ESCOLA DE DOUTORAMENTO
INTERNACIONAL DA USC

Nuria
López Lorenzo

Tese de doutoramento

Therapeutical approaches for prion diseases and characterization of recombinant prion strains from different perspectives

Santiago de Compostela, 2023

Programa de Doutoramento en Medicina Molecular

USC
UNIVERSIDADE
DE SANTIAGO
DE COMPOSTELA

ESCOLA DE DOUTORAMENTO
INTERNACIONAL DA USC

TESE DE DOUTORAMENTO

THERAPEUTICAL APPROACHES FOR PRION DISEASES AND CHARACTERIZATION OF RECOMBINANT PRION STRAINS FROM DIFFERENT PERSPECTIVES

Autor

Nuria López Lorenzo

Director: Jesús R. Requena

PROGRAMA DE DOUTORAMENTO EN MEDICINA MOLECULAR

SANTIAGO DE COMPOSTELA

USC
UNIVERSIDADE
DE SANTIAGO
DE COMPOSTELA

DECLARACIÓN DA AUTORA DA TESE

Dna. **Nuria López Lorenzo**

Título da tese: **Therapeutical approaches for prion diseases and characterization of recombinant prion strains from different perspectives**

Presento a miña tese, seguindo o procedemento axeitado ao Regulamento, e declaro que:

1) A tese abarca os resultados da elaboración do meu traballo.
2) De ser o caso, na tese faise referencia ás colaboracións que tivo este traballo.
3) Confirmo que a tese non incorre en ningún tipo de plaxio doutros autores nin de traballos presentados por min para a obtención doutros títulos.
4) A tese é a versión definitiva presentada para a súa defensa e coincide a versión impresa coa presentada en formato electrónico

E comprométome a presentar o Compromiso Documental de Supervisión no caso de que o orixinal non estea na Escola.

En **Santiago de Compostela**, **18 de Agosto de 2023**.

Sinatura electrónica

USC UNIVERSIDADE DE SANTIAGO DE COMPOSTELA

A doutoranda declara non ter ningún conflito de interese en relación coa tese de doutoramento.

A doutoranda declara ser autora de todas as figuras recollidas nesta tese de doutoramento agás daquelas que o indiquen no pé de imaxe.

USC
UNIVERSIDADE DE SANTIAGO DE COMPOSTELA

A presente tese de doutoramento contou coas seguintes fontes de financiamiento:

- Financiamiento do Ministerio de Economía, Industria y Competitividad (MINECO),Plan Nacional 2017 (BFU2017-86692-P)

- Financiamento da Agencia Española de Investigación (PID2020-117465GB-I00), financiado parcialmente polo Fondo Europeo de Desenvolvemento Rexional.

- Axuda de investigación “Sergio Rubio Muñóz” 2020-2021, da Fundación Española de Enfermedades Priónicas.

- A doutoranda foi beneficiaria dunha axuda de apoio a etapa predoutoral do Sistema galego de I+D+i, cofinanciadas parcialmente no ámbito das universidades do Sistema universitario de Galicia polo programa operativo Fondo Social Europeo Galicia 2014-2020, na súa convocatoria no ano 2019, pola Consellería de Cultura, Educación e Ordenación Universitaria de la Xunta de Galicia.
-

USC
UNIVERSIDADE DE SANTIAGO DE COMPOSTELA

"What I love about science is that as you learn, you don't really get answers. You just get better questions."

- John Green, Turtles All the Way Down

USC UNIVERSIDADE DE SANTIAGO DE COMPOSTELA

Agradecimientos

Recuerdo cuando estaba en el colegio y en los libros de biología aparecían fotografías de los grandes científicos de los siglos XIX y XX. A menudo nos los presentan con imágenes de investigadores solitarios mirando a través de las lentes del microscopio, ¿quién no tiene en la mente esa imagen de Fleming con la única compañía de cientos de placas Petri? Sin embargo, si algo he aprendido durante estos años es que el camino de la ciencia es de todo menos solitario. Compañeros, amigos, familia y colaboradores han recorrido este trayecto conmigo y han dejado su granito de arena en esta tesis o en mí. Por ese motivo quiero dedicarles unas palabras de agradecimiento, ya fuera por su contribución a este trabajo o por su compañía en esta aventura.

Por supuesto, las primeras palabras de agradecimiento van dedicadas a mi director de tesis, Jesús Requena. Llegué al laboratorio para hacer el TFM y en principio no estaba en mis planes hacer el doctorado, pero los priones resultaron ser más fascinantes de lo que esperaba, y en parte tú los haces así. Creo que han sido unos años productivos, aunque quizás los resultados no siempre fueron los que esperábamos. En todo momento me has dado la libertad de ir a mi ritmo, de organizarme a mi manera y de hacer los experimentos que consideraba, pero con sutiles sugerencias demostrando en todo momento que estabas ahí, y por eso te lo agradezco.

Secondly, I want to thank Emiliano Biasini and Ines Mancini for opening the doors of their laboratories at the University of Trento, and also to all the members of the Dulbecco Telethon Laboratory for Prions and Amyloids at CIBIO: Valerio, Giovanni, Tania, Serena, Elisa, and Laura. I know it was not the best time to go: a pandemic, lockdowns, limited capacity in the laboratories, movement restrictions, and I am aware that it would have been easier for you to prioritize your

USC UNIVERSIDADE DE SANTIAGO DE COMPOSTELA

experiments and send the visiting Ph.D. student home, but you always counted on me and included me in the work plans. Grazie mille!

Ir de estancia a otros laboratorios fue de las experiencias más enriquecedoras del doctorado. Aprender técnicas nuevas, conocer otras perspectivas o adaptarse a distintas formas de trabajar te hacen crecer a nivel profesional y yo tuve la suerte de vivir esta experiencia por partida doble. Mi segunda estancia fue en el laboratorio de Joaquín Castilla, en el CIC bioGUNE, grupo con el que la relación ya estaba más que consolidada desde mucho antes de que yo llegara. Con Hasier, Patricia, Jorge, Carlos, Cristina, Nuno, Leire y Juan, aprendí lo que era el trabajo en equipo y que el buen ambiente también se puede mantener en grupos más grandes. En estos agradecimientos creo que Hasier merece una mención especial por estar siempre dispuesto a echar una mano, por ser el primero en contestar a los correos, y junto con Patricia, por ayudarnos con esas técnicas que todavía se nos resisten. Además, si algo aprendí de vosotros es que el networking se hace mejor si va acompañado de txakoli y queso.

También quiero agradecerle a Enric Vidal y Samanta Giler, del CReSa-IRTA, por los estudios histopatológicos, incluso bajo presión, mandándonos los resultados siempre a tiempo para los congresos.

También agradecerle a Susana Bravo del servicio de proteómica del IDIS, a Manuel Martín de la unidad de resonancia magnética del CACTUS y a Víctor Sánchez por su contribución a los análisis de espectrometría de masas y resonancia magnética nuclear de estado sólido y por ayudarnos a interpretar los resultados.

Special thanks go to Professor Holger Wille from the University of Alberta (Canada) for sharing his scFvG1 antibody with us. Also thanks to Professor Glenn Telling, from Colorado State University (US), for sharing his TgVole model with us. I extend my gratitude to Professor Vincent Beringue, Professor Human Rezaei, and Doctor Davy Martin from INRAE (France) for fibrillating for us an amyloid with such unexpected properties. Lastly, I express my gratitude to Professor

USC UNIVERSIDADE DE SANTIAGO DE COMPOSTELA

Romolo Nonno for agreeing to study the biological properties of the amyloid in his bank voles.

Por último, a las técnicos del CIMUS, Pili, Lucía, Ana, Ángela y Jose, por estar siempre dispuestos a echar una mano y por su gestión de los recursos comunes que permiten que todos le saquemos el mejor provecho. Sin olvidarme del personal del CEBEGA, Anxo, Silvia, las dos Anas, Laura y Pablo, por cuidar de los ratones y mantenernos siempre informados sobre su estado.

Sin embargo, el día a día de un doctorado va mucho más allá del trabajo en el laboratorio y colaboraciones, y esas personas que están alrededor, apoyándote, escuchándote o simplemente poniéndote un café al lado del ordenador mientras trabajas; al final son las que más aportan porque no dejan que tires la toalla. Esas personas están en muchas partes, pero en mi caso, están en el laboratorio y en casa.

Empezando por el laboratorio, si hay alguien que merece un pedestal por aguantarme día sí y día también, esa es Sonia. Sonia, podría ponerte con la gente que contribuyó de una forma más práctica en la tesis, porque por supuesto lo hiciste, pero creo que te debo mucho más a nivel personal. Gracias por escucharme todos los días, por tomarte cafés conmigo (y algún que otro vino cuando teníamos algo que celebrar u olvidar) y por decirme que a veces también hay que pararse y tomar tiempo para uno mismo. A Yaiza, por enseñarme que en todo caos hay un orden y en todo orden hay un caos. De ti también aprendí que a veces también hay que disfrutar de la vida y tomársela un poco más a la ligera. A Leticia, sabes que, aunque estés en Göttingen, yo te considero una más del laboratorio. Hasta que te conocí no sabía que se podía llegar a ser tan intensa y tenaz. Me enseñaste a que si la vida te la limones, hay que hacer litros de limonada y seguir hacia delante, siempre “digna y regia”, como dices tú. Gracias también a Alex, Raúl, Sanaz, por compartir conmigo estos meses en el laboratorio, aunque creo que no conocisteis mi mejor versión. Alba, Rafa, Jesuína, Maite, Charlene, Sonia, Laura, Álvaro, Michael, Nicolás, Lucía, y todos los estudiantes

USC UNIVERSIDADE DE SANTIAGO DE COMPOSTELA

de TFM, TFG y prácticas que habéis pasado por el laboratorio, gracias a vosotros también por recordarme a mí misma de dónde vengo y por qué estoy aquí.

Gracias también a las chicas del laboratorio de al lado, las plaquetas. A Irene y María, cuyas tesis fueron mis primeras referencias y mi camino a seguir. Gracias especialmente a Lidia y Alberto (que te incluyo aquí aunque no seas de este grupo) por los cafés y las eternas conversaciones de pasillo. Por compartir conmigo vuestras experiencias, consejos y por escucharme, aún ahora, que ya terminasteis vuestra etapa en el CiMUS.

Por último, solo me queda agradecerles a esas personas que están a mi lado cuando salgo del laboratorio. A mis amigas, que sin tener ni idea de priones me preguntan cómo me va la tesis y cómo se encuentran los ratones; que a día de hoy se ofrecen para que practique con ellas las presentaciones de congresos o la de la tesis, y que me animan diciendo que en unos meses seré “Dra. López”.

A mis padres por apoyarme en todas mis decisiones y por enseñarme que los límites me los pongo yo. Por alegrarse conmigo de los pequeños logros y por intentar entender de qué va todo esto. A mi hermano, Iván, porque sí, porque me achucha cada vez que llego de Santiago y con eso le basta para demostrarme su apoyo.

Y a Germán, porque lo que llevamos vivido en estos cuatro años de tesis solo los sabemos tú y yo. Porque una tesis no es un camino de rosas y las alegrías se celebran con los compañeros y los amigo, pero la frustración se lleva y se paga en casa. Gracias por soportarme en los malos momentos y no dejar que tire la toalla. Gracias también por aguantar que antepusiera la tesis a todo lo demás. Gracias por estar ahí y ser un pilar fundamental de esta tesis.

USC
UNIVERSIDADE DE SANTIAGO DE COMPOSTELA

Abstract

Transmissible spongiform encephalopathies, also known as prion diseases, are neurodegenerative disorders caused by prions. These infectious proteins result from misfolding of the cellular prion protein, PrP^{C}, into its pathogenic isoform, PrP^{Sc}. Transmissible spongiform encephalopathies affect humans and other mammals and can manifest as idiopathic, genetic, or acquired diseases. Although PrP^{C} and PrP^{Sc} share the same amino acid sequence, they differ in their secondary, tertiary, and quaternary structures, leading to distinct biological and biochemical properties. Furthermore, PrP^{Sc} can exhibit conformational variants called strains, which display different phenotypes and even resistance to certain compounds with anti-prion properties.

Prion diseases are fatal. Despite the evaluation of various candidates with therapeutic potential, there are currently no treatments or vaccines available for them. In this thesis, three therapeutic candidates are assessed as proof of concept, tackling prion diseases from different aspects of their biology in a rapid murine model of prion disease. The first candidate is a porphyrin termed Fe(III)-TMPyP, which acts as a molecular chaperone, stabilizing the native conformation of PrP^{C} and hindering its conversion into PrP^{Sc}. The second therapeutic strategy proposed involves the use of a single-chain antibody, scFv-G1, designed to recognize PrP^{Sc} specifically. The third therapeutic approach employs a recombinant self-propagating PrP amyloid that aims to prevent the conversion of PrP^{C} into PrP^{Sc} and compete with PrP^{Sc} for the substrate.

Unfortunately, the results obtained from these therapeutic approaches were not as expected; similar to other studies in search of treatments for prion diseases, they were unable to demonstrate beneficial effects in animal models.

USC UNIVERSIDADE DE SANTIAGO DE COMPOSTELA

One reason for therapeutic failure in prion diseases is attributed to the ability of prions to evade treatment through adaptation to the presence of the pharmacological agent or the selection of prion strains that propagate more effectively in its presence. Both mechanisms result in the generation of drug-resistant strains and are mainly due to slight conformational arrangements in prion structure. Therefore, a thorough characterization of diverse prion strains can provide crucial information about the differences between them, allowing for the design of effective therapies and addressing the adaptation and selection mechanisms that lead to therapeutic failure. Furthermore, studying the diversity of prion strains and their differences involves significant biochemical and structural interest. For these reasons, the last chapter of this doctoral thesis aims to study various recombinant prion strains generated spontaneously by PMSA using different biological, biochemical, and biophysical approaches.

Overall, this work addresses prion diseases through the use of three pharmacological candidates, each approaching prion disorders from different perspectives. Although the results have not met expectations in terms of efficacy, they have shed light on the limitations of each candidate. Additionally, it has been possible to characterize recombinant prion strains from different approaches, establishing differences among them and redefining the role of cofactors in the diversity of prion strains.

USC UNIVERSIDADE DE SANTIAGO DE COMPOSTELA

Resumen

Las encefalopatías espongiformes transmisibles, también conocidas como enfermedades priónicas, son trastornos neurodegenerativos causados por priones, proteínas infecciosas que surgen del malplegamiento de la proteína priónica celular, PrP^{C}, en su isoforma patogénica, PrP^{Sc}. Las encefalopatías espongiformes transmisibles afectan al ser humano y otros mamíferos y pueden presentarse como enfermedades idiopáticas, genéticas, o adquiridas. Aunque la PrP^{C} y la PrP^{Sc} comparten la misma secuencia aminoacídica, difieren en sus estructuras secundaria, terciaria y cuaternaria, lo que se traduce en distintas propiedades biológicas y bioquímicas. Por otra parte, la PrP^{Sc} puede presentar variantes conformacionales, denominadas cepas, que se manifiestan con distintos fenotipos e incluso resistencia a ciertos compuestos con propiedades antipriónicas.

Las enfermedades priónicas son mortales. Aunque se han estudiado diversos candidatos con potencial terapéutico, a día de hoy no existen tratamientos ni vacunas para ellas. En la presente tesis se evalúan tres candidatos terapéuticos como prueba de concepto, abordando las enfermedades priónicas desde distintos aspectos de su biología, en un modelo murino rápido de enfermedad priónica. El primer candidato es una porfirina, llamada Fe(III)-TMPyP, que actúa como una chaperona molecular estabilizando la conformación nativa de la PrP^{C} e impidiendo su conversión en la PrP^{Sc}. La segunda estrategia terapéutica que se plantea es el uso del anticuerpo de cadena sencilla, scFv-G1, diseñado para reconocer específicamente la PrP^{Sc}. El tercer abordaje terapéutico consiste en el uso de un amiloide de PrP recombinante autopropagativo que tiene como objetivo bloquear la conversión de la PrP^{C} en PrP^{Sc} y competir con la PrP^{Sc} por el sustrato.

USC UNIVERSIDADE DE SANTIAGO DE COMPOSTELA

Desafortunadamente, los resultados obtenidos con los abordajes terapéuticos no fueron los esperados; al igual que otros trabajos en la búsqueda de un tratamiento para las enfermedades priónicas, no pudieron mostrar efectos beneficiosos en modelos animales.

Un motivo de fracaso terapéutico en las enfermedades priónicas se atribuye a la capacidad de los priones de evadir el tratamiento mediante la adaptación a la presencia del agente farmacológico o a la selección de las cepas de priones que mejor se propagan en su presencia. Ambos mecanismos tienen como consecuencia la generación de cepas resistentes al tratamiento y se deben principalmente a ligeros cambios conformacionales en la estructura de los priones. Por este motivo, una caracterización minuciosa de diversas cepas puede proporcionar información crucial sobre las diferencias entre ellas, lo que permitiría diseñar terapias efectivas y abordar los mecanismos de adaptación y selección que conducen a la ineficacia del tratamiento. Por otro lado, el estudio de la diversidad de cepas de priones y las diferencias existentes entre ellas es de gran interés bioquímico y estructural. Por todo ello, el último capítulo de la presente tesis de doctorado tiene como propósito el estudio mediante métodos biológicos, bioquímicos y biofísicos de diversas cepas de priones recombinantes, generadas espontáneamente mediante PMSA.

En definitiva, ha sido posible estudiar el efecto terapéutico de tres candidatos que abordan las enfermedades priónicas desde distintas perspectivas y, aunque los resultados no han sido los esperados en términos de eficacia, han arrojado luz sobre las limitaciones que presenta cada una de ellas en la terapia de las enfermedades priónicas. Además, ha sido posible caracterizar desde distintas perspectivas cepas recombinantes de priones, estableciendo diferencias entre ellas y redefiniendo el role de los cofactores en la diversidad de cepas de priones.

USC UNIVERSIDADE DE SANTIAGO DE COMPOSTELA

Resumo

As encefalopatías esponxiformes transmisíbeis, tamén coñecidas como enfermidades priónicas, son trastornos neurodexenerativos causados por prións, proteínas infecciosas que xorden do mal-pregado da proteína priónica celular, PrP^{C}, na súa iso-forma patóxena, PrP^{Sc}. As encefalopatías esponxiformes transmisíbeis son enfermidades raras; a súa incidencia é de 1-2 casos por cada millón de habitantes e ano, fronte aos 11000 casos por millón de habitantes e ano que se diagnostican de enfermidade de Alzheimer, a doenza neurodexenerativa máis común. As enfermidades priónicas non só afectan ao ser humano, tamén a outros mamíferos, e poden presentarse como enfermidades xenéticas, adquiridas ou idiopáticas, sendo estas últimas as máis comúns. As enfermidades priónicas xenéticas son aquelas que están vinculadas con mutacións no xene PRNP, que codifica a PrP^{C} e para as que hai máis de 40 mutacións descritas. Son enfermidades dominantes e con elevada penetrancia, o que quere dicir que un portador dunha mutación relacionada cunha destas doenzas xenéticas, ten unha alta probabilidade de desenrolar a enfermidade ao longo da súa vida. Por outra banda, as enfermidades priónicas menos comúns son as adquiridas, que se relacionan co consumo de alimentos, co contacto con materiais cirúrxicos, ou coa recepción de órganos ou tecidos contaminados con prións. Aínda que as enfermidades priónicas adquiridas son as menos común, son probablemente as máis coñecidas debido á encefalopatía esponxiforme bovina, coñecida popularmente como a enfermidade das vacas tolas. Esta doenza xurdiu en Reino Unido como consecuencia da alimentación do gando vacún con fariñas cárnicas, que resultaron estar contaminadas con prións. O brote de encefalopatía esponxiforme bovina levou ao sacrificio de máis de 4 millóns de reses e incontábeis perdas económicas. Pero o máis desalentador foi que, como consecuencia do consumo de carne contaminada, esta enfermidade deu orixe a unha nova zoonose, coñecida como a variante da enfermidade

USC UNIVERSIDADE DE SANTIAGO DE COMPOSTELA

de Creutzfeldt-Jakob. Este feito desencadeou unha crise de saúde pública en Europa a finais dos anos 90 e comezos dos 2000.

A PrP^{C} é una glicoproteína de membrana altamente conservada entre os mamíferos. A súa función non está ben definida, aínda que se coñece que participa en diversos procesos biolóxicos e patolóxicos coma o mantemento da mielina, a homeostase de certos metais, proporcionando protección contra o estrés oxidativo, preservando a plasticidade sináptica, regulando o ritmo circadiano, regulando o sistema inmune, tamén participa na sensibilidade á dor, na bioloxía do cancro e en enfermidades neurodexenerativas. Porén, o desenrolo de ratos transxénicos que carecen desta proteína demostrou que a súa función non é vital ou que na súa ausencia existen mecanismos compensatorios que permiten o desenrolo da vida.

Malia que a PrP^{C} e a PrP^{Sc} comparten a mesma secuencia aminoacídica, ambas iso-formas presentan distintas arquitecturas nas súas estruturas secundaria, terciaria e cuaternaria. Mentres que a PrP^{C} é una proteína globular, cunha gran presencia de hélices α na súa estrutura secundaria e cun extremo N-terminal intrinsecamente desordenado, a PrP^{Sc} ten unha elevada presenza de follas β na súa estrutura secundaria e presenta unha arquitectura de follas β intermolecular en rexistro paralelo, PIRIBS (do inglés, *Parallel In-register Intermolecular β-Sheet Architectures*). Ademais, as súas diferencias estruturais vense reflectidas nas propiedades biolóxicas e bioquímicas de ámbalas dúas iso-formas. Mentres que a PrP^{C} é unha proteína fisiolóxica, que se atopa como monómero ancorada ás membranas celulares e é solúbel e sensíbel á dixestión con proteasas; na PrP^{Sc}, os monómeros asócianse formando fibras amiloides que son insolúbeis e crean depósitos no cerebro, ademais a PrP^{Sc} é parcialmente resistentes á dixestión con proteasas. Por outra banda, a PrP^{Sc} pode presentar variantes conformacionais que difiren lixeiramente na súa arquitectura, denominadas cepas, e que presentan certas diferenzas biolóxicas e bioquímicas, como distinta resistencia á dixestión con proteasas, á desnaturalización con axentes caotrópicos, distinta afinidade polas

USC UNIVERSIDADE DE SANTIAGO DE COMPOSTELA

áreas cerebrais, distintos tempos de incubación, e incluso resistencia a certos compostos con propiedades antipriónicas.

A arquitectura da PrP^{Sc} foi recentemente descuberta. Ata ese momento existían dous modelos conformacionais para a iso-forma patóxena da PrP^{C}, o PIRIBS e o β-solenoide de 4 chanzos (4RβS, do inglés, *4-Run-β-Solenoid*). Na conformación PIRIBS, cada monómero está pregado en follas β que se atopan completamente aliñadas, de tal xeito que cada aminoácido se atopa enriba ou debaixo do mesmo aminoácido do monómero consecutivo. Pola contra, o 4RβS implica que cada monómero se atopa pregado sobre sí mesmo nunha configuración helicoidal, na que cada monómero distribúese ao longo de 4 chanzos. A escasa resolución dos métodos disponíbeis ata o momento, as dificultades que incumben á purificación da PrP^{Sc} de cerebro e as limitacións das ferramentas informáticas non permitían determinar cal dos dous modelos era o correcto e as evidencias que se obtiñan eran compatíbeis cos dous. Non foi ata o ano 2021 cando Allison Kraus e os seus colegas obtiveron imaxes por criomicroscopía electrónica que permitiron a resolución da primeira cepa de prións illada de cerebro de hámsteres inoculados. En cuestión de meses, o mesmo grupo e outros foron quen de resolver a estrutura doutras cepas de prións, evidenciando que as diferencias entre elas residen en lixeiras variacións estruturais. A resolución da estrutura dos prións considérase un dos grandes fitos dos últimos anos no campo dos prións.

Desafortunadamente, as enfermidades priónicas son mortais. Ata o momento diversas estratexias terapéuticas foron avaliadas intentando abordar as enfermidades priónicas dende distintos aspectos da súa bioloxía, pero con escasa ou nula efectividade. Dado que a presenza da PrP^{C} é imprescindíbel para o desenrrolo das enfermidades priónicas, moitos esforzos centráronse en diminuir ou impedir a expresión da PrP^{C}. Esta estratexia sería altamente vantaxosa para os portadores de mutacións relacionadas con enfermidades priónicas xenéticas, xa que se fora posíbel anular por completo a expresión da PrP^{C}, eliminaríase o risco de padecer estas enfermidades. Esta estratexia terapéutica é a máis

USC UNIVERSIDADE DE SANTIAGO DE COMPOSTELA

prometedora dos últimos anos xa que é a que mellores resultados mostrou en ratos. Outras estratexias terapéuticas estudadas foron aquelas que teñen como diana a PrP^{C}, e son coñecidas como chaperonas moleculares. Estes compostos teñen como obxectivo unírense á PrP^{C} estabilizándoa, reducindo a súa enerxía libre de Gibbs, e impedindo a súa conversión na PrP^{Sc}. Por outra banda, a PrP^{Sc} tamén foi o obxectivo de diversas terapias que pretendían estabilizala para evitar a súa conversión, aumentar a súa eliminación ou bloquear a súa interacción coa PrP^{C}. Outra estratexia terapéutica prometedora no ámbito das enfermidades priónicas e tamén no das enfermidades neurodexenerativas en xeral, son as inmunoterapias, e concretamente a inmunización pasiva. Esta abordaxe terapéutica foi recentemente levada a un ensaio en pacientes con enfermidades priónicas e, aínda que o número de pacientes foi moi limitado para extraer conclusións sobre a efectividade do tratamento, verificouse que a inmunización pasiva e, canda menos, segura, sentando as bases para futuros ensaios clínicos nos que se poida valorar a súa eficacia. Porén, malia a diversidade de candidatos terapéuticos estudados, na actualidade non existen tratamentos nin vacinas para as enfermidades priónicas.

Na presente tese de doutoramento preséntanse tres posíbeis candidatos terapéuticos que abordan as enfermidades priónicas dende tres puntos de vista distintos da súa bioloxía: unha chaperona molecular que actúa sobre a PrP^{C} estabilizando a súa conformación; inmunización pasiva cun anticorpo tipo scFv específico fronte a conformación da PrP^{Sc}; e un amiloide da PrP autopropagativo mais inocuo, que uniríase á PrP^{Sc} impedindo a súa conversión e empregando o seu substrato, a PrP^{C}, para propagarse. Como proba de concepto da actividade *in vivo* dos candidatos terapeúticos mencioados, o modelo animal empregado foi un rato transxénico que expresa a proteína priónica dunha especie de roedor silvestre (*Myodes glareolus*), e que alberga concretamente o polimorfismo 109I (TgVole), e cuns niveis de expresión próximos aos fisiolóxicos, ~1-1,2x. Este modelo animal é altamente susceptíbel a desenrolar enfermidades priónicas. Por outra banda, o axente infeccioso

USC UNIVERSIDADE DE SANTIAGO DE COMPOSTELA

contra ao que foron testados os candidatos terapéuticos foi una cepa de prións da caquexia crónica dos cervos, unha doenza priónica que afecta cérvidos, que foi adaptada previamente ao noso modelo animal.

O primeiro candidato abordado foi un tetrapirrol, chamado Fe(III)-TMPyP. A capacidade antipriónica do Fe(III)-TMPyP foi amplamente descrita. Coñécese que o Fe(III)-TMPyP únese á PrP^{C}, interactuando coa rexión C-terminal da hélice α 3 e a primeira folla β; deste xeito, estabiliza a conformación nativa da PrP^{C} e inhibe a súa conversión na PrP^{Sc} tanto *in vitro* como en cultivos celulares. Ademais, o Fe(III)-TMPyP foi testado fronte diferentes cepas de prións en cultivos celulares, demostrando que a súa actividade é independente da cepa fronte a que se atope. Porén, os datos da súa actividade *in vivo* son mínimos, e limítanse a unha avaliación en hámsteres na que foi administrado á vez que o inóculo, prolongando a supervivencia dos animais ao neutralizar ao axente infeccioso na súa administración conxunta. Para avaliar a súa actividade nunhas condicións máis realistas que puidesen parecerse ao tratamento dun pacente, deseñouse unha posoloxía crónica que consistíu nunha administración semanal do tetrapirrol, por vía intracerebral, durante cinco semanas e comezando co tratamento dúas semanas despois da inoculación co axente infeccioso.

Os datos de supervivencia indicaron que o tratamento crónico con Fe(III)-TMPyP non aumentou a esperanza de vida dos ratos, aínda que se detectaron niveis de PrP^{Sc} lixeiramente inferiores naqueles ratos tratados cronicamente con respecto aos que recibiron o soro salino. Dado o resultado negativo respecto a eficacia in vivo do Fe(III)-TMPyP, fíxose un seguimento cinético da distribución do composto no cerebro aproveitando a súa autofluorescencia. Dito ensaio demostrou que incluso despois de 24 horas, o tetrapirrol mantíñase localizado nas zonas da administración, indicando que é incapaz de difundir a través do parénquima cerebral. Polo tanto, concluíuse que o efecto sobre a cantidade de PrP^{Sc} podería deberse a un efecto local, pero tal efecto non

USC UNIVERSIDADE DE SANTIAGO DE COMPOSTELA

é suficiente como para verse reflectido nunha demora no inicio dos signos clínicos ou nunha prolongación da supervivencia.

A segunda estratexia terapéutica que se prantexou foi o uso do anticorpo conformacional scFv-G1. Este traballo foi parte dunha colaboración co grupo de Holger Wille, da Universidade de Alberta, o cal desenrolou dito anticorpo. A orixe do scFv-G1 está nunha vacina fronte unha conformación da PrP nunha arquitectura 4RβS. Aínda que agora sábese que a arquitectura da PrP^{Sc} é un PIRIBS, cabe resaltar que este traballo comezou antes de tal descubrimento. Esta vacina baseada na arquitectura do 4RβS empregou un prión fúnxico, chamado HET-s, cuxa estrutura é un β-solenoide de dous chanzos. Unindo dúas moléculas de HET-s simularon a estrutura do 4RβS e crearon a andamiaxe perfecta para albergar un epítopo da PrP. Para isto, os investigadores basáronse na modelización da PrP na arquitectura 4RβS mediante dinámicas moleculares e seleccionaron aminoácidos inmunoxénicos que introduciron na andamiaxe do HET-s. Ratos inmunizados con esta vacina presentaron una prolongación da supervivencia de ata o 250% e células B produtoras de anticorpos foron illadas. Entre os anticorpos producidos escolleuse unha IgG que era capaz de recoñecer PrP^{Sc} *in vitro* procedente de homoxenados cerebrais de distintas orixes. Finalmente, secuenciouse o epítopo que recoñecía a IgG e produciuse o fragmento variábel de cadea sinxela de xeito recombinante en *Escherichia coli*, dando lugar ao scFv-G1. A aproximación terapéutica que se prantexou na presente tese para avaliar a actividade de scFv-G1, como proba de concepto, foi semellante á do Fe(III)-TMPyP, consistindo nun tratamento crónico por vía intracerebral, durante cinco semanas e comezando dúas semanas despois da inoculación, no mesmo modelo animal e co mesmo inóculo. Lamentablemente, os datos de supervivencia dos ratos indicaron que o tratamento non melloraba a esperanza de vida dos ratos nin tampouco modulaba outros parámetros que indicasen un efecto sobre a enfermidade.

USC UNIVERSIDADE DE SANTIAGO DE COMPOSTELA

A terceira abordaxe terapéutica consistiu no uso dun amiloide non infeccioso, autopropagativo, de PrP recombinante. Aparte das isoformas PrP^{C} e PrP^{Sc}, tamén é posíbel obter no laboratorio outras formas amiloide da proteína priónica. Estes amiloides difiren da PrP^{Sc} en aspectos bioquímicos e biolóxicos. Ao igual que a PrP^{Sc}, os amiloides da PrP son parcialmente resistentes á dixestión con proteasas, pero o núcleo resistente é de menor tamaño. Ademais, o tropismo cerebral dos amiloides é distinto do da PrP^{Sc}. Por outra banda, aínda que amiloides se propagan e acumúlanse no cerebro dos animais inoculados con eles, non desencadean unha enfermidade priónica no primeiro pase; porén, tras tres pases seriados, os animais desenrolan a enfermidade, pero nese caso, o material que acumulan no cerebro é similar á PrP^{Sc} e xa non mostra as particularidades dos amiloides.

A abordaxe terapéutica empregando un amiloide recombinante da PrP foi previamente estudada en hámsteres, con resultados satisfactorios nos que víase unha prolongación da supervivencia cando se administraban antes da inoculación. Para verificar que dita abordaxe terapéutica tamén era válida no noso modelo animal, fibrilamos no laboratorio un amiloide cun núcleo resistente a proteasas C-terminal e administrámollelo aos ratos profilácticamente, dúas semanas antes da inoculación. Os resultados mostraron que o amiloide, non só non foi efectivo extendendo a supervivencia dos animais, senón que resultou ser infeccioso no modelo animal empregado, desencadeando unha enfermidade priónica no grupo control que unicamente recibiu o amiloide. Estes animais presentaban no cerebro material con resistencia á proteasa cun perfil electroforético distinto ao da PrP^{Sc}, dado que o núcleo resistente á dixestión era de menor tamaño, e só era recoñecido por anticorpos do extremo C-terminal. Por outra banda, ao aplicaren un protocolo de concentración de prións, identificouse a maiores unha banda N-terminal pouco abundante pero presente en todos os animais. Curiosamente, mentres que a banda C-terminal coincidía coas propiedades do amiloide administrado, a banda N-terminal resistente a

USC UNIVERSIDADE DE SANTIAGO DE COMPOSTELA

proteasa non estaba presente no amiloide recombinante, suxerindo que se xerou no cerebro dos animais a raíz da inoculación co amiloide.

Para determinar se este amiloide infeccioso mantiña as súas propiedades tras pases seriadas ou finalmente emerxía PrP^{Sc}, a enfermidade transmitiuse seriadamente por tres pases. Á diferencia doutros amiloides descritos previamente, este amiloide mantivo as súas propiedades respecto ao patrón electroforético ou patoloxía durante os tres pases, indicando que o amiloide comportábase como un prion *bona fide*.

Os resultados obtidos co estudo das abordaxes terapéuticas foron desalentadores; ao igual que outros traballos na procura dun tratamento para as enfermidades priónicas, non puideron mostrar efectos beneficiosos en modelos animais.

Un motivo de fracaso terapéutico nas enfermidades priónicas débese á capacidade dos prións a adaptarse á presenza do axente farmacolóxico, dando lugar a cepas resistentes ao tratamento. Ditas resistencias débense principalmente a lixeiros cambios conformacionais na estrutura dos prións, en consecuencia, o estudo estrutural e bioquímico de diversas cepas de prións pode aportar información moi relevante sobre os mecanismos moleculares involucrados nas resistencias aos tratamentos destas doenzas. Tendo isto en conta, o último capítulo da presente tese de doutoramento ten como obxectivo o estudo das propiedades biolóxicas, bioquímicas e biofísicas de diversas cepas de prións recombinantes.

Con dito fin, este traballo describe a xeración espontánea de diversos confórmeros de PrP recombinante mediante a técnica da amplificación de proteínas mal-pregadas por axitación (PMSA, do inglés Protein Misfolding Shaking Amplification) en presenza de tres cofactores distintos. As técnicas de propagación de prións *in vitro* presentan diversas vantaxes coma reducir o número, os custos e o tempo derivados de estudos en animais, estudar a eficacia de diferentes moléculas terapéuticas, obter grandes cantidades de prións infecciosos

USC UNIVERSIDADE DE SANTIAGO DE COMPOSTELA

para análises estruturais, amplificar pequenas cantidades de prións, como ferramenta para o diagnóstico ou para estudar os compoñentes mínimos necesarios para obter partículas infecciosas, entre outros. Entre as técnicas de amplificación *in vitro* dispoñíbeis foi escollida a PMSA, dado que o equipamento e a metodoloxía son sinxelos, pouco custosos, o material xerado mediante esta técnica é infeccioso, e unha vez inoculados, recapitulan enfermidades priónicas comparábeis ás dos prións illado de cerebro e ademais pódense obter grandes cantidades de prións recombinantes en pouco tempo. Por outra banda, esta técnica permite mater un control sobre os reactivos empregados, ao contrario daquelas técnicas que requiren o uso de homoxenados de cerebro como fonte PrP^{C}, e polo tanto, permite avaliar o efecto dos cofactores sobre a xeración e propiedades dos prión xerados mediante esta técnica. Os cofactores son moléculas de diversas naturezas, como lípidos, ácidos nucleicos, polisacáridos ou outras proteínas, que se asocian ás fibras de PrP^{Sc}. A función concreta dos cofactores descoñécese, aínda que se pensa que poden participar no proceso de conversión, estabilizando á proteína durante o malpregamento. Tamén suxeriuse que os cofactores poden definir as propiedades das cepas de prións. Por outra banda, creese que os cofactores xogan un rol determinante na xeración de prión espontaneamente *in vitro*, de tal xeito que o cofactor pode guiar á proteína para a conversión nunha determinada cepa, polo tanto, limitando a diversidade de cepas que se poden xerar na súa presencia.

Para estudar a diversidade de confórmeros que se poden orixinar na presencia de tres cofactores de natureza glicosaminoglicana (heparina, condroitín sulfato e polisulfato de pentosano), a PrP^{C} recombinante someteuse á PMSA en presenza dun cofactor e esferas de vidro, e a mobilidade electroforética do produto final analizouse tras a súa dixestión cunha proteasa. Os resultados amosaron que a lo menos tres confórmeros con diferentes perfís electroforéticos foron xerados en presenza de cada cofactor.

Para caracterizar cada un dos confórmeros e determinar as diferenzas entre eles empregáronse diversos métodos bioquímicos, biofísicos e

USC UNIVERSIDADE DE SANTIAGO DE COMPOSTELA

biolóxicos. As análises mediante espectrometría de masas, resonancia magnética de estado sólido e Western blot, determinaron que os confórmeros analizados presentaban distintas propiedades bioquímicas e biofísicas, indicando que eran estruturalmente diferentes. Ademais, os resultados obtidos por espectrometría de masas comparáronse con datos previos procedentes de mostras de pacientes, animais inoculados, o doutras cepas de prión recombiantes xeradas con outras técnicas, demostrando que os nosos datos eran consistentes co previamente descrito e concluíndo que os confórmeros xerados mediante PMSA compartían propiedades con prións *bona fide*.

Por outra banda, para caracterizar as propiedades biolóxicas dos confórmeros, estes foron inoculados intracerebralmente no mesmo modelo de rato transxénico empregado nas abordaxes terapéuticas, o TgVole. Trala inoculación, todos os animais adoeceron, presentando signos compatíbeis con enfermidades priónicas. Cando os seus cerebros foron analizados, atopáronse en todos eles PrP resistente a proteasa, e a análise histopatolóxica confirmou que os ratos padecerán unha enfermidade priónica. Estes resultados demostraron que os confórmeros eran infecciosos, e polo tanto trátabanse de prións *bona fide.*

Os prións xerados con PrP^{C} recombinante a miúdo sofren un proceso de adaptación cando son inoculados en animais. Esta adaptación débese principalmente ás diferencias entre a PrP^{C} recombinante e a nativa do cerebro; esta última presenta modificación postraducionais, en forma de glicosilacións e unha áncora de glicofosfatidilinositol. Ademais o ambiente cerebral é moito máis complexo que os reactivos que se empregan para xerar prións *in vitro*. Para comparar as características biolóxicas de cada un dos confórmeros realizouse un segundo pase, para asegurar que o material xerado nos cerebros, froito da inoculación dos confórmeros, estaba totalmente adaptado ao cerebro dos animais. Ao igual que no primeiro pase, todos os animais sucumbiron a unha enfermidade priónica. Neste segundo pase, estudáronse os tempos de incubación, os patróns electroforéticos, e os perfís de lesións cerebrais.

USC UNIVERSIDADE DE SANTIAGO DE COMPOSTELA

Aínda que moitos tempos de incubación se viron unificados, estas análises permitiron identificar cepas de prións que presentaban diferente afinidade polas áreas cerebrais e con patróns de resistencia a proteasa distintos. Estes resultados permitiron concluir que diferentes cepas de prións foron xeradas nas mesmas condición e en presenza do mesmo cofactor, pero por outra banda os resultados tamén indicaron que confórmeros xerados con cofactores distintos deron lugar a enfermidades con características moi similares, suxerindo que con cofactores distintos podería xerarse a mesma cepa.

En resumo, neste traballo foi posíbel estudar o efecto terapéutico de tres candidatos con potencial antipriónico e, malia que os resultados non foron os esperados en termos de eficacia, arroxaron luz sobre as limitacións que presenta cada un deles na terapia das enfermidades priónicas. Ademais, foi posíbel caracterizar por medios biolóxicos, bioquímicos e biofísicos cepas recombinantes de prións, establecendo diferenzas entre elas e redefinindo o papel dos cofactores na diversidade de cepas de prións.

USC UNIVERSIDADE DE SANTIAGO DE COMPOSTELA

List of Abbreviations

°C	Celsius degree
Å	Angstroms
%	Percentage
µg	Microgram
µL	Microliter
µM	Micromolar
λ_{ex}	Wavelength of excitation
λ_{em}	Wavelength of emission
12B2	Anti-PrP monoclonal antibody
22L	Mouse-adapted prion strain
263K	Hamster-adapted prion strain
3F10	Anti-PrP monoclonal antibody
4RβS	4-rung-β-solenoid
6C2	Anti-PrP monoclonal antibody
9A2	Anti-PrP monoclonal antibody

A

Aβ	Amyloid-β
a22L	GPI-anchorless 22L prion strain
AAV	Adeno-associated viruses
ADAM	a disintegrin and metalloproteinase
Adgrg6	Adhesion G Protein-Coupled Receptor G6
ALS	Amyotrophic lateral sclerosis
APP	Amyloid precursor protein
aRML	GPI-anchorless RML prion strain
ASA	Amyloid Seed Assay
ASO	Antisense oligonucleotide
ATM	Atomic force microscopy
AU	Arbitrary units

B

BBB	Blood-brain barrier
BSE	Bovine spongiform encephalopathy

USC UNIVERSIDADE DE SANTIAGO DE COMPOSTELA

BV	Bank vole
BVPrP	Bank vole prion protein

C

C1	C-terminal fragment generated by α-cleavage
C2	C-terminal fragment generated by β-cleavage
cAMP	Cyclic adenosine monophosphate
CB	Conversion buffer
C-BSE	Classical bovine spongiform encephalopathy
CC1	Charged cluster 1
CC2	Charged cluster 2
CD	Circular dichroism
CJD	Creutzfeldt-Jakob disease
CNS	Central nervous system
CoS	Chondroitin sulfate
CPD	Camel prion disease
Cryo-EM	Cryo-electron microscopy
CSF	Cerebrospinal fluid
CTF12/13	C-terminal fragments of 12 and 13kDa
CWD	Chronic wasting disease

D

Da	Dalton
DAPI	4 ',6-diamidino-2-fenilindol
DARR	Dipolar assisted rotational resonance
Dex	Dextran sulfate
DNA	Deoxyribonucleic acid
DNase	Deoxyribonuclease
OD_{600}	Optical density at 600nm
dpi	Days post-inoculation
Dy	Drowsy, hamster prion strain

E

E. coli	*Escherichia coli*
EEG	Electroencephalogram
ELISA	Enzyme-linked immunosorbent assay

USC UNIVERSIDADE DE SANTIAGO DE COMPOSTELA

EM	Electron microscopy
ER	Endoplasmic reticulum
ERAD	Endoplasmic-reticulum-associated protein degradation

F

FDA	Food and drug administration
Fe(III)-TMPyP	Fe(III) tetrakis(4- N-methylpyridinium)porphyrin
FFI	Fatal familial insomnia
FTIR	Fourier-transform infrared spectroscopy

G

g	Centrifuge force
gCJD	Genetic Creutzfeldt-Jakob disease
GFAP	Glial fibrillary acidic protein
Gdn	Guanidine
GPI	Glycosylphosphatidylinositol
Gpr126	G-protein coupled receptor Adgrg6
GSS	Gerstmann-Sträussler-Scheinker syndrome

H

H	Hours
H-BSE	H-type atypical bovine spongiform encephalopathy
HC	Hydrophobic core
Hep	Heparin
HR	Hydrophobic region
HRP	Horseradish peroxidase
Hu	Human
Hy	Hyper, hamster prion strain

I

i.c.	Intracerebral
iCJD	Iatrogenic Creutzfeldt-Jakob disease
i.p.	Intraperitoneal
IPTG	Isopropyl β-d-1-thiogalactopyranoside

K

USC UNIVERSIDADE DE SANTIAGO DE COMPOSTELA

kDa	Kilo Dalton
kHz	Kilohertz

L

L	Liter
LB	Luria Bertoni, bacteria growth medium
L-BSE	L-type atypical bovine spongiform encephalopathy
LCP	Luminescent conjugated polymers
LOTSS	Low Toxicity Synthetic Strain
LTP	Long-term potentiation

M

M	Molar
M7	Mouse-adapted prion strain
MBM	Meat and bone meal
MeOH	Methanol
MES	2-(N-morpholino)ethanesulfonic acid
mg	Milligram
min	Minutes
miRNA	Micro ribonucleic acid
mL	Milliliter
mM	Millimolar
Mo	Mouse
mQ	Milli-Q water
MRI	Magnetic resonance imaging
mRNA	Messenger ribonucleic acid
MS	Mass spectrometry
ms	Milliseconds
MSE	Mink spongiform encephalopathy
MW	Molecular weight
NBH	Normal brain homogenate

N

N1	N-terminal fragment generated by α-cleavage
N2	N-terminal fragment generated by β-cleavage
N3	N-terminal fragment generated by γ-cleavage

USC UNIVERSIDADE DE SANTIAGO DE COMPOSTELA

NaPTA	Sodium phosphotungstate
Ni-NTA	Nickel-nitrilotriacetic acid
NMDA	N-methyl-D-aspartate
NMR	Nuclear Magnetic Resonance
Nor98	Norway 98, atypical prion strain
ns	Nanoseconds

O

OD	Optical density
on	Overnight
OPR	Open reading frame
OR	Octarepeats

P

PBS	Phosphate-buffered saline
PERK	PKR-like endoplasmic reticulum kinase
PIRIBS	Parallel-in-register-intermolecular-β-sheets
PK	Proteinase K
PMCA	Protein misfolding cycling amplification
PMSA	Protein misfolding shaking amplification
ppm	Parts per million
PPS	Pentosan polysulfate sodium
PRND	Prion-like protein Doppel gene
PRNP	Prion protein gene
PRNT	Putative testis-specific prion protein gene
PrP27-30	Scrapie isoform of the prion protein PK treated
PrP	Prion protein
PrP^{C}	Cellular prion protein
PrP^{res}	PK-resistant PrP
PrP^{Sc}	Scrapie prion protein
PrP^{Ss}	Sslow prion protein
PVDF	Polyvinylidene difluoride

Q

q.s.	Quantum Satis

USC UNIVERSIDADE DE SANTIAGO DE COMPOSTELA

R	
recPrP	Recombinant prion protein
RML	Rocky Mountain Laboratory prion strain
RNAi	Ribonucleic acid interference
rpm	Revolutions per minute
RT	Room temperature
RT-QuIC	Real-time quaking-induced conversion
S	
s	Seconds
SAF	Scrapie associated fibrils
SAF83	Anti-PrP monoclonal antibody
SAF84	Anti-PrP monoclonal antibody
SAXS	Small Angle X-ray Scattering
scFv	Single chain variable fragment
sCJD	Sporadic Creutzfeldt-Jakob disease
SD	Standard deviation
SEM	Standard error of the mean
sFI	Sporadic fatal insomnia
siRNA	Small interfering ribonucleic acid
shRNA	Short hairpin ribonucleic acid
SMA	Spinal muscular atrophy
SPRN	Shadow of prion protein gene
SSLOW	Synthetic Strain Leading to OverWeight
ssNMR	Solid-state nuclear magnetic resonance
T	
TBS-T	Tris buffer saline - tween
TEM	Transmission electron microscopy
Tg	Transgenic
TgVole	Transgenic mice bearing bank vole PrP sequence
ThT	Thioflavin-T
TI	Thymus-independent antigens
TMB	3,3´,5,5´-tetramethylbenzidine
TSE	Transmissible spongiform encephalopathy

USC UNIVERSIDADE DE SANTIAGO DE COMPOSTELA

U

UPR	Unfolded protein response
UPS	Ubiquitin proteasome system

V

vCJD	Variant Creutzfeldt-Jakob disease
v/v	Volume/volume
VPSPr	Variably protease-sensitive prionopathy

W

w/v	Weight/Volume
WT	Wild-type

Amino acid	Three-letter abbreviation	One-letter abbreviation	Amino acid	Three-letter abbreviation	One-letter abbreviation
Alanine	Ala	A	Leucine	Leu	L
Arginine	Arg	R	Lysine	Lys	K
Asparagine	Asn	N	Methionine	Met	M
Aspartic acid	Asp	D	Phenylalanine	Phe	F
Cysteine	Cys	C	Proline	Pro	P
Glutamic acid	Glu	E	Serine	Ser	S
Glutamine	Gln	Q	Threonine	Thr	T
Glycine	Gly	G	Tryptophan	Trp	W
Histidine	His	H	Tyrosine	Tyr	Y
Isoleucine	Ile	I	Valine	Val	V

USC UNIVERSIDADE DE SANTIAGO DE COMPOSTELA

INDEX

Abstract xv
Resumen xvii
Resumo xix
List of Abbreviations xxxi
INDEX xxxix
1. GENERAL INTRODUCTION 1
1.1. Prion diseases 3
1.1.1 Human prion diseases 4
1.1.2 Animal prion diseases 12
1.2 Historical landmarks in prion research 19
1.3 Molecular bases of prion diseases 25
1.3.1 The cellular prion protein (PrP^C) 25
1.3.1.1 PrP^C structure and biosynthesis 25
1.3.1.2 Functions of the PrP^C 29
1.3.2 The scrapie prion protein (PrP^{Sc}) 34
1.3.2.1 Understanding the structure of PrP^{Sc} 34
1.3.2.2 PrP^{Sc} models 39
1.3.3 Conversion of PrP^C into PrP^{Sc} 43
1.3.4 Neurotoxicity in prion diseases 44
2. OBJECTIVES 47
3. CHAPTER I: THERAPEUTICAL POTENTIAL OF A PORPHYRIN AND A SCFV ANTIBODY FOR PRION DISEASES 51
3.1 Introduction 53
3.2 Specific aims 69
3.3 Methods 71
3.3.1 Ethical statement 71

USC UNIVERSIDADE DE SANTIAGO DE COMPOSTELA

3.3.2 Animal model and housing conditions *71*

3.3.3 Prion inoculation *72*

3.3.4 Mice treatment *73*

3.3.4.1 Chronic treatment with Fe(III)-TMPyP *73*

3.3.4.2 Therapeutic treatment with scFv-G1 ..... *74*

3.3.5 Assessment of scFv-G1 activity by ELISA *75*

3.3.6 Preparation of brain homogenates *76*

3.3.7 Proteinase K digestion and Western blot analysis. *76*

3.3.8 Histopathological and immunohistochemical analysis *77*

3.3.9 Kinetics of Fe(III)-TMPyP distribution in brain *79*

3.3.10 Statistical analysis *79*

3.4 Results 81

3.4.1 Assessment of the anti-prion activity of Fe(III)-TMPyP in a fast murine model of prion disease *81*

3.4.2 scFv-G1 antibody as a therapeutic strategy for prion diseases *84*

3.4.3 Chronic treatment with Fe(III)-TMPyP and scFv-G1 of mice challenged with lower doses of prions *89*

3.4.3.1 Fe(III)-TMPyP does not delay the prion disease in TgVole mice infected with a diluted vole-adapted CWD inoculum. *89*

3.4.3.2 Fe(III)-TMPyP does not efficiently spread throughout the brain parenchyma *92*

3.4.3.3 A therapeutic administration of scFv-G1 does not delay the clinical course of prion disease with a diluted inoculum *94*

3.4.4. A chronic intracranial treatment does not reduce the mice life expectancy *96*

3.5 Discussion 99

3.5.1 Assessment of the anti-prion activity of Fe(III)-TMPyP in a fast murine model of prion disease *99*

USC UNIVERSIDADE DE SANTIAGO DE COMPOSTELA

3.5.2 scFv-G1 antibody as a therapeutic strategy for prion diseases 103

3.6 Salient Remarks..... 111

4. CHAPTER II: A NON-PrP^{Sc} PRP PRION..... 113

4.1 Introduction 115

4.1.1 Protein folding and amyloid formation 115

4.1.2 PrP amyloids 119

4.2 Specific aims 127

4.3 Methods..... 129

4.3.1 Expression and purification of BVPrP 109I..... 129

4.3.2 PrP fibrillation and monitoring of fibril formation..... 130

4.3.3 Negative stain TEM..... 130

4.3.4 PrP amyloid digestion with PK 131

4.3.5 Animal model and housing conditions..... 131

4.3.6 TgVole mice inoculation and treatment. 131

4.3.7 Brain homogenate preparation and Western blot analysis... 132

4.3.8 Prion concentration and purification from brain homogenates 133

4.3.9 Protein deglycosylation with PNGase F..... 133

4.3.10 Histopathological and immunohistochemical analysis. 134

4.3.11 Statistical analysis 134

4.4 Results 135

4.4.1 A self-replicating full-length PrP amyloid as a therapeutic approach for prion diseases 135

4.4.2. Serial transmission of PrP^{Ss} did not entail the emergence of classical PrP^{Sc} 145

4.5 Discussion 153

USC UNIVERSIDADE DE SANTIAGO DE COMPOSTELA

4.5.1 A self-replicating full-length PrP amyloid as a therapeutic approach for prion diseases? 153

4.5.2 The recombinant PrP amyloid propagated in mice brains and caused a fatal disease 155

4.6 Salient Remarks 161

5. CHAPTER III: CHARACTERIZATION OF RECOMBINANT PRION STRAINS GENERATED BY PMSA WITH DIFFERENT COFACTORS 163

5.1 Introduction 165

5.1.1 Prion strains 165

5.1.2 Transmissibility of prion strains and transmission barriers . 170

5.1.3 Synthetic prions and in vitro propagation methods 172

5.1.4 Role of cofactors in synthetic prions 178

5.2 Specific aims 181

5.3 Methods 183

5.3.1 De novo generation of PrPSc by PMSA with different cofactors 183

5.3.2 Propagation of PrP^{Sc} by PMSA 184

5.3.3 Mice inoculation 184

5.3.4 Histopathological and immunohistochemical analyses 184

5.3.5 Western blot of recombinant PrP^{Sc} 185

5.3.6 Western blot of brain homogenates 185

5.3.6 Mass spectrometry-based analysis 185

5.3.7 Expression of recombinant PrP (109I) with uniformly labeled (^{13}C, ^{15}N) phenylalanine residues 187

5.3.8 Solid-state nuclear magnetic resonance measurements (ssNMR) 187

5.4 Results 191

5.4.1 De novo generation of diverse conformers with different polysaccharide cofactors by PMSA 191

USC UNIVERSIDADE DE SANTIAGO DE COMPOSTELA

5.4.2 Characterization of the recombinant conformers by limited proteolysis coupled to mass spectrometry 198

5.4.3 Study of the infectivity of the conformers generated by PMSA 208

5.4.4 Biochemical features of the different recombinant prion strains 211

5.4.5 Characterization of different strains generated with dextran sulfate by ssNMR 221

5.5 Discussion 225

5.5.1 Generation and characterization of different recombinant prions strains de novo generated by PMSA with different cofactors 225

5.6 Salient Remarks..... 237

6. CONCLUSIONS 239

7. REFERENCES 243

8. SUPPLEMENTARY INFORMATION 290

Annex I: Listing of materials used in this thesis..... 290

Annex II: Listing of reagents used in the present thesis 292

Annex III: Listing of buffers used in the present thesis and their composition 296

Annex IV: Listing of apparatus used in this thesis..... 298

Annex V: Listing of software used in this thesis 300

Annex VI: Bank vole PrP 23-231 109I sequence 301

Annex VII: Supplementary images 302

Annex VIII: Chromatogram and mass/charge spectra 303

Annex IX: Games-Howell's multiple comparison post hoc test of the conformers.....311

Annex X: Ethics Committee Report / Infome del Comité de Ética 319

Annex XI: Copyright permissions..... 322

USC UNIVERSIDADE DE SANTIAGO DE COMPOSTELA

USC UNIVERSIDADE DE SANTIAGO DE COMPOSTELA

1. GENERAL INTRODUCTION

USC
UNIVERSIDADE
DE SANTIAGO
DE COMPOSTELA

1.1. PRION DISEASES

Prion diseases are neurodegenerative disorders that belong to the group of protein misfolding diseases or proteinopathies, a heterogeneous group of conditions that also includes cystic fibrosis, Alzheimer's disease, type II diabetes, and several others. All these diseases are characterized by the aggregation of structurally abnormal proteins that failed in acquiring their native three-dimensional conformation or lost it, leading to the accumulation of protein aggregates in different organs and tissues that disrupt their normal functioning [1]. In the case of prion diseases, the central event in their pathogenesis is the conformational conversion of the host-encoded cellular prion protein (PrP^{C}) into its pathogenic isoform (PrP^{Sc}). This conformational rearrangement involves important changes in the biochemical and biological properties of the protein, such as the formation of insoluble proteins and partial resistance to digestion with proteases.

Prion diseases are fatal and incurable conditions that affect humans and other species of mammals consisting of an extended asymptomatic incubation period followed by a rapidly progressive disease that leads to the death of the patients in a matter of months or few years. While patients manifest various clinical signs depending on the prion disease, the predominant symptoms include motor dysfunctions, cognitive impairment, behavior abnormalities, and cerebellar ataxia. Unfortunately, these clinical presentations are not pathognomonic; quite the opposite, they are common to many other neurodegenerative disorders. This fact, added to the low incidence of these illnesses, the rapid progression of the disease, and the lack of specific biomarkers, difficult an early and accurate diagnosis. Although techniques such as electroencephalogram (EEG), magnetic resonance imaging (MRI), or cerebrospinal fluid (CSF) analysis can be helpful in the diagnosis, the

USC UNIVERSIDADE DE SANTIAGO DE COMPOSTELA

confirmation of prion disease is generally *post-mortem* after neuropathological brain examinations [2,3]. In this regard, prion diseases are also known as transmissible spongiform encephalopathies (TSE) in reference to the appearance of the brain tissue that presents multiple rounded vacuoles in the grey matter that provide a sponge-like aspect. Apart from the spongiform degeneration, other histopathological features that also characterize prion diseases are the presence of reactive gliosis involving astrocytes and microglia, neuronal loss, and accumulation of prion protein aggregates (Fig 1.1).

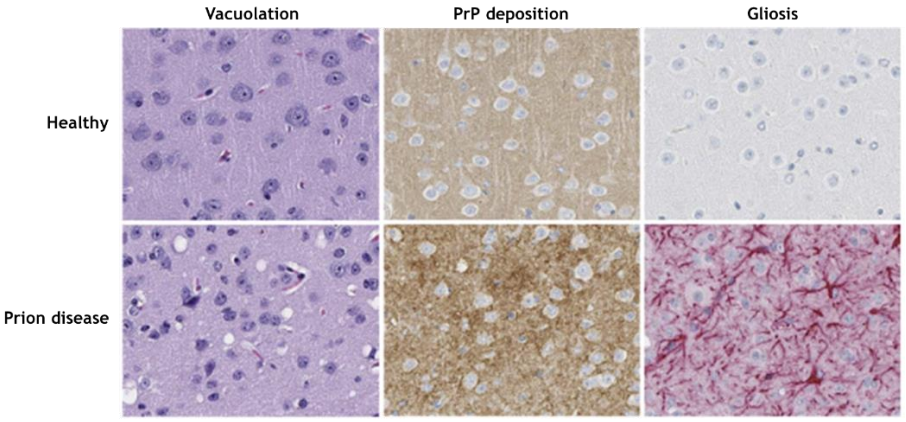


Figure 1.1 Neuropathological features of prion diseases in comparison with healthy brains. Abnormalities in the brain of affected individuals include vacuolation visible with hematoxylin-eosin staining, accumulation of prion protein deposits detectable with immunohistochemical staining with an anti-PrP antibody, and astrogliosis perceivable after staining with anti-glial fibrillary acidic protein antibody (GFAP). Adapted from Raymond et al 2019[4].

1.1.1 Human prion diseases

Human prion diseases are rare neurodegenerative conditions that affect approximately 1-2 persons per million of population worldwide and annually [5]. They comprise a heterogeneous group of diseases with different clinical presentations, molecular and histopathological

USC UNIVERSIDADE DE SANTIAGO DE COMPOSTELA

features. According to their etiology, prion diseases can be classified into three subgroups: sporadic, genetic, and acquired disorders (Table 1.1).

Sporadic prion diseases

Sporadic prion diseases are the most common subgroup of prion diseases that encompasses 85% of the cases. Sporadic prion diseases have been documented globally, displaying a random distribution and lacking any association with environmental, social, or occupational risk factors. Although the incidence varies among countries, these divergences are most likely due to limitations in the detection and reporting of the cases rather than a different distribution. The event that triggers the development of sporadic prion disease is unknown. Epidemiological studies have ruled out the hypothesis that an external exposure to the infectious agent triggered sporadic cases, and there is no evidence of spatial or temporal clustering, or a connection with outbreaks of animal prion diseases. Instead, studies suggest that sporadic cases arise from a random conversion of the protein into its pathogenic form [6].

The most common sporadic prion disease is sporadic Creutzfeldt-Jakob disease (sCJD). In Spain, the incidence of sCJD is 1,14 cases per million population and year [7], sharing a similar frequency with other European countries. The distribution of patients by gender and age reveals that the frequency in women is slightly higher than in men (1,4:1), and the mean age at the diagnosis was between 60 and 79 in both sexes [8].

USC UNIVERSIDADE DE SANTIAGO DE COMPOSTELA

Table 1.1 Classification of human prion diseases according to their etiology.

Etiology	Frequency	Prion disease	Age at onset (years)	Mean duration	Clinical features	Neuropathological features
Sporadic prion diseases	~85-90%	Sporadic Creutzfeldt-Jakob disease (sCJD)	60 (17-83)	4-6 months	Dementia, ataxia, myoclonus	Gray matter vacuolation and gliosis
		Variably protease-sensitive prionopathy (VPSPr)	65 (48-81)	1-5 years	Behavioral changes, dementia, ataxia	Cortical vacuolation and microplaques
		Sporadic fatal insomnia (sFI)	50 (36-71)	1-3 years	Rapidly progressive ataxia and cognitive decline	Thalamic and olivary severe atrophy
Genetic prion diseases	~10-15%	Genetic CJD (gCJD)	60 (20-80)	1-5 years	Dementia, ataxia, myoclonus	Gray matter vacuolation and gliosis
		Gerstmann- Sträussler-Scheinker syndrome (GSS)	20-60	3-6 years	Ataxia, late dementia and parkinsonism	PrP plaques, gliosis and vacuolation
		Fatal familial insomnia (FFI)	35-55	1 year	Insomnia, dysautonomia, ataxia, dementia	Thalamic and olivary gliosis
Acquired prion diseases	<1%	Kuru	40 (4-60)	3-12 months	Tremor, ataxia, pyramidal and extrapyramidal dysfunctions	Kuru plaques
		Variant CJD (vCJD)	28 (20-60)	18 months	Behavioral changes, late dementia	Florid plaques and diffuse spongiosis
		Iatrogenic CJD (iCJD)	1-30 years after exposure	<1 year	Cerebellar ataxia	Florid plaques and diffuse spongiosis

sCJD exhibits a wide range of clinical manifestations: dementia, ataxia, myoclonic involuntary movements, language disorders, visual impairments, behavioral changes, or spasticity, for instance[6]. Moreover, it also displays various molecular and histological features, such as the electrophoretic pattern of PrP resistant to digestion with the protease proteinase K (PK), or the brain lesion profile. The clinical symptoms, life expectancy, and molecular properties strongly correlate with the polymorphic variations of the prion protein gene (PRNP) [9], to the point that sCJD has been categorized according to amino acid present at codon 129 and their molecular features. Therefore, six subtypes of sCJD exist based on the presence of methionine, valine or both, in case of heterozygous: MM1, MV1, VV2, MV2, MM2-C, VV1, and MM2-T, this last subtype is also known as sporadic fatal insomnia (sFI) due to the main clinical sign is the difficulty to fall asleep or stay asleep, resulting in severe sleep deprivation[2,3].

In 2008, a new prion disease was described, termed variably protease-sensitive prionopathy (VPSPr) [10,11], and due to its lack of association with mutations in the PRNP gene, it was classified as a sporadic prion disease. The progression of this disease is slightly slower than sCJD (>2 years), and the most common clinical signs are cerebellar ataxia, movement disorders, cognitive impairments, or extrapyramidal symptoms. Neuropathological examinations show spongiform degeneration and PrP amyloid plaques. However, the most remarkable feature of this disorder, which gives this disease its name, is the high sensitivity of the misfolded form of the prion protein to digestion with PK, which is reflected as a characteristic multiple-band pattern upon immunoblotting [12].

Genetic prion diseases

While the majority of prion diseases are idiopathic approximately 10-15% of the cases are linked to a mutation in the PRNP sequence and are referred to as genetic prion diseases. Genetic prion disorders are autosomal-dominant diseases with high penetrance, meaning that

USC UNIVERSIDADE DE SANTIAGO DE COMPOSTELA

carriers of mutations associated with genetic prion diseases almost certainly will develop the condition in their lifetime. These mutations could be point mutations in the PRNP sequence, insertions and deletions in the region of the octapeptide repeats, or nonsense mutations[13] (Fig 1.2).

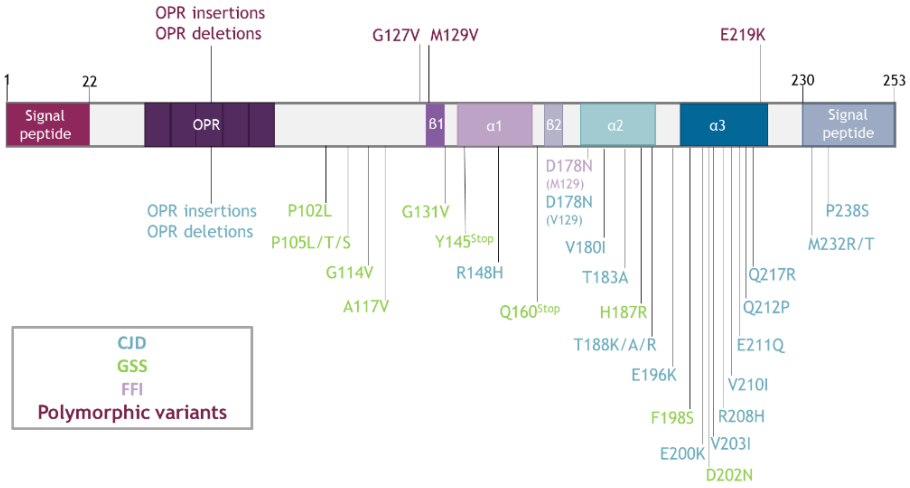


Figure 1.2 Schematic representation of the prion protein gene and the most relevant polymorphisms and disease-associated mutations. The polymorphic variants are above the gene schematic colored in red; mutations responsible for prion diseases are below the gene schematic and colored in blue, green, or lilac according to the condition that they trigger: gCJD, GSS, and FFI, respectively[14].

Unlike sporadic diseases, which exhibit a homogeneous worldwide incidence, genetic prion diseases have an irregular geographical distribution and frequency since they have been transmitted in regional clusters[15]; for instance: the E200K mutation is common in Slovakia and Israel, mostly in people of Libyan origin [16–18]; the V180I substitution is common in Japan; the V210I is localized in Italy [19]; and the F198S mutation is commonly found in Indiana and is known as Indiana

USC UNIVERSIDADE DE SANTIAGO DE COMPOSTELA

kindred variant of Gerstmann–Sträussler–Scheinker (GSS) syndrome [20]. Depending on the mutation and the polymorphism at codon 129, genetic prion diseases can display different phenotypes and are classified into three subtypes: genetic CJD (gCJD), GSS syndrome, and fatal familial insomnia (FFI).

gCJD can be caused by a large number of mutations in the PRNP gene: over 40 pathogenic mutations have been described, so far. The clinical and pathological features are comparable to those found in patients with sCJD, although the age at onset is usually younger and the disease duration slightly longer [13]. On the other hand, GSS syndrome was first reported in an Austrian family in 1936. It is characterized by chronic progressive cerebellar ataxia, terminal dementia, and parkinsonism, and extended clinical duration compared to other prion diseases (3-10 years) [14].

FFI is caused by a mutation at codon 178, where an aspartic acid is substituted by an asparagine, and is accompanied by methionine at the polymorphic codon 129. As the name suggests, FFI is characterized by severe sleep disturbances as a result of a thalamic affectation; nonetheless, this is not the only symptom that patients develop, and pyramidal signs, dysautonomia, and motor dysfunction are also common[21,22].

Acquired prion diseases

Acquired prion diseases are caused by exogenous exposure to prions, which could be present in food, surgical material, or biological samples. Although this subgroup is the less common (<1%), it is probably the most famous among the population due to the social, historical, and economic implications they had. This subgroup involves three prion diseases: Kuru, variant CJD (vCJD), and iatrogenic CJD (iCJD).

Kuru is an eradicated prion disease; however, it deserves a space in this introduction since it provided the first evidence that human prion diseases could be transmitted between individuals. Kuru was a

USC UNIVERSIDADE DE SANTIAGO DE COMPOSTELA

neurological disorder endemic in the Fore tribe of Papua New Guinea, reported and studied by Gajdusek and Zigas in the 1950s [23]. In the Fore language, *kuru* means "to tremble" since people that developed this disease presented tremors, ataxia, and other motor dysfunctions. The transmission of kuru was due to rituals of endocannibalism, an extended cultural mourning practice. Specifically, during funeral rituals, it was a tradition for the Fore people to consume organs and tissues of the deceased, especially by women and children, who in turn were the members of the tribe most affected by kuru, while men rarely participated in these practices [24]. Gadjusek and colleagues demonstrated the transmission of kuru to human and nonhuman primates, which was the first evidence that human spongiform encephalopathies were infectious diseases[25,26]. These demonstrations led to Gajdusek's Nobel Prize in 1976. Even though the origin of Kuru remains unknown, it has been suggested that it commenced with a member who died of sCJD and whose brain was consumed by relatives. This hypothesis is supported by works that studied the transmissibility and biochemical similarities between kuru and sCJD-infected mice. Apart from similar incubation periods or electrophoretic patterns, both diseases display a neuropathological key feature that consists of an amyloid plaque with an eosinophilic core and radially orientated fibrils that accumulate in the cerebellum, termed florid plaques [27].

Another acquired prion disease, which is probably the most famous human prion disease, is vCJD. vCJD is associated with the consumption of meat from cattle affected by bovine spongiform encephalopathy [28,29]. vCJD was first reported in the United Kingdom in 1996 and later in other European (France, Spain, Ireland, Netherlands, Italy, or Portugal) and non-European countries (United States, Canada, Saudi Arabia, Japan, China, or Taiwan). Although only 232 cases had been reported until July 2021 [30], the occurrence of this zoonotic disease presented a major public health concern because of its extended incubation period and the potential exposure of a significant portion of the population to the infectious agent. Fortunately, the peak of cases was in 2000, and

USC UNIVERSIDADE DE SANTIAGO DE COMPOSTELA

from 2006, cases decreased drastically [5]. More than 90% of cases of vCJD patients were homozygous for methionine at codon 129; however, since the incubation period strongly depends on the PRNP genotype, there is still the possibility of further cases in heterozygous in codon 129 that were in contact with contaminated meat during the outbreak of BSE, and for which the incubation period would be much more extended [6].

While the oral route is implicated in cases of kuru and vCJD, it is important to note that human prion diseases can also be transmitted iatrogenically, through the contact with infected human tissues or contaminated surgical materials. This fact became evident when individuals who had received human-derived grafts or hormones, or underwent surgical procedures, subsequently developed CJD. The first case of iatrogenic Creutzfeldt-Jakob disease (iCJD) was reported in 1974 [31]; nevertheless, some suspicious cases were mentioned even years before [32]. The majority of iCJD cases are associated with dura mater grafts and growth hormone treatments. Additionally, there have been documented iCJD transmission through gonadotropin administration, corneal transplants, and even red blood cell transfusions. It must be mentioned that prions are highly resistant to standard sterilization and decontamination procedures, remaining in surgical materials. Notably, two cases of iCJD have been linked to the use of electrodes for intracerebral EEG that had previously been employed in a patient later diagnosed with CJD [33]. Most of the iCJD cases are thought to be due to biological samples from sCJD patients; nevertheless, it is known that the cases of iCJD transmitted through transfusion of blood components were donated by vCJD patients [34]. Fortunately, the implementation of rigorous decontamination methods and the development of recombinant hormones dramatically reduced the occurrence of iCJD.

Epidemiological studies carried out in historical samples of tonsils and appendices donated before[35], during [36,37], and after the outbreak of BSE in the United Kingdom detected the accumulation of PK-resistant prion

USC UNIVERSIDADE DE SANTIAGO DE COMPOSTELA

protein in lymphoid tissues of donors belonging to all groups. That meant that prions were present regardless of whether the samples were collectec from people who may have been exposed or not. Importantly, these works estimated that the prevalence of prion accumulation was 1 in 4000, raising two concerns. Firstly, the exposure to BSE-contaminated food may have occurred before 1970 and continued after 1996, which is a more extended period than previously estimated, since samples of patients who lived before the outbreak of BSE or after controlling of the epidemic of BSE, also presented accumulation of PK-resistant prion protein in their lymphoid tissues. Secondly, in case the accumulation of abnormal prion protein is independent of the exposure to contaminated food, in an important proportion of the population there is a low background of PrP deposition in lymphoid tissues that can progress or not to vCJD [5]. In any case, the potential risks of the presence of abnormal prion protein deposits in human tissues require adequate surveillance programs, effective decontamination methods, and measures to prevent occupational hazards.

1.1.2 Animal prion diseases

The connection between humans and animals started more than 16.000 years ago with the domestication of dogs. During the Neolithic period, agriculture and livestock flourished, leading to the domestication of other animal species, including sheep, goats, and cattle. Animals have been used for centuries as sources of meat, milk, wool, and leather, as beasts of burden, pets, and more recently as animals of rescue, assistance, or therapy. Thus, the connection between humans and animals has many economical, socio-cultural, and health implications. In this regard, the close interaction between humans and animals led to the transmission of animal diseases to humans, known as zoonoses. In fact, 60% of human pathogens are considered to have a zoonotic origin, and most animal diseases involve a zoonotic risk for human beings [38].

USC UNIVERSIDADE DE SANTIAGO DE COMPOSTELA

Prion diseases affect both wild and domestic mammals. For decades, the zoonotic potential of animal prion diseases was considered negligible since a transmission barrier phenomenon seemed to limit the propagation between different species; however, in 1996, the emergence of vCJD was associated with the outbreak of BSE in cattle, demonstrating the zoonotic potential and triggering a public health crisis in Europe.

Scrapie

Scrapie is a prion disease that naturally affects sheep. The first report od scrapie dates from the year 1732, when infected Spanish merino sheep were imported to the United Kingdom causing some outbreaks. Nowadays, scrapie is endemic in several countries worldwide. Even though sheep and goats can present a large variety of phenotypes, such as trembling, pruritus, incoordination of gait, behavioral changes, or weight loss. Prions have been found in saliva, milk, blood, and soil where sick animals used to graze, suggesting both vertical and horizontal transmission of the disease. In 1998, a new type of scrapie was found in Norway, called Nor98[39], which differed from the classical cases in the deposition of abnormal PrP in the brain[40]. Nor-98 was the first case of a subgroup termed atypical scrapie. Atypical scrapie was suggested to have a sporadic origin since it occurred in old animals and with low incidence; nonetheless, further studies demonstrated that atypical scrapie could also be horizontally transmissible. The emergence of scrapie cases in flocks causes severe economic losses; thus, many efforts have been made to eradicate or, at least, reduce the incidence of the disease. In this regard, as well as human prion diseases, the susceptibility to scrapie is highly linked to the PRNP background; for instance: atypical scrapie is more common in $A_{136}R_{154}R_{171}$ and $A_{136}H_{154}R_{171}$ genotypes, whereas classical scrapie is more common in $V_{136}R_{154}Q_{171}$ genotype [41]. Therefore, selective breeding strategies have arisen in order to select polymorphic variations that show resistance to prion diseases [42]. Despite the fact that no cases of transmission of scrapie to humans through the consumption of products of ovine origin

USC UNIVERSIDADE DE SANTIAGO DE COMPOSTELA

have been reported to date, some studies carried out in humanized transgenic mice and non-human primates have demonstrated a zoonotic potential [43].

Bovine spongiform encephalopathy

In 1986 a new prion disease that affected cattle emerged, commonly known as *mad cow disease* [44]. Bovine spongiform encephalopathy (BSE) spread to 28 countries and soon became an epidemic. In the United Kingdom, the most affected country, around 4,4 million animals were culled to contain the spread of the disease; of those, roughly 180.000 were infected. The economic impact resulted in losses of £4 billion [45], and, despite the efforts, it has been estimated that over 1 million BSE-infected animals could have entered the human food chain [43]. The clinical signs of those animals affected with BSE were cachexia, ataxia, behavioral changes, lethargy, and hyperreactivity. The origin of BSE remains unknown; however, since the ban on the use of meat and bone meal (MBM) to feed livestock in 1988 resulted in a drastic decline in BSE cases, the most likely explanation is that the MBM used to feed livestock was contaminated with prions[46] and the disease was transmitted orally to cattle. Moreover, three hypotheses about the provenance of the contaminated MBM were formulated. The first hypothesis proposed that the contamination may have come from sheep infected with atypical scrapie, as indicated by the biochemical similarities observed when Nor98 is transmitted to bovine transgenic mice [47,48]. The second explanation suggests that MBM could be contaminated with remains of animals with subclinical sporadic or genetic bovine spongiform encephalopathy [49,50]. Lastly, the third theory proposed that MBM could contain human remains infected with CJD [51].

The outbreak of BSE was responsible for the emergence of vCJD (Fig 1.3); additionally, BSE was also transmitted to other animals fed with contaminated meat, such as domestic cats and some zoological ruminants, ungulates, felines, and non-human primates [52]. Moreover,

USC UNIVERSIDADE DE SANTIAGO DE COMPOSTELA

BSE has also been transmitted experimentally to hamsters, mice, minks, sheep, goats, and pigs, demonstrating that BSE has a high capacity to cross the species barrier [42]. The active surveillance to detect BSE cases found out atypical BSE variants, namely H-BSE or L-BSE, according to their biochemical properties [53,54]. Since atypical BSE variants have a low incidence and mostly affect old animals, it was suggested that they may consist of sporadic cases; however, the zoonotic risk and the potential transmission of these atypical variants have been demonstrated experimentally and were proposed as the origin of the BSE epidemic [55–58].

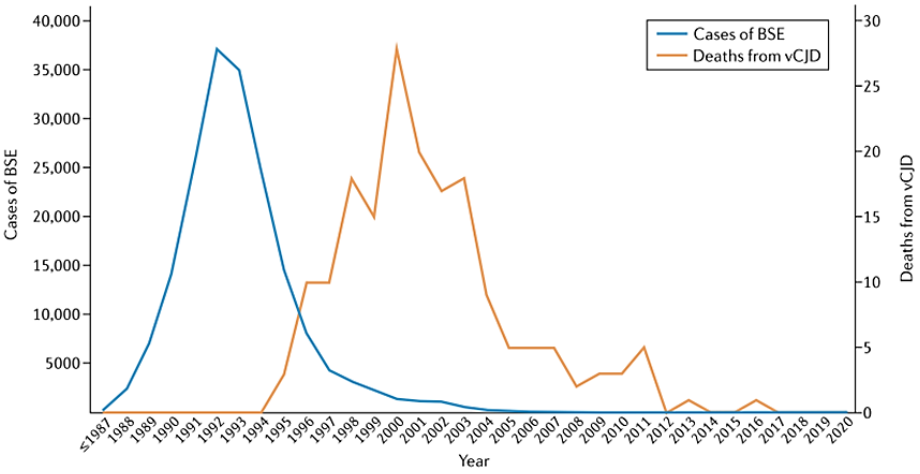


Figure 1.3 Comparison between BSE and vCJD cases. The graph represents the reported cases of bovine spongiform encephalopathy and the subsequent emergence of variant Creutzfeldt-Jakob disease in the United Kingdom. Graph available in Watson et al 2021[5].

Chronic wasting disease

Chronic wasting disease (CWD) is a prion disease that affects free-ranging and captive cervids. It was first reported in 1967, in Colorado,

USC UNIVERSIDADE DE SANTIAGO DE COMPOSTELA

and in a few years, it had rapidly spread in North America promoted by natural migrations of free-ranging populations and commercial exports. Furthermore, some cases have been reported in South Korea due to animal importations from Canada. Recently, in 2016, CWD was also identified in wild reindeer and moose in Norway, followed by the detection of more cases in a semi-isolated reindeer population in the region of Nordfjella. In an attempt to control the spread of cases in this area, the Norwegian authorities took the drastic decision to cull this reindeer population and test them for CWD, finding 18 positive cases out of 2400 samples. Currently, CWD cases have also been reported in Sweden and Finland (Fig 1.4) [59].

CWD affects different species of cervids, such as deer, reindeer, elk, and moose, among others, and sick animals are popularly called *zombie deers* because of the clinical signs that they present, characterized by cachexia, excessive salivation, behavioral changes such as loss of fear to humans, dropping ears and lowered head. CWD is highly contagious among individuals[60]; prion infectivity was found in saliva[61], urine[62], feces[63], and placenta, confirming vertical and horizontal transmission. Likewise, prions have been detected in grazing areas, soil[64], and water[65], raising concern about significant environmental contamination and the risk of transmission among individuals [66]. Moreover, the high prevalence of CWD in some states of the U.S. is a major cause for concern, particularly in Wyoming, where the population of mule deer is facing significant declines as a result of this prion disease[67] .

While no natural transmission to other species or humans has been reported to date, experimental studies have successfully transmitted CWD to various animal species that cohabitate with cervids or act as scavengers, such as cattle, sheep, goats, ferrets, minks, raccoons, mice, and non-human primates as well [68], supporting the potential zoonotic risk and a possible cross-species transmission.

USC UNIVERSIDADE DE SANTIAGO DE COMPOSTELA

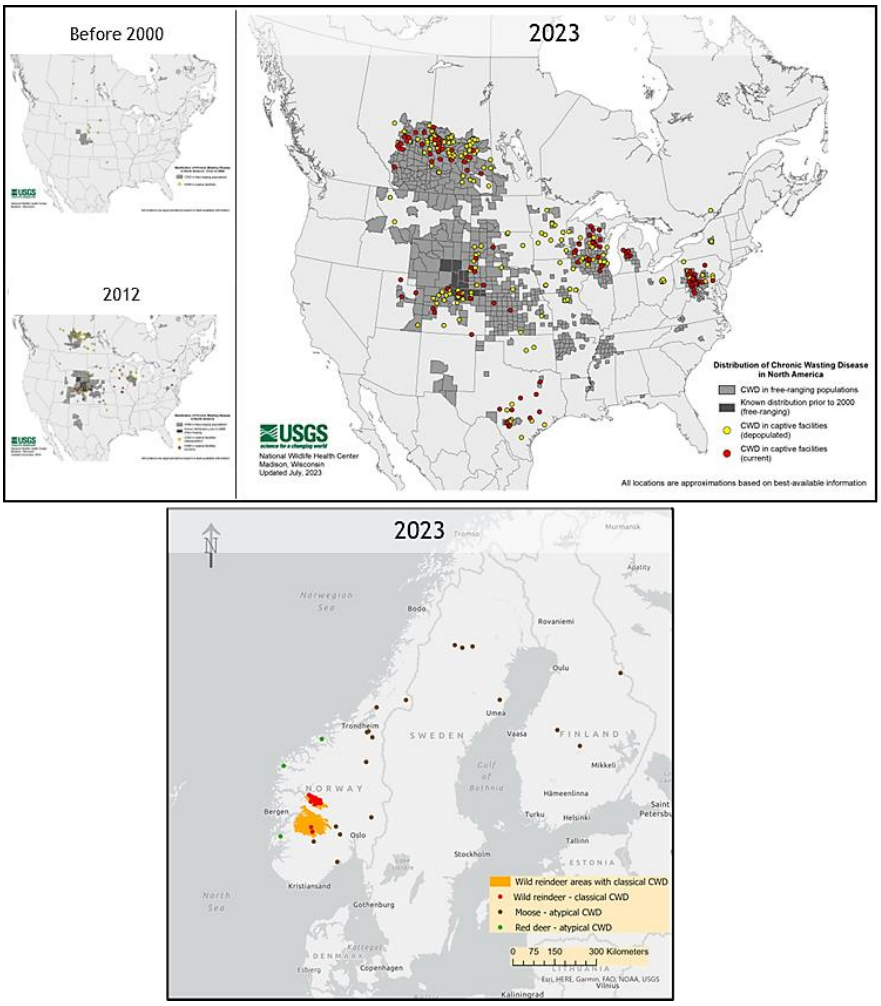


Figure 1.4. Cases of CWD in North America and Northern Europe. Maps of CWD distribution in North America (left panel) and the Nordic countries (right panel). Maps of public domain obtained from the National Wildlife Health Center (available on https://www.usgs.gov/centers/nwhc/science/expanding-distribution-chronic-wasting-disease) and the Norwegian Institute for Nature Research (available on https://www.hjortevilt.no/skrantesjuke-cwd/cwd-in-norway-english/), respectively.

USC UNIVERSIDADE DE SANTIAGO DE COMPOSTELA

Mink spongiform encephalopathy

Mink spongiform encephalopathy (MSE) was first detected in 1947 in farmed minks for fur in Wisconsin and Minnesota. Subsequently, more cases were reported in Canada, Germany, or Finland, always in captive animals [69]. Although the origin of MSE is unknown, it was most likely transmitted by scrapie-contaminated feed since simultaneous outbreaks occurred in different farms sharing the same feed supplier [70]. Infected animals display behavioral changes like aggressiveness, compulsive biting, or depression, and also motor impairments such as ataxia, incoordination, and hindlimb weakness [52], and horizontal transmission is the most plausible spreading route among individuals. While MSE did not hold as much socioeconomic impact as BSE or CWD, it provided significant contributions to prion research. After transmission of MSE to hamsters, two prion variants were isolated, which triggered different clinical signs, biochemical properties, and neuropathological features. These two variants, called "hyper"(Hy) and "drowsy" (Dy), have been extensively studied and characterized, contributing to the understanding of the diversity and complexity of prion strains.

Camel prion disease

In 2018, camel prion disease (CPD) was identified in three individuals of dromedary camel in Algeria, and one year later, some cases were also reported in Tunisia, increasing concern about a possible epizootic and zoonotic risk that this disease could entail [71,72]. It should be noted that in some countries in Africa and the Middle East, camels are an essential source of meat, milk, and leather. Likewise, they are also used for the transportation of both people and goods, and they are used for leisure, such as dromedary races. As a result, camels hold important economic value for the local population.

CPD was detected in young and old animals, suggesting both horizontal and vertical transmission. Nonetheless, the origin remains unknown, and a cross-species transmission seems unlikely since neither scrapie nor BSE cases have been reported in these areas [5].

USC UNIVERSIDADE DE SANTIAGO DE COMPOSTELA

1.2 HISTORICAL LANDMARKS IN PRION RESEARCH

Prion diseases have over 300 years of history. Despite numerous progresses in deciphering the infectious agent, especially in recent decades, many details still need to be unveiled.

For centuries, a neurological disorder was known to affect sheep. The earliest written documentation of scrapie date back to 1732 and consisted of a request to the United Kingdom Parliament urging the regulation of the entry of sheep into the country after some farmers reported outbreaks originating from imported livestock. At that time, various causes were attributed to it, from parasites to viruses, thunderstorms or hereditary diseases [24].

It was in the 1930s when Cuille and Chelle demonstrated the infectious nature of the disease, transmitting scrapie experimentally to healthy sheep and goats and suggesting that the infectious agent should be a filterable virus[73]. Simultaneously and serendipitously, Gordon conducted an experiment that supported Cuille and Chelle's evidence. Between 1931 and 1934, Gordon was developing a vaccine for the looping-ill disease; for this purpose, he inoculated some sheep intracranially with the looping-ill virus. To prepare the vaccines, he obtained the infected animals' brains, spinal cords, and spleens and mixed these tissues with 0.35% formalin to inactivate the virus and subsequently, he immunized sheep with these preparations. Years later, the vaccine was demonstrated to be effective against the looping-ill virus, but, unexpectedly, immunized animals developed scrapie. This fact evidenced that scrapie was transmissible between individuals and, most importantly, the infectious agent was resistant to formalin [74].

On the other side of the world, in Papua New Guinea, another neurodegenerative disease was emerging [75]. In 1950, Vincent Zigas, an Estonian doctor, moved to Papua New Guinea where he worked as a medical officer. Soon after arriving, he heard about a unique unreported disorder affecting people in the Fore tribe. Along with Carleton Gajdusek, an American physician, thoroughly studied the disease named kuru[23]. Despite the extensive clinical description and *post-*

USC UNIVERSIDADE DE SANTIAGO DE COMPOSTELA

mortem findings, Gajdusek and Zigas did not identify the etiological agent; hence, they proposed that the disease might be hereditary or caused by a toxic sustance. Later, Igor Klazto, a Russian neuropathologist, joined Gajdusek and Zigas in describing the neuropathological findings in the brains of kuru-affected patients[76]. During those examinations, Klazto noted some similarities with another neurological disorder reported a few years earlier, in 1920 and 1921, by two German neuropathologists, Alfons Maria Jakob and Hans Gerhardt Creutzfeldt [34], who independently reported cases of patients with motor impairments and progressive dementia associated with neuronal degeneration. In 1959, Klazto participated in a convention in London where he presented kuru-affected brain micrographs. It was in this meeting where William Hadlow, a veterinary pathologist, recognized histopathological analogies between kuru and scrapie[77]. Thus, the intricate puzzle linking kuru, scrapie, and CJD gradually came together.

During the following years, significant advances were made in the experimental transmission of these disorders, demonstrating that they consisted of infectious diseases and evidencing the existence of different variants, termed strains, responsible for various clinical and neuropathological features. In this regard, Gajdusek and Gibbs proved the transmission of kuru and CJD to human and non-human primates [25,26,78], Pattison and Millson transmitted scrapie to goats [79], and Chandler transmitted scrapie to mice [80]. The demonstration that kuru was an infectious disease led Gajdusek to win the Nobel Prize in 1976. At that point, the most accepted hypothesis was that slow viruses caused spongiform encephalopathies; however, unsuccessful attempts to isolate the infectious agent, its minute size[81], and certain resemblances to the protein known to induce allergic encephalomyelitis [82] raised doubts about the viral origin of the scrapie agent. To determine the size of the scrapie agent, Alper and colleagues irradiated samples with ionizing radiation and ultraviolet light. According to their results, they proposed that the scrapie agent may lack nucleic acids given its high resistance to radiation and small size [83]. Regarding these findings, a

USC UNIVERSIDADE DE SANTIAGO DE COMPOSTELA

mathematician called Griffith proposed the breakthrough idea that proteins could self-replicate, and presented three models based on mathematical equations to explain how proteins could propagate themselves without the involvement of nucleic acids. One of the models explained that a distinct structural version of the same protein could self-template, propagating its conformation to native proteins in thermodynamically feasible ways[84]. This model laid the foundations of the "protein-only hypothesis", a controversial theory that proposed that proteins could propagate their conformation. Although this hypothesis went unnoticed at the time, years later it would be the key to understanding the propagation of prions[85].

In 1980, Cho determined that a protein component was required for scrapie infectivity [86], and in 1982, Prusiner, Bolton, and McKinley extracted a protein from scrapie-infected hamster brains that was not present in healthy animals [87,88]. Such protein was highly hydrophobic, presented an elevated resistance to proteolytic digestion with PK, was resistant to inactivation with non-denaturing detergents, and had a molecular weight of 27-30kDa.

Based on these findings, Prusiner enunciated the prion concept, which postulated that the causative agent of prion disease lacked nucleic acids and consisted of proteinaceous infectious particles, termed prions[89]. The identification of the causal agent of prion diseases was the first support for the protein-only hypothesis and opened a new paradigm for comprehending not only prion diseases, but also other neurodegenerative disorders, and challenged the previous understandings of the protein biology.

Prusiner would win the Nobel Prize in Physiology or Medicine in 1997 for his enunciation of the prion concept. Later on, the term prion would be used not only to designate the infectious agent of TSE, but also to refer to other self-propagating proteins, such as the fungal and yeast proteins HET-s, or URE3, among others [90].

Prion purification led to the identification and cloning of the encoding gene for the prion protein, the PRNP gene. The PRNP gene encodes

USC UNIVERSIDADE DE SANTIAGO DE COMPOSTELA

both isoforms of the prion protein, the cellular prion protein, and the scrapie isoform [91,92]. Additionally, the documentation of the prion protein gene also permitted the identification of prion diseases linked to mutations in this gene [93] or the development of transgenic mice. Almost in parallel with these discoveries, the outbreak of BSE emerged in the United Kingdom [44].

Another remarkable finding that resulted from the identification of the PRNP gene was that the ablation of this gene prevented the acquisition of prion diseases. Büeler and Weissmann developed transgenic mice lacking PRNP and demonstrated that these animals did not succumb to prion disease, not even presented a subclinical prion replication; in addition, heterozygous animals with a lower expression of PrP showed longer periods of incubation [94–97]. This crucial role of the prion protein in developing prion diseases was the last piece of evidence confirming the protein-only hypothesis. Moreover, the cellular prion protein was established as a potential therapeutic target for treating prion disorders.

Once the causal agent and the involvement of the prion protein in prion disease were discovered, efforts shifted toward studying the disparities between the two isoforms and the triggers that led to their conversion.

In this regard, Kocisko and colleagues developed the first method of prion propagation *in vitro* using cell extracts and partially purified prions, called cell-free conversion assay [98]; this method was later substituted for more efficient techniques for prion detection or amplification, such as the protein misfolding cyclic amplification (PMCA) [99], real-time quaking-induced conversion (RT-QuIC)[100], or protein misfolding shaking amplification (PMSA)[101]. These techniques have not only contributed greatly to the understanding of the propagation process, but have also been useful in studying species barrier phenomena, as diagnostic tools, and in structural studies. Moreover, assays for therapeutic candidates have also benefited from these methods, which will be described in detail below.

USC UNIVERSIDADE DE SANTIAGO DE COMPOSTELA

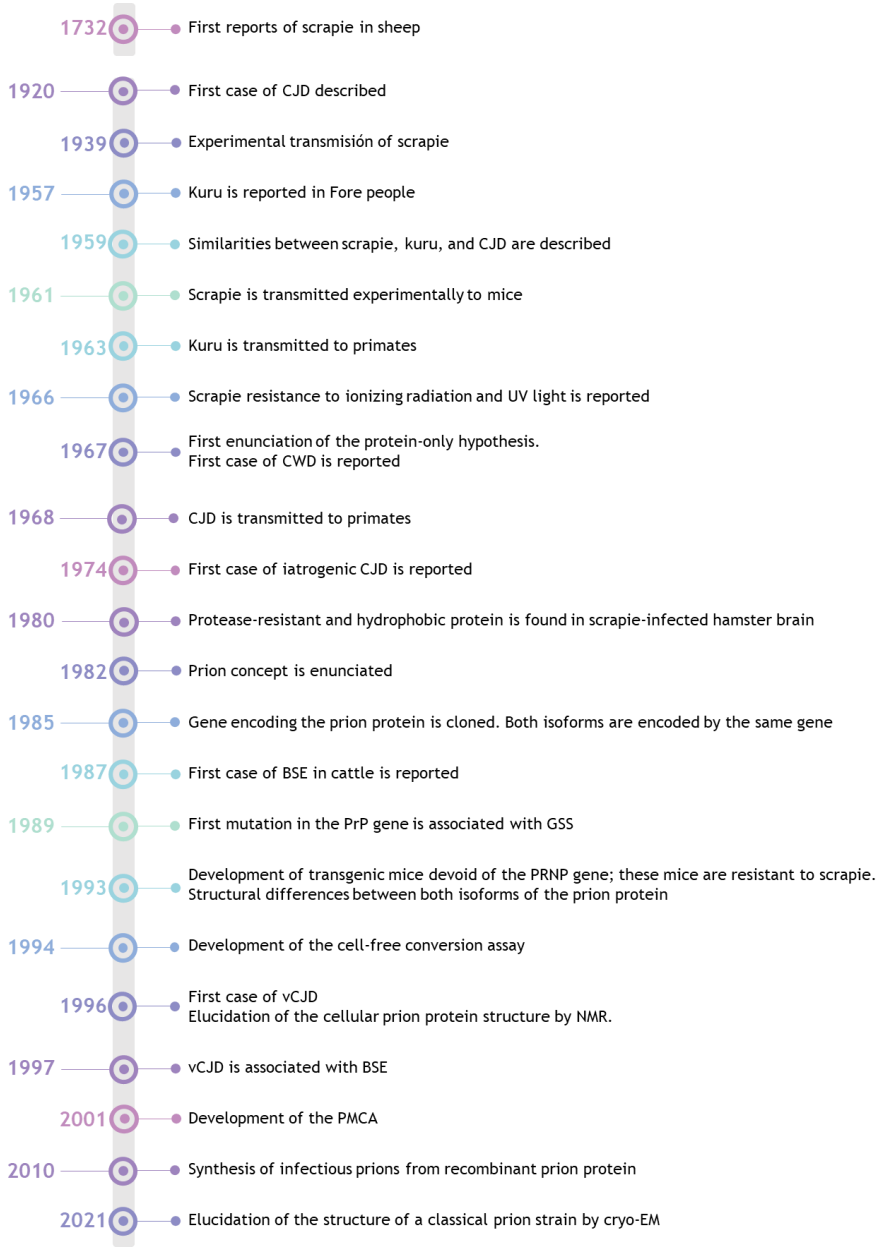


Figure 1.5 Timeline summarizing the historical hallmarks in the prions field. Image created with BioRender.

USC UNIVERSIDADE DE SANTIAGO DE COMPOSTELA

In 1996, the structure of the cellular prion protein was elucidated at the atomic level by nuclear magnetic resonance spectroscopy (NMR) [102] by Riek and colleagues under the direction of Wüthrich, and later by X-ray crystallography by Knaus and colleagues [103]. These studies showed that the cellular prion protein was a globular protein that consisted of an unstructured amino-proximal tail, three α-helices, and two antiparallel β-sheet. The development of NMR for studying macromolecules such as proteins would lead Wüthrich to win the Nobel Prize in chemistry in 2002.

The globular structure of the cellular prion protein contrasted with the images of scrapie-associated fibrils (SAF) obtained by negative-stain transmission electron microscopy purified from infected rodents and CJD patients. These fibrils resembled those present in Alzheimer's disease [104,105] and, according to the data obtained by biophysical methods, such as Fourier transform infrared (FTIR) and circular dichroism spectroscopy, presented a high content on β-sheet [106,107].

During the 2000s, significant efforts were directed toward four areas related to prion research. These areas include understanding the function of the cellular prion protein, developing therapies against prion diseases, propagating and generating infectious prion *in vitro*, and elucidating the prion structure. Although more details on these topics will be provided later, it should be noted that, despite being linked with different physiological processes, the function of the prion protein remains incompletely understood; additionally, no effective treatment, cure, or vaccine has been developed so far for prion diseases.

In 2010, Ma and colleagues were the first to synthesize infectious prions generated from recombinant prion protein without any external prion seed by PMCA [108]. But overall, the greatest breakthrough in the field of prions in the last decades was elucidating the prion structure (Fig 1.5). The prion architecture has been extensively characterized for years by diverse methods, such as FTIR, CD spectroscopy, hydrogen/deuterium exchange, limited proteolysis, electron crystallography, or cryogenic electron microscopy [109]; however, the prion conformation was not fully

USC UNIVERSIDADE DE SANTIAGO DE COMPOSTELA

elucidated until 2021, when Kraus and colleagues solved the structure of an *ex vivo* prion strain by cryo-electron microscopy (cryo-EM)[110], demonstrating that classical prions consist of a Parallel-In-Register- β-Sheet (PIRIBS) amyloid.

1.3 MOLECULAR BASES OF PRION DISEASES

1.3.1 The cellular prion protein (PrP^C)

1.3.1.1 PrP^C structure and biosynthesis

PrP^C is a cell surface glycoprotein constitutively expressed in several tissues (Fig 1.6)[111]. PrP^C is encoded by the PRNP gene, located on the short arm of chromosome 20 in humans, and consists of three exons, although the open reading frame (ORF) lies in the third exon[112–114]. PrP^C is highly conserved among mammalian species[115]; additionally, ortholog proteins were also described in avians[116], amphibians, and reptiles[117]. PRNP also has three homolog genes, called PRND, PRNT, and SPRN, which encode Doppel, prion protein testis-specific, and Shadoo, respectively[118]. Although these proteins share structural similarities with PrP^C, there is no evidence of their implication in prion diseases.

PrP mRNA is expressed early in the embryogenesis in the neural tube in mice, and, in adulthood, it is expressed mainly in cells of the nervous system, gastrointestinal tissue, muscle, skin, uterus, and testis. However, the highest abundance of the protein is found in cells of the central and peripheral nervous system[119,120]. The unprocessed human PrP is 253 amino acids in length, whereas the mature protein is composed of 209 residues. The immature protein consists of the following motifs: a signal peptide (1-22), one nonapeptide and four octapeptide repeats (OR) (51-91) flanked by two positively charged regions, CC1 (23-27) and CC2 (95-110); a highly conserved hydrophobic region (HR) (113-135), one disulfide bridge between two

USC UNIVERSIDADE DE SANTIAGO DE COMPOSTELA

cysteine residues at positions 179 and 214, two N-linked glycosylation sites at asparagines 181 and 197; and a C-terminal signal peptide (232-253) which is substituted by a glycophosphatidylinositol-anchor (GPI) [111,121].

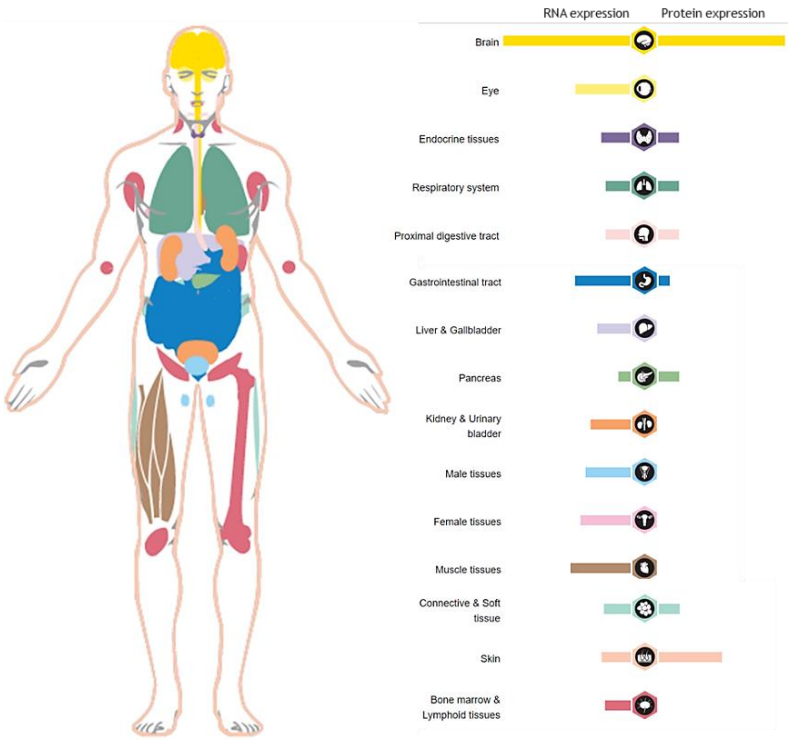


Figure 1.6. RNA and protein expression levels of the prion protein in human tissues. Data from Human Protein Atlas, image available in https://www.proteinatlas.org/ENSG00000171867-PRNP/tissue

As well as other secreted proteins, PrP is synthesized in the endoplasmic reticulum (ER). The N-terminal signal peptide guides the prion protein to the ER, where it is recognized and bound by the signal-recognizing particles (SRP). Then, the protein is translocated into the ER lumen, and the signal peptide is cleaved. In the ER lumen, the

USC UNIVERSIDADE DE SANTIAGO DE COMPOSTELA

immature PrP is subjected to various post-translational modifications; for instance: multimeric transamidases preassembled the GPI anchor, the disulfide bond is formed between both cysteines, and the N-linked oligosaccharides chains are added to the asparagines. Subsequently, the protein is trafficked to the Golgi, where the GPI and N-linked sugars are modified into more complex and longer glycans, rich in sialic acid. After maturation, PrP^C is transported to the cell surface, where it is attached by the GPI-anchor to detergent-resistant raft domains rich in sphingolipids, cholesterol, other GPI-anchored proteins, and protein tyrosine kinases [122].

The average half-life of PrP^C in the cell surface is over 5h; after this time, PrP^C can be internalized by two different endocytosis routes: clathrin-dependent and clathrin-independent pathways [123], such as caveolae-mediated [124] or lipid rafts-dependent endocytosis [125]. At this point, PrP^C can be recycled and sent again to the cell surface, delivered to the Golgi by endosomes [126], or sent to degradation. In normal circumstances, internalized PrP^C is degraded in the endolysosome compartment (Fig 1.7 A). Alternatively, endoproteolytic processing of the PrP^C can also occur in the cell surface or the secretory pathway; thus, metalloproteinases of the A disintegrin and metalloproteinase (ADAM) family can α-, β-, and γ-cleave PrP^C, generating the corresponding N1 and C1, N2 and C2 or N3 fragments[127,128], which play essential roles in physiological and pathological processes[129].

As well as other proteins, PrP^C is subjected to quality control to ensure that is correctly folded. Failures during the processing of proteins suppose dramatic consequences for the cell; hence, the cell uses several pathways to degrade altered proteins. In the ER, incorrectly folded forms of the prion protein are retrotranslocated to the cytosol, where they are removed by proteasomal degradation; an excess of abnormally folded protein in the cytosol results in toxicity to the cell and interferes with cell viability.

USC UNIVERSIDADE DE SANTIAGO DE COMPOSTELA

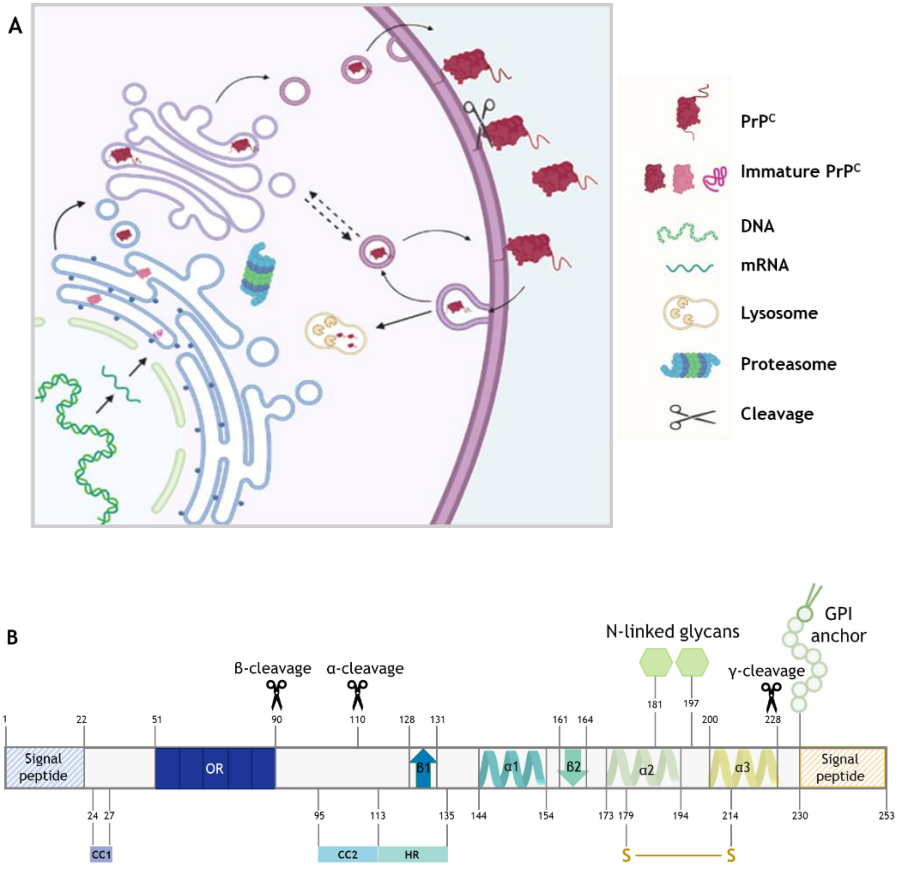


Figure 1.7 PrP^C synthesis and structure. A) Schematic representation of the PrP^C biology since the mRNA is transcribed until the protein is degraded in the lysosomes. Image created with BioRender on https://www.biorender.com/. B) Illustration of the structural motifs of the PrP^C.; CC1: positively charged region 1; CC2: positively charged region 2; OR:octarepeats; S-S indicates the disulfide bound.

A properly folded and mature PrP presents two well-differentiated regions: an N-terminal unstructured and highly flexible domain (23-124) and a C-terminal globular domain (125-231). The globular domain of the prion protein was first solved by NMR in solution using

USC UNIVERSIDADE DE SANTIAGO DE COMPOSTELA

recombinant PrP expressed by *Escherichia coli* [102], since the low yield of prion purification methods difficulted the study of *ex vivo* PrP^C, and the need to have isotopically labeled PrP^C to apply this method. The C-terminal structured domain is composed of three α-helices that contribute to the 42% approximately of the PrP structure: helix α1 (144-154), helix α2 (173-194), and helix α3 (200-228), and two short antiparallel β-strands, strand β1 (128-131) and strand β2 (161-164, mouse numbering), that contribute to the 3% of the total structure. Helices α2 and α3 are covalently linked by the disulfide bond (Fig 1.7 B).

1.3.1.2 Functions of the PrP^C

Due to its involvement in various physiological and pathological processes, it has been suggested to categorize PrP^C as a multifunctional protein[129]. Despite the large number of attributed functions, PrP^C is not essential for life. PrP^C-devoid transgenic mice present minor phenotypic changes as compared with wild-type mice [130,131]. Likewise, PrP-null wild-type goats[132,133] present normal breeding and do not report any histopathological alterations. Hence, PrP^C functions are redundant or there are compensatory mechanisms that participate in its absence (Fig 1.8).

Early studies on PrP^C function determined that OR could bind divalent cations like copper, nickel, iron, or zinc [134]. NMR spectroscopy demonstrated that PrP^C binds copper ions by coordination with nitrogen atoms in the imidazole side chains of histidines in a pH-dependent manner. This evidence may indicate that PrP^C could be involved in copper transport from the extracellular medium to endosomal compartments [135]. *In vitro*, PrP^C and copper interactions have been related to the activity of NMDA receptors and protection against oxidative stress, although these activities have not been demonstrated *in vivo* [136]. PrP^C has also been related to iron homeostasis since PrP^C overexpression protected cells from iron toxicity[137], showed a higher uptake of iron, and increased ferritin expression. [138]. Additionally, PrP^C-null transgenic mice displayed lower levels of metal ions in blood and

USC UNIVERSIDADE DE SANTIAGO DE COMPOSTELA

tissues, such as iron, copper, and zinc, presenting signs of anemia that evidenced the relation between metal ions and the PrP^C [139].
Another phenotypic difference between wild-type and PrP^C-devoid mice was demyelination of the peripheral nervous system, suggesting that PrP^C would be involved in myelin maintenance. Bremer and colleagues confirmed this hypothesis demonstrating that the demyelination could be rescued by triggering neuron-specific PrP^C expression [140]. This function depends on the interaction between the region of the PrP^C comprising amino acids 23-33 and the G-protein coupled receptor Adgrg6 (Gpr126) on the Schwann cell surface. In this regard, the N1 fragment that contains such sequence is released to the extracellular compartment after α-cleavage; subsequently, it binds to the Gpr126 expressed on Schwann cells activating Adgrg6, which via cyclic adenosine monophosphate (cAMP), triggers a downstream signaling cascade that leads to the myelination [141].
PrP^C is mostly localized in pre-and postsynaptic compartments along axons and in pre-synaptic terminals. This expression pattern suggests that PrP^C could also be involved in preserving normal synaptic transmission and plasticity. Moreover, while knockout mice presented weakened inhibitory GABAergic synaptic transmission and reduced long-term potentiation (LTP) in hippocampal cells, animals overexpressing PrP^C presented supra physiological synaptic transmission[142]. Additionally, LTP is related to synaptic plasticity, and, due to memory and learning processes lie in the hippocampus, deficits in synaptic plasticity in this brain area would be related to prion-associated cognitive impairment.

The prion protein may also play a role in Alzheimer's disease and other neurodegenerative diseases. It has been reported that PrP^C inhibits β-secretase 1, an enzyme that participates in the synthesis of amyloid-β (Aβ) by cleaving the amyloid precursor protein (APP). According to this hypothesis, the expression of PrP^C would be protective against Alzheimer's disease, while the ablation of PrP expression would increase the formation of Aβ [143]. However, studies exploring this theory

USC UNIVERSIDADE DE SANTIAGO DE COMPOSTELA

found contradictory results, and while patients of Alzheimer's disease non-associated to genetic mutations presented a lower expression of PrP^C, familial cases of Alzheimer's disease did not display altered levels of PrP^C[144]. Likewise, PrP^C-null mice did not display altered levels of Aβ [145].

On the other hand, the direct interaction between the N-terminal domain of the PrP^C and Aβ oligomers has also been described [146,147]. It has been suggested that PrP^C may act by transducing the toxic signaling pathway that triggers the pathological phenotype in neurons. It was suggested that the neurotoxicity would be mediated by the dysregulation of the glutamate receptor mGluR5, which causes dendritic spine loss and long-term depression. Moreover, PrP^C, may also be involved in Aβ oligomer-induced tau hyperphosphorylation, which is associated with neurofibrillary tangle formation[148]. PrP^C also binds other amyloids related to neurodegenerative disorders, such as α-synuclein and the scrapie isoform of the prion protein, reinforcing the idea that PrP^C could act as receptor for these amyloids triggering a neurotoxic signaling cascade[149,150].

Since the most notable sign of FFI patients is sleep-wake cycle disruption, the role of PrP^C in circadian rhythm was suspected [151]. Studies with PrP^C-null mice showed that animals exhibited sleep dysregulation; [152,153] this sleep-wake cycle alteration was related to melatonin serum levels [154], and this phenotype was rescued after inducing PrP^C expression. This evidence suggested that the FFI phenotype could be related to a loss of function of the PrP^C. Moreover, in rat forebrain and suprachiasmatic nucleus, PrP mRNA seemed to be subjected to circadian oscillations[155]. However, many studies disagree about the causes of the sleep-wake cycle dysregulation, and some authors suggested that it was related to the malfunction of cation channels and receptors such as calcium-dependent potassium channels, voltage-gated calcium channels or NMDA receptors that lead to hyperexcitability. On the other hand, other works suggested that the effect of PrP^C on NMDA receptors containing the subunit GluN2D

USC UNIVERSIDADE DE SANTIAGO DE COMPOSTELA

confered neuroprotection facing synaptotoxicity[156], due to the fact that it was shown that PrP^C modulates NMDA-mediated excitotoxicity after acute cerebral ischemia *in vivo* [157]. This interaction showed that, while PrP^C-deficient mice presented more extended brain lesions after cerebral ischemia, in mice overexpressing PrP^C the extent of the damage was minor [158].

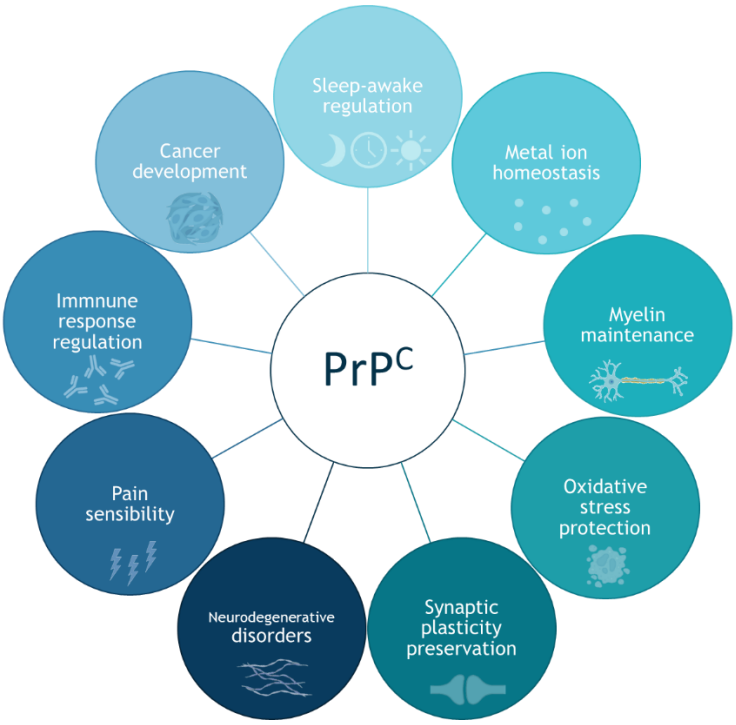


Figure 1.8 Schematic representation of the functions of the cellular prion protein. Image created with BioRender on biorender.com

Apart from the nervous system, PrP^C is highly expressed in cells of the immune system, such as mast cells, T-lymphocytes, natural killer cells,

USC UNIVERSIDADE DE SANTIAGO DE COMPOSTELA

and macrophages. *In vitro* experiments showed that activation of mast cells is translated into the secretion of the inflammatory mediators, but also in the release of the N3 fragment, suggesting that PrP^C may be involved in inflammatory responses [159]. PrP^C has also been associated with T lymphocyte differentiation, since PrP^C knock-out mice present more T cells with pro-inflammatory phenotype. Another evidence of PrP^C role in the immune system was provided by the aforementioned wild-type goats lacking PrP^C. These animals presented higher levels of neutrophils in comparison with other animals; however, the implications of this alteration remain unknown [132,133].

PrP^C has also been related to pain sensibility, and some works demonstrated that the expression of PrP^C protects against both inflammatory and neuropathic pain when comparing wild-type and PrP^C-null mice. This effect is due to the inhibition of NMDA receptors related to the transmission of pain at the spinal cord level[160].

While the primary implications of PrP^C are typically associated with the proper functioning of the nervous system or neurodegenerative disorders, this protein has also been linked to various biological aspects of cancer development, such as cell proliferation, migration, and chemoresistance[161]. PrP^C has been identified as an upregulated protein in various cancers, indicating that its involvement is attributed to a gain of function. Overall, PrP^C is associated with several signaling pathways that activate the transcription of genes involved in cell growth, metabolism (e.g., GLUT1 gene) [162], multidrug resistance proteins (e.g., MDR1)[163,164], and cytoskeleton rearrangement, facilitating epithelial-to-mesenchymal transition[165]. Moreover, it has been demonstrated that PrP^C directly interacts with doxorubicin, a chemotherapeutic drug, sequestering the molecule through the utilization of its N-terminal tail[166].

USC UNIVERSIDADE DE SANTIAGO DE COMPOSTELA

1.3.2 The scrapie prion protein (PrP^{Sc})

The scrapie isoform of the prion protein (PrP^{Sc}) is the pathogenic conformer associated with prion disorders. While PrP^{Sc} and PrP^{C} have the same primary sequence and post-translational modification, they differ in their secondary, tertiary, and quaternary structures. Although PrP^{C} has been solved by NMR and X-ray crystallography, the conformational change of the PrP^{Sc} confers it distinct biological and biochemical properties. Unlike PrP^{C}, this isoform tends to form insoluble aggregates making it impossible to use those structural techniques that require the protein to remain in a soluble state; thus, the elucidation of the structure of PrP^{Sc} posed a great challenge for decades. However, after many efforts, the structure of PrP^{Sc} has been recently deciphered and it is expected that, in the near future, further research based on these findings will shed light on mechanisms that are still poorly understood, such as the conversion or the pathogenesis. Notwithstanding, it is important to note that this thesis was already in progress when the structure of PrP^{Sc} was published and, even though we now know that classical PrP^{Sc} consists of a parallel in-register β-sheet (PIRIBS), it is crucial to comprehend the previous structural models as well as the analytical pieces of evidence that supported them, in order to fully understand some of the hypotheses and experiments conducted in the present work.

1.3.2.1 Understanding the structure of PrP^{Sc}

While cryogenic electron microscopy was the technique used to solve the structure of PrP^{Sc}, various imaging, biochemical, and spectroscopic techniques were also employed to gather data from *ex vivo* or synthetic prions. Low- and high-resolution methods were equally crucial in providing valuable insights into the architecture of PrP^{Sc}.

Electron microscopy was the first technique employed to visualize prion fibrils [104,167]. Despite the high tendency to form aggregates, negative stain electron microscopy observations led to perceiving some similarities between PrP^{Sc} and the fibrils of Aβ present in the brains of Alzheimer's disease patients. Some years after these first observations,

USC UNIVERSIDADE DE SANTIAGO DE COMPOSTELA

negative stain electron microscopy was also used in independent works to measure the fibrils diameter, suggesting that 10-20nm fibrils may be constituted by two 4-6nm width intertwined protofilaments [168,169].

Early structural studies based on FTIR[170,171] and CD analyses determined that, unlike PrP^{C}, the secondary structure of PrP^{Sc} contained more β-sheet and substantially less α-helices. Nonetheless, a later reinterpretation of this data, revealed that PrP^{Sc} is spared of α-helical structures. The misinterpretation was due to the presence of an absorption band in the spectrum at ~1660 cm^{-1} attributed to α-helical structures. However, this band was also identified in amyloids lacking any α-helix in their structure. Such band overlaps with the assignment of other structural motifs, such as turn or coils, which are present in amyloid structures [106,107,172]

X-ray diffraction experiments importantly contributed to shedding light on the PrP^{Sc} structure[173]. The application of this technique was possible thanks to the improvements in prion purification methods, using phosphostungstate anions to precipitate the protein, and advances in the alignment of fibril preparation. X-ray diffraction determined that the amyloid fibril was composed of the repetition of 1,92nm units along the fibril axis, and most importantly, the absence of equatorial diffraction at 1,0nm was indicative of stacked β-sheet amyloid structures[169]. Altogether, these findings suggested that the PrP^{Sc} structure may be a β-helical architecture, such as a β-solenoid[174]. Also based on X-ray technology, synchrotron-based small-angle X-ray scattering (SAXS) was applied to describe prion features. The results obtained by this method corroborated previous findings indicating that the fibril had a diameter of ~11nm. The sizes of the diameter and the units of repetition were compatible with two intertwined protofilaments consisting of four β-strands in a β-solenoid configuration. This hypothesis was supported by solid-state nuclear magnetic resonance (ssNMR) spectroscopic analyses of a fungal prion, HET-s, which structure was a two-rungs β-solenoid[175,176].

USC UNIVERSIDADE DE SANTIAGO DE COMPOSTELA

Another imaging technique employed to visualize PrP^{Sc} was atomic force microscopy (ATM). This approach permits the visualization of different surfaces or biomolecules immobilized on different materials providing a 3D image. Using ATM, PrP^{Sc} was observed on the surface of neuroblastoma cells persistently infected with murine prions[177]. Moreover, it was also used to compare and estimate the height and helical periodicity of purified or synthetic prions[178].

One of the main biochemical differences between PrP^{C} and PrP^{Sc} is the partial resistance of PrP^{Sc} to proteolytic degradation with PK. This proteinase cleaves unstructured and flexible regions of the PrP^{Sc}, whereas β-strand and inaccessible motifs would remain intact. PK-resistant fragments of hamster-adapted prion strains, 263K, Dy[179], and GPI-anchorless RML[180], were analyzed by mass spectrometry to identify the PK cleavage sites. Overall, the analyses of these three strains agreed on the high resistance of the C-terminal region to proteolytic degradation [181,182]. Moreover, minor differences in the cleavage sites were reported. Limited proteolysis analyses of samples from CJD patients agreed with these results reporting similar cleavage sites; further, N-terminal truncated PK-resistant fragments were also described [183]. Altogether, these data allowed designing a preliminary map of the β-strands of the PrP^{Sc} [184].

Hydrogen/deuterium exchange mass spectrometry provides structural information based on the accessibility of different structural motifs to the solvent; those flexible secondary structures present rapid hydrogen for deuterium exchange, whereas the exchange is moderately or largely slower when the structure consists of α-helices and β-sheets, respectively. In this regard, hydrogen/deuterium exchange analyses determined that the region comprising amino acids 90-224 presented low exchange rates, suggesting that this region has a high content of β-strands connected by turns or loops [185,186].

ssNMR is a spectroscopic method employed to determine the chemical structure, three-dimensional arrangement, and dynamic properties of

USC UNIVERSIDADE DE SANTIAGO DE COMPOSTELA

solids or semi-solids. It has been successfully employed to solve the architecture of amyloids such as the fungal prion, HET-s, which was a β-solenoid configuration [175], or Aβ, which unlike HET-s, presents a parallel in-register β-sheet conformation [187,188]. Structural characterization of prions using ssNMR had been restricted due to the limited amount obtained from *in vitro* amplification techniques; nonetheless, the development of the protein misfolding shaking amplification (PMSA), a technique that allowed obtaining a large amount of recombinant prions isotopically labeled needed for ssNMR analysis [101,189]. Although the prion structure could not be solved by this method, measurements of distances between amino acids typically located in β strand were compatible with a PIRIBS architecture.

The application of cryo-EM technology has revolutionized structural studies in the prion field representing a major milestone. In recent years cryo-EM technology improved so much that the images obtained reached a near-atomic resolution [190]. Moreover, the structural model supported by this technique also changed with the progressive improvement in the cryo-EM resolution.

Vazquez-Fernández and colleagues employed Cryo-EM to examine GPI-anchorless RML prions directly, in the absence of any staining that could introduce possible artifacts and provided consistent measurements of the prion fibrils. The helical symmetry within the PrP^{Sc} fibrils made it possible to perform 3D reconstruction and analyses of the individual fibrils. These determinations indicated that each PrP^{Sc} particle had an average height of 1,8nm, which coincided with the expected height of a four-rung β-solenoid monomer, 1,92nm (4 rungs x 0,48nm) [191]; these measurements were also consistent with single particle averaging, an alternative processing approach that classifies and averages hundreds of images of fibril sections. Moreover, volumetric analyses supported the idea that fibrils were composed of two intertwined protofilaments, which agreed with previous findings by X-ray diffraction [169]. Unfortunately, this attempt to solve the prion

USC UNIVERSIDADE DE SANTIAGO DE COMPOSTELA

structure did not obtain a sufficient resolution to achieve an all-atom reconstruction.

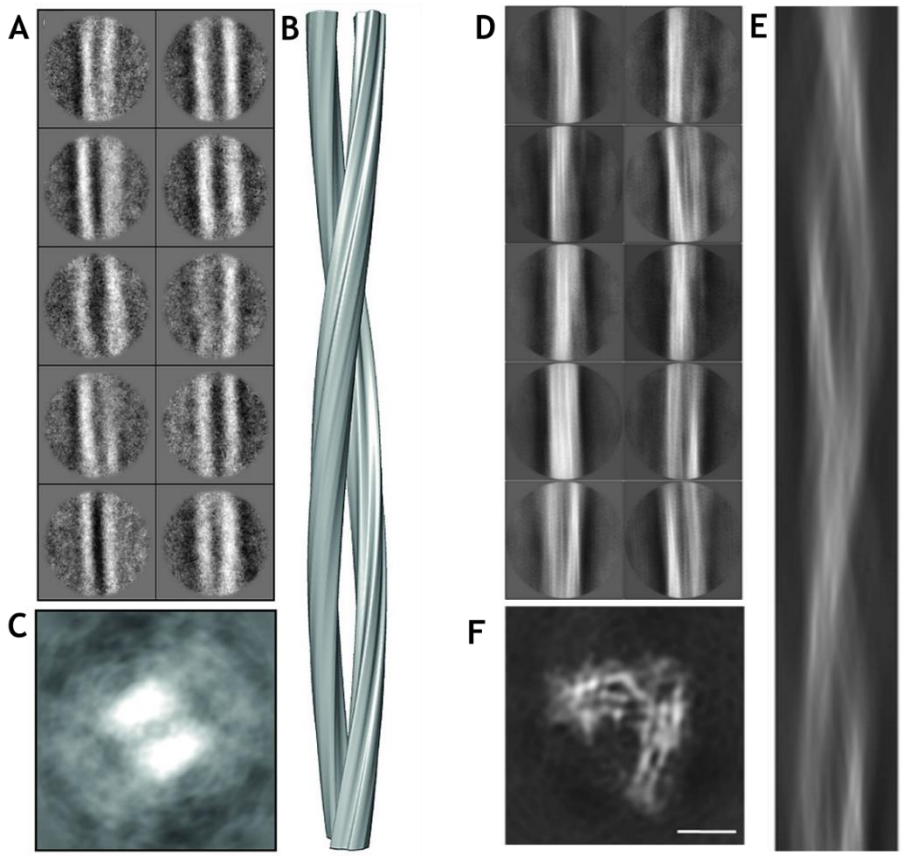


Figure 1.9. Cryo-EM data obtained from *ex vivo* GPI-anchorless RML prions. Improvements in purification, resolution, and cryo-EM data collection were translated into a different interpretation regarding the structure of the same prion strain. Comparison of the data collected by Vázquez-Fernández et al., (A-C) and Kraus et al., (D-F). A and D correspond to 2D class averages; B and E consist of the lateral view of the 3D reconstruction; and C and F correspond to the cross-section projection of the density map. Adapted from Vázquez-Fernández et al 2016 [191] (open access) and Kraus et al 2021 [192].

USC UNIVERSIDADE DE SANTIAGO DE COMPOSTELA

The definitive confirmation that *bona fide* brain-derived prions have a PIRIBS architecture was the fruit of the work of Kraus and colleagues, who solved the hamster-adapted 263K prion strain by cryo-EM with a 3,1Å resolution [192]. Soon after these findings, more *ex vivo* prion strains were solved, reinforcing Kraus's results [190,193,194]. Thus, ex vivo classical prions, such as 263K, RML, 22L, or M7, consist of left-handed helical twist single-protofilament. PrP^{Sc} monomers display a parallel-in register β-sheet architecture and present two lobes, an N-terminal and a C-terminal lobe which are connected by continuous electron density, refusing the idea that both halves belong to independent protofilaments. The fibril core of 263K comprises amino acids ~95-227 and is ~3,5nm in its narrowest dimension, whereas it is ~13nm in its longest.

1.3.2.2 PrP^{Sc} models

Based on the pieces of evidence provided by all the aforementioned structural methods, at the beginning of the present thesis, two possible conformational models were competing: the 4-Rung β-Solenoid (4RβS) and the Parallel In-Register Intermolecular β-Sheet (PIRIBS).

4-Rung β-Solenoid (4RβS)

Overall, the β-solenoid configuration consists of elongated fibrils comprising repetitive arrangements of β-strands connected by loops resulting in a helical shape. Coils are made up of linear β-strands joined with tight turns, termed β-arcs, or loops around the axis of the solenoid. This architecture creates a stable and rigid structure in which stacked coils are coordinated by hydrogen bonds contributing to strands of different coils forming parallel β-sheets. The β-solenoid inter-coil distance is well established and consists of the distance between hydrogen-bonded β-strands, 4.8±0.2Å. β-solenoids have the distinctive property of having a clear boundary between the interior side chains, that compose the hydrophobic core, and the side chains on the surfaces exposed to solvent. This boundary is formed by a tightly packed layer of polypeptide backbones linked by hydrogen bonds, which wraps around the hydrophobic core [195].

USC UNIVERSIDADE DE SANTIAGO DE COMPOSTELA

The 4RβS model proposed that each PrP monomer was folded into four consecutive left-handed rungs. The fibril core comprised residues 89-230 (mouse numbering) and each rung contained three β-strands connected by turn or loops, coinciding with the identified PK cleavage sites. The disulfide bond would remain intact connecting cysteines located in consecutive rungs. This model was in complete agreement with the data obtained by the aforementioned structural studies regarding the fibril size [191] and permitted the accommodation of N-linked complex glycans. In addition, molecular dynamic simulations determined that this arrangement was thermodynamically plausible. Moreover, the possible folding pathway was reconstructed and simulated by computational methods, leading to a complete conversion of PrP^{C} into this PrP^{Sc} model [196]

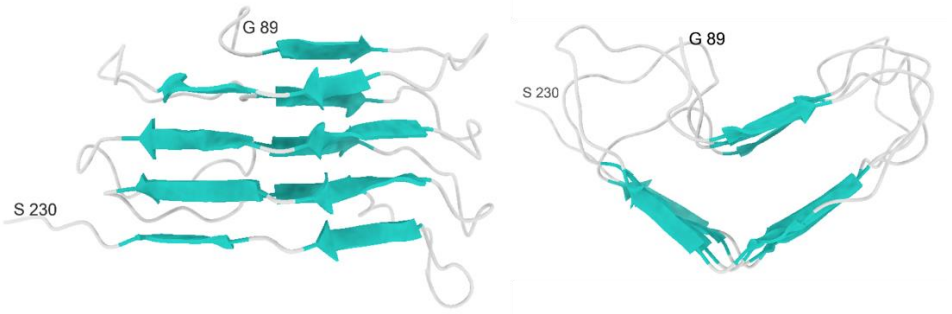


Figure 1.10. 4RβS model. PrP^{Sc} structure modeled as a 4RβS (left) and cross-sectional representation of the structure (right). β-strands are represented as turquoise arrows, and turns and loops in light gray. Image created with Chimera X [197](Coordinates available on https://doi.org/10.1371/journal.ppat.1007864) [196]

Parallel In-Register Intermolecular β-Sheet (PIRIBS)

Parallel in-register architecture is the most common conformation among amyloid fibrils. It consists of strands stacked on top of each other in the same orientation, coinciding equivalent residues of consecutive

USC UNIVERSIDADE DE SANTIAGO DE COMPOSTELA

strands along the axis. This conformation maximizes the contacts between residues, the number of hydrogen bonds, and hydrophobic interactions. Moreover, charged residues, that could destabilize this conformation, are located in loops or compensated by oppositely charged ions when orientated to the aqueous phase [198].

The first PrP^{Sc} PIRIBS model was proposed by Groveman and colleagues, based on ssNMR and negatively stained electron microscopy data obtained from PrP amyloids propagated by prion-seeded RT-QuIC. These synthetic amyloids presented a major advantage over brain-derived samples, which was that they lacked the heterogeneous glycans composing the GPI anchor and the N-linked glycosylations, which negatively affect the resolution of the protein. Based on their results, the authors suggested that PrP^{Sc} fibrils consisted of a single protofilament, and each PrP^{Sc} monomer contained two domains separated by a cleft [199]. However, the acceptance of this model was limited since it was based on data collected from non-infectious amyloids and its stability in molecular dynamics simulations, poor. In this regard, it was suggested that the difference between infectious and non-infectious PrP amyloids could lie in their structural differences. Moreover, computational simulations initially failed to accommodate the glycosylations into this model because of the excessive steric clashes [109].

Subsequently, other recombinant amyloids were solved by cryo- EM. However, working with recombinant samples also entails certain drawbacks. These amyloids are not infectious, or their infectivity is orders of magnitude lower than *bona fide* brain-derived prions; additionally, their PK-resistant cores are smaller. Moreover, the diverse range of sequences employed in these experimental approaches, such as proteins from different species[200], truncated forms of the PrP, or sequences with disease-associated mutations[201–203], led to obtaining results with remarkable heterogeneity regarding the cores forming the fibril, as well as the interactions between protofilaments. Nonetheless, setting aside these divergences, all these studies with recombinant PrP

USC UNIVERSIDADE DE SANTIAGO DE COMPOSTELA

amyloids presented higher resolution than the previous attempt using GPI-less *ex vivo* prions and converged on one crucial aspect: the fibril was composed of two protofilaments whose monomers presented a PIRIBS conformation.

Despite the divergences with Groveman's model, the PIRIBS architecture was definitely confirmed using cryo-EM [204,205]. Thus, prion fibrils are constituted by one single left-handed helical twist protofilament. The fibril core is composed of stacked PrP monomers that typically span from residue ~95 to ~227, although the size of the core slightly varies among strains.

The PrP monomer folds to form an N-terminal and C-terminal lobe that are connected by a central staggered interface. The N-terminal lobe includes residues 94 to 170 and this region can be subdivided into three structural elements: a steric zipper (residues ~95-110 and ~133-152); an N β-arch, consisting of hydrophobic residues with a relatively conserved topology between strains, and a conformationally variable region; and a middle β-arch. On the other hand, the C-terminal lobe contains the disulfide β-arch, and spans from residue ~179 to ~214, which contains both N-linked glycans [110,190].

Soon after the publication of Kraus's work, the structure of four more prion strains were solved also with the application of cryo-EM, marking a significant breakthrough in the field of prions [190,193,194,205]. Based on these recent findings, it is expected that great advances will soon be achieved, especially the elucidation of the mechanism of conversion, the pathogenesis, and the development of structure-based therapeutic approaches.

USC UNIVERSIDADE DE SANTIAGO DE COMPOSTELA

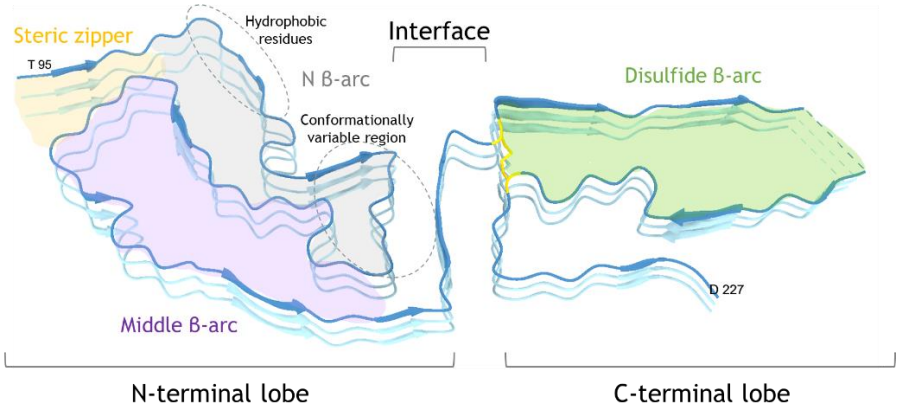


Figure 1.11. Structural motifs of 263K. Cross-section of 263K fibril with the main structural motifs. Cysteines involved in the disulfide bond are colored in yellow. Posttranslational modifications are not included. Image created with Chimera (PDB 7LNA)[110,197].

1.3.3 Conversion of PrP^{C} into PrP^{Sc}

One of the most striking properties of PrP^{Sc} is its capacity of self-propagation, templating correctly folded PrP^{C} into the PrP^{Sc} conformation. While the exact mechanism of conversion remains unclear, understanding the conformation of PrP^{Sc} has provided insights into important steps that may occur during the structural rearrangement. It was suggested that the restructuration process may occur through a partially unfolded intermediate, which would be originated from the dissociation of the loop containing β1, helix α1, and β2, and the hairpin consisting of helices α2 and α3. After this first movement, a multi-step process, in which all intramolecular interactions become intermolecular, culminates in the formation of a flat, β-sheet-rich molecule, in which only the disulfide bond remains intact [110]. It is thought that the self-propagating mechanism begins with the interaction with the protruding ends, the sticky N-terminal tail, or an unfolded intermediate. Subsequently, the refolding could extend along the polypeptide backbone towards the N- and C-termini [204].

USC UNIVERSIDADE DE SANTIAGO DE COMPOSTELA

The generation of a highly compacted fibril core with extensive intermolecular β-sheets along the fibril axis requires a complete unrolling of the helices and unfolding of the β-sheets. Additionally, it was proposed that the interaction with polyanionic cofactors and other molecules present in the cell membrane may also play a crucial role in this conversion process [204].

1.3.4 Neurotoxicity in prion diseases

The structural configuration of PrP^{Sc} confers it different biochemical and biological properties from those of PrP^{C}. Prion fibrils aggregate leading to the formation protein depositions, which are insoluble in non-denaturing detergents and partially resistant to proteolytic degradation. The presence of PrP^{C} is a *sine qua non* condition to develop prion diseases. Notwithstanding, the neurotoxic mechanism is poorly understood, and pieces of evidence suggest that the neurotoxicity and the presence of PrP^{Sc} deposits are not directly related. Indeed, Brandner and colleagues elegantly demonstrated PrP^{Sc} was not solely responsible for the damage observed in prion diseases. For this purpose, they transplanted brain tissue of prion-infected mice into knock-out mice, observing that despite the chronic presence of PrP^{Sc} deposits, mice bearing the graft did not develop prion diseases, and the lesion was limited to the tissue expressing PrP^{C} [206].

The relation between PrP^{C} expression and neurodegeneration was also demonstrated using a conditional knock-out mouse model with floxed PRNP gene and inducible expression of the Cre recombinase; thus, when the Cre recombinase expression was induced, the PRNP gene was deleted. Inoculation of animals before PRNP gene excision resulted in the onset of clinical signs; however, the interruption of the PrP^{C} expression gave rise to a reversion of the disease [207]. Additional observations also demonstrated that classical PrP^{Sc} can be detected in the brain of inoculated animals before the onset of clinical signs, and it was proposed that the neurotoxicity could be mediated by species of the

USC UNIVERSIDADE DE SANTIAGO DE COMPOSTELA

prion protein different from PrP^{Sc}, such as PK-sensitive forms of the prion protein or oligomers [208,209]; moreover, these toxic species are not necessarily the infectious forms of the prion protein[210].

Regarding the molecular mechanism of how PrP^{Sc} could be related to neurotoxicity, many theories have been proposed. It has been proposed that, as well as PrP^{C} may act as a cell-surface receptor of different amyloids such as Aβ or α-synuclein, it should also bind PrP^{Sc} or other PrP oligomers, transducing a downstream toxic signaling cascade [211].

Moreover, the ER could play a crucial role in genetic prion disease pathogenesis, since mutated proteins could misfold during their synthesis in the ER, causing ER stress and proteostasis impairment. Apart from increasing PrP^{Sc} level, ER stress can also lead to the accumulation of incorrectly folded forms of the PrP, which could be more susceptible to prion conversion [212].

Sustained ER stress has nefarious consequences for the cell, for this reason, cells count on quality control mechanisms to restore ER function and ensure the removal of misfolded proteins, such as the unfolded protein response (UPR) and the ER-associated degradation (ERAD). Both systems coordinately interact with the ubiquitin-proteasome system (UPS), a protein degradation pathway that clearances ubiquitinated proteins in the cytosol by the action of the 26S proteasome. In prion-infected animals, ER stress and UPS dysfunction are detected in the early stages of the disease [213]; furthermore, ubiquitin deposits have been found as granules surrounding PrP^{Sc} amyloid plaques [214].

The accumulation of misfolded proteins in prion diseases can overwhelm the capacity of the proteasome, that can result in a proteasomal insufficiency and impairment of protein regulatory pathways. This dysfunction in the UPS can lead to a loss of protein homeostasis and activation of proapoptotic pathways, resulting in cell death.

USC UNIVERSIDADE DE SANTIAGO DE COMPOSTELA

To summarize, the study of prions represented, and still represents an amazing challenge to the scientific community. The concept of prion has expanded the traditional concept of infectious agents by demonstrating that misfolded proteins can also be transmissible among individuals. In addition, although transmissible spongiform encephalopathies are rare diseases, their contemplation can also have a significant impact on advancing other neurodegenerative diseases, such as Alzheimer's and Parkinson's, which share common features with prion diseases, such as protein misfolding and the formation of toxic aggregates in the brain. Finally, in view of the common features between prions and proteins involved in other neurodegenerative disorders, by better understanding prions, it is possible to gain valuable insights for the development of therapies and therapeutic approaches for these more common diseases that currently lack a cure.

USC UNIVERSIDADE DE SANTIAGO DE COMPOSTELA

2. OBJECTIVES

USC
UNIVERSIDADE DE SANTIAGO DE COMPOSTELA

The present thesis is organized into three chapters, two of which are dedicated to the assessment of three therapeutic candidates for prion diseases. The third chapter tackles the study of the biochemical and biological properties of different recombinant prion strains. Thus, the objectives of this work were classified according to the chapter they belong.

Prion diseases are rare and fatal neurodegenerative disorders for which there is no treatment. The global objective of the first chapter is to evaluate two therapeutic strategies in a fast murine model of prion disease; these pharmacological approaches tackle prion diseases from two different perspectives, targeting PrP^{C} and PrP^{Sc}.

The global goal of the first chapter has been broken up into two specific objectives according to the therapeutic compound employed in each approach:

1. Evaluation of the chronic administration of a tetrapyrrole, Fe(III)-TMPyP, as a treatment against prion diseases.
2. Evaluation of the single-chain fragment variable, scFv-G1, as a chronic treatment for prion diseases.

Similarly, the global objective of the second chapter was to assess the therapeutic potential of a PrP amyloid in a fast murine model of prion disease. However, in view of the results that arose from the first experiments performed, new objectives were incorporated:

1. Evaluation of the prophylactic administration of a recombinant PrP amyloid as a treatment of prion diseases.
2. Serial transmission of the infectious PrP amyloid.
3. Biochemical and biological characterization of the infectious PrP amyloid.

USC UNIVERSIDADE DE SANTIAGO DE COMPOSTELA

Due to the involvement of diversity of prions strains in the capacity to cause diseases with different phenotypes and their implication in the development of resistances to pharmacological treatments, the characterization of different prion strains could shed light on the mechanisms associated to therapeutical failure. Hence, the main objective of the third chapter is to generate *de novo* different PrP conformers by PMSA in the presence of different polysaccharide cofactors. This global objective has been broken up into the following specific aims:

4. Determination of the biological, biochemical, and biophysical properties of the recombinant conformers.
5. Comparison of the properties of the generated conformers to determine if they exhibit different features.
6. Assessment of the infectious potential of the generated conformers to determine if they exhibit characteristics of *bona fide* prions.
7. Comparison of the properties of the conformers *in vivo* to determine if they consist of different prion strains.
8. Comparison of the effect of the different cofactors on the generation of the conformers.

USC UNIVERSIDADE DE SANTIAGO DE COMPOSTELA

3. CHAPTER I: THERAPEUTICAL POTENTIAL OF A PORPHYRIN AND A scFv ANTIBODY FOR PRION DISEASES

USC
UNIVERSIDADE DE SANTIAGO DE COMPOSTELA

3.1 INTRODUCTION

Prion diseases or transmissible spongiform encephalopathies are fatal neuropathological disorders for which there is no cure. Three decades ago, it was discovered that prions cause transmissible spongiform encephalopathies; however, the efforts to find a treatment that could extend survival or even ameliorate the symptoms of those patients suffering from these conditions failed.

Many attempts have been made in order to find an effective treatment against prion diseases. Nonetheless, there are critical aspects still poorly understood, completely unknown, or which have been recently discovered that could be contemplated as possible therapeutic targets, such as the PrP^{C} function, the pathogenesis, the mechanism of conversion of PrP^{C} into PrP^{Sc} and the PrP^{Sc} structure[110].

A large variety of drugs have been tested *in vitro*, *in cellula* or *in vivo* [215–220]: from small compounds commonly used as a treatment for other disorders to large and complex molecules, immunotherapie, or gene therapies specially designed for these diseases. However, only six treatments have been clinically tested: amantadine, flupirtine, pentosan polysulfate, quinacrine, doxycycline, and PRN100 [221–228], unfortunately, all of them with little or no improvement over controls.

The search for a prion treatment was tackled from different points of view regarding the target molecule (Fig 2.1). Most of the approaches were based on the PrP^{C} because it is the best-known molecule involved in prion disorders and its essential role in prion pathogenesis as the substrate for PrP^{Sc} propagation; however, other key points of the prion biology have also been explored, tackling TSE from the expression of

USC UNIVERSIDADE DE SANTIAGO DE COMPOSTELA

the PrP, to the conversion of PrP^{C} into PrP^{Sc} or the toxicity derived from the conversion, among others.

Targeting the PrP expression

PrP^{C} is essential for the development of prion diseases. This fact was demonstrated in the early '90s when the first PRNP knock-out mice revealed to be resistant to prion diseases[96,207]. Moreover, heterozygous and knock-down animals had an extended incubation time compared to wild-type animals, which means that even a partial suppression of PrP expression could have beneficial effects[96,229]. Hence, reducing the PrP expression is currently the most promising approach to finding a therapy for prion diseases. Although this approach would be beneficial for all patients, it would be especially advantageous for carriers of genetic prion diseases, since a complete the suppression of the expression of the PrP would permit them to evade the disease, even after the onset.

In this regard, two strategies based on decreasing mRNA have been assessed: small interference RNA (siRNA) and antisense oligonucleotides (ASOs).

RNA interference (RNAi) is a noncoding RNA naturally synthesized as a conserved response against double-stranded RNA, generally from a viral origin. Its function is to regulate gene expression in a sequence-specific manner[230]. This biological mechanism could be used from a therapeutic perspective by designing an RNAi targeting PrP mRNA. Two varieties of RNAi share the exact mechanism of action, although they differ in the way they are synthesized: small interfering RNA (siRNA) and microRNA (miRNA) (also called short hairpin RNA, shRNA, if its origin is synthetic).

SiRNA was successfully tested in chronically infected cells showing PrP^{Sc} inhibition[231]. However, its inability to cross the blood-brain barrier was evidenced in the first attempt to use it in infected animals [232]. This handicap was overcome by binding the siRNA to the rabies

USC UNIVERSIDADE DE SANTIAGO DE COMPOSTELA

virus glycoprotein (RVG), which uses the nicotinic acetylcholine receptor (AchR) to enter into the neurons overcoming the BBB[233], or encapsulating the siRNA in liposomes-siRNA-peptide complexes. This last strategy showed an increase in the survival of mice of up to threefold in comparison with the control group[234,235].

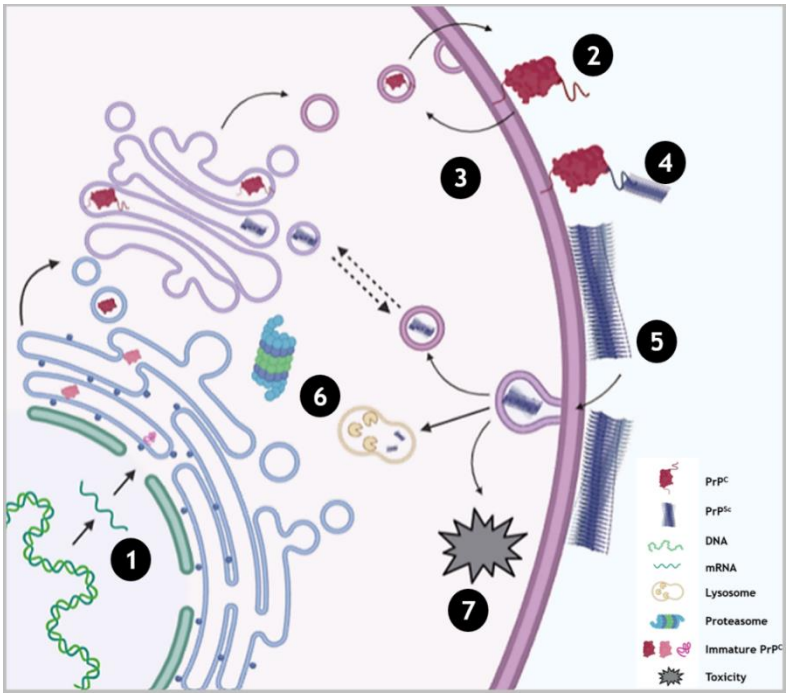


Figure 2.1. Scheme of therapeutic approaches for prion diseases. 1. Reducing the expression level of PrP. 2. Targeting PrP^{C}. 3. Targeting PrP trafficking. 4. Impeding PrP^{Sc} propagation 5. Increasing the PrP^{Sc} clearance. 6. Increasing the degradation of misfolded proteins. 7. Interrupting the cell signaling cascade that triggers the toxicity. Picture created with BioRender.com

On the other hand, shRNA encoded in adeno-associated virus (AAV) vector type 2 was also tested *in vivo* by thalamic infusion. However,

USC UNIVERSIDADE DE SANTIAGO DE COMPOSTELA

there was no beneficial effect, probably because of an inefficient distribution throughout the brain[236].

The second strategy to knock down PrP expression is using antisense oligonucleotides (ASOs). ASOs are short synthetic single-stranded DNA molecules that bind sequence-specifically to a mRNA, leading to their degradation[237]. Like RNAi, ASOs do not cross the BBB and must be injected into CSF or into the brain parenchyma. Moreover, these oligonucleotides must be modified as phosphorothioate oligonucleotides in order to avoid their degradation[238]. The most encouraging figure about ASOs is that they have been successfully tested in animal models for other neurodegenerative disorders. Currently, clinical trials are ongoing to assess their safety and tolerability in patients in the early stages of Alzheimer's disease[239,240]; furthermore, in 2016, the FDA approved the first treatment with ASOs for spinal muscular atrophy (SMA)[241,242].

Regarding prion diseases, ASOs efficacy was assessed in mouse models [243], demonstrating prophylactic and therapeutic effects, even when the treatment started at the onset of the clinical stage of prion disease, and its effectivity against different prion strains[4,244].

Targeting PrP^C

Independently of the origin of the prion disease, PrP^C is a common factor in all of them. Therefore, targeting PrP^C has been a promising approach to tackling prion disorders. Different bioinformatic tools, such as *in silico* screenings and cell-based or cell-free high-throughput screenings, have allowed the identification of several molecules that interact with PrP^C [245–248]. In this group of molecules are included molecular chaperones, which are compounds that bind PrP^C, stabilizing its native conformation, reducing the Gibbs free energy, and hindering its conversion. Porphyrins such as Fe(III)-TMPyP, phenothiazines, or diphenylmethane derivatives are some examples of chemical compounds which act as molecular chaperones and have demonstrated efficacy *in vitro* and *in vivo* [249,250]. Apart from its efficacy in decreasing

USC UNIVERSIDADE DE SANTIAGO DE COMPOSTELA

the accumulation and propagation of PrP^{Sc}, Fe(III)-TMPyP also showed a reduction of PrP^{C}-mediated synaptotoxicity of Aβ oligomers in cell models and the inhibition of the cytotoxic effect of a PrP mutant carrying the Δ105-125 deletion; these features make it a great candidate for anti-prion therapy.[251,252]

Pentosan polysulfate (PPS), doxycycline, or quinacrine are also drugs included in the group of PrP^{C} targeting compounds. However, these molecules interact in a non-specific manner[250]. All of them have been tested in clinical trials; however, there was no apparent amelioration in the clinical symptomatology or survival[223–227,253–256]. Currently, there is an ongoing clinical trial whose purpose is to establish if the prophylactic use of doxycycline avoids or delays the disease in carriers of the FFI mutation[257].

Targeting PrP^{Sc}

PrP^{Sc} is the causal agent of prion disorders; this fact focused many efforts on reducing the amount of PrP^{Sc} as a therapeutic strategy. Even though the PrP^{Sc} structure has only recently been elucidated, the lack of knowledge about the PrP^{Sc} structure did not impede to find different compounds that bind it.

Even though stabilizing PrP^{Sc} might initially sound counterproductive, it is one plausible strategy to avoid prion propagation due to PrP^{Sc} seeding capacity based on its facility to generate small oligomers from larger fibrils (frangibility). These small oligomers have nucleation properties and can incorporate more monomers expanding the fibril. Thus, decreasing the frangibility of the aggregates, the propagation would be reduced; moreover, stabilized aggregates are susceptible to degradation[258,259].

Congo red is a diazo dye that binds amyloid fibrils emitting green birefringence under polarized light; this property was employed for the diagnosis of amyloidoses and the use of this dye became a gold standard. Congo red was one of the first patented molecules against

USC UNIVERSIDADE DE SANTIAGO DE COMPOSTELA

prion diseases, and it significantly prolonged the survival of scrapie-infected hamsters without affecting PrP^C normal metabolism. However, its interaction with other molecules and carcinogenicity discouraged its use in humans[260–263]. On the other hand, luminescent conjugated polythiophenes (LCP) are also fluorescent dyes that bind and stabilize protein aggregates with repetitive cross-β sheet structures by cooperative electrostatic interactions [259]. Moreover, it was also hypothesized that LCPs could discern between different prion strains based on the emission of conformation-dependent fluorescent spectra[264]. LCP derivatives were tested in vitro showing a reduction of the infectivity of prion-infected brain homogenates and cultuted organotypic cerebellar slides. Furthermore, LCPs were also tested *in vivo* by continuous intracerebral infusion in prion-infected mice. This therapeutic strategy was approached from two perspectives, prophylactically, starting the treatment 7 days before the inoculation, and therapeutically, initiating the treatment 49 days after inoculation. Although both approaches increased the survival of prion-infected mice, the symptomatic treatment showed a moderate effect on the life expectancy of the animals, extending the survival by 22% over the mice treated with the vehicle[265].

Targeting PrP conversion

One key point in prion diseases is the interaction between PrP^C and PrP^{Sc} and the subsequent conversion of physiological form into the pathogenic one. Although the process of conversion is poorly understood, it is clear that interfering with the interaction between both conformers would cease the prion propagation.

β-sheet breakers are short synthetic peptides designed to have a region of homology with the central hydrophobic region of Aβ and another region of different amino acids which do not fit with the Aβ sequence. These peptides specifically bind to Aβ oligomers, but they prevent from the extension of the fibril, avoiding the incorporation of more monomers. This was translated into the prevention of neuronal death *in*

USC UNIVERSIDADE DE SANTIAGO DE COMPOSTELA

vitro, reduction of brain deposition, and blockage of amyloid fibrils formation in animal models[266]. This strategy was transferred to prion disease models designing β-sheet breakers tackling the conserved PrP residues 115-122, with an extra proline to prevent the peptide from acquiring the β-sheet structure. These β-sheet breakers avoided the PrP^{C} recruitment and reversed the PrP^{Sc} conformation to the cellular form, *in vitro*. In animal models, β-sheet breakers delayed the onset of clinical signs when the inoculum was incubated with the β-sheet breakers before inoculation. Even though this approach demonstrate that β-sheet breakers can interfere prion propagation, it would be necessary to assess that they have a similar effect in the brain, administered separately from the inoculum. Moreover, due to the poor permeability of the BBB to proteins and peptides and their high susceptibility to protease degradation, it would be of vital importance to study the pharmacological properties of these β-sheet breakers[267].

Targeting PrP trafficking

Previous studies showed that the depletion of PrP^{C} from the cell surface blocked prion propagation, supporting the idea that prion conversion requires the presence of PrP^{C} on the membrane; thus, tackling the PrP trafficking from the intracellular compartment to the cell surface and *vice versa* could reduce prion propagation [268–270].

Chlorpromazine was first hypothesized to bind PrP^{C}; however, several experiments, such as NMR and X-ray crystallography, showed that the interaction was too weak. Moreover, chlorpromazine could not avoid PrP conversion by PMCA, while the efficacy *in cellula* was evident. Further experiments in cell cultures demonstrated that chlorpromazine induces PrP^{C} and PrP^{Sc} relocalization by clathrin-mediated endocytosis, reducing PrP levels on the plasma surface[271,272] One advantage of chlorpromazine over other drugs is its capacity to cross the BBB. This fact, added to the experience of its use as an antipsychotic drug, led to combine it with quinacrine to treat prion diseases, particularly two FFI

USC UNIVERSIDADE DE SANTIAGO DE COMPOSTELA

patients. However, the combined treatment had no effect on the clinical course of the disease[273].

Promoting PrP degradation

GPI-anchored proteins, such as PrP, when aberrantly folded in the ER follow the ER-to-lysosome-associated degradation pathway in order to avoid the accumulation of toxic aggregates. Although this physiological mechanism of proteostasis just takes place in early stages of protein expression, this degradation pathway can be exploded to decrease the amount of PrP in the cell [274,275]. Based on molecular dynamics simulations, Spagnolli and collaborators rationally designed small chemical compounds that target PrP folding intermediates that would be generated in the ER during PrP expression and folding processes. These compounds bind PrP hindering the acquisition of its native conformation; therefore, it is recognized as an aberrant folded form and sent to degradation. Cell-based assays performed with these compounds demonstrated that they decrease the amount of mature PrP, and as a result, they inhibit prion replication; notwithstanding, there is still no data on its efficacy in vivo [276].

On the other hand, lysosomes also play a crucial role in PrP recycling routes: PrP in the plasma membrane is endocytosed and can be recycled and re-routed to the cell surface or sent to degradation by the lysosomes[277]. Moreover, PrP^{Sc} can be routed to lysosomes by autophagy[278]. In this regard, rapamycin, tacrolimus, or polyamines were reported to increase PrP^{Sc} clearance by promoting autophagy or lysosomal degradation. Nonetheless, when these candidates were tested *in vivo*, in prion-infected mice, they demonstrated a poor or null effect on the survival; while tacrolimus did not increase the survival of prion-infected mice, rapamycin and a polyamine, astemizole specifically, presented a modest prolongation on the survival over the control mice, 10% and 4% respectively[268,279–283].

USC UNIVERSIDADE DE SANTIAGO DE COMPOSTELA

Interfering the post conversion toxic cascade

Although many efforts have been made to target PrP^{Sc}, the mechanism of toxicity in prion diseases remains poorly understood, and although PrP^{Sc} is present in prion diseases, there is evidence that the amount of PrP^{Sc} or its infectivity are not directly related to the neurotoxicity [95,207,208,284–286]. One well-known factor involved in prion toxicity is ER stress. In prion diseases, the accumulation of misfolded PrP entails ER malfunction, and as a consequence, unfolded proteins accumulate in the cell. Moreover, aberrant forms of PrP^{C} also concentrate in the cell with a high propensity to misfold into PrP^{Sc}. The UPR is a protective cellular mechanism triggered in ER stress situations that enhances chaperone synthesis by different transcriptional pathways[287,288]. Increasing the expression of GADD34 (a phosphatase involved in UPR), the survival of prion-infected mice was prolonged and synaptic deficits and neuronal loss were rescued[289]. Guanabenz and its derivative, Sephin1, are drugs that promote the UPR response. In animal models, Sephin1 increased prion clearance in the spleen; nevertheless, it did not show an effect on the mice lifespan, probably because of its poor capacity to cross the BBB [290].

Immunotherapies for prion diseases

Even though prion diseases mainly affect the central nervous system, PrP^{C} is ubiquitously expressed. Moreover, as PrP^{C} and PrP^{Sc} share the same primary sequence and both are tolerated by the host's immune system, hampering an immune response against PrP^{Sc}. Many attempts have been made in order to overcome this tolerance and boost the activation of an immune response. Indeed, several immunization strategies showed encouraging results in misfolding protein disorders and neurodegenerative diseases, tackling both active and passive immunotherapy as promising therapeutic strategies[291–293].

Active immunization strategies are focused on breaking self-tolerance and inducing an immune response against PrP. These approaches are also based on the fact that animals in the terminal stage of prion disease

USC UNIVERSIDADE DE SANTIAGO DE COMPOSTELA

generate antibodies against PrP, denoting that misfolded PrP can promote some sort of immune response[294,295]. To explore this concept, bacterially expressed C-terminal (211-230) or PrP peptides from the central region (131-150) were inoculated in wild-type mice and demonstrated to trigger an important immune response in these animals. Moreover, antibodies generated by the host did not recognize the native PrP^{C}, which means that such epitopes could be hidden in the mature PrP^{C} after post-translational modifications[296–298]. This immunoreactivity was also obtained by inoculating truncated, modified, crosslinked PrP peptides or even heterologous PrP. However, the effect on the survival of prion-infected animals was minimal[299–303]. The use of adjuvants such as alum or Freund's adjuvant[304–306], but specially CpG-oligodeoxynucleotides (CpG) also demonstrated to boost the immune response and break the self-tolerance[307–309].

The efforts mentioned above were attempts to overcome self-tolerance, enhance the immunogenicity of PrP peptides and promote an immune response against PrP^{C}; nevertheless, PrP^{Sc} and its structural difference regarding PrP^{C} would be the ideal target of active immunization. Some attempts were focused on identifying epitopes that only were available in PrP^{Sc}. However, the PrP^{Sc} structure was not available at that moment, and the selected epitopes had not a preventive effect or even accelerated prion disease[310–313].

On the other hand, passive immunization is based on the use of PrP^{C} or PrP^{Sc}-specific antibodies. This promising approach would offer a complete abolition of PrP propagation by three mechanisms: stabilizing PrP^{C}, sterically impeding the interaction between PrP^{C} and PrP^{Sc}, and stabilizing PrP^{Sc}. In this regard, knock-out mice entailed a critical tool to develop a large variety of antibodies targeting PrP epitopes which were tested in prion-infected animals to assess their specificity and capability to delay the onset of prion diseases[314,315].

Although several antibodies demonstrated to decrease prion pathology, their efficacy essentially depends on the epitope, and targeting the

USC UNIVERSIDADE DE SANTIAGO DE COMPOSTELA

wrong epitope could trigger neurotoxicity, such as nerve cell loss, gliosis, and microglial activation. Thus, antibodies targeting the N-terminal flexible tail resulted in neuroprotective, while antibodies targeting the globular domain, especially helices α1 and α3, are neurotoxic. It was hypothesized that the toxicity of such antibodies was mediated by the PrP N-terminal tail and activated the same toxic pathways to PrP^{Sc}, including PERK, activating calpains and promoting the production of reactive oxygen species[316].

Apart from ASOs, currently, the most promising treatments against prion diseases are therapeutic antibodies. *In vivo*, the most encouraging results were obtained by intraperitoneal treatment with ICSM18 (IgG1 recognizing PrP 146–159) or ICSM35 (IgG2 targeting PrP 91-110) after inoculation. These mice accumulated much less PrP^{Sc} in the spleen and brain and lived more than 500 days with no clinical signs; thus, they were postulated for clinical trials[317]. Nonetheless, independent studies showed controversial results regarding the safety of both antibodies: one of them reported no-drug-related toxicity, whereas the other one demonstrated dose-dependent neurotoxic effects [215,317–319].

Recently, in 2018 the first-in-human treatment with a therapeutic antibody for prion diseases was conducted. The procedure enrolled 6 patients diagnosed with CJD, 5 with sCJD, and 1 with iCJD, and untreated historical controls. This study was conducted under a UK Special Licence instead of a clinical trial; the UK Special Licence allows treating individual patients with an unlicensed drug if the clinical condition cannot be treated with a licensed product on the market, such as prion diseases. The antibody, PRN100, is a humanized monoclonal antibody derived from ICSM18 (IgG4κ) and was administered intravenously. The number of patients was too small to draw conclusions about the therapeutic properties of PRN100. However, it permitted monitoring of the concentrations of the antibody in serum and CSF and to assess the safety. This study allowed to conclude that the intravenous treatment with PRN100 can cross the BBB and reach the expected therapeutic concentrations in CSF. Moreover, the absence of

USC UNIVERSIDADE DE SANTIAGO DE COMPOSTELA

side effects and the results of the autopsy showed that the treatment did not induce neurotoxicity, demonstrating that the treatment is safe [228].

Limitations in prion disease therapies

Despite years of effort looking for a treatment for prion diseases, these disorders are still uncurable. Researchers found many obstacles to overcome, some of them physiological, others derived from the pathology, and others due to the wrong designs of the experiments that were fruitless in drawing conclusions.

One of the main issues is that a large percentage of the chemical compound tested for prion diseases does not cross the BBB[216,243,251,254,320]. In animals, this handicap is overcome by injecting the treatment directly into the brain; however, this approach can hardly be translated to humans. An alternative is an intrathecal administration or the use of osmotic pumps, which connect an intraventricular catheter to allow a continuous administration of the treatment into the brain; these pumps have a homologous device for use in humans, called the Ommaya reservoir. All these approaches carry risks like infections, partial loss of brain function, or subdural hematoma, among others[321,322].

On the other hand, when PrP^{Sc}-targeting compounds were tested, it was discovered that some molecules were only effective against specific prion strains. This is the case of cpd-B or some tetracyclic antibiotics[323,324]. Although PrP^{Sc} is the same molecule, there are some architectural differences between prion strains that make them susceptible or not to be inactivated by different drugs, called strain specificity[325]. Also related to prion strains, another difficulty that limits the treatment with some promising drugs is the emergence of drug resistance[326,327]. This disappointing effect was seen after the treatment with quinacrine or IND24 and could be due to two reasons: 1) the presence of two different strains in the same host and the selection of the resistant one after the treatment or 2) the adaptation of the prion strain to the treatment[325]. The combination of different treatments was

USC UNIVERSIDADE DE SANTIAGO DE COMPOSTELA

proposed as a strategy to evade this obstacle; nevertheless, the combination of IND24 and Anle138b also concluded with the acquisition of drug resistance[328].

Finally, regarding clinical trials, many factors difficult obtaining statistically significant data. The low incidence, the rapid progression, the difficulties in obtaining an accurate diagnosis in the early stages, and the paperwork involving a clinical trial contribute to a small number of participants enrolled and patients in an advanced stage of the disease, who sometimes died before receiving the treatment. Moreover, the diversity of prion diseases regarding the origin, polymorphisms, mutations, and age at the onset entail a high heterogeneity. Finally, the difference in clinical trial design, sample collection, and the lack of standardized outcome measures make the comparison of different studies and meta-analyses a challenge[215,218,329].

Palliative cares

The absence of therapies for curing prion diseases limits the treatments to palliative care to ameliorate the condition. Most patients suffer from psychological and psychiatric symptoms, such as depression, anxiety, psychosis, and hallucinations, but also motor disorders like myoclonic jerking, rigidity, or akinesia, which require pharmacological treatments such as anxiolytics, antipsychotics, or neuroleptics. However, non-pharmacological assistance is also essential to maintain motor capabilities as long as possible; for example, a physical or speech therapist to alleviate swallowing difficulties and avoid choking and suffocation risks[330,331]

Prion diseases are rare fatal disorders with rapid progression. The diagnosis supposes to be a severe blow, not only for patients but for relatives as well; for this reason, psychological support is fundamental to deal with the situation.

USC UNIVERSIDADE DE SANTIAGO DE COMPOSTELA

Given the null therapeutic alternatives for prion, we aimed to contribute to the search for candidates to treat these disorders. Thus, this chapter describes the evaluation of two therapeutic candidates, a molecular chaperone and a conformational scFv antibody.

One of the possible therapeutical strategies against TSE is PrP^{C} stabilization by molecular chaperones, which avoid the conversion of PrP^{C} into PrP^{Sc}. Certain cyclic tetrapyrroles, such as porphyrins, were demonstrated to bind to PrP^{C}, inhibiting prion propagation *in cellula* and animal models[332].
Fe(III)-TMPyP is a cationic tetrapyrrole that binds to the structured domain of huPrP, interacting with the C-terminal region of helix α3 and the first β-strand, (Fig 2.2) and acts as a pharmacological chaperone preserving its native conformation and preventing it from misfolding. Fe(III)-TMPyP was demonstrated to inhibit prion replication *in vitro*[333] and *in cellula*, against different prion strains[334–336].
Based on the recognized activity of Fe(III)-TMPyP, we selected it as a potential candidate for the chronic treatment of prion disorders.

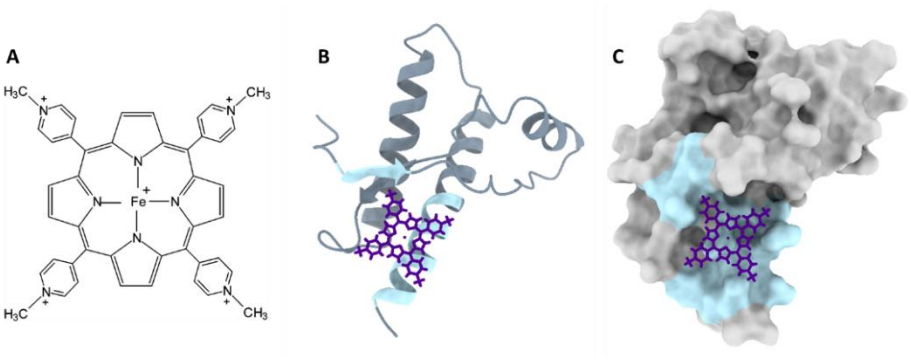


Figure 2.2. Fe(III)-TMPYP and its interaction with PrP^{C}. A) Chemical structure of Fe(III)-TMPyP. B) Cartoon image of huPrP (PDB 1QLX) and Fe(III)-TMPyP (PubChem 126456051). Fe(III)-TMPyP (purple) interacts with the C-terminal region of helix α3 and the first ß-strand (light blue) of human PrP91-231(gray). C) Surface model of huPrP (gray) and Fe(III)-TMPyP (purple) interaction. Light blue areas of huPrP indicate the site of interaction.

USC UNIVERSIDADE DE SANTIAGO DE COMPOSTELA

The second candidate was based on a passive immunization with a scFv antibody. This scFv antibody was obtained from an IgG isolated from mice immunized with a vaccine based on the 4RβS structural model, but which recognized PrP^{Sc} from brain homogenates. Given the significant interest in passive immunization for diseases like Alzheimer's, exemplified by the approval of aducanumab and lecanemab, we considered this approach based on passive immunization could also be useful in treating prion diseases.

To assess the potential anti-prion activity of these two candidates, we conducted experiments using a fast murine model of prion disease. This murine model involved transgenic mice bearing the bank vole (109I) prion protein (TgVole). Such model was selected based on the high susceptibility of bank voles to developing prion disease within a relatively short timeframe. Thus, we considered these TgVole mice as an appropriate model for evaluating the proof-of-concept of *in vivo* anti-prion activity.

USC UNIVERSIDADE DE SANTIAGO DE COMPOSTELA

3.2 SPECIFIC AIMS

Prion diseases are rare and fatal neurodegenerative disorders for which there is no treatment. The global objective of this chapter is to evaluate two therapeutic strategies in a fast murine model of prion disease. These pharmacological approaches tackle prion diseases from two different perspectives, targeting PrP^{C} and PrP^{Sc}. This global goal has been broken up into two specific objectives according to the therapeutic compound employed in each approach:

1. Evaluation of the chronic administration of a tetrapyrrole, Fe(III)-TMPyP, as a treatment against prion diseases.

2. Evaluation of the single-chain fragment variable, scFv-G1, as a chronic treatment for prion diseases.

USC UNIVERSIDADE DE SANTIAGO DE COMPOSTELA

3.3 METHODS

Reagents, materials, buffers composition, and the equipment used in this doctoral thesis are collected in Annexes I, II, III, IV, and V.

3.3.1 ETHICAL STATEMENT

All described experiments were in compliance with the guidelines included in the current Spanish regulations "Real Decreto 118/2021 de 23 de Febrero" which modifies the "Real Decreto 53/2013 de 1 de Febrero" on the protection of animals used for experimental and other scientific purposes. Both are based on the European Directive 2010/63/EU on Laboratory Animal Protection. All experiments described were performed under animal experiment permit 15005/16/006, approved by the Ethical Committee of the University of Santiago de Compostela and the Consellería del Medio Rural of the Xunta de Galicia. The procedures were carried out at Centro de Biomedicina Experimental (CEBEGA) de la Universidad de Santiago de Compostela, registered in the Spanish Register of breeding, supplier and user centers with the number ES150780292901.

3.3.2 ANIMAL MODEL AND HOUSING CONDITIONS

Bank voles (*Myodes glareolus*) are wild rodents used in prion research. Their experimental use in the prion field was first reported in the 70's decade, in a test with different rodents; in this study, bank voles (BV) were the fastest animal model in developing prion disease[337]. Later experiments demonstrated that BVs were also prone to propagate different prion strains, even from other species, developing prion

USC UNIVERSIDADE DE SANTIAGO DE COMPOSTELA

diseases in short incubation periods[338–341]. Such studies revealed their high susceptibility to prion diseases, and BVs were considered universal acceptors for prions[342].

BVPrP is polymorphic at position 109, where methionine (M) or isoleucine (I) can be present[343], and depending on the polymorphic variation, they are susceptible to different prion strains[344]. In an attempt to adapt the particularities of BVs to a laboratory animal, which is more accessible and easier to acquire, different transgenic mice bearing BVPrP sequences were developed.

The animal model used in this thesis, hereinafter TgVole, is a transgenic mouse expressing BVPrP sequence encoding isoleucine at codon 109 and with an expression level approximate that of wild-type BVs, ~1-1,2x [101]. This model was developed and generously provided by Dr. Glenn Telling from the University of Colorado.

A breeding colony was established at the Faculty of Medicine at Universidade de Santiago de Compostela. Throughout 2020, the experiments with animals at the University of Santiago were centralized at CEBEGA (Centro de Biomedicina Experimental da Universidade de Santiago de Compostela) and faced the impossibility of sending the current colony to CEBEGA, a second group of animals was sent by Dr. Joaquin Castilla, from the CIC bioGUNE, in Bilbao, and a new breeding colony of TgVole mice was established. In both cases, animals were housed in groups of 2 to 6 animals, at 22–24 °C and 60% humidity, with a controlled light/dark cycle (12 h light, 12 h darkness), food and drink *ad libitum,* and environmental enrichment.

3.3.3 PRION INOCULATION

All the procedures were conducted in microbiological containment level 2 facilities. Prion inoculation was performed in the class II microbiological safety cabinet.

USC UNIVERSIDADE DE SANTIAGO DE COMPOSTELA

Males and females of TgVole mice at the age of 4 to 8 weeks were assigned to groups of 6 to 14 individuals and were anesthetized intraperitoneally with 0.2ml/10g body weight of a 1.2%(w/v) solution of tribromoethanol (also known as Avertin). Before inoculation, the absence of paw withdrawal reflex was assessed to ensure deep anesthesia. Mice were then inoculated using a disposable 29-gauge needle with 20µL of a 1% or 0,1%(w/v) brain homogenate diluted in filtered PBS, from a terminally ill mouse inoculated with a vole-adapted CWD strain, kindly provided by Dr. Romolo Nonno, from the Istituto Superiore di Sanità, in Rome [345].

Mice were observed twice a week until the onset of clinical signs; from that moment on, they were monitored daily until they reached a terminal stage when they were euthanized by cervical dislocation and subsequent decapitation. The terminal stage was established when the animal presented feeding difficulties or body weight loss. The main clinical signs identified were kyphosis, ataxia, tremor, spastic tail, lethargy, hyperactivity, scratching, head bobbing, dull hair coat, circling, aberrant gait, priapism, dragging of hind limbs, and body weight loss.

Brains were removed and sagittally cut into two halves. One half was frozen for biochemical characterization, and the other half was fixed in 10% PFA in PBS for histopathological and immunohistochemical analysis.

3.3.4 MICE TREATMENT

Before the treatment, mice were anesthetized as was previously described in section "*3.3.3 Prion inoculation*".

3.3.4.1 Chronic treatment with Fe(III)-TMPyP

Previous works reported a neutralization of the infectious agents present in the inoculum by the therapeutic candidate at the site of inoculation when both were administrated simultaneously [346,347] In order to avoid this artifactual and therapeutically irrelevant *in situ* inactivation of the

USC UNIVERSIDADE DE SANTIAGO DE COMPOSTELA

inoculum, the treatment started 2 weeks after inoculation. The inoculation was performed as previously described and inoculated mice were divided into 2 groups: Fe(III)-TMPyP group and saline group. The Fe(III)-TMPyP group received an intracranial injection with a disposable 29-gauge needle of 20µL 0,5mM Fe(III)-TMPyP in PBS for 5 consecutive weeks, while the saline group received a similar volume of PBS for 5 weeks.

Although no side effects were reported in previous works with Fe(III)-TMPyP, mice were monitored after treatment in order to identify possible toxicity such as death, convulsions, tremor, excitation, akinesia, piloerection, scratching, spastic tail, or other evident behavioral changes[348]. Only local irritation at the site of injection was detected when we saw some mice with acute pruritus, which resolved a few hours after the treatment.

After the treatment, mice were monitored twice weekly until the onset of clinical signs.

3.3.4.2 Therapeutic treatment with scFv-G1

The scFv-G1 antibody was developed and sent by Holger Wille from the University of Alberta. After assessing its activity by ELISA (see below), the antibody was diluted to a final concentration of 0,5mg/mL. A group of mice was inoculated as previously described, and 2 weeks after inoculation, mice were separated into 2 groups, the scFv-G1 group and the saline control group. The scFv-G1 group received an intracranial injection of 20µL of 0,5mg/mL of scFv-G1 with a disposable 29-gauge needle, whereas the saline control group received 20µL of PBS by the same route. The treatment was repeated weekly for 5 weeks. Mice were monitored twice a week until the onset of clinical signs.

It was previously reported that intracranial injection of antibodies which recognize the globular domain of the native PrP could trigger neurotoxicity and neuronal death[265,349]. Although this antibody is structurally specific for PrP^{Sc}, mice were monitored after the treatment

USC UNIVERSIDADE DE SANTIAGO DE COMPOSTELA

in order to identify possible side effects such as death, convulsions, tremor, excitation, akinesia, piloerection, scratching, spastic tail, or other evident behavioral changes[348]. After assessing the innocuity of the treatment, mice were then monitored twice a week until the onset of clinical signs.

3.3.5 Assessment of scFv-G1 activity by ELISA

Every day before treating the mice, the activity of the antibody was assessed by competitive enzyme-linked immunosorbent assay (ELISA) to test whether the shipping conditions and thawing process did not affect its quality (Fig 2.3).

Holger Wille's group provided us with small aliquots of scFv-G1 antibody, an ELISA plate with 5 µg of antigen-coated, and an unmodified G1 antibody.

The strip was washed 3 times with 200µL 0.05% PBS-T. Subsequently, 100µL of the scFv-G1 antibody was added at different dilutions in PBS (1:200 and 1:50) and incubated for 3h RT. After the incubation, the strip was washed 3 times with 200 µL 0.05% PBS-T, followed by the addition of 100µL of the parent G1 antibody at a concentration of 1:15000, and it was incubated for 1h RT. The strip was then washed again with 200µL 0.05% PBS-T followed by the addition of 100µL of goat anti-mouse conjugated with horseradish peroxidase (HRP) secondary antibody at a concentration of 1:50000. The secondary antibody was incubated for 1h RT and washed with 200µL 0.05% PBS-T. Then, 100µL of TMB was added and incubated at RT for 10min until the blue color was developed. Finally, the reaction was stopped by adding 50µL 2M H_2SO_4 and the plate was read at 450nm.

A negative control was also included, which consisted of incubating the G1 parent antibody with the antigen in the absence of the scFv-G1 antibody.

USC UNIVERSIDADE DE SANTIAGO DE COMPOSTELA

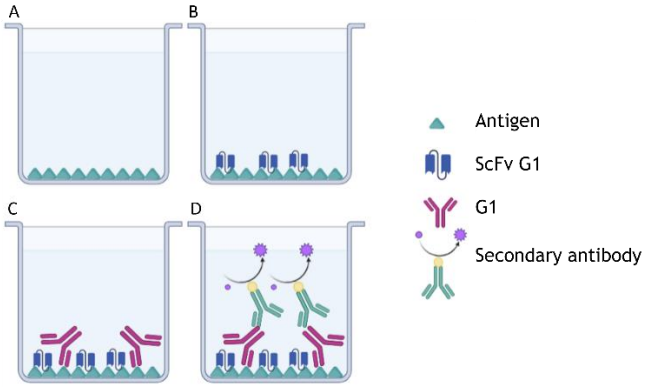


Figure 2.3. Outline of competitive ELISA assay. A) Antigen-coated plate. B) scFv-G1 antibody was added and bonded to the antigen. C) G1 antibody, which also recognizes the antigen, competed with scFv-G1. D. An enzyme-conjugated secondary antibody that only binds to the effector part of the G1 antibody was added. The intensity of the coloured solution is inversely proportional to the binding of scFv-G1 to the antigen.

3.3.6 PREPARATION OF BRAIN HOMOGENATES

Frozen brains were suspended at 10% (w/v) in PBS and protease inhibitors cocktail and were homogenized using a Dounce homogenizer until it was a homogeneous mixture. Brain homogenates were stored at -80°C.

3.3.7 PROTEINASE K DIGESTION AND WESTERN BLOT ANALYSIS.

For biochemical characterization of PK-resistant material by Western blot, 10µL of brain homogenate were diluted with the same volume of PBS and digested with PK at a final concentration of 50µg/mL for 1h at 42°C and 800rpm. Subsequently, 5x Laemmli sample buffer was added and heated for 10min, at 99°C and 800 rpm. Proteins were then separated in 4-12% precast Bis-Tris gels and transferred to a 0,45µm polyvinylidene fluoride (PVDF) membrane. The membrane was blocked for 1h in a 5% blocking buffer. Subsequently, the membrane was incubated with SAF83 (1:400) (epitope 130-160) or anti-β-tubulin

USC UNIVERSIDADE DE SANTIAGO DE COMPOSTELA

(1:1000) in a 1% blocking buffer. After incubation, the membrane was washed 3 times with TBS-T for 10min, and then the HRP conjugated anti-mouse secondary antibody (1:10000) diluted in TBS-T was added and incubated for 1h. After washing three times with TBS-T, the signal was revealed using Pierce ECL Western Blotting substrate or Immobilon Forte Western HRP substrate. Images were obtained with ChemiDoc MP Imaging System and analyzed using Image Lab software.

3.3.8 HISTOPATHOLOGICAL AND IMMUNOHISTOCHEMICAL ANALYSIS

Histopathological and immunohistochemical assays were carried out by Enric Vidal and Samanta Giler at CRESA.

For histopathological analysis, transversal sections of the fixed brains were performed at the levels of the medulla oblongata, piriform cortex, and optic chiasm. Samples were embedded in paraffin-wax after dehydration through increasing alcohol concentrations and xylene. For morphological evaluation, 4µm sections were mounted on glass microscope slides and stained with hematoxylin and eosin.

For immunohistochemical analysis, sections were mounted in 3-trietoxysilil-propilamine-coated glass microscope slides. Deparaffinized sections were subjected to epitope unmasking treatments immersing in formic acid and boiling at low pH (6.15) in a pressure cooker and pre-treating with proteinase K. Endogenous peroxidases were blocked by immersion in a 3 % H_2O_2 in methanol solution. Subsequently, sections were incubated overnight with anti-PrP 6C2 monoclonal antibody(1:1000), and visualized with the Goat anti-mouse EnVision system, using 3,3'-diaminobenzidine as the chromogen substrate. As a background control, incubation with the primary antibody was omitted.

Mouse spongiform lesions and PK-resistant immunolabeling were evaluated following a semiquantitative approach previously described

USC UNIVERSIDADE DE SANTIAGO DE COMPOSTELA

[350]. Briefly, fourteen different brain areas were examined (Fig 2.4): piriform cortex (Pfc), hippocampus (H), occipital cortex (Oc), temporal cortex (Tc), parietal cortex (Pc), frontal cortex (Fc), striatum (S), thalamus (T), hypothalamus (HT), mesencephalon (M), medulla oblongata (Mobl), cerebellar nuclei (Cm), cerebellar vermis (Cv) and cerebellar cortex (Cc), and the spongiform lesion for each area was scored from (0) absence of spongiosis, (1) mild, (2) moderate, (3) intense and (4) maximum level of lesion. Each area was investigated globally as region for the scoring. Brain lesion profiles were plotted considering the anatomical regions and the mean of the semiquantitative score for each area. Error bars represent the standard error of the mean [350].

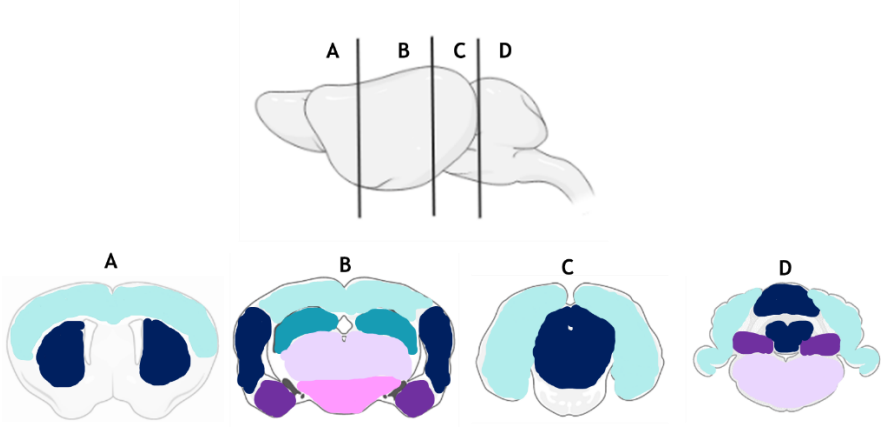


Figure 2.4. Brain sections for histopathological analysis. Mice brains were cut in four sections (A, B, C and D) and the following brain areas were examined: A) frontal cortex (Fc), in light blue; striatum (S), in dark blue; B) parietal cortex (Pc), in light blue; temporal cortex (Tc), in dark blue; piriform cortex (Pfc), in dark purple; hippocampus (H),in turquois; thalamus (T) in light lilac; hypothalamus (HT), in pink; C) occipital cortex (Oc), in light blue; mesencephalon (M), in dark blue; D) cerebellar cortex (Cc), in light bue; cerebellar nuclei (Cm), in dark purple; cerebellar vermis (Cv), in dark blue and medulla oblongata (Mobl), in light lilac.

USC UNIVERSIDADE DE SANTIAGO DE COMPOSTELA

3.3.9 KINETICS OF FE(III)-TMPYP DISTRIBUTION IN BRAIN

A group of 16 mice was anesthetized with Avertin, as previously described. An incision was performed to expose the skull and Fe(III)-TMPyP was injected intracerebrally approximately 1mm lateral to the bregma and 3mm deep perpendicularly to the skull surface in order to reach the lateral ventricle. Mice were euthanized immediately after the injection or after 10min, 30min, 1h, 2h, 3h, or 24h. Two mice received saline buffer instead of Fe(III)-TMPyP as negative controls and were euthanized immediately after the administration.

Mice were euthanized at different time points, and their brains were collected and immersed in 4% paraformaldehyde in PBS for 24h at 4°C. Subsequently, brains were cryopreserved and immersed in 30% sucrose at room temperature. Samples were frozen at -20°C, and caudal sections at 30µm thickness were obtained using a cryostat. The cryosections were stained with 4 ',6-diamidino-2-fenilindol (DAPI), and slides were visualized using a microscope of fluorescence Leica DM4 B, with the 10X objective. Images were then analyzed with LAS X software.

3.3.10 STATISTICAL ANALYSIS

Statistical analyses were performed using Graph Pad Prism 8.

Descriptive statistics such as mean, standard deviation, or the standard error of the mean were calculated for each group of mice. Survival time was expressed as mean±SEM.

Kolmogorov–Smirnov test for individual datasets was tested for normality. Student's t-test was applied to all datasets with two tails, according to the result of the Kolmogorov–Smirnov test.

The graphical representation of survival time was plotted as the percentage of survival and was analyzed by the Kaplan-Meier test. The results were contrasted by the *log-rank* (Mantel-Cox) test, and a ρ value$\leq$0.05 was considered statistically significant.

USC UNIVERSIDADE DE SANTIAGO DE COMPOSTELA

All groups of mice were tested for outliers by Grubbs' test with $\alpha=0.05$. Identified outliers were removed.

A one-way ANOVA followed by *post hoc* tests was also performed to assess the difference between treated and control groups. A ρ value≤ 0.05 was considered statistically significant.

USC UNIVERSIDADE DE SANTIAGO DE COMPOSTELA

3.4 RESULTS

3.4.1 ASSESSMENT OF THE ANTI-PRION ACTIVITY OF FE(III)-TMPYP IN A FAST MURINE MODEL OF PRION DISEASE

The broad knowledge about the mechanism of action of Fe(III)-TMPyP and its previous encouraging results led us to test a chronic administration in a fast murine model of prion disease. This study was a proof of concept with a view to assessing it in a human model of prion disease in case of promising results were achieved.

A total of 28 mice were inoculated intracerebrally with 20µL of 1% brain homogenate from a terminally sick mouse inoculated with a vole-adapted CWD strain. Two weeks after inoculation, mice were divided into two groups: one group of mice was treated intracerebrally with 20µL 0.5mM Fe(III)-TMPyP, and the other group, a saline control group, received 20µL of a saline buffer. After the treatment, mice were observed in order to identify possible side effects due to the intracranial administration of Fe(III)-TMPyP. Some animals displayed slight pruritus at the site of inoculation minutes after administration. This local irritation lasted a few hours after the treatment. The treatment was repeated weekly for 5 weeks. At the end of the treatment, 7 out of the 28 mice had died because of the anesthesia, the procedure, or intercurrent diseases; 3 animals belonged to the treated group, while 4 mice belonged to the saline group.

The attack rate for both groups was 100%, and all the mice presented neurological signs such as ataxic gait, head bobbing, and hyperactivity. The mean survival time of mice treated with Fe(III)-TMPyP was 71,2 ± 1,2dpi, while the saline group had an average survival time of 71,0 ± 2,1dpi; the log-rank statistical analysis demonstrated that there were no statistically significant differences between both groups indicating that

USC UNIVERSIDADE DE SANTIAGO DE COMPOSTELA

Fe(III)-TMPyP did not delay the onset of clinical signs neither prolonged the survival time of mice inoculated with a vole-adapted CWD strain (Fig 2.5).

A

Group	Inoculation	Treatment	Dosing regimen	Attack rate	Mean ± SEM	p value
Fe(III)-TMPyP	20µL 1% BH	20µL 0,5mM Fe(III)-TMPyP, i.c.	Days 14, 21, 28, 35, 42 after inoculation	11/11*	71,2 ± 1,2	0,4970
Saline		20µL 0,9% saline, i.c.		10/10*	71 ± 2,1	

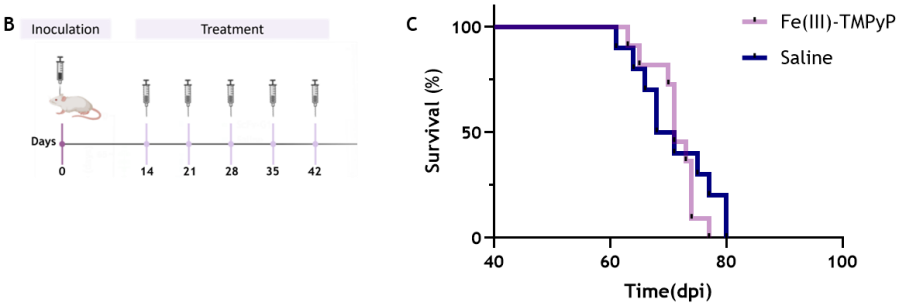


Figure 2.5. Chronic treatment with Fe(III)-TMPyP did not prolong the survival of prion-infected mice. A) Two groups of mice were inoculated with 20µL of 1% brain homogenate from a terminally ill mouse inoculated with vole-adapted CWD. All the mice succumbed to prion disease, and the mean incubation time was calculated for both groups. Log-rank test showed no statistically significant differences between the group of mice that received Fe(III)-TMPyP and the saline group (p=0.4970). Asterisk (*) indicates that one or more mice died during the procedure or due to intercurrent diseases; these mice were not included in the statistical analysis or the Kaplan-Meier curve. B) Time course of the treatment. Two weeks after inoculation, mice were treated intracerebrally with Fe(III)-TMPyP or saline. The treatment was repeated weekly for 4 weeks. C) Survival curve of mice treated with Fe(III)-TMPyP or saline. The survival endpoint of animals treated with Fe(III)-TMPyP (light purple)(n=11) or saline (dark blue)(10) was plotted on a Kaplan-Meier survival curve.

USC UNIVERSIDADE DE SANTIAGO DE COMPOSTELA

Proteinase K digestion and Western blot analysis performed with frozen brains demonstrated that both groups accumulated PrP^{Sc}. Unexpectedly, densitometric and statistical analysis of Western blots showed that the amount of PrP^{Sc} in the brains of mice treated with Fe(III)-TMPyP was lower in comparison with non-treated animals (ρ=0,0246), displaying a reduction of the PrP^{Sc} accumulation of 49%, while there was no statistically significant difference in the amount of total PrP (ρ=0,6773) (Fig 2.6).

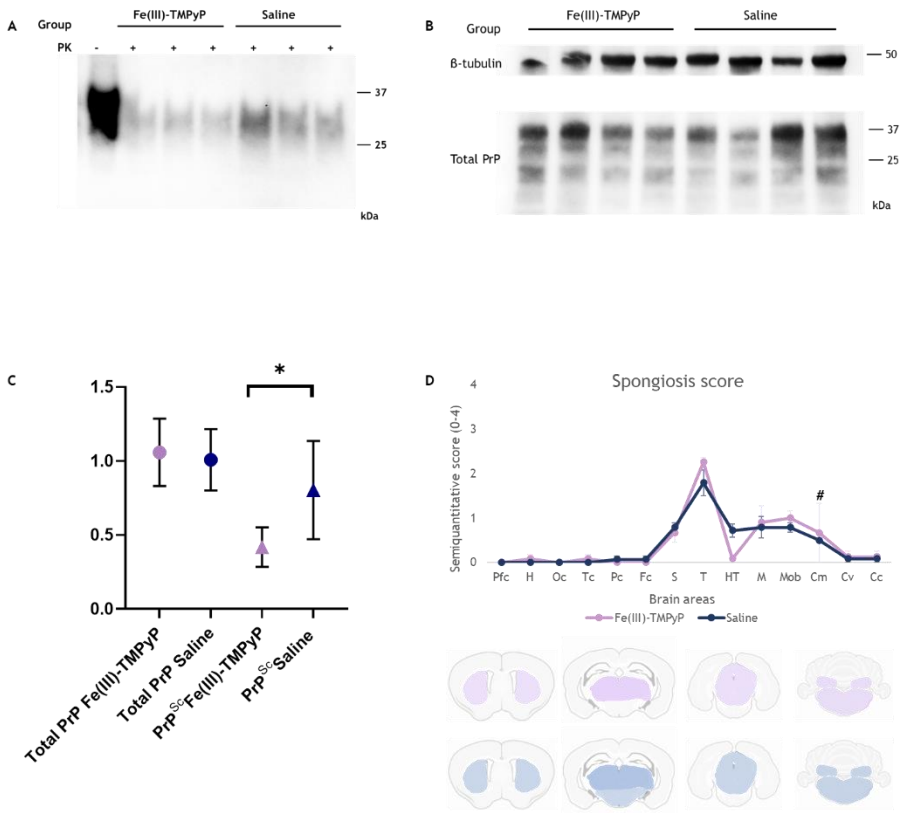


Figure 2.6. Chronic treatment with Fe(III)-TMPyP did not modify the pathology compared to the saline group A) The accumulation of PK-resistant material was

USC UNIVERSIDADE DE SANTIAGO DE COMPOSTELA

assessed by Western blot using SAF83 antibody (1:400) (epitope 130-160). B) Western blot of total PrP and tubulin of treated and control mice. Undigested samples from brain homogenates were subjected to Western blot analysis to assess the total amount of PrP and the loading control, ß-tubulin (1:1000). C) Densitometric analysis of total PrP (circle) and PrP^{Sc} (triangle) normalized by the loading control showed statistically significant less amount of PrP^{Sc} (ρ=0,0246) in brains of mice treated chronically with Fe(III)-TMPyP(light purple) in comparison with control mice (dark blue), whereas the total PrP of mice treated with Fe(III)-TMPyP (light purple) and control mice (dark blue) is essentially the same (ρ=0,6773). Error bars represent the SD and asterisk (*) indicates statistical significance. D) The brain lesion profile of mice traeated with Fe(III)-TMPyP (light purple line) (n=6) or saline buffer (dark blue line) (n=7) represents the mean semi-quantitative scoring (0–4, vertical axis) of the spongiform lesions against the following brain regions: Pfc: piriform cortex, H: hippocampus, Oc: occipital cortex, Tc: temporal cortex, Pc: parietal cortex, Fc: frontal cortex, S: striatum, T: thalamus, HT: hypothalamus, M: mesencephalon, Mob: medulla oblongata, Cm: cerebellar nuclei, Cv: cerebellar vermis, Cc: cerebellar cortex. The spongiosis score was essentially similar for both groups that presented moderate vacuolation in the thalamus, and slight affectation of the striatum, mesencephalon and medulla oblongata. Error bars represent the SEM and hash (#) indicates that the pointed-out brain area could not be examined in all the samples.

To determine the effect of the treatment on the microscopic pathology, fixed brains were stained with hematoxylin and eosin. Histopathological examination of the brains of both groups showed a characteristic spongiform lesion profile of prion disease. This pattern was essentially the same for both groups demonstrating that the chronic treatment with Fe(III)-TMPyP did not modify the pathology in comparison with the saline group. The spongiosis score determined moderate vacuolation in the thalamus and mild affectation of the basal ganglia, concretely the corpus striatum, in addition to the mesencephalon and medulla oblongata. Immunohistochemical staining using the monoclonal antibody 6C2 did not successfully detect PK-resistant PrP (PrP^{res}) deposits in the brains of both animal groups.

3.4.2 scFv-G1 antibody as a therapeutic strategy for prion diseases

Passive immunization is one of the few therapeutic strategies that has achieved successful enough results *in vivo* to reach clinical trials, not only for prion diseases[228] but also for other neurodegenerative diseases

USC UNIVERSIDADE DE SANTIAGO DE COMPOSTELA

such as Alzheimer's disease[351], Parkinson's disease[292], Huntington disease[293] or ALS[352].

Based on the structural differences among the PrP^{C} and the 4RβS model proposed for the PrP^{Sc} structure[353], Holger Wille and colleagues from the University of Alberta designed a structure-based vaccine for prion diseases.

For this purpose, they used the fungal prion HET-s as the scaffold to harbor the epitope based on specific amino acids displayed on the surface of the 4RβS. HET-s has a two-rung β-solenoid architecture [354] ; thus, to simulate the 4RβS structure and bear the epitope, two molecules of HET-s were linked (HET-2s) and mutated strategically to replace certain amino acids for others present in the prion protein (353)[355,356]. This molecule was bacterially expressed and fibrillated, assessing that the fibrils morphology was similar to the native HET-s fibrils.

The epitope of the vaccine was composed of two clusters of amino acids located in the intrinsically disordered region and the helix α1, respectively, Lys 105, Ans 107, Lys109, and His110, and Asp143, Glu145, and Asp146 (mouse sequence), in the PrP^{C} conformation. These two clusters of amino acids are separated by a distance of 35Å in the native conformation, while in the model of the 4RβS, both groups of amino acids are located in the first and second rung, one on top of the other, specifically separated by a distance of 4,8 Å, which is the distance between hydrogen-bonded β-strands. In contrast, in the PIRIBS architecture, the distance that separates both clusters of amino acids is approximately 27Å (measured with ChimeraX).

Against all odds, Wille and collaborators showed that mice immunized with this vaccine developed antibodies that specifically recognized PrP^{Sc} present in brain homogenates from mice inoculated with different prion strains[357]. Furthermore, TgP101L mice immunized with this vaccine, a mouse model that naturally develops a GSS syndrome, experimented an extension of the survival of 250% in comparison with

USC UNIVERSIDADE DE SANTIAGO DE COMPOSTELA

unimmunized animals or animals that received the HET-2s scaffold without the PrP epitope (Fig 2.7) [357].

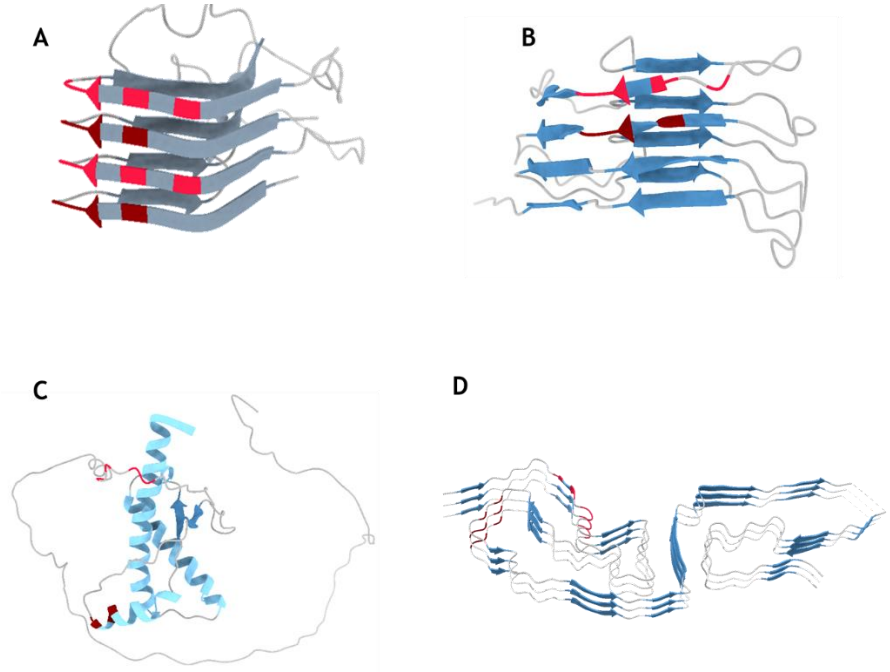


Figure 2.7 Epitope locations in different PrP architectures. The epitope, Lys105, Asn107, His110, and Lys109 are in light red, Asp143, Glu145, and Asp146 are in dark red. A) HET-s (PDB 2KJ3) dimer with the epitope in red. The HET-s sequence was mutated to link two monomers and display the epitope on its surface. HET-s ß-solenoid architecture is similar to the 4RßS model and served as a scaffold to harbor the epitope[354]. B) 4RßS model with the epitope in red. The 4RßS was proposed as possible architecture of PrP^{Sc}; in this conformation, a monomer or PrP is organized in 4 rungs, and the epitope is comprised of amino acids located in the first and second rungs[196]. C) Structure of mouse PrP^{C} obtained from AlphaFold (UniProt P04925) with the amino acids involved in the antibody epitope in red[358]; one part of the epitope is located in the intrinsically unstructured domain (light red), while the other amino acids are in the helix α 1 (dark red)[359] D) PIRIBS architecture with the epitope in red [110]. In contrast with the 4RßS model, in the PIRIBS conformation (PDB 7LNA) the amino acids that comprise the epitope are separated by a distance of 27Å approximately. Image created with ChimeraX(359)

USC UNIVERSIDADE DE SANTIAGO DE COMPOSTELA

A monoclonal IgG antibody (YEG mAb G1) was selected and engineered to be expressed in *E.coli* as humanized recombinant single chain variable region antibody (scFv-G1). In this thesis, the anti-prion activity of scFv-G1 was assessed in TgVole mice from the point of view of a chronic treatment.

Several studies demonstrated that chronic passive immunization extended the survival of prion-infected mice when they were administered either via intraperitoneal or intraventricular infusion[320,360–362].

Based on these previous studies, we decided to try a therapeutic approach focused on chronic treatment via intracerebral. Thus, a group of 24 mice was inoculated intracerebrally with 20µL of 1% brain homogenate of a vole-adapted CWD strain. Two weeks after inoculation, animals were divided into 2 groups of 12 mice each and were treated weekly for 5 weeks with 20µL 0.5mg/mL of scFv-G1 or 20µL of a saline buffer. Mice were observed after administering the antibody in search of acute side effects, but fortunately, the antibody was well-tolerated, and none was observed. Subsequently, animals were monitored and euthanized when they were terminally sick. At the end of the treatment 4 mice, 2 of each group, had died during the procedure or because of intercurrent diseases.

All mice developed clinical signs characterized by kyphosis, ataxia, hyperactivity, head bobbing, and body weight loss. The group of mice that receive the antibody had an average survival time of 63,3±0,7 dpi, whereas the incubation period for control mice was 61,9±1,0 dpi. The log-rank test showed no statistically significant differences between the group of mice that received the treatment and the saline group (ρ=0,3094). The Western blot performed with brain homogenates from animals of both groups revealed that the presence of PK-resistant material in the samples was essentially the same (Fig 2.8).

Anatomopathological analysis of brains of mice belonging to both groups showed that, independently of the treatment, all the animals

USC UNIVERSIDADE DE SANTIAGO DE COMPOSTELA

presented a similar lesion profile with vacuolation in the brain stem and the striatum. Immunolabeling of PrP^{res} using the monoclonal antibody 6C2 could not detect deposits in the brains of these animals.

A

Group	Inoculation	Treatment	Dosing regimen	Attack rate	Mean ± SEM	p value
ScFv-G1	20µL 1% BH	20uL 0,5mg/mL, i.c.	Days 14, 21, 28, 35, 42 after inoculation	10/10*	63,3 ± 0,7	0,3094
Saline		20µL 0,9% saline, i.c.		10/10*	61,9 ± 1,0	

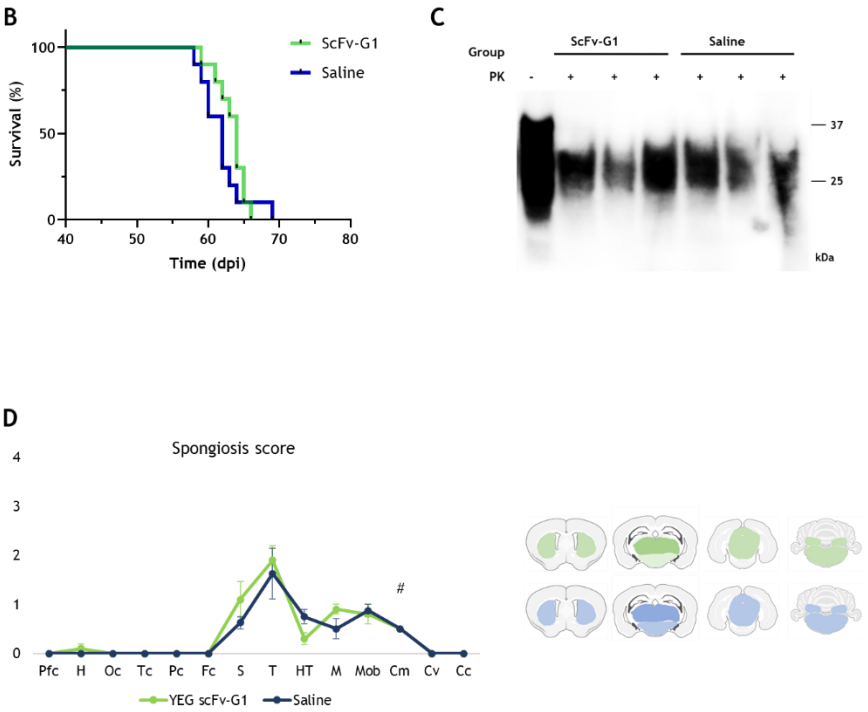


Figure 2.8 Therapeutic treatment with scFv-G1 did not extend the survival time of prion-infected mice nor modified the pathology in comparison with the saline group. A) Two groups of mice were inoculated with 20µL of 1% brain homogenate from a terminally ill mouse inoculated with vole-adapted CWD. All the mice succumbed to prion disease and the mean incubation time was calculated for both

USC UNIVERSIDADE DE SANTIAGO DE COMPOSTELA

groups. Log-rank test showed no statistically significant differences between the group of mice that received scFv-G1 (n=10) and the saline group (n=10) (p=0.3094). Asterisk (*) indicates that one or more mice died during the procedure or due to intercurrent diseases; these mice were not included in the statistical analysis or the Kaplan-Meier curve. B) Survival curve of mice treated with scFv-G1 or saline. The survival endpoint of animals treated with scFv-G1 (light green)(n=10) or saline (dark blue)(n=10) was plotted on a Kaplan-Meier survival curve. C) The accumulation of PK-resistant material was assessed by Western blot using SAF83 antibody (1:400) (epitope 130-160). D) The brain lesion profile of mice treated with scFv-G1 (light green) (n=5) or saline buffer(n=4) represents the mean semi-quantitative scoring (0-4, vertical axis) of the spongiform lesions against the following brain regions: Pfc: piriform cortex, H: hippocampus, Oc: occipital cortex, Tc: temporal cortex, Pc: parietal cortex, Fc: frontal cortex, S: striatum, T: thalamus, HT: hypothalamus, M: mesencephalon, Mob: medulla oblongata, Cm: cerebellar nuclei, Cv: cerebellar vermis, Cc: cerebellar cortex. The spongiosis score was essentially similar for both groups that presented moderate vacuolation in the thalamus, and slight affectation of the striatum, mesencephalon, hypothalamus and medulla oblongata. Error bars represent the SEM and hash (#) indicates that the pointed-out brain area could not be examined in all the samples.

3.4.3 Chronic treatment with Fe(III)-TMPyP and scFv-G1 of mice challenged with lower doses of prions

The negative results obtained after a chronic treatment with Fe(III)-TMPyP and scFv-G1 led us to consider that the lack of activity could be due to the high concentration and aggressivity of the inoculum. For this reason, both experiments were repeated using a diluted version of the same vole-adapted CWD inoculum, in order to assess if both treatments showed *in vivo* efficacy in mice inoculated with lower doses of prions.

3.4.3.1 Fe(III)-TMPyP does not delay the prion disease in TgVole mice infected with a diluted vole-adapted CWD inoculum.

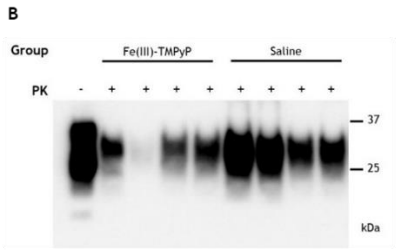
A group of 18 mice was inoculated intracerebrally with 20µL of 0,1% brain homogenate from a terminally sick mouse inoculated with vole-adapted CWD. The posology was similar to the previous experiment. Briefly, one group of 7 mice was treated intracerebrally with 20µL

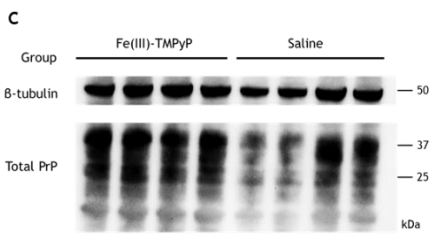
USC UNIVERSIDADE DE SANTIAGO DE COMPOSTELA

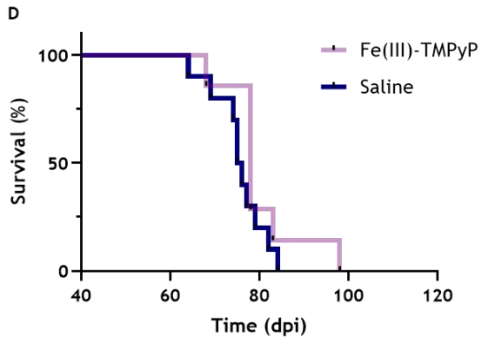
0.5mM Fe(III)-TMPyP, and the control group, composed of 11 mice, received 20µL of a saline buffer. The treatment started 14 days after inoculation, and it was repeated weekly for 5 weeks.

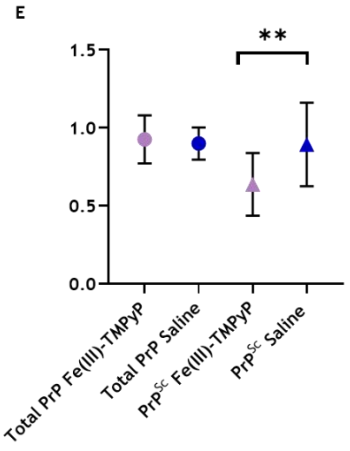
A

Group	Inoculation	Treatment	Dosing regimen	Attack rate	Mean ± SEM	p value
Fe(III)-TMPyP	20µL 0,1% BH	20µL 0,5mM Fe(III)-TMPyP, i.c.	Days 14, 21, 28, 35, 42 after inoculation	7/7	80,1 ± 3,4	0,1809
Saline		20µL 0,9% saline, i.c.		10/10	75,5 ± 1,8	









USC UNIVERSIDADE DE SANTIAGO DE COMPOSTELA

Figure 2.9 Chronic treatment with Fe(III)-TMPyP after inoculation with a diluted inoculum neither extend the survival of prion-infected mice nor modified the pathology in comparison with the saline group. A) Two groups of mice were inoculated with 20µL of 0.1% brain homogenate from a terminally ill mouse inoculated with vole-adapted CWD. All the mice succumbed to prion disease, and the mean incubation time was calculated for both groups. Log-rank test showed no statistically significant differences between the group of mice that received Fe(III)-TMPyP and the saline group (p=0.1809). B) The accumulation of PK-resistant material was assessed by Western blot using SAF83 antibody (1:400) (epitope 130-160). C) Western blot analysis of non-digested samples showed a similar amount of tubulin and total PrP in brain homogenates of both groups). D) Survival curve of mice treated with Fe(III)-TMPyP or saline. Mice were observed twice a week to identify clinical signs, after the onset of the clinical phase, mice were monitored daily and euthanized when they were terminally sick. The survival endpoint of animals treated with Fe(III)-TMPyP (light purple)(n=7) or saline (blue)(n=10) was plotted on a Kaplan-Meier survival curve. E) Statistical analysis demonstrated that animals treated with Fe(III)-TMPyP accumulated less amount of PK-resistant PrP (light purple triangle) compared to control mice (dark blue triangle) when the samples were normalized by the loading control; on the contrary, the amount of total PrP (circles) was essentially the same in both groups. Error bars represent the SD and asterisk (*) indicates statistical significance.

The incubation period of mice treated with Fe(III)-TPMyP was 80,1±3,4 dpi, while for mice treated with saline buffer, the mean incubation time was 75,5±1,8dpi. The log-rank test showed no statistically significant differences between the group of mice that received Fe(III)-TMPyP and the saline group (ρ=0,1809), demonstrating again that Fe(III)-TMPyP does not delay the prion disease, even in a better scenario with a diluted inoculum.

However, as seen with the more concentrated inoculum, Western blot analysis of PK-digested brain homogenates also showed that mice treated with Fe(III)-TMPyP accumulated statistically significant less amount of PK-resistant PrP (ρ=0,0020), although this difference was not reflected in their survival time. Regarding total PrP, there were no statistically significant differences between the group treated with Fe(III)-TMPyP and the saline group (ρ=0,5975). Mice treated with Fe(III)-TMPyP presented 28,6% less PK-resistant PrP in comparison with those animals that received saline buffer.

USC UNIVERSIDADE DE SANTIAGO DE COMPOSTELA

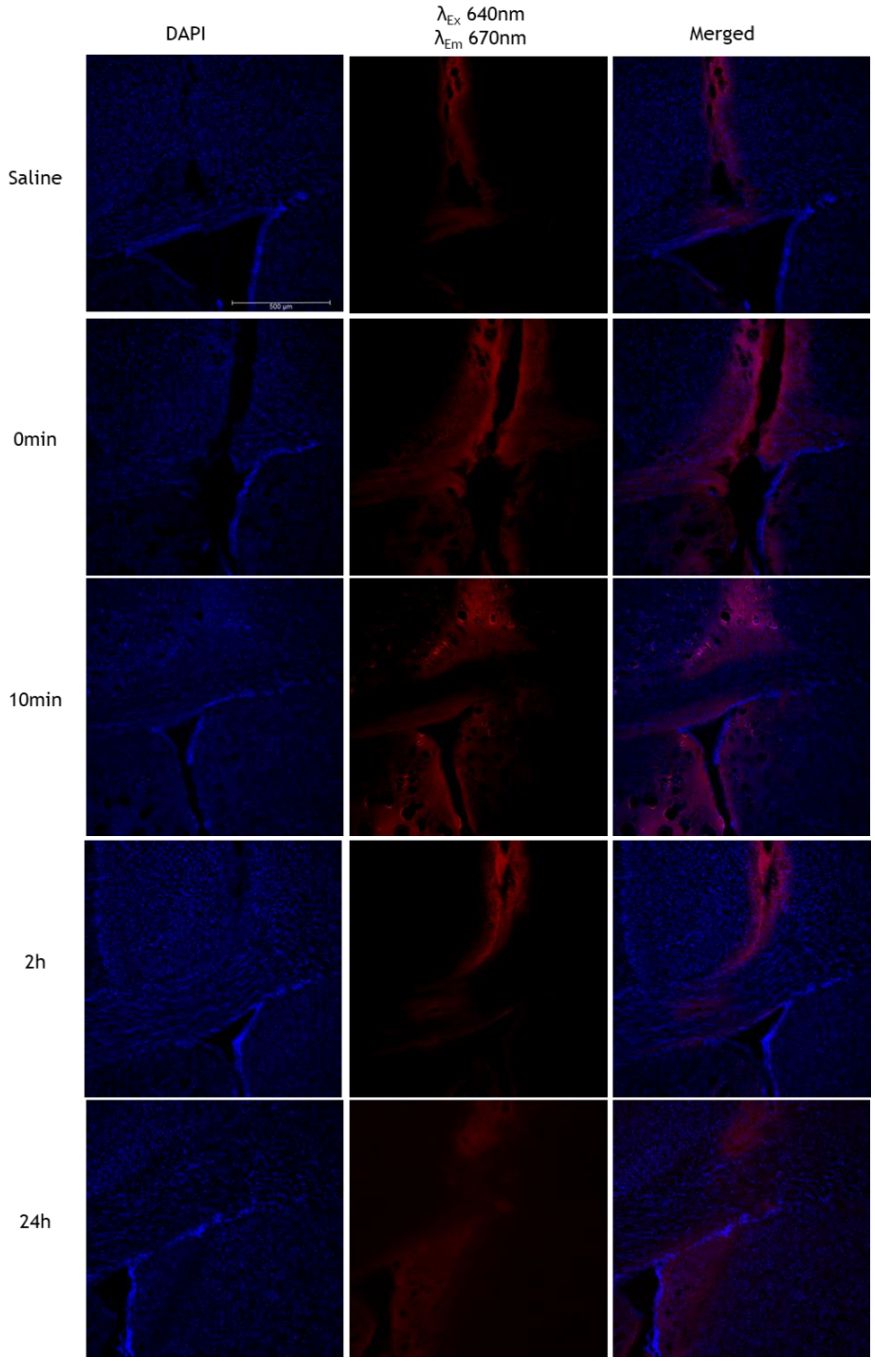
3.4.3.2 Fe(III)-TMPyP does not efficiently spread throughout the brain parenchyma

In view of the slight but significant decrease of PrP^{Sc} in the brains of animals treated with Fe(III)-TMPyP we wondered if such a result was due to a local effect of Fe(III)-TMPyP in the site of injection.

In order to study Fe(III)-TMPyP kinetics of distribution throughout the brain, a preliminary evaluation was carried out, taking advantage of the natural autofluorescence of porphyrins (λ_{ex}~450-650nm, λ_{em}~600-700nm)[363]. Fe(III)-TMPyP was injected intraventricularly, and mice were euthanized at different time points. Nuclei were stained with DAPI, and slides were visualized under the fluorescence microscope. Fe(III)-TMPyP autofluorescence was visualized in the red channel using λ_{ex} 640nm and λ_{em} 670nm. Red fluorescence was observed at different time points in the lateral ventricle, even after 24h; however, this fluorescence was limited to the area surrounding the site of injection, and there was no evidence of spreading throughout the parenchyma.

It would be expected to observe a spread of the fluorescence in case of diffusion throughout the brain or a decrease on the fluorescence, in case of clearance of Fe(III)-TMPyP; nonetheless, between 2 and 24h, the intensity of the fluorescence and the area encompassed was essentially similar, indicating that Fe(III)-TMPyP could be very slowly cleared from the site of inoculation.

USC UNIVERSIDADE DE SANTIAGO DE COMPOSTELA



USC UNIVERSIDADE DE SANTIAGO DE COMPOSTELA

Figure 2.10. Fluorescence images of brain cryosections. Cryosections of the lateral ventricle were visualized with the blue (DAPI) and red (Fe(III)-TMPyP) channels, and both images were merged. A group of 16 mice was anesthetized, and Fe(III)-TMPyP was injected into the brain, taking as reference the bregma to deposit the treatment in the lateral ventricle. Two mice received saline instead of Fe(III)-TMPyP. The mice that received saline and two mice injected with Fe(III)-TMPyP were euthanized immediately after the administration. The remaining mice were euthanized after 10min, 30min, 1h, 2h, 3h, and 24h. Their brains were fixed and cryopreserved before taking coronal slides with a cryostat. Nuclei were stained with DAPI while it was taken advantage of the natural autofluorescence of Fe(III)-TMPyP to visualize the distribution. It can be observed the red fluorescence of Fe(III)-TMPyP surrounding the site of inoculation at different time points.

3.4.3.3 A therapeutic administration of scFv-G1 does not delay the clinical course of prion disease with a diluted inoculum

To assess if the treatment with scFv-G1 antibody was effective in more favorable conditions, a group of 26 TgVole mice receive an intracranial inoculation with 20µL of 0,1% brain homogenate of a vole-adapted CWD strain. After 2 weeks, mice were grouped into treatment and control groups, which received 20µL 0.5mg/mL of scFv-G1 antibody or 20µL of a saline buffer. The treatment was repeated weekly for 5 weeks via intracerebral. At the end of the treatment, mice were monitored twice a week before the onset of the prion disease or daily during the course of the illness until they reach the terminal stage. At this point, mice were euthanized.

All the animals developed neurological signs characterized by kyphosis, ataxia, head bobbing, and body weight loss. The group of mice that receive the antibody had an average survival time of 72,8±1,6 dpi, whereas the incubation period for control mice was 75,1±1,7 dpi. The log-rank test showed no statistically significant differences between both groups of mice (ρ=0,2508).

The Western blot analysis performed with brain homogenates from animals of both groups revealed that both groups accumulated PK-resistant material in equal proportions.

USC UNIVERSIDADE DE SANTIAGO DE COMPOSTELA

A

Group	Inoculation	Treatment	Dosing regimen	Attack rate	Mean ± SEM	p value
ScFv-G1	20µL 0,1% BH	20uL 0,5mg/mL, i.c.	Days 14, 21, 28, 35, 42 after inoculation	13/13#	72,8 ± 1,6	0,2508
Saline		20µL 0,9% saline, i.c.		13/13#	75,1 ± 1,7	

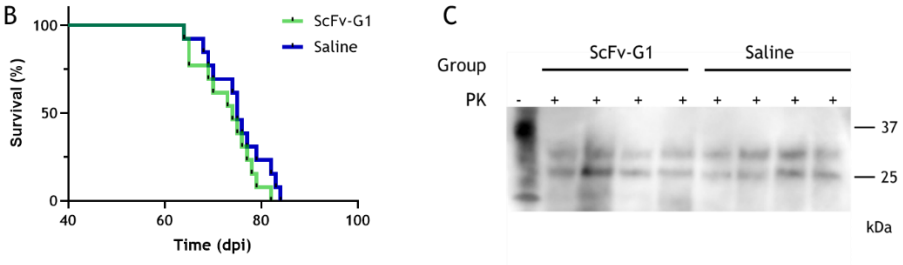


Figure 2.11 Therapeutic treatment with scFv-G1 did not extend the survival time of prion-infected mice nor modified the pathology in comparison with the saline group even when the inoculum was diluted. A) Two groups of mice were inoculated with 20µL of 0,1% brain homogenate from a terminally ill mouse inoculated with vole-adapted CWD. All the mice succumbed to prion disease and the mean incubation time was calculated for both groups. Log-rank test showed no statistically significant differences between the group of mice that received scFv-G1 and the saline group (p=0.2508). Hash (#) indicates that outliers were detected by Grubbs' test; these outliers were removed before the statistical analysis (Annex VII Fig S1). B) Survival curve of mice treated with scFv-G1(n=13) or saline buffer (n=13). Mice were monitored twice a week to identify clinical signs, after the onset of the clinical phase, mice were observed daily and euthanized when they were terminally sick and the survival endpoint of animals treated with scFv-G1 (light green) or saline (dark blue) was plotted on a Kaplan-Meier survival curve. C) The accumulation of PK-resistant material was assessed by Western blot using SAF83 antibody (1:400) (epitope 130-160).

USC UNIVERSIDADE DE SANTIAGO DE COMPOSTELA

3.4.4. A CHRONIC INTRACRANIAL TREATMENT DOES NOT REDUCE THE MICE LIFE EXPECTANCY

The results presented above showed that neither a chronic treatment with Fe(III)-TMPyP nor with scFv-G1 were effective in TgVole mice inoculated with a vole-adapted CWD strain. These results contrasted with preliminary studies *in vitro* and in cell-based bioassays that suggested that both treatments would be active against prion diseases.

We reasoned that one possible argument could be that the continuous intracerebral treatment could weaken the mice. This effect, plus the proper prion disease, could hide the beneficial effect of both treatments. In order to assess whether the repetition of intracranial injections affected the lifespan of infected mice, a control group was inoculated with 20µL of 0.1% brain homogenate from a terminally sick mouse inoculated with vole-adapted CWD and the average survival time was then compared with the saline group of mice that was previously used in the section *3.4.2.3 A therapeutic administration of scFv-G1 does not delay the clinical course of prion disease with a diluted inoculum.* The mean survival time of mice just inoculated with a 0,1% brain homogenate (that did not receive repeated intracranial administrations of saline buffer) was 76,6±1,8 dpi, whereas the mean incubation period of mice inoculated and treated intracerebrally weekly for 5 weeks, was 75,1±1,7 dpi.

The log-rank test showed that the difference was not statistically significant, with a ρ value=0,3953. Moreover, the histopathological analysis did not show brain damage as a consequence of repetitive brain injection derived from the chronic treatments, in comparison with those mice that were just inoculated.

USC UNIVERSIDADE DE SANTIAGO DE COMPOSTELA

A

Group	Inoculation	Treatment	Dosing regimen	Attack rate	Mean ± SEM	p value
Inoculated	20µL 0,1% BH	-	-	11/11	76,6 ± 1,8	0,3953
Inoculated + saline		20µL 0,9% saline, i.c.	Days 14, 21, 28, 35, 42 after inoculation	13/13	75,1 ± 1,7	

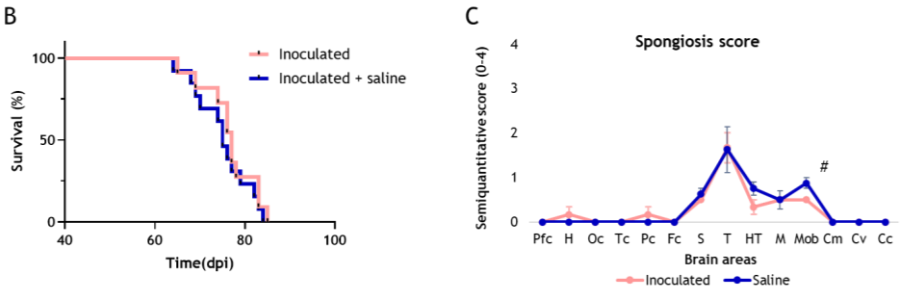


Figure 2.12 The chronic intracranial treatment did not affect the mice lifespan. A) Two groups of mice inoculated with 20µL of 0,1% brain homogenate from a terminally ill mouse inoculated with vole-adapted CWD were compared. One group of mice was just inoculated (pink) while the other group was inoculated and treated weekly for 5 weeks with saline buffer (blue). All the mice succumbed to prion disease and the mean incubation time was calculated for both groups. Log-rank test showed no statistically significant differences between both groups of mice (p=0.3953). B) Kaplan-Meier survival curve. The survival curve of both groups was practically similar; the mean survival time of mice just inoculated (pink) was 76,6±1,8dpi (n=11), while the survival of mice that were also treated with saline (blue) was 75,1±1,7 dpi (n=13). C) The histopathological profile of mice just inoculated (pink line)(n=5) or inoculated and treated with saline buffer (blue line) (n=4) represents the mean semi-quantitative scoring (0–4, vertical axis) of the spongiform lesions against these brain regions: Pfc: piriform cortex, H: hippocampus, Oc: occipital cortex, Tc: temporal cortex, Pc: parietal cortex, Fc: frontal cortex, S: striatum, T: thalamus, HT: hypothalamus, M: mesencephalon, Mob: medulla oblongata, Cm: cerebellar nuclei, Cv: cerebellar vermis, Cc: cerebellar cortex. The spongiform change of both groups is similar, meaning that the chronic intracranial treatment did not cause a change in the lesion profile. Hash (#) indicates that the pointed-out brain area could not be examined in all the samples.

USC UNIVERSIDADE DE SANTIAGO DE COMPOSTELA

3.5 DISCUSSION

3.5.1 ASSESSMENT OF THE ANTI-PRION ACTIVITY OF FE(III)-TMPYP IN A FAST MURINE MODEL OF PRION DISEASE

Porphyrins are organic heterocyclic molecules with essential functions in animals, plants, algae, and also bacteria; in consequence, they are known as "pigments of life". They play crucial roles in oxygen transport, photosynthesis, and enzymatic reactions. Moreover, porphyrins have intrinsic properties with industrial and medical interest; for instance, one of the main porphyrin features is their capability to absorb light in the visible region and transmission of energy through the coordinated metal, called light-harvesting system. This process is the basis of their function in photosynthesis; for this reason, porphyrin-based materials have been used in the fabrication of organic photovoltaic devices. Furthermore, their flat and symmetric architecture is useful for building units of supramolecular polymers[364]. Medical interest in porphyrins lies in the porphyrin-mediated photodynamic therapy. Their natural fluorescence and the capability to chelate superparamagnetic metal ions allow *in vivo* imaging and guiding of porphyrins to the place of interest by MRI. Moreover, porphyrins can encapsulate drugs and molecules of interest and release them by ultrasounds in concrete tissue[252]. These examples show the potential and interest harbored in porphyrin compounds.

Anti-prion properties of porphyrins and phthalocyanines have been studied *in vitro*, *in cellula* for decades with encouraging results[251,332–335,346,365]. Fe(III)-TMPyP is a cationic tetrapyrrole that acts as a molecular chaperone binding to huPrP^{C} residues 160-180 in an equimolar ratio[365]. Previous studies demonstrated that such porphyrin

USC UNIVERSIDADE DE SANTIAGO DE COMPOSTELA

inhibits prion propagation by PMCA and in cell cultures infected with different prion strains in a micromolar range: 6,21μM *in vitro* and 1.61μM *in cellula*. Moreover, Fe(III)-TMPyP also demonstrated to reduce the synaptotoxicity of PrP^C-mediated Aβ oligomers[335]. In addition, experiments in transgenic mice overexpressing hamster PrP (Tg7) showed 90 days of prolongation of survival over the untreated animals. These animals were inoculated and treated intraperitoneally with Fe(III)-TMPyP, 3 times a week for 4 weeks, starting the treatment on the day of the inoculation. Nonetheless, when the treatment started in an advanced stage of the disease (56dpi), it did not report an increase in the incubation time. Additionally, further experiments demonstrated that the effect was due to an inactivation of the infectious agent in the place of inoculation. As consequence, the authors of this work concluded that Fe(III)-TMPyP would be better used as a prophylactic agent in case of peripheral incidental contact with prions, rather than as a therapeutic agent[346].

In the present thesis, Fe(III)-TMPyP was assessed in a fast murine model of prion disease. For this purpose, a group of TgVole mice was inoculated intracranially with a vole-adapted CWD strain. This CWD strain causes a prion disease in a short incubation period of approximately 70dpi, which was considered to be helpful in getting fast results that could be useful as proof of concept. Furthermore, the i.c. route was selected over the i.p. via, as it better mimics the pathogenesis of sporadic prion diseases, which are the most common forms of prion diseases, while i.p. route would be more suitable for targeting acquired prion diseases.

The treatment with Fe(III)-TMPyP started 2 weeks after inoculation in order to avoid the inactivation of the infectious agent at the site of inoculation, as was previously reported[346]. The treatment was repeated weekly for 4 weeks and finished approximately 2 weeks before the onset of clinical signs.

USC UNIVERSIDADE DE SANTIAGO DE COMPOSTELA

Unfortunately, our attempt failed to prolong the survival or delay the onset of clinical signs. Based on the previous experiments, our first interpretation was that the prion strain might be extremely aggressive or that prion titters in the inoculum was too high to be neutralized by Fe(III)-TMPyP. For this reason, a second attempt was performed with a higher dilution of the inoculum, 0,1% instead of 1%, while the administration route or dosing regimen were preserved. This second approach did not provide the expected results either, dismissing the hypothesis that the prion concentration in the inoculum was too harmful.

Although mice did not experience an extension on the survival, analysis of the PrP^{Sc} present in their brains revealed a reduced amount of protease-resistant PrP. Despite the fact that Western blot is not a quantitative technique and the statistical results derived from its densitometric analysis should be cautiously interpreted, this reduction in the PrP^{Sc} was consistent, since it was observed in both groups of animals treated with Fe(III)-TMPyP regardless the dilution of the inoculum.

The reason why this reduction was not translated into a lifespan extension could be that Fe(III)-TMPyP cannot distribute throughout the brain parenchyma. The kinetics of Fe(III)-TPMyP diffusion revealed that after 24h, it remained in the site of administration. This should be enough to obtain a local reduction of PrP^{Sc} but not sufficient to obtain a global effect reflected in a delay in the onset of the disease. Moreover, since stereotaxic devices were not used during the treatment, the site of administration of Fe(III)-TMPyP slightly varied among the repetitive injections and most likely allowed to cover a wider treated area, reinforcing the hypothesis that Fe(III)-TMPyP had local effect reflected in the amount of PrP^{Sc}, though insufficient to increase the survival.

Very recently, Chiesa and colleagues identified another cationic tetrapyrrole with anti-prion properties, Zn(II)-BnPyP. Although Fe(III)-TMPyP and Zn(II)-BnPyP share the same chemical nature, they differ

USC UNIVERSIDADE DE SANTIAGO DE COMPOSTELA

on the mechanism of action. While Fe(III)-TMPyP acts as a molecular chaperones stabilizing PrP^{C}, Zn(II)-BnPyP binds to two distinct sites of PrP^{C} and destabilizes its native conformation; as a result, Zn(II)-BnPyP shows a dual effect: on one hand, it hinders PrP^{C} conversion into PrP^{Sc} and, on the other hand, it promotes the degradation of the complex Zn(II)-BnPyP - PrP^{C}. Despite the encouraging results that Zn(II)-BnPyP showed *in vitro* and in cell-based assays, attempts to treat prion infected mice failed in showing an effect on the survival over the vehicle-treated mice, even when Zn(II)-BnPyP was administered either by direct intracerebral injections and chronic infusion with osmotic pumps to bypass the BBB. Consistently with our findings, Zn(II)-BnPyP presented poor diffusion into the brain parenchyma[366]; thus, despite the interesting anti-prion properties that porphyrins show *in vitro* these results suggest that their poor pharmacokinetics is responsible for their pharmacological failure *in vivo*.

In addition, since Fe(III)-TMPyP had apparently a local effect, it would be expected that this effect would also have an impact on the histopathological profile of treated mice. Specifically, since the treatment was attempted to be deposited in the lateral ventricle, a reduction in vacuolization in the brain areas adjacent to the lateral ventricles could be expected. Considering that the inoculated CWD strain mainly affects the brainstem and basal ganglia, brain areas such as the striatum and thalamus might be expected to show less vacuolation. However, the anatomopathological examinations did not reveal any differences in spongiosis in any region. Moreover, the immunohistochemical labeling failed in exhibiting PrP^{res} deposition in both, control and treated mice, even when two different primary antibodies were tested, 6C2 and SAF84 (data not shown). The absence of PrP^{res} may be due to the incubation time of this strain, which may be too short to obtain an accumulation of PrP^{res} deposits. On the other hand, it may also be due to the fact that this strain is affected by the unmasking process to which samples are subjected during their preparation for the immunohistochemical analysis.

USC UNIVERSIDADE DE SANTIAGO DE COMPOSTELA

A reasonable argumentation for the discrepancy between the absence of activity of Fe(III)-TMPyP regarding the survival or the lesion profile, and the levels of PrP^{Sc}, could be that the amount of PrP^{Sc} might not be directly related to the neurotoxicity. This idea was proposed by Collinge and colleagues[208,209,286] and hypothesizes that prion disease takes place in two distinct phases. During the silent phase 1, infectious prion titers exponentially rise until they reach a plateau (phase 2) In this second phase, clinical signs begin, and the duration is inversely related to the PrP^{C} expression levels, being shorter in mice that overexpress PrP^{C} and longer in heterozygous animals. Classical PrP^{Sc} just emerges at the end of the incubation period, implying that the neurotoxicity might be mediated by different PrP species such as PK-sensitive PrP species or PrP oligomers. Consistent with this data and based on the mechanism of action, we consider that Fe(III)-TMPyP might bind PrP^{C} and decrease the conversion into the PrP^{Sc}; however, it does not affect the toxic PrP conformers or does not interrupt the toxic signaling cascade.

In summary, the most reasonable argument for why Fe(III)-TMPyP did not ameliorate the prion diseases is because it cannot diffuse throughout the brain parenchyma or it does not avoid the formation of toxic species of PrP.

3.5.2 scFv-G1 antibody as a therapeutic strategy for prion diseases

In 1986, muromonab, the first therapeutic antibody was approved by the FDA. Nowadays, there are more than 130 therapeutic antibodies authorized; most of them, 45%, are commonly used in oncology, while antibodies against neurological disorders represent approximately 7%. The reason why the number of antibodies targeting neuropathological diseases is too low is that most of them do not cross the BBB due to their large size, added to the t he tight junctions formed by endothelial cells in the BBB, for these reasons typically less than 0,05% of the initial dose reaches the targeted brain region. This fact implies the use

USC UNIVERSIDADE DE SANTIAGO DE COMPOSTELA

of large doses of the treatment and increasing the costs of the therapy, forcing the use of invasive routes such as the intrathecal route, or employing encapsulated or vectored antibodies to overcome the BBB[367–369]. However, some engineered antibodies like nanobodies or single-chain antibodies offer promising alternatives to traditional monoclonal antibodies because some of them have shown the ability to cross the BBB through transcytosis [370–372]. As a result, these engineered antibodies are attractive candidates for passive immunization approaches in addressing neurodegenerative disorders

In the present thesis, a scFv antibody developed by Wille and colleagues was directly administered in the brain of mice in an attempt to treat prion diseases. The therapeutical antibody carried an epitope structurally specific for PrP misfolded into a β-solenoid architecture. This antibody was obtained after immunizing mice with a vaccine composed of two linked molecules of the fungal prion HET-s, which was engineered to serve as a scaffold for the epitope. TgP101L mice (an animal model that naturally develops GSS syndrome) immunized with this vaccine experimented an extension of the lifespan in comparison with mice vaccinated with the HET-2s scaffold without the PrP epitope, or non-immunized controls. Antibodies obtained from immunized mice were purified and engineered to be expressed in *E. coli* as scFv, which demonstrated to recognize *in vitro* different prion strains from various species, such as GSS (A117V), FFI (D178N/129M), fCJD(E200K), vCJD, CWD (transgenic mice), BSE (transgenic mice), Hy and Dy among others[357]. It should be noted that this project started before Kraus and colleagues demonstrated by cryo-EM that the PrP structure is a PIRIBS[110]; hence, obtaining positive results with this conformationally specific antibody would support the hypothesis that the PrP^{Sc} architecture would be a 4RβS.

In an attempt to assess whether scFv-G1 could be a candidate for passive immunization in prion diseases, we tested its efficacy in a fast murine model of prion disease. However, since we did not know whether scFv-G1 could cross the BBB, we to overcome this possible

USC UNIVERSIDADE DE SANTIAGO DE COMPOSTELA

challenge by injecting it directly intracerebrally in mice that had been previously inoculated with a vole-adapted CWD strain.

Disappointingly, the treatment neither had effect on the survival nor the pathology. Despite the lack of efficacy against prion diseases, we were able to verify that the use of this antibody by intracerebral route was safe, since none of the animals presented adverse effects after the administration of the repeated doses. Although in-depth analyses including immunolabeling of apoptotic cells would be necessary to confirm the absence of neurotoxicity related to the administration of the scFv-G1 antibody, anatomopathological examinations of brain slides stained with hematoxylin eosin did not reveal cerebellar or hippocampal damage, the presence of shrunken or pyknotic nuclei, or disorganizations of the neuropil, like those that have been described in cases on neurotoxicity associated with the intracerebral administration of anti-PrP antibodies [316,349]

In view of the lack of effectivity of scFv-G1, we considered that the inoculum might have a high titer of prions, and the antibody was ineffective because it could not neutralize such amount of infectious agents; for this reason, the chronic treatment was repeated using a lower concentration of the inoculum, 0,1% instead of 1%. However, this attempt also failed in ameliorating the prion disease.

The lack of effect of scFv in these experiments contrasted with the results obtained with the vaccine in different animal models and against different prion strains. On one hand, a justification for the absence of activity could be that the selected IgG recognizes the antigen *in vitro* but not *in vivo*. On the other hand, the lack of activity could be due to the sort antibodies selected to generate the scFv-G1 antibody. It is known that polymeric structures with repetitive antigens could behave as thymus-independent (TI) antigens. Unlike conventional antigens that require T cell involvement to activate B lymphocytes, thymus-independent antigens can directly stimulate B lymphocytes and trigger antibody production. Although most of TI antigens are polysaccharides

USC UNIVERSIDADE DE SANTIAGO DE COMPOSTELA

or glycolipids, a short fraction of polymeric proteins, such as flagella, can also promote the generation of antibodies by B cells without the participation of T lymphocytes. It is possible that HET-s behaved as a TI antigen. Thus, the vaccine promoted the generation of antibodies against the epitope and extended the mice survival. However, these TI antigens only stimulate the synthesis of IgM antibodies, whereas scFv-G1 had its origin in an IgG. So that, although scFv-G1 somehow recognizes the epitope *in vitro*, it is not effective *in vivo* [266,373]. The hypothesis that the specific immune response against PrP^{Sc} would trigger the synthesis of IgM instead of IgG would be supported by Korth's work[374], in which the authors describe a monoclonal IgM, 15B3 that specifically recognizes PrP^{Sc} but not PrP^{C} [375]. Additionally, Jones and colleagues [376] also isolated an IgM that selectively bonded to brain-derived PrP^{Sc}, while this antibody failed in recognizing the native isoform of the PrP. Taken together, these pieces of evidence support the idea that IgM antibodies, rather than IgG, might be conformationally specific, triggering an immune response against PrP^{Sc}.

However, one of the most intriguing questions is why a vaccine targeting a nonexistent epitope could be effective in extending the survival of prion-infected mice? Further experiments are still needed to shed light on this question. Notwithstanding, it could be hypothesized that the immunization with a fungal protein, rather than the selection of the 4RβS epitope, gave rise to the immune response against PrP^{Sc}. Since HET-s is a fungal protein, its inoculation would most likely trigger a strong immune response. The contact with an antigen triggers a humoral reaction with a primary antibody response. During this response, B cells are activated and differentiated into antibody-secreting cells, producing antibodies against the antigen. These antibodies (typically IgG and IgM) are highly variable and present low average affinity towards the antigen and, in order to increase the affinity, plasma cells produce a large repertoire of antibodies. The process of increasing the diversity of antibodies involves random recombination of the gene segments that encode the variable regions of the heavy and light chains of antibodies,

USC UNIVERSIDADE DE SANTIAGO DE COMPOSTELA

as well as the addition of nucleotides during the recombination process[377] and, despite the fact that HET-s and PrP^{Sc} present different amino acid sequences and structural arrangements, it is plausible that as a consequence of a strong immune response, during the expansion of antibodies certain epitopes randomly generated would present affinity towards PrP^{Sc}.

The negative results obtained with Fe(III)-TMPyP and scFv-G1 led us to consider that perhaps the posology and the route of administration of the treatment was too aggressive, and after 5 weeks of intracranial injections, mice were extremely weak to face the prion disease, despite the fact that we based our dosing regimen and the route of administration in previous works[251].

To assess whether the dosing regimen might have a negative effect on the mice survival, we compared a group of mice inoculated and treated for 5 weeks with saline buffer and a group of mice that was just inoculated. We found that there were no statistically significant differences in the average survival time or the lesion profile, dismissing the idea that the repetitive treatment was the cause of the lack of efficacy in our mice model. Therefore, we reasoned that the animal model and the prion strain employed in these studies might not be suitable for testing anti-prion therapies. We used TgVole mice due to their high susceptibility to different prion strains and the short incubation time, which made this model attractive to test our compounds as proof of concept. Nonetheless, the best models to evaluate candidates for prion therapies are humanized mice[378]. However, this and other human models have longer incubation periods, involving more time. Besides, experiments with these transgenic mice must be conducted in microbiological containment level 3 laboratory, which are unavailable in our animal facilities.

On the other hand, it is possible that other routes of inoculation and administration would provide better results. It is possible that peripheral routes of inoculation and treatment would allow the interaction of

USC UNIVERSIDADE DE SANTIAGO DE COMPOSTELA

inoculum and treatment in the spleen or lymph nodes, decreasing the amount of infectious agents that reach the brain and extending the survival. However, results obtained with peripheral routes of inoculation and treatment would only be translated to acquired prion diseases, which are the least common and we reasoned that i.c. inoculation is the route that most closely approximates what happened in sporadic or familial prion diseases. Moreover, we also considered that the i.c. administration was the most suitable route to administer the treatments, since we did not know if they could cross the BBB and by the i.c. pathway we could overcome it. The BBB represents the major challenge for all those treatments that have their target in the brain; nevertheless, there exist some strategies to improve the diffusion of drugs through the BBB and the brain. In case of small chemical compounds, such as the Fe(III)-TMPyP, one approach to improve it bioavailability would be to modify the chemical structure to increase the liposolubility or reduce the size, without compromising its activity. Another strategy to obtain better results in terms of bioavailability for small molecules or scFv antibodies, would be using specialized delivery systems, such as nanoparticles, liposomes or extracellular vesicles. These systems encapsulate the drug and improve the transport across the BBB and protect the treatment from degradation increasing the half-life. Moreover, the surface of these carriers could be decorated with ligands of receptor-mediated transporters, permitting an efficient delivery across the BBB[379]. Additionally, the concentration of a therapeutic candidates in the brain could be also achieved by increasing the permeability of the BBB. The disruption of the BBB or a temporary permeabilization could be achieved by different methods, such as through electric stimulation [380] or localize low-intensity ultrasounds [381]. Moreover, certain drugs can also increase the permeability of the BBB, such as mannitol, a hyperosmotic sugar alcohol that induce osmotic blood-brain barrier opening. This effect has been applied to reduce the intracranial or intraocular pressure, and to improve the delivery of chemotherapeutics in cases of brain tumors [382]; thus, its use could improve the bioavailability of treatments against prion diseases in case

USC UNIVERSIDADE DE SANTIAGO DE COMPOSTELA

of peripheral administrations. Thus, the use of one or more of these approaches would increase the diffusion of Fe(III)-TMPyP and scFv antibodies across the BBB and brain parenchyma and the application of these strategies may have a beneficial effect in prion-infected mice.

USC UNIVERSIDADE DE SANTIAGO DE COMPOSTELA

3.6 SALIENT REMARKS

1. The molecular chaperone, Fe(III)-TMPyP, neither had effect on the survival nor the pathology of TgVole mice inoculated with a vole adapted-CWD strain after a chronic treatment.

2. A chronic treatment with Fe(III)-TMPyP reduced the accumulation of PrP^{Sc} in the brain of mice inoculated with a vole adapted-CWD strain.

3. A preliminary kinetic evaluation of Fe(III)-TMPyP showed that the tetrapyrrole cannot diffuse throughout the brain parenchyma.

4. Given the poor penetrance of Fe(III)-TMPyP, the reduction in the accumulation of PrP^{Sc} might be due to a local effect in the site of administration.

5. The conformational antibody, scFv-G1, neither had effect on the survival nor the pathology of TgVole mice inoculated with a vole adapted-CWD strain after a chronic treatment.

USC UNIVERSIDADE DE SANTIAGO DE COMPOSTELA

4. CHAPTER II: A NON-PRP^{Sc} PrP PRION

USC
UNIVERSIDADE DE SANTIAGO DE COMPOSTELA

4.1 INTRODUCTION

4.1.1 PROTEIN FOLDING AND AMYLOID FORMATION

One of the most important properties of proteins is their capability to fold from unfolded polypeptides into complex and biologically active three-dimensional structures. *In vivo*, large proteins require the support of chaperones to fold correctly; however, small proteins can self-assemble into specific and identical structures, even *in vitro*, away from a cellular environment. The total number of possible folding pathways from a polypeptide to the native state of a protein is infinite; nonetheless, energetic states guide the process to the most thermodynamically stable conformation in physiological conditions: the folding pathway follows a stochastic search of different energetically stable intermediate conformations until the polypeptide finds the lowest-energy structure. The folding pathway is encoded in the amino acid sequence, especially hydrophobic and polar residues rapidly interact, generating a compact nucleus excluding water from the protein core; subsequently, the remaining residues condensate surrounding the nucleus. Secondary structures composing globular domains, such as α-helices, are rapidly folded in terms of nanoseconds, while β-sheets take more orders of magnitude of time. In addition, these first well-defined structures are stabilized by hydrogen bonds between the amide and carbonyl groups [383–385].

Intermediate states during the folding process are particularly important in large proteins, due to the fact that in these proteins the architecture is sequentially acquired in different steps. In cells, protein folding is highly regulated, and failures in this process raise the malfunction or loss of activity of the molecule, which can lead to cell damage, toxic events, and eventually, cell death.

USC UNIVERSIDADE DE SANTIAGO DE COMPOSTELA

Under certain conditions, unfolded or partially unfolded polypeptides can interact with each other leading to the formation of protein aggregates. Initially, earlier aggregates present weak intermolecular interactions and can easily dissociate and reverse to soluble peptides or to the native state. However, if the interaction is not reversed, these aggregates can evolve into amorphous deposits of native-like assemblies or reorganize their structures into amyloid fibrils. Generally, large proteins tend to form amorphous aggregates, whereas short proteins usually generate amyloid fibrils (Fig 3.1).

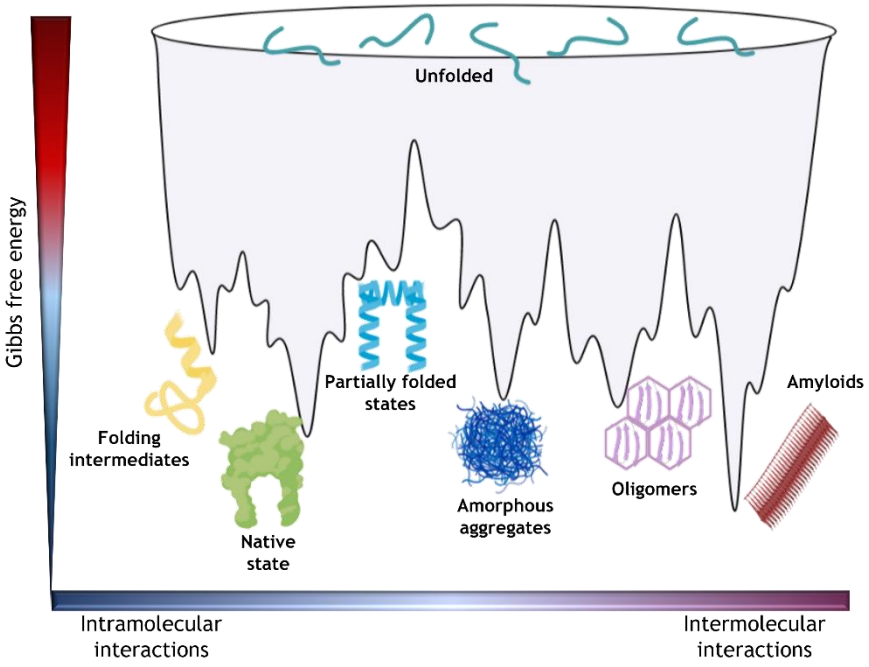


Figure 3.1. Schematic representation of the energy landscape and the different protein conformations. The protein folding process follows different pathways from the unfolded polypeptide chain (dark green) to reach the bioactive native architecture (green), such as folding intermediates (yellow) and partially folded

USC UNIVERSIDADE DE SANTIAGO DE COMPOSTELA

states (light blue). Mutations, intermolecular interaction, and certain environmental conditions lead to misfolded forms of the protein, such as amorphous aggregates (dark blue), oligomers (pink), or amyloids (red). These structures are responsible for protein depositions causing pathological conditions.

Amyloid architecture is a thermodynamically stable protein conformation characterized by highly organized hydrogen-bonded β-sheets. These β-sheets strands are perpendicularly repeated throughout the fibril axis. Independently of the native state of the protein, all amyloids share common features, such as insolubility, affinity for dyes such as Congo red, fibrillar morphology characterized by long, generally twisted, and unbranched structures of a few nanometers in diameter, and optical properties such as birefringence (optical property whereby a ray of light incident in a material with this feature, is split into two rays taking slightly different paths), which are indicative of cross β-structure [386].

Amyloid formation involves a complete rearrangement of the protein that requires the exposure of hydrophobic amino acids to the solvent and can be triggered by partially denaturing environmental conditions, such as low pH, the presence of chemical denaturants, or high temperatures. Generally, proteins with a high tendency to aggregate into amyloids present disordered regions. Furthermore, mutations affecting the primary sequence of the protein can decrease the stability and increase the propensity to aggregate by enhancing the hydrophobicity.

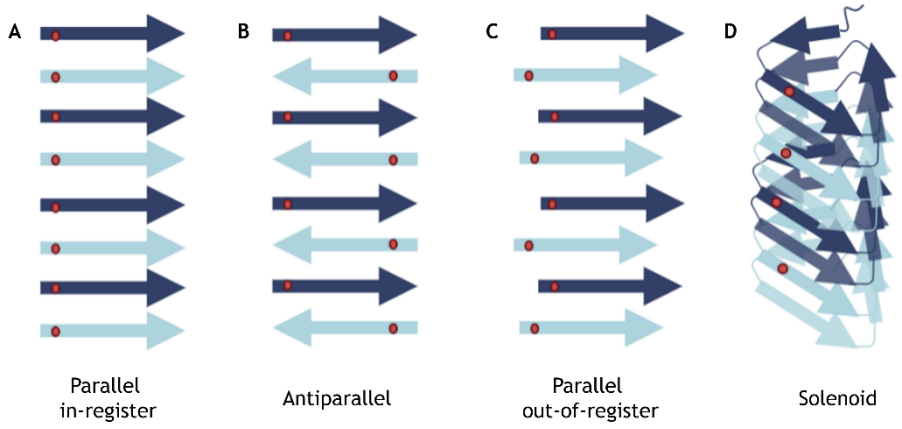
Amyloid generation occurs in three phases: a lag phase, also known as nucleation, where totally or partially unfolded monomers form the nuclei through nonspecific interactions; exponential growth, also called fibrillation or polymerization phase, in which fibrils elongate by the addition of monomers; and equilibrium phase or plateau. The nucleation phase can be accelerated by adding preformed amyloids, known as seeds, due to the property of amyloids to induce the conformational change of native proteins onto the amyloid architecture. This process can take place among similar or different proteins (cross-

USC UNIVERSIDADE DE SANTIAGO DE COMPOSTELA

seeding); indeed, amyloid aggregates involving different proteins are often found in amyloid-related diseases, known as heterologous cross-seeding [387,388].

It is thought that oligomers are the initial species implicated in protein aggregation, playing a key role in amyloid formation. In contrast to amyloids, oligomers have a small size, do not bind dyes, or present a β-sheet architecture. Moreover, oligomers and protofilaments, rather than mature fibrils have been proposed to be responsible for the toxicity in amyloid-related diseases, by interacting with the cell membrane, disrupting the cell balance, or by other specific mechanisms [385].

The amyloid backbone is very compact and is stabilized by hydrogen-bonded, hydrophobic, and van der Waals forces. Depending on the monomers disposition regarding each other, amyloids can present the following architectures (Fig 3.2): parallel in-register structure, when one β-strand is orientated in the same direction as the β-strand below it and the residues of both strands are completely aligned; parallel out-of-register, both strands are orientated in the same direction but the residues are not aligned; antiparallel, when one β-strand is in the opposite direction than the β-strand below it; solenoid, each β-strand is folded in more than one rung following a solenoidal conformation[389].



USC UNIVERSIDADE DE SANTIAGO DE COMPOSTELA

Figure 3.2. Amyloid structures. A) Parallel in-register is the most common architecture and the most thermodynamically stable in comparison with the antiparallel and the parallel out-of-register. Residues interact by hydrogen bonds with identical amino acids (red) in the strands above or below. B) Antiparallel conformation presents strands in opposite directions and is common in amyloids with charged side chains. C) Parallel out-of-register is the less common conformation; the strands must be stabilized by salt bridges to maintain the architecture. D) Two-rung solenoid. Each monomer is folded into more than one layer and residues are in the same orientation but in different layers.

Many amyloids responsible for neurodegenerative diseases, such as tau[390], Aβ [391], α-synuclein[392], and PrP[393], were demonstrated to share a parallel-in-register architecture.

Even though amyloids are generally associated with pathologies, there have also been described functional amyloids, especially in bacteria and fungi, but in mammals and fish as well. Some of these functions are chemical storage, epigenetic inheritance, memory, cell signaling, structural properties, and activation and inactivation of cellular functions [394].

4.1.2 PRP AMYLOIDS

Apart from the PrP^{C} and PrP^{Sc} architectures, other structures have been described for PrP. These conformers are designated with the general term "PrP amyloids". PrP amyloids comprise a large variety of molecules e.g., recombinant proteins[202], ex vivo particles[393], truncated or mutated forms of the PrP protein [203], disease-associated[201], or non-infectious particles [395,396]. Although PrP prions are also amyloids, they have features that those conformers included in the term PrP amyloids do not; for this reason, PrP prions receive the proper sobriquet of PrP^{Sc}. One of the main characteristics that differentiate PrP^{Sc} and PrP amyloids is infectivity. *Bona fide* PrP^{Sc} is, by definition infectious; this means that when brain-derived or recombinant PrP^{Sc} is inoculated in a wild-type animal, it triggers a prion disease that eventually kills the

USC UNIVERSIDADE DE SANTIAGO DE COMPOSTELA

animal. However, the infectivity is a controversial property of PrP^{Sc}; several animal models recapitulate prion diseases triggering reminiscent clinical signs and the pathognomonic histopathological changes in the brain, but failed in transmitting the disease to wild-type animals or entailed incomplete attack rates, the need to use animal models that overexpress PrP, or serial passages through different transgenic models to show little evidence of transmissibility[397–405].

Regarding their structure, like PrP^{Sc}, PrP amyloids share a PIRIBS conformation[201–203,393,395]. However, while brain-derived PrP^{Sc} encompasses a single protofilament[110,190,194,205,406], it seems that different PrP amyloids consist of the interaction of two, three, or even four intertwined protofilaments, whose interactions stabilize the fibril[201,393]. Additionally, the fibril core of PrP amyloids is smaller than PrP^{Sc} (Fig 3.3).

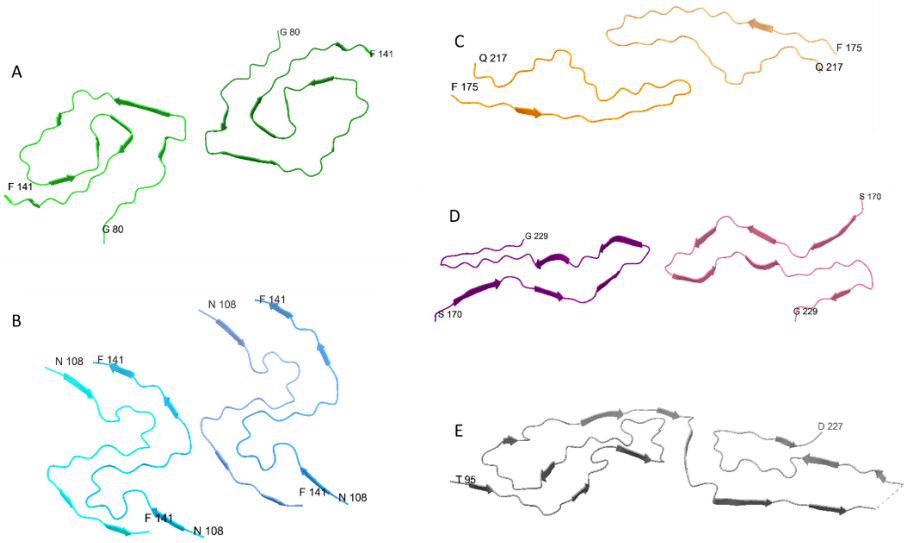


Figure 3.3. Comparison of different PrP amyloid structures elucidated by cryo-EM and *bona fide* PrP^{Sc}. A) Structure of ex vivo GSS (F198S) fibrils. Cryo-EM analysis

USC UNIVERSIDADE DE SANTIAGO DE COMPOSTELA

of GSS(F198S) fibrils obtained post-mortem from a symptomatic patient showed two left-handed symmetric protofilaments, whose core is comprised of amino acids G80-F141 (PDB 7UMQ)l[393]. B) Structure of recombinant huPrP23-144 amyloid fibrils. Cryo-EM analysis of *in vitro* prepared huPrP23-144 amyloid fibrils, which is associated with the Y145Stop mutation that causes GSS syndrome, showed four-protofilament fibrils. These symmetric protofilaments have an S shape and are arranged in a head-to-tail direction. The fibril core encompasses residues N108-F141 (PDB 7RL4)[201]. C) Structure of full-length huPrP bearing the E196K mutation. Cryo-EM analysis of recombinant huPrP23-231 bearing the E196K mutation associated with a familial form of CJD revealed two symmetric left-handed protofilaments. The core comprises residues F175-Q217 (PDB 7DWV)[202] D) Structure of wild-type full-length huPrP. Cryo-EM analysis of recombinant full-length huPrP fibrils revealed two symmetric, left-handed intertwined protofilaments. The fibril core encompasses residues S170-G229 (PDB 6LNI)[395]. E) Structure of brain-derived 263K prions. *Bona fide* PrP^{Sc} obtained from hamsters inoculated with the prion strain 263K were purified and analyzed by cryo-EM. Fibrils are composed of a single protofilament whose core contains residues T95-D227 (PDB 7LNA).

Hallinan and colleagues were the first authors to describe the structure of PrP amyloids from patients affected by a prion disease solved by cryo-EM. These patients carried a mutation in the PRNP gene that resulted in the substitution of phenylalanine for serine at position 198, which causes GSS syndrome. The authors of this work analyzed brain-derived PrP fibrils nondigested with PK. The fibrils of ~11nm in diameter and a helical pitch of ~100nm were composed of different numbers of protofilaments (two, three, or four units) intertwined into a left-handed fibrils. Protofilaments shared a C2 symmetry, and the core encompassed residues G80-F141. Monomers stacked along the fibril axis are stabilized by hydrogen bonds, as well as the protofilaments among them, that establish hydrogen bonds through the GGG motif of residues 90-93. In addition, each monomer entailed nine short β-strands distributed in a spiral-like shape.

Although patients that suffer from this prion disease express the full-length PrP protein, the above-mentioned results evidenced that the fibril core only encompasses the N-terminal region and that the mutated residue is not included in the fibril core. Additionally, the theoretical

USC UNIVERSIDADE DE SANTIAGO DE COMPOSTELA

molecular weight of the fibril core is ~6,2kDa, whereas biochemical characterization by Western blot of the brain-derived sample shows a PK-resistant band of ~8-11kDa which does not include the post-translational modifications such as the GPI-anchor or the glycosylations [407]. The authors reasoned that the core might encompass amino acids 70-150, although some residues might belong to more flexible architectures excluded from the core proper [393].

Likewise, cryo-EM studies of PrP amyloid fibrils prepared *in vitro* with the recombinant protein huPrP23-144 share parallel in-register intermolecular β-sheet architecture. This protein is associated with GSS syndrome, as well, which is triggered by a mutation that results in a substitution of tyrosine to a stop codon at position 145 (Y145Stop)[408]. The fibril is ~20nm in width and has a helical pitch of ~70nm. Furthermore, its core comprises residues 108-141 and has a diameter of 10nm. The fibril involves four symmetric protofilaments arranged in a head-to-tail direction stabilized by intermolecular interaction among hydrophobic residues; moreover, the inner protofilaments establish intermolecular hydrogen bonds. Furthermore, these protofilaments have a S shape intertwined in a left-handed helix, and each monomer has two short β-strands[201]. These results are consistent with previous findings obtained by ss-NMR, which indicated the existence of a flexible 23-111 region and a partially ordered C-terminal domain and three β-strands encompassing residues from position 109 to 140[409,410].

While F198S and Y145Stop PrP amyloid fibril cores encompass the N-terminal region, wild-type and E196K PrP amyloids differ and have a structured C-terminal core based on disulfide β-arches. Therefore, cryo-EM images of recombinant E196K huPrP fibrils, synthesized *in vitro* under partially denaturing conditions, showed a fibril core entailing residues 175-217. The architecture of this mutated huPrP, responsible for a familial CJD form[411], showed fibrils of ~21nm width consisting of two symmetric protofilaments intertwined into a left-handed twist with a helical pitch of ~280nm. Both protofilaments are stabilized by salt bridges involving four amino acids. The fibril core of ~11nm width, is

USC UNIVERSIDADE DE SANTIAGO DE COMPOSTELA

composed of 5 β-strands; additionally, the authors identified density regions, termed islands, which were hypothesized to be comprised of residues 136-142, located on the opposite side of the hydrophobic side chains of V180 and I182 and I184 [202].

Similarly, wild-type full-length huPrP amyloid fibrils encompass the C-terminal fibril core. As well as the E196K PrP amyloid, these fibrils were synthesized *in vitro* under partially denaturing conditions. Such fibrils have a width of ~25nm and a pitch of ~155nm. Moreover, the fibril core has a diameter of ~14nm and entails residues 170-229. Like the E196K huPrP amyloid, the fibril is composed of two symmetric protofilaments, intertwined into a left-handed fibril and both protofilaments establish salt bridges that stabilize the fibril. Moreover, the fibril core encompasses six β-strands [395].

Biochemical and biological features of this full-length PrP amyloid have been characterized for a long time. Previous studies related it with certain subpopulations of PK-resistant material found in patients with sCJD, regarding the size of the PK-resistant core, which is shorter than classical PrP^{Sc}, and the C-terminal sequence involved[412,413]. Nonetheless, this recombinant amyloid resulted non-infectious on the first passage when it was inoculated in wild-type animals. Interestingly, although this material was innocuous, atypical PK-resistant material was propagating in the brain during this silent stage[400]; additionally, this "atypical" material preserved the biochemical properties of the amyloid employed as inoculum. After serial passages, this amyloid suffered structural, biological, and biochemical changes that were evidenced by the onset of clinical signs, a change in the electrophoretic mobility (with the emergence of a classical PK-resistance pattern), and a variation of the neuropathological lesion profile. This conformational change was termed by the authors "deformed templating" (Fig 3.4). While classical templating is defined as a folding pathway that faithfully reproduces the pattern of the template, deformed templating could be described as an alternative cross-β folding pattern that only partially overlaps with the folding pattern of the original template. This process would be

USC UNIVERSIDADE DE SANTIAGO DE COMPOSTELA

responsible for the conformational diversity of fibrils, and the emergence of a concrete population of fibrils would be influenced by environmental conditions[400,414,415].

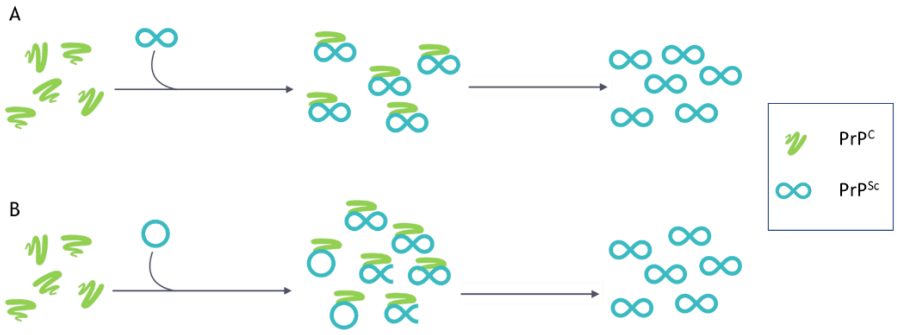


Figure 3.4. PrP protein misfolding pathways. A) Classical templating. The amyloid fibrils reproduce the same folding pattern as the template. B) Deformed templating. The amyloid fibrils acquire alternative patterns that fit partially with the template and only the most suitable can propagate.

Based on the ability of recombinant PrP amyloid to propagate and accumulate in hamster brains in a clinically-silent way [400,414–416], Diaz-Espinoza and colleagues hypothesized that it could be used for therapeutic purposes, since this amyloid could most likely compete against PrP^{Sc} for the substrate PrP^{C} and delay the onset of the disease. Certainly, when the authors administered intracerebrally their amyloid (called anti-prion 1, AP1) at different time points before the inoculum, they observed a prolongation in the survival of prion-infected hamsters. In fact, when the animals were treated prophylactically with AP1 63 days before inoculation with 263K at a concentration of 10^{-5}, 3 out of 5 animals did not develop clinical signs and lived more than 500 days[417].

In this chapter we describe an attempt to tackle prion diseases using a therapeutic amyloid, to assess that Diaz-Espinoza's results could be also translated to different animal models, in this case, the TgVole mice.

USC UNIVERSIDADE DE SANTIAGO DE COMPOSTELA

While Diaz-Espinoza and colleagues suggested that the amyloid would compete with PrP^{Sc} for the substrate, we contemplate a dual mechanism of action. On one hand, since PrP^{Sc} and the recombinant PrP amyloid share the same primary sequence and both are PIRIBS, we consider that the PrP amyloid would incorporate to the extreme of the PrP^{Sc} fibril, and instead of propagate PrP^{Sc}, it would propagate the amyloid. On the other hand, as Diaz-Espinoza indicates, the self-replicating amyloid would also compete for the substrate. Regarding these hypothetical mechanisms of action, we consider that a self-replicating full-length PrP amyloid, would be an interesting candidate for prion diseases.

USC UNIVERSIDADE DE SANTIAGO DE COMPOSTELA

4.2 SPECIFIC AIMS

Prion diseases are rare and fatal neurodegenerative disorders for which there is no treatment. The global goal of this chapter was to assess the therapeutic potential of a PrP amyloid in a fast murine model of prion disease. However, in view of the results that arose from the first experiments performed, new objectives were incorporated:

1. Evaluation of the prophylactic administration of a recombinant PrP amyloid as a treatment of prion diseases.

2. Serial transmission of the infectious PrP amyloid.

3. Biochemical and biological characterization of the infectious PrP amyloid.

USC UNIVERSIDADE DE SANTIAGO DE COMPOSTELA

4.3 METHODS

Reagents, materials, buffers composition, and devices used in this doctoral thesis are comprised in Annexes I, II, III, IV, and V.

4.3.1 EXPRESSION AND PURIFICATION OF BVPRP 109I

Recombinant full-length BVPrP (I109) (23-231) was expressed by *E. coli Rosetta* (DE3) Competent Cells harboring the pOPIN E expression vector containing I109 BV PRNP [101]. Bacteria from a glycerolate stored at -80°C were grown in a 250mL Erlenmeyer flask containing 50 mL of LB broth overnight at 37°C and 225rpm. The culture was then transferred to two 2L Erlenmeyer flasks containing each 500 mL of minimal medium supplemented with glucose, NH_4Cl, $MgSO_4$, $CaCl_2$, thiamine, biotin, and ampicillin. When the culture reached an OD_{600} of 0.8-1.2 AU, 1mM Isopropyl β-D-1-thiogalactopyranoside (IPTG) was added to induce expression of PrP overnight under the same temperature and agitation conditions. Bacteria were then pelleted by centrifugation for 15min at 5000g and 4°C, pellets were frozen for 2h at -80°C. Subsequently, bacteria were lysed with 60mL of lysis buffer for 1h under shaking at 225rmp and centrifuged 20min at 20000g and 4°C to obtain the inclusion bodies containing the expressed protein. Inclusion bodies were then solubilized in the buffer of solubilization of inclusion bodies and centrifuged for 1h at 20000g and 4°C.

Although the protein does not contain a His-tag, purification of the protein was performed with a histidine affinity column taking advantage of the natural His present in the octapeptide repeat region of PrP. After elution, the quality and purity of protein batches were assessed by BlueSafe staining after electrophoresis in SDS-PAGE gels.

USC UNIVERSIDADE DE SANTIAGO DE COMPOSTELA

Finally, Gdn/HCl was added to a final concentration of 6M. For long-term storage of purified protein preparations were frozen at -80°C.

4.3.2 PRP FIBRILLATION AND MONITORING OF FIBRIL FORMATION

Due to logistic reasons, PrP fibrillation was performed by Davy Martin at French National Institute for Agriculture, Food and Environment (INRAE), in Paris, France. PrP protein stored at -80°C in elution buffer with 6M Gdn/HCl was filtered with a 0,22µm filter and subsequently was dialyzed against fibrillation buffer 4 times (4h, ON, 4h, 4h). Aggregated material was removed by centrifugation for 10min at 16000g and 4°C. Protein concentration was then adjusted at 1mg/mL using the fibrillation buffer to dilute the sample. The protein was incubated at 37°C under continuous rotation in a wheel at 8rpm. PrP amyloid formation was monitored using ThT binding assay: aliquots were withdrawn and diluted into 10mM sodium acetate buffer, pH5.0 to a final PrP concentration of 0.3µM. Then ThT was added to a final concentration of 10µM, and fluorescence was measured at λ_{ex}450nm, λ_{em}485nm. When ThT fluorescence reached the plateau stage, samples were dialyzed in 10mM sodium acetate, pH5.0, 4 times (4h, ON, 4h, 4h) to ensure that Gdn/HCl had been completely removed. PrP fibers were collected by ultracentrifugation for 1h at 228147g using a Beckman Optima TL100 Ultracentrifuge and TLA-100.3 rotor, and resuspended in 10mM sodium acetate, pH5.0. A washing step was performed by repeating the ultracentrifugation and resuspension steps. The final pellet was resuspended in deionized water [418].

4.3.3 NEGATIVE STAIN TEM

Sedimented recBVPrP23-231 amyloid fibers were adsorbed on Formvar carbon-coated gold grids, washed with water thrice, negatively stained with freshly filtered 2% uranyl acetate, air-dried and imaged using a JEOL JEM-F200CF-HR electron microscope.

USC UNIVERSIDADE DE SANTIAGO DE COMPOSTELA

4.3.4 PrP amyloid digestion with PK

Recombinant PrP amyloid fibers were digested by the addition of PK from a concentrated stock solution to final concentrations (2mg/mL, 5mg/mL, 10mg/mL and 25mg/ml) and incubated at 42°C for 1h. Samples were mixed with Laemmli sample buffer and heated at 95°C for 10min, followed by SDS-PAGE 4-12% Tris/glycine gels. After electrophoresis, gels were stained with BlueSafe stain.

4.3.5 Animal model and housing conditions

The animal model, housing conditions and ethical considerations are described in the previous sections *3.3.1 Ethical statement* and *3.3.2 Animal model and housing conditions*.

4.3.6 TgVole mice inoculation and treatment.

Prion inoculation and mice treatment were conducted as it was previously described in sections *3.3.3 Prion inoculation* and *3.3.4 Mice treatment* with the following modifications.

Twenty-eight TgVole mice expressing ~1x BVPrP carrying the polymorphism 109I were anesthetized intraperitoneally with 0.2ml/10g body weight of a 1.2%(w/v) solution of tribromoethanol. The absence of paw withdrawal reflex was assessed to ensure deep anesthesia. Animals were then divided into one group of 12 individuals and 2 groups of 8 animals. The group of 12 animals and one group of 8 mice were treated intracerebrally with 20µL 0,5mg/mL of PrP amyloid in PBS. The remaining group of 8 mice received an intracerebral administration of 20µL of a saline buffer. Two weeks after the prophylactic treatment, the group of 12 mice that received the PrP amyloid and the group of 8 mice that received the saline buffer were inoculated intracranially using a disposable 29-gauge needle with 20µL of a 1% brain homogenate diluted in PBS, from a terminally ill mouse inoculated with a vole-adapted CWD strain.

USC UNIVERSIDADE DE SANTIAGO DE COMPOSTELA

Mice were observed twice a week until the onset of clinical signs; from that moment on, they were monitored daily until they reach a terminal stage when they were euthanized by cervical dislocation and subsequent decapitation.

Brains were removed and cut sagittally into two halves. One half was frozen for biochemical characterization and the other half was fixed in 10% formalin in PBS for histopathological and immunohistochemical analysis.

4.3.7 BRAIN HOMOGENATE PREPARATION AND WESTERN BLOT ANALYSIS

Brain homogenates and Western blot analysis were performed as it was previously mentioned in sections *3.3.6 Preparation of brain homogenates* and *3.3.7 Proteinase K digestion and Western blot analysis* with some minor modifications described below.

Frozen brains were suspended with PBS and protease inhibitors cocktail at 10% (w/v) and homogenized. For biochemical characterization of PK-resistant material by Western blot, 20µL of brain homogenates were digested with PK at a final concentration of 50µg/mL for 1h at 42°C and 800rpm. Subsequently, proteins were precipitated by the addition of MeOH and kept at -20 for 30min. Samples were centrifuged for 30min at 23000g, the supernatant was discarded and the pellet was resuspended in Laemmli sample buffer and heated for 10min, at 99°C and 800 rpm. Proteins were then separated electrophoretically in pre-cast 4-12% Bis-Tris gel and transferred to a PVDF membrane. The membrane was blocked for 1h in 5% blocking buffer and incubated with SAF83 (1:400) (epitope 130-160), SAF84 (1:400) (epitope 160-170), 12B2 (1:1000) (epitope 86-93) in 1% blocking buffer. After incubation, the membrane was washed three times with TBS-T for 10min, and then, the HRP conjugated anti-mouse secondary antibody (1:10000) diluted in TBS-T was added and incubated for 1h. After washing three times with TBS-T, the signal was revealed using Pierce ECL Western

USC UNIVERSIDADE DE SANTIAGO DE COMPOSTELA

Blotting substrate or Immobilon Forte Western HRP substrate. Images were obtained with ChemiDoc MP Imaging System and analyzed using Image Lab software.

4.3.8 PRION CONCENTRATION AND PURIFICATION FROM BRAIN HOMOGENATES

Aliquots of 200µL of 10% brain homogenates were treated with 100µg/mL Pronase E for 30min at 37°C and 800rpm. Samples were then incubated with 10mM EDTA, 2% (w/v) sarkosyl, and 50U of Benzonase for 10min, at 37°C and 800rpm. Subsequently, sodium phosphotungstate (NaPTA) was added to give the final concentration in the sample at 0,3% (w/v). After incubation for 30min at 37°C and 800rpm, iodixanol and NaPTA were added for final concentrations of 35% (w/v) and 0,3%(w/v), respectively, and centrifuged for 90min at 16100g. The clarified supernatant was transferred to a new tube and mixed with a buffer containing 2% (w/v) sarkosyl and 0.3% (w/v) NaPTA, incubated for 10min at 37°C and 800rpm and then centrifuged for 90min at 16100g. The clarified supernatant was discarded, and the insoluble pellet was resuspended in 20uL of wash buffer composed of 17,5% (w/v) iodixanol and 0,1% (w/v) sarkosyl and digested with PK for a final concentration of 10ug/mL for 1h at 37°C and 800rpm. After digestion, wash buffer and NaPTA for a final concentration of 0,3% (w/v) and centrifuged 30min at 16100g. The supernatant was discarded, and the previous step was repeated, and the final pellet was resuspended in NuPage loading buffer 1:3 (v/v)[419].

4.3.9 PROTEIN DEGLYCOSYLATION WITH PNGASE F

N-linked glycans were removed using PNGase F following the manufacturer's instructions. Briefly, 9µL of 10% brain homogenate was digested with PK as described above. Subsequently, 1µL of Glycoprotein Denaturing Buffer (10x) was added and incubated at 100°C for 10min. After heating, 5µL of water, 2µL of GlycoBuffer 2

USC UNIVERSIDADE DE SANTIAGO DE COMPOSTELA

(10x), 2µL NP-40 and 2µL PNGase F were added and incubated at 37°C, 800rpm, overnight.

4.3.10 HISTOPATHOLOGICAL AND IMMUNOHISTOCHEMICAL ANALYSIS.

The histopathological and immunohistochemical analysis were developed as it was described in section *3.3.8 Histopathological and immunohistochemical analysis.*

4.3.11 STATISTICAL ANALYSIS

Statistical analyses were performed using Graph Pad Prism 8 as it was described in section *3.3.9 Statistical analysis.*

USC UNIVERSIDADE DE SANTIAGO DE COMPOSTELA

4.4 RESULTS

4.4.1 A SELF-REPLICATING FULL-LENGTH PrP AMYLOID AS A THERAPEUTIC APPROACH FOR PRION DISEASES

In order to assess if this effect is independent of the animal model and the prion strain, we studied a therapeutic full-length BVPrP amyloid, that we termed "theraloid", in mice expressing ~1x BVPrP (109I). For this purpose, a recombinant full-length BVPrP protein expressed in E coli was fibrillated into an amyloid under partially denaturing conditions in a buffer containing 2M guanidine. The fibrillation was monitored by the ThT curve, and the fibrillation product was characterized by TEM and digestion with increasing concentrations of PK (Fig 3.1).

A group of 29 TgVole mice expressing ~1x BVPrP 109I sequence were divided into three groups: the theraloid group, saline control group, and amyloid control group, including 12, 8, and 9 mice, respectively. Mice from the theraloid group and the amyloid control group received an intracranial administration of 20µL 0,5mg/mL of the theraloid in PBS, whereas mice from the saline control group received an intracranial administration of 20µL of a saline buffer. After 2 weeks, mice from the theraloid group and the saline control group were inoculated intracerebrally with 20µL 1% BH from a terminally ill mouse inoculated with a bank vole-adapted CWD prion strain.

USC UNIVERSIDADE DE SANTIAGO DE COMPOSTELA

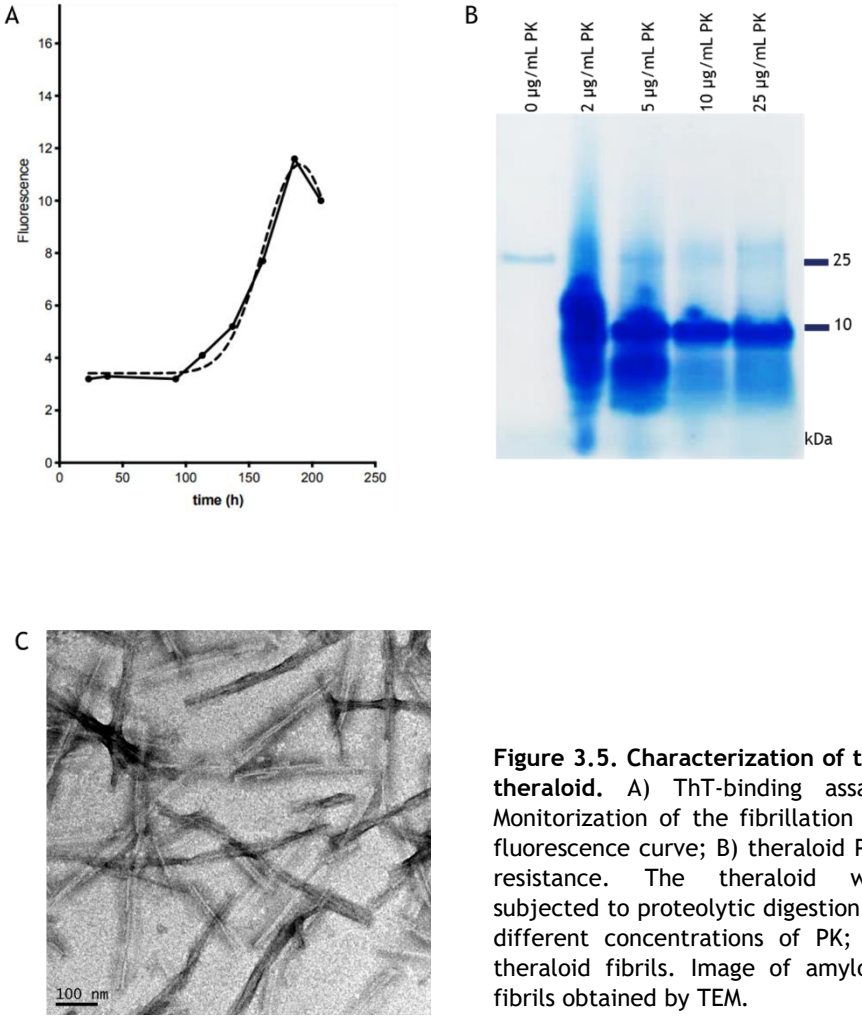


Figure 3.5. Characterization of the theraloid. A) ThT-binding assay. Monitorization of the fibrillation by fluorescence curve; B) theraloid PK-resistance. The theraloid was subjected to proteolytic digestion at different concentrations of PK; C) theraloid fibrils. Image of amyloid fibrils obtained by TEM.

Mice from the amyloid control group were only inoculated with the recombinant amyloid in order to assess that the amyloid was innocuous and that propagated in the brain, as well as it was previously reported.

USC UNIVERSIDADE DE SANTIAGO DE COMPOSTELA

After inoculation, mice were observed twice a week until the onset of clinical signs, after which they were monitored daily until they reached the terminal stage. At this point, mice were euthanized, and their brains were collected. One-half brain was immediately frozen for Western blot analysis, and the other half brain was fixed in paraformaldehyde for histopathological characterization.

After 60 days, all mice of the theraloid and the saline control group developed clinical signs characterized by kyphosis, ataxia, head bobbing, and body weight loss. The main survival time of mice treated prophylactically with the theraloid was 63,8±1,3dpi, while the survival of mice from the saline control group was 68,1±3,1dpi. There were no statistically significant differences between both groups (ρ=0,2756).

At that moment, all mice belonging to the amyloid control group were alive and with no apparent clinical signs.

Hematoxylin and eosin-stained brains showed statistically significant differences in the lesion profile in the hippocampus. While mice from the saline control group presented a classical pattern with characteristic lesions with moderate spongiosis in the thalamus and mild vacuolation in the striatum, hypothalamus, and brain stem; mice treated with the therapeutic amyloid presented, in addition to the previously mentioned lesions, moderate spongiosis in the hippocampus, indicating that the theraloid was probably propagating in this area. Interestingly, while the immunohistochemical analysis of those animals that received the saline buffer failed to reveal PrP^{res} deposits, in some of the mice treated prophylactically with the theraloid it could be discerned a weak and diffuse punctate staining in the hippocampus. This immunolabeling was only appreciated in those mice with the higher vacuolation in the hippocampus.

USC UNIVERSIDADE DE SANTIAGO DE COMPOSTELA

A

Group	Inoculation	Treatment	Dosing regimen	Attack rate	Mean ± SEM	p value
Theraloid	20µL 1% BH	20µL 0,5mg/mL PrP amyloid, i.c.	Days 14 prior prion inoculation	12/12	63,8 ± 1,3	0,2756
Saline		20µL 0,9% saline, i.c.		8/8	68,1 ± 3,1	
Amyloid	20µL 0,5mg/mL PrP amyloid, i.c.	-	-	-/8*	-	-

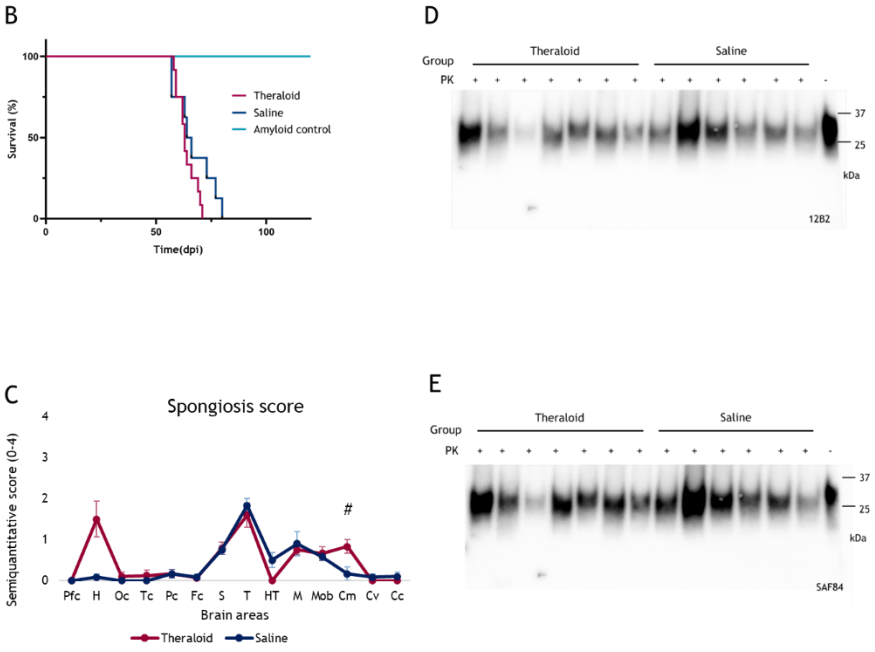


Figure 3.6. Prophylactic treatment with the theraloid did not prolong the survival of TgVole mice. A) Summary of the groups of mice and their corresponding treatment. Mice were separated into three groups: the theraloid group received a prophylactic administration of a PrP amyloid two weeks before inoculation; the saline control group received saline buffer two weeks before prion inoculation; and animals from the amyloid control group were inoculated solely with the amyloid. There were no statistically significant differences in the survival time between the theraloid and saline groups. Asterisk (*) indicates that one or more mice died during the procedure or due to intercurrent diseases. B) Kaplan-Meier curve. Seventy days

USC UNIVERSIDADE DE SANTIAGO DE COMPOSTELA

post-inoculation, all mice of the theraloid (dark red line) (n=12) and saline (dark blue line) (n=8) groups had died, while all mice inoculated just with the amyloid (turquoise line) (n=8) were alive with no clinical signs. C) Brain lesion profile. The spongiosis score represents the mean semi-quantitative scoring (0–4) of the spongiform lesions, which was essentially the same in both groups except for the lesion pattern in the hippocampus. While brains of untreated mice (dark blue) (n=6) did not show vacuolation in the hippocampus, all the animals treated with the theraloid (dark red) (n=6) presented different levels of spongiosis in this brain area. Pfc: piriform cortex; H: hippocampus; Oc: occipital cortex; Tc: temporal cortex; Pc: parietal cortex; Fc: frontal cortex; S: striatum; T: thalamus; HT: hypothalamus; M: mesencephalon; Mob: medulla oblongata; Cm: cerebellar nuclei; Cv: cerebellar vermis; Cc: cerebellar cortex. Error bars represent the SEM and hash (#) indicates that the pointed-out brain area could not be examined in all the samples. D) and E) Western blot analysis of mice brains from theraloid and saline control groups after performing a protocol of prion concentration. Brain homogenates were digested with PK 50µg/mL, and both groups of mice presented PK-resistant material. The same membrane was incubated with both 12B2 (1:2000) and SAF84 (1:400) antibodies showing the same electrophoretic pattern with both antibodies.

Western blot analysis of PK-digested brain homogenates showed PK-resistant material in the brains of mice from the theraloid and saline control groups. This PK-resistant material was incubated with two different antibodies, 12B2 and SAF84. Although the differences at the histopathological level, the electrophoretic pattern was similar in both groups of animals and with both antibodies (Fig 3.6).

Surprisingly, after 150 dpi, mice from the amyloid control group, which was initially a control group to assess the propagation and accumulation of the amyloid in the absence of the CWD prion strain, started displaying clinical signs. However, the symptoms of animals from this group were completely different from those inoculated with the vole-adapted CWD strain; indeed, these animals presented a long clinical period until they reach the terminal stage, characterized by reduced activity, aberrant gait (tiptoe walking), scruffy coat, and body weight loss. Finally, all the mice reached a terminal state and were euthanized. The average survival time was 198,7 ± 8,3dpi (Fig 3.7).

USC UNIVERSIDADE DE SANTIAGO DE COMPOSTELA

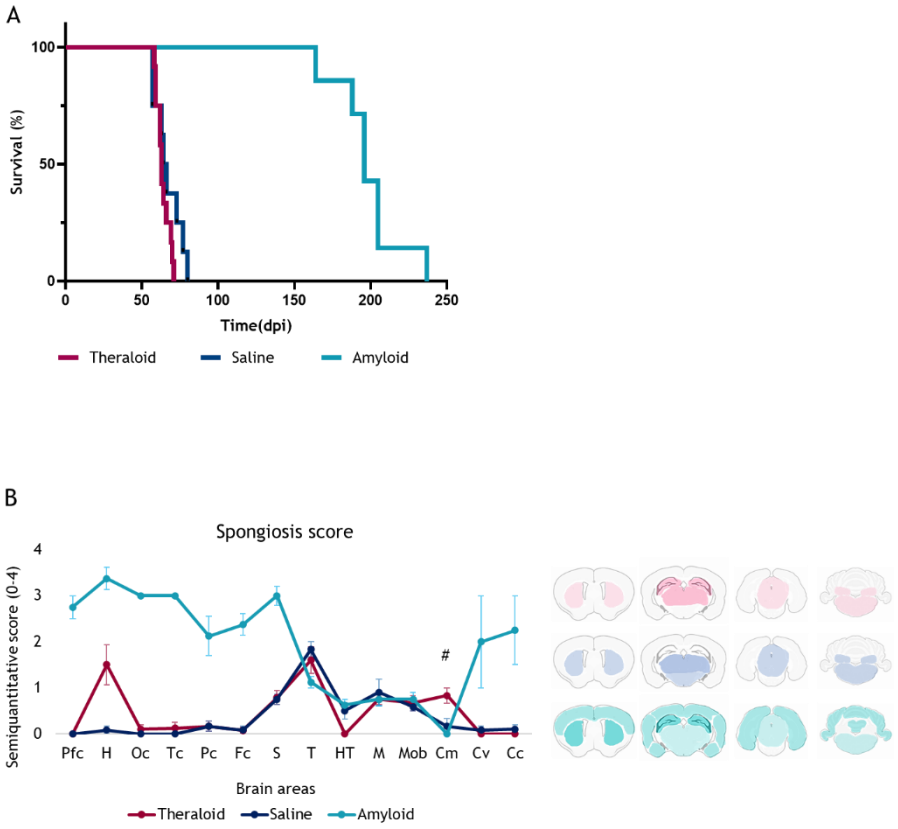


Figure 3.7 Control mice inoculated with the amyloid succumbed to a prion disease. A) Kaplan-Meier curve. Comparison of the survival time of mice from the theraloid (dark red) (n=12), saline (dark blue) (n=8), and amyloid group (turquoise) (n=8). The survival period was 63,8±1,3dpi, 68,1±3,1dpi, and 198,7±8,3dpi, respectively. B) Lesion profile and schematic representation of the brain affected areas. The histopathological profile represents the mean semi-quantitative scoring (0–4, vertical axis) of the spongiform lesions against these brain regions: Pfc: piriform cortex, H: hippocampus, Oc: occipital cortex, Tc: temporal cortex, Pc: parietal cortex, Fc: frontal cortex, S: striatum, T: thalamus, HT: hypothalamus, M: mesencephalon, Mob: medulla oblongata, Cm: cerebellar nuclei, Cv: cerebellar vermis, Cc: cerebellar cortex. In contrast to animals inoculated with the vole-adapted CWD strain, which presented a classical lesion pattern with spongiform changes in the brain stem, those animals inoculated just with the amyloid (n=4) presented an atypical pattern characterized by intense vacuolation in the neocortex,

USC UNIVERSIDADE DE SANTIAGO DE COMPOSTELA

hippocampus, and striatum. Error bars represent the SEM and hash (#) indicates that the pointed-out brain area could not be examined in all the samples.

The histopathological analysis showed clear differences in the lesion profile of mice inoculated with the vole-adapted CWD strain and the amyloid. While animals belonging to the theraloid and saline groups presented a classical lesion profile with spongiosis focus mainly in the basal ganglia, concretely in the corpus striatum, and in the brain stem, those animals belonging to the amyloid group displayed an atypical pattern whose most affected brain areas were the hippocampus and the neocortex. This group presented intense gliosis and loss of pyramidal neurons in the hippocampus, and granular cell loss in the cerebellar cortex. Moreover, in contrast to mice inoculated with the vole-adapted CWD strain that had no detectable PrP^{res} deposits, immunohistochemical staining of brains of mice inoculated with the amyloid showed clear subventricular plaques, additionally, diffuse punctate staining was observed in the oriens layer of the hippocampus. These immunolabeling was also detected in some animals belonging to the theraloid group, as was aforementioned (Fig 3.8).

To further characterize the material that was propagating in these animals, brain homogenates were digested with PK and subjected to western blot analysis. The electrophoretic pattern was compared with a classical prion strain, 263K.

USC UNIVERSIDADE DE SANTIAGO DE COMPOSTELA

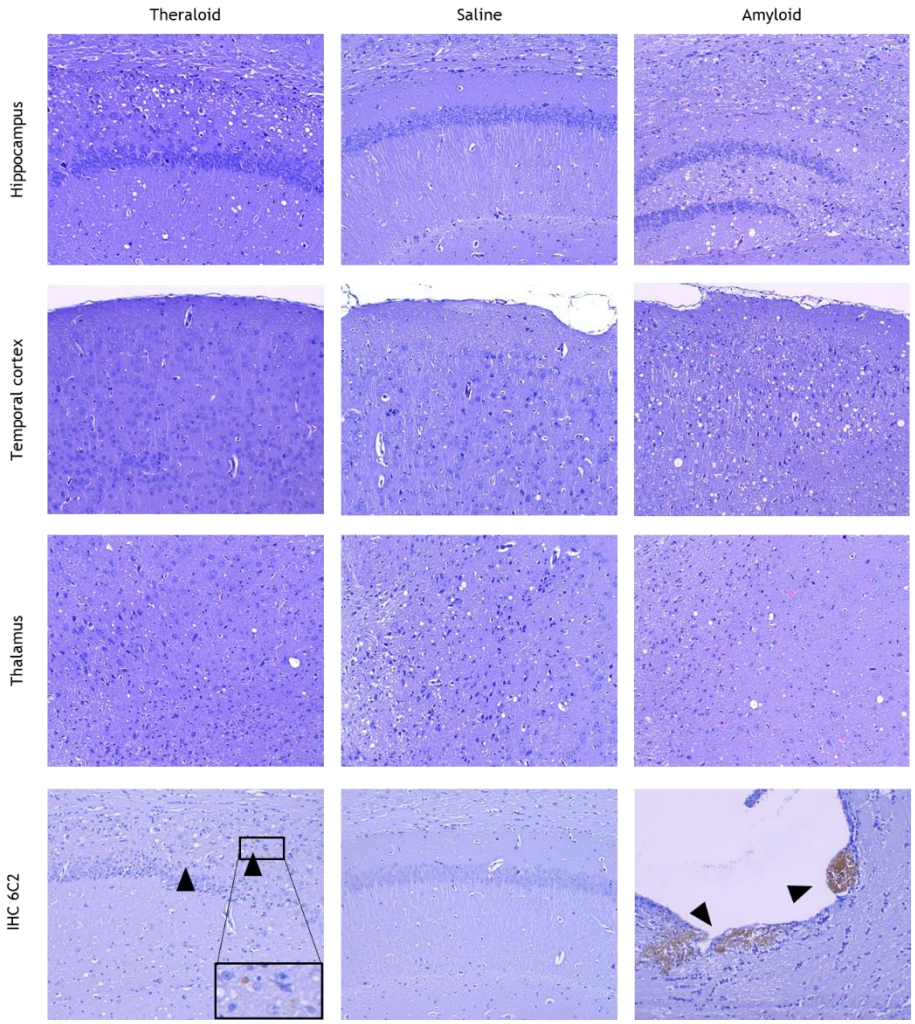


Figure 3.8. Hematoxylin-eosin staining and immunohistochemistry. Histopathological examinations confirmed the presence of vacuolation in all animals independently whether they belonged to the theraloid (n=7), saline (n=6) or amyloid control group (n=4). Moderate vacuolation in the thalamus was common to all groups. Animals that received the amyloid, either accompanied by the vole-adapted CWD inoculum or alone, presented vacuolation in the hippocampus, intense gliosis and, loss of pyramidal neurons in this brain area. A spongiform change was also perceivable in the temporal cortex of mice belonging to the amyloid control group.

USC UNIVERSIDADE DE SANTIAGO DE COMPOSTELA

Immunostaining with the monoclonal antibody 6C2 (1:1000) revealed PrP deposits only in those animals that received the amyloid, whereas the immunolabeling was negative in mice of the saline group. Such deposits were extremely weak and diffuse in the theraloid group, while animals of the amyloid group presented clear subventricular plaques. Arrowheads indicate deposits of PrP^{res}.

PK-resistant material was recognized by the C-terminal antibody, SAF84 (epitope 160-170), while it was not detected using SAF83, an antibody that recognizes the central region of the PrP sequence (epitope 130-160). The visible bands with SAF84 had an approximate molecular weight of ~21, ~17, and ~13kDa. When this material was treated with PNGase F, the three bands merged in a single band of ~13kDa, which corresponded to the PK-resistant core of the amyloid, which size is 10kDa, plus the GPI anchor (~3kDa). Thus, the fragments present in the brain homogenate and recognized by SAF84 corresponded to the di-glycosylated, mono-glycosylated, and non-glycosylated bands. The size of such bands contrasted with the molecular weight of classical prions such as 263K, which sizes are approximately ~30, ~27, and ~21kDa. These results showed that the atypical material that was spreading and accumulating in the brain of mice from the amyloid group was originated from the recombinant amyloid, which PK-resistant core comprise from position 153/154 to 231 (Fig 3.9).

These results demonstrate that the PrP amyloid was fully infectious in TgVole mice expressing physiological levels of PrP and with an attach rate of 100%. Furthermore, the mean incubation time of 200 days, a period of incubation lower than some recombinant prion strains [420].

USC UNIVERSIDADE DE SANTIAGO DE COMPOSTELA

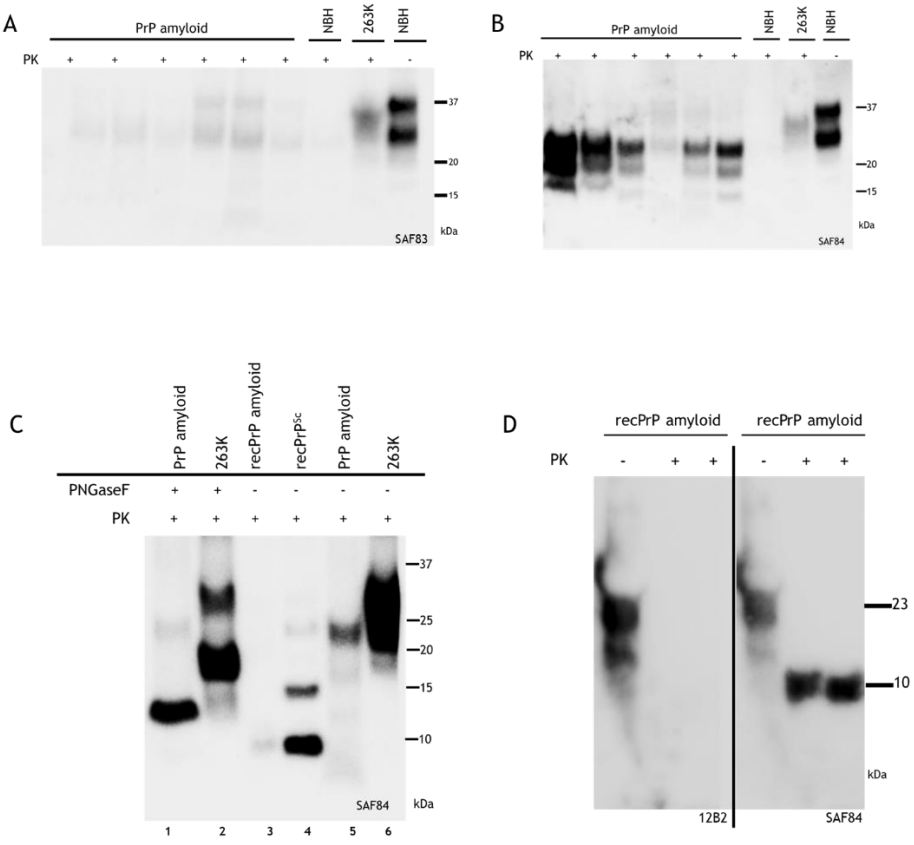


Figure 3.9. Biochemical characterization of brain-derived material from mice inoculated with the recombinant PrP amyloid. A) Brain homogenates were digested with PK and subjected to Western blot analysis. No PK-resistant material from mice inoculated with the amyloid was detected with the central-region antibody, SAF83 (1:400). B) Western blot incubated with the C-terminal antibody, SAF84 (1:4000), showed an atypical electrophoretic pattern with ~21, ~17, and ~13kDa bands. C) Brain homogenate of animals inoculated with the PrP amyloid (lane 1) and also brain homogenate of a hamster inoculated with 263K prion strain (lane 2) were deglycosylated with PNGaseF and compared with the recombinant amyloid used as inoculum (lane 3); a recombinant prion strain (lane 4) and both brain homogenates treated with PK but non-deglycosylated (lanes 5 and 6). D) Western blot of the recombinant PrP amyloid digested with PK revealed that the material inoculated consisted of a C-terminal PK-resistant core recognized with the antibody SAF84 (epitope 160-170) but not with 12B2 (epitope 86-93).

USC UNIVERSIDADE DE SANTIAGO DE COMPOSTELA

4.4.2. SERIAL TRANSMISSION OF PrP^{Ss} DID NOT ENTAIL THE EMERGENCE OF CLASSICAL PrP^{Sc}

In previous works, Makarava and colleagues described different PrP amyloids which propagated in hamster brains, although the propagation was silent and none of the amyloids triggered clinical signs on the first passage [400,416]. In one of their works, the authors presented the first PrP amyloid, which inoculated in Syrian hamsters propagated following a PrP^{Sc} pattern and sharing biological features with classical strains such as 263K. This amyloid was called SSLOW (Synthetic Strain Leading to OverWeight) [416]. Nonetheless, in other work, the authors showed a different PrP amyloid, called LOTSS (Low Toxicity Synthetic Strain), whose electrophoretic pattern was atypical (featuring a C-terminal PK-resistant core), instead of classical such as SSLOW. The first and the second passages of this amyloid were innocuous for the hamsters, which did not develop clinical signs, although they accumulated PK-resistant material. However, animals from the third passage developed clinical signs and presented classical PrP^{Sc} in their brains [400].

The emergence of classical PrP^{Sc} after inoculation of a recombinant PrP amyloid was also described by Choi and colleagues. To summarize, these authors inoculated an N-terminal amyloid, product of the fibrillation of the PrP peptide 23-144, into a mouse model that overexpressed PrP and wild-type mice. This amyloid triggered a prion disease, evidenced by the emergence of clinical signs on the first passage and the accumulation of PK-resistant material. Although the inoculated amyloid was N-terminal, the PK-resistant material found in these animals was a mixture of atypical and classical patterns; nonetheless, this material evolved after serial transmission while the atypical pattern decreased, the classic was the predominant one [421].

The PrP amyloid that we presented in this work shared similarities with LOTSS regarding the electrophoretic pattern. Thus, serial transmission of this PrP amyloid was carried out to assess whether the biological and biochemical features changed in subsequent passages, as well as the previously reported recombinant PrP amyloids. We assigned the name

USC UNIVERSIDADE DE SANTIAGO DE COMPOSTELA

PrP^{Ss}, to this amyloid, from $\mathbf{S}_{SLOW}$, the first infectious recombinant PrP amyloid.

For this purpose, a group of 8 TgVole mice was inoculated with 20µL of 1% BH from a terminally sick animal inoculated with the recombinant PrP amyloid, henceforth, the first passage of PrP^{Ss}. All the mice succumbed to prion disease and presented a long clinical period before reaching the terminal stage. This group of mice showed signs such as kyphosis, reduced activity, tiptoe walking, and scruffy coat. Such symptoms were similar to those displayed in animals from the first passage. The main incubation time was 118,1 ± 7,1dpi, lower than the first passage, which could indicate an adaptation of PrP^{Ss}. When all the mice from the second passage had died, a third group of 8 mice was inoculated with a pool of brain homogenates of mice from the second passage, at a concentration of 1% in PBS. Likewise, this group of animals developed clinical signs similar to the first and second passage, characterized by reduced activity, kyphosis, scruffy coat, and tiptoe walking. The duration of the clinical stage of this group was shorter in comparison with the previous passages, 96,4 ± 4,3dpi (Fig 3.10), and the difference in the average incubation time between the second and third passage was statistically significant (ρ=0,0202).

USC UNIVERSIDADE DE SANTIAGO DE COMPOSTELA

A

Group	Inoculum	Attack rate	Mean ± SEM
1st passage PrP^{Ss}	20µL 0,5mg/mL recPrP amyloid	8/8*	198,7 ± 8,3
2nd passage PrP^{Ss}	20µL 1% BH 1st passage	8/8	118,1 ± 7,1
3rd passage PrP^{Ss}	20µL 1% BH pool 2nd passage	8/8	96,4 ± 4,3

B

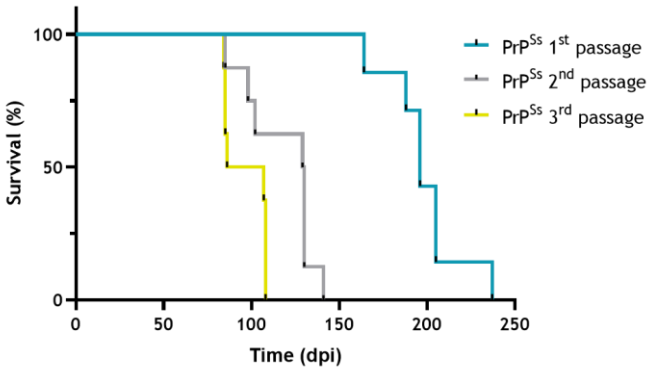


Figure 3.10. Serial transmission of PrP^{Ss} showed an adaptation manifested by the reduction in the time of incubation. A) Summary table of the three passages. All passages had an attack rate of 100% and periods of incubation were clearly shorter. B) Kaplan-Meier curve. Survival curve of the three passages. Although the average incubation time of the second and third passages was closer, there were statistically significant differences between them (ρ=0,0202).

Brain homogenates of mice from the three passages were subjected to Western blot analysis and revealed an evident reduction in the amount of PrP^{Ss}, while the pattern was apparently similar among the three passages. There was no evidence of classical PrP^{Sc} propagation when samples were incubated with different antibodies, SAF84 and 12B2 (Fig 3.11).

USC UNIVERSIDADE DE SANTIAGO DE COMPOSTELA

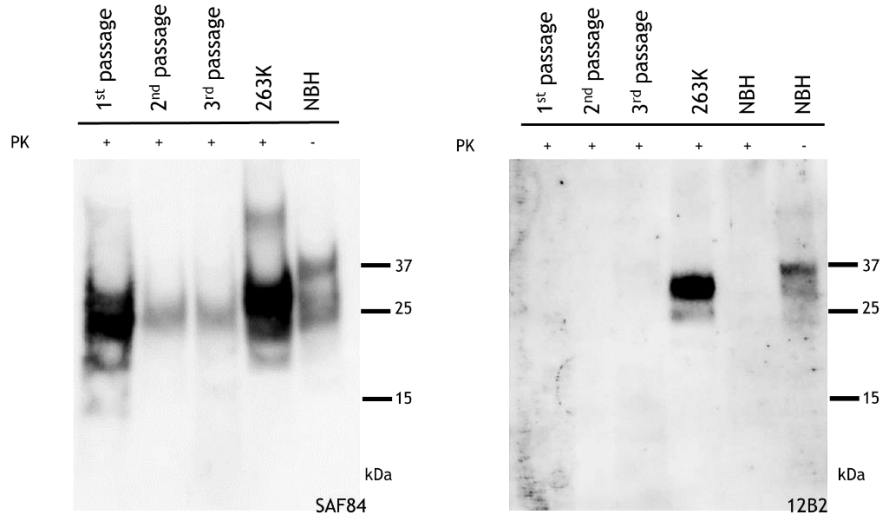


Figure 3.11 Western blot analysis of brain homogenates of mice from the three passages. The Western blot showed much less amount of PK-resistant material, even when the volume of brain homogenates from the second and third passage used for this Western blot was three times the volume of brain homogenate from the first passage. Although the low signal, the pattern seemed the same, and classical PrP^{Sc} was not distinguished either when the antibody SAF84 was used, or with the antibody 12B2.

Although N-terminal antibodies, such as 12B2 or 9A2, did not recognize PK-resistant material when regular volumes of brain homogenate were analyzed, when 10 times of brain homogenates were subjected to a protocol of concentration and prion purification[419], N-terminal low molecular weight bands (~8kDa) arose in samples from the three passages (Fig 3.12). Such N-terminal low molecular weight fragments were similar to the atypical material found in brains of transgenic mice that overexpress the BV (109I) prion protein, and which develop sporadically a prion disease.

USC UNIVERSIDADE DE SANTIAGO DE COMPOSTELA

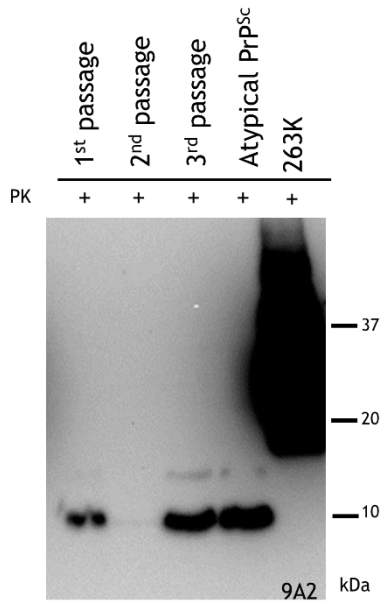


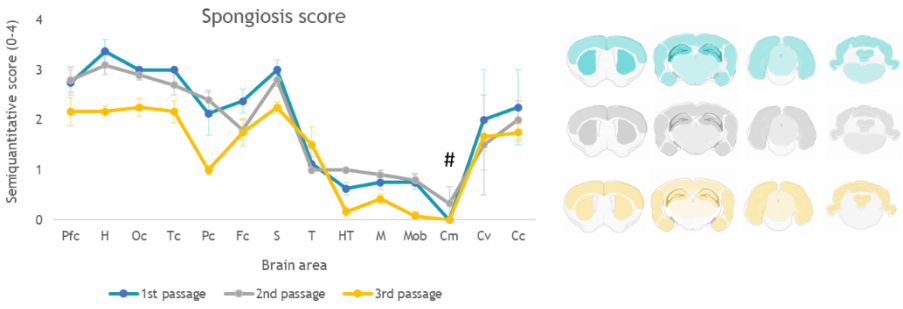
Figure 3.12. Western blot analysis after performing a protocol for prion concentration. Atypical PrP^{Sc} was detected in samples from the three passages with the N-terminal antibody 9A2 after carrying out a protocol for prion concentration. 263K and a sample from TgVole 4x mice were included as controls.

Examinations of fixed brains revealed that the lesion profile, as well as the location of PrP^{res} deposits remain invariablle along the serial transmission. Spongiform changes mainly affected the neocortex, archicortex and cerebellar cortex. In this last brain area, moderate vacuolation was accompanied by loss of neurons of the granular layer, with an absence of PrP^{res} deposits. The inspection of the hippocampus showed a clear gliosis and loss of pyramidal neurons, with punctate granular deposits of PrP^{res}, which are more intense in the oriens layer. These results indicate that the agent responsible for the spongiform lesions was the same in the three passages (Fig 3.13).

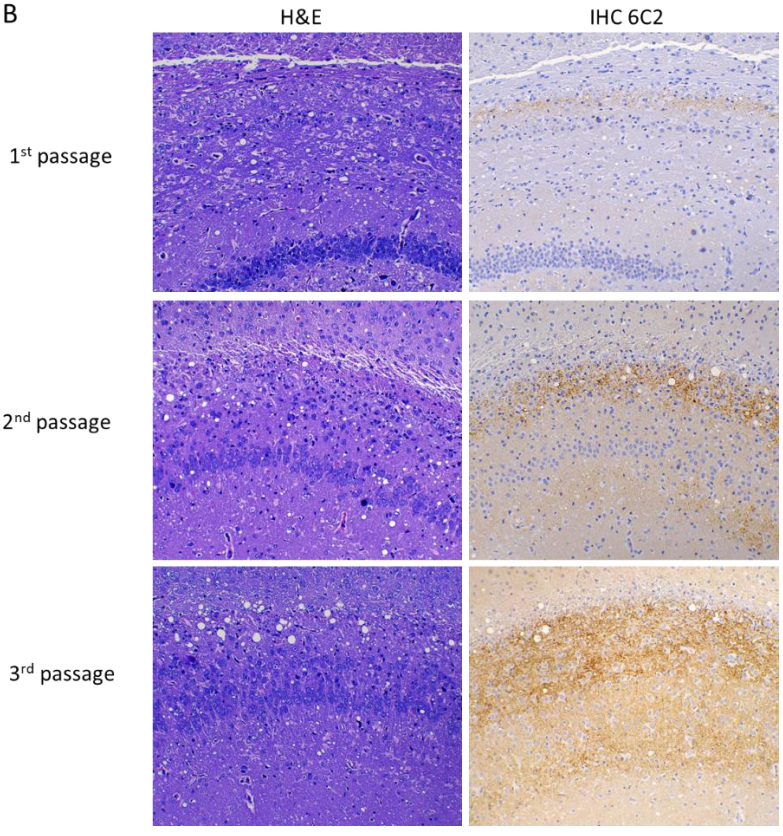
Taken together, these results determined that the PrP amyloid behaved as a *bona fide* prion, and after serial transmission, this prion stabilized with an average incubation time close to 100dpi and propagated both, C-terminal and N-terminal atypical PK-resistant fragments.

USC UNIVERSIDADE DE SANTIAGO DE COMPOSTELA

A



B



USC UNIVERSIDADE DE SANTIAGO DE COMPOSTELA

Figure 3.13. Histopathological and immunohistochemical analysis of mice from the three passages of PrP^{Ss}. A) Brain lesion profile and schematic representation of the brain affected areas. The histopathological profile represents the mean semi-quantitative scoring (0–4, vertical axis) of the spongiform lesions against these brain regions: Pfc: piriform cortex, H: hippocampus, Oc: occipital cortex, Tc: temporal cortex, Pc: parietal cortex, Fc: frontal cortex, S: striatum, T: thalamus, HT: hypothalamus, M: mesencephalon, Mob: medulla oblongata, Cm: cerebellar nuclei, Cv: cerebellar vermis, Cc: cerebellar cortex. All the mice present a similar pattern of spongiform change that mainly affect the neocortex, archicortex, cerebellar cortex, corpus striatum and thalamus. Hash (#) indicates that the pointed-out brain area could not be examined in all the brains. B) Immunolabeling of PrP^{res} deposits with the monoclonal antibody 6C2 (1:1000) revealed punctate granular deposits in the hippocampus.

USC UNIVERSIDADE DE SANTIAGO DE COMPOSTELA

4.5 DISCUSSION

4.5.1 A SELF-REPLICATING FULL-LENGTH PRP AMYLOID AS A THERAPEUTIC APPROACH FOR PRION DISEASES?

Prion diseases are fatal and incurable neurodegenerative conditions and despite decades of efforts, there is still no treatment for these illnesses. One therapeutic strategy that exhibited moderate results in preventing prion diseases in animals was based on the use of a PrP amyloid[417]. This PrP amyloid shared a homologous primary sequence with PrP^{Sc} but differed in the quaternary structure[110,395] and was hypothesized to compete with PrP^{Sc} for the substrate (PrP^{C}) while it was innocuously accumulating in the brain. In hamsters, this competition resulted in a delay in the onset of clinical signs when amyloid was administered some weeks before prion inoculation. Moreover, when animals were exposed to low titers of prions, the prophylactic treatment with the PrP amyloid prevented some animals from acquiring a prion disease, while all animals that did not receive the treatment succumbed to the disease [417]. In addition, the silent propagation of this and other PrP amyloids were also corroborated by other authors [186,395,400,416,422–424].

In the current work, the same strategy was tackled but by using a different animal model, a transgenic mouse expressing ~1-1,2x BVPrP (109I) (TgVole). Hence, recombinant BVPrP bearing the polymorphism 109I was fibrillated into an amyloid and characterized by different techniques. Mice were divided into three groups and intervened as follows: one group of mice, called theraloid group, received a prophylactic intracranial administration of the amyloid, and two weeks later animals were inoculated with a vole-adapted CWD

USC UNIVERSIDADE DE SANTIAGO DE COMPOSTELA

prion strain; another group of mice, called saline control group, received an intracranial administration of saline buffer, and two weeks later mice were inoculated by the same route with a vole-adapted CWD prion strain; the last group, called amyloid control group, received only an intracranial administration of the recombinant PrP amyloid.

In contrast to previous works[417], the prophylactic administration of the recombinant amyloid did not delay the onset of prion disease. Although the theraloid did not prolonged the survival, detailed anatomopathological examinations demonstrated that the theraloid was propagating and accumulating in the brain [400,416]. Animals treated prophylactically with the theraloid presented a noticeable affectation of the hippocampus and the presence of periventricular and hippocampal PrP^{res} deposits. Such histopathological features were not perceivable in brains of mice from the saline control group; therefore, these features could only be caused by the theraloid. Nonetheless, Western blot analysis revealed a similar electrophoretic pattern in both groups of animals and with analogous amounts of PrP^{Sc}. The most reasonable explanation why at this point PrP^{Ss} was not detected by Western blot is that the timeframe that PrP^{Ss} had to accumulate in the brain was too short, and when mice succumbed to the prion disease caused by the CWD inoculum (68dpi), the amount of PrP^{Ss} was minuscule in comparison to the classical material.

One possible reason why the treatment with the recombinant PrP amyloid was not effective, could be the period of time between the prophylactic treatment and the inoculation. Diaz-Espinoza and colleagues treated prophylactically hamsters at different time points (15, 36, and 63 days) before the inoculation with the 263K strain. Although the longest survival was obtained when hamsters were treated 63 days before inoculation, the treatment 15 days before also demonstrated a clear effect, and was the posology chosen for this work. Nonetheless, at the same inoculum concentration (1% of brain homogenate), 263K spread slower than the vole-adapted CWD strain (~85 vs ~68dpi); thus, the timeframe the amyloid had to propagate and

USC UNIVERSIDADE DE SANTIAGO DE COMPOSTELA

start recruiting PrP^C was shorter in our model and it is most likely that this time was not sufficient to see an effect on the survival.

4.5.2 THE RECOMBINANT PRP AMYLOID PROPAGATED IN MICE BRAINS AND CAUSED A FATAL DISEASE

Unexpectedly, mice from the amyloid control group recapitulated a prion disease, and all the mice died at approximately 198dpi. The clinical symptoms of these mice were completely different from those observed in animals inoculated with the CWD strain, ruling out the possibility of cross-contamination with CWD prions as the origin of the prion disease in this group. In addition, the PK-resistant material present in the brain of these mice displayed an atypical electrophoretic pattern, composed of C-terminal fragments whose PK-resistant core was 154-230 and a minority N-terminal band of ~8kDa that was only detected when large amounts of brain homogenates were analyzed. Previous works documented the propagation and accumulation of PK-resistant material in the brains of animals after inoculation of a full-length recombinant PrP amyloid; however, the propagation was subclinical, and no animals displayed clinical signs compatible with prion disease on the first passage [178,186,400,416,422,423,425]. Only Choi and colleagues synthesized an amyloid from a truncated PrP protein (23-144) that triggered a prion disease in wild-type and Tga20 mice (this model overexpresses 10x the PrP protein [426]), which had an average incubation time of ~534 and ~254dpi, respectively[421], much longer than the animal model used in the present work.

Serial transmission of the material generated in the brain of mice inoculated with PrP amyloids led to the origin of classical PrP^{Sc}, which was accompanied by a reduction in the incubation period. The deformed templating process was postulated as the origin of classical PrP^{Sc} from the amyloids synthesized by Makarava et al and Choi et al. The deformed templating theory supports the idea that an environmental change is an event that boosts the generation of conformational variants,

USC UNIVERSIDADE DE SANTIAGO DE COMPOSTELA

"strains", in a sort of trial-and-error seeding event, and eventually, one strain that fits in the new scenario emerges from the pool [415]. In the case of Makarava and Choi's works, the deformed templating phenomenon would be triggered by the inoculation of the recombinant PrP amyloid in the brain, which presents a different environment than that of the buffer where the amyloid was synthesized and propagated initially and the presence of native PrP^{C} instead of recombinant PrP.

Serial transmission of the material generated in the brain of our mice after inoculation of the PrP amyloid, that we have called PrP^{Ss}, resulted in an adaptation evidenced by the reduction in the average incubation time throughout the subsequent passages. Based on Makarava and Choi's results, we expected that PrP^{Ss} would be subjected to deformed templating, leading to the emergence of classical PrP^{Sc} species after serial passages. Nonetheless, this molecular change did not take place, and PrP^{Ss} remained invariable throughout the passages.

Regarding the biochemical features of PrP^{Ss}, the C-terminal PK-resistant material undoubtedly corresponds to the inoculated recombinant amyloid, which had a C-terminal PK-resistant core; however, the origin of the N-terminal PK-resistant material is unclear. The analysis by Western blot of the inoculum prior inoculation demonstrated that no N-terminal PK-resistant material was present in the inoculum. Consequently, this material might be originated in the brain of mice after inoculation.

Since both N-terminal and C-terminal material propagated invariably after serial transmission, a possible explanation is that both residues are complementary parts of the same PrP molecule, meaning that both compose PrP^{Ss}. Therefore, when the recombinant amyloid was inoculated, instead of being subjected to deformed templating to originate classical PrP^{Sc}, the deformed templating process would had been incomplete and led to the formation of two PK-resistant fragments joined by a PK-sensitive central region. Based on the fact that the

USC UNIVERSIDADE DE SANTIAGO DE COMPOSTELA

deformed templating did not progress to classical PrP^{Sc} after serial transmission, this PrP^{Ss} particle might be stable.

On the other hand, the idea that the C-terminal (PrP^{Ss}) and the N-terminal species are different entities that propagate simultaneously, cannot be ruled out. The presence of mixtures of prions strains propagating together was described in numerous works, reporting cases of patients and animals that got naturally sick, but also animals inoculated incidentally in the laboratory [340,427–430]. Based on the idea that PrP^{Ss} and the N-terminal strain are different species, the provenance of the N-terminal strain would lie in the proper animal model. Interestingly, transgenic mouse models such as Tg3574, TgVole (4x), and Tg3581, that overexpress three-, four-, and five-fold the BVPrP 109I protein, respectively, develop spontaneously a prion disease. The onset of the disease occurs after 340 (Tg3574), 182 (TgVole 4x), and 218 days (Tg3581), and is characterized by the accumulation of a N-terminal PK-resistant fragment similar to that we identified in our mice [431–434].

Although information about the accumulation of PrP^{res} in age-matched mice or the susceptibility to develop spontaneous prion diseases in our animal model has not been published, it is worth noting that these mice express approximately physiological levels of BVPrP 109I (~1-1,2x) and we have not found evidence of the accumulation of PrP^{res} after 120, 300 or 400 days (Fig 3.14)[101]. However, it is possible that the inoculation with the recombinant amyloid accelerated or promoted the accumulation of a prion strain that animals with this genetic background tends to accumulate naturally[435]. Therefore, in normal conditions, it is most likely that the accumulation of PrP^{res} our mice is so gradual that it is undetectable within their lifespan [429,436–440]. Nevertheless, the inoculation of the recombinant amyloid accelerates the generation such prion strain that then coexist with PrP^{Ss} in an apparent equilibrium.

At this point the question that arises is, which of the two species, PrP^{Ss} or the N-terminal strain, is responsible for the prion disease in these

USC UNIVERSIDADE DE SANTIAGO DE COMPOSTELA

animals? To address this query, we assumed that the initial event after the PrP amyloid inoculation is the propagation of PrP^{Ss}, followed by the subsequent the emergence of the N-terminal strain. Considering this premise, we turn to the histopathological findings. The main feature that distinguishes the prion disease in animals inoculated with the amyloid from those with the CWD strain is the impact on the hippocampus and cerebral cortex. Interestingly, an incipient vacuolation in the hippocampus was even appreciated in those mice inoculated with both, the PrP amyloid and the CWD strain, which succumbed after 68dpi. This observation implies that spongiosis due to the amyloid is already evident after this timeframe. Since the hippocampal affectation is the first histopathological feature that emerge after inoculation of the amyloid and is consistent throughout the passages, we consider that the specie responsible for the disease would be PrP^{Ss}.

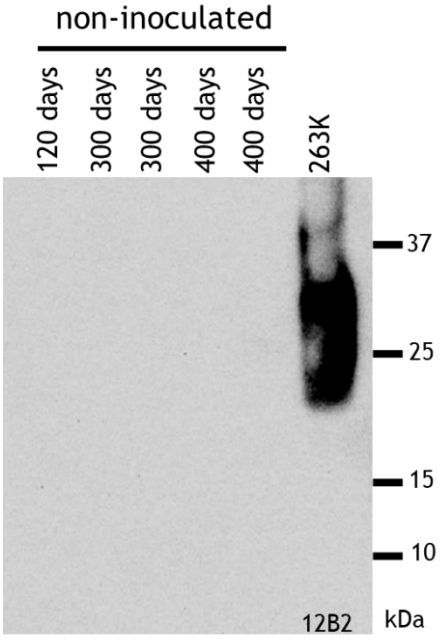


Figure 3.14. Non-inoculated TgVole mice did not accumulate PK-resistant PrP. TgVole mice were culled at different time points to assess if at different ages it was possible to detect PK-resistant PrP after subjected the brain homogenates to a protocol of prion concentration. Samples were challenged with the N-terminal antibody 12B2 (1:1000).

USC UNIVERSIDADE DE SANTIAGO DE COMPOSTELA

To summarize, the present work demonstrated that a recombinant PrP amyloid can behave as a *bona fide* prion triggering a prion disease in an animal model that expresses ~1x the PrP protein. This work also shows the narrow border between infectious and non-infectious PrP proteins, and why amyloids, independently of the size of their core, must also be considered as potentially infectious agents, since their infectivity most likely depends on the selection of a suitable animal model.

USC UNIVERSIDADE DE SANTIAGO DE COMPOSTELA

4.6 SALIENT REMARKS

1. The prophylactic administration of the recombinant PrP amyloid, termed theraloid, had no effect on the survival of prion infected mice.

2. Animals treated with the theraloid presented distinct histopathological features, indicating that the theraloid was propagating.

3. The theraloid resulted infectious in TgVole mice, triggering a prion disease in those animals that were solely inoculated with the amyloid.

4. Mice inoculated with the theraloid accumulated and propagated two different prion strains.

5. The amyloid was serially transmitted to TgVole mice, indicating that the recombinant PrP amyloid was a *bona fide* prion.

6. The biological and biochemical properties of the amyloid were maintained after serial transmission.

USC UNIVERSIDADE DE SANTIAGO DE COMPOSTELA

5. CHAPTER III: CHARACTERIZATION OF RECOMBINANT PRION STRAINS GENERATED BY PMSA WITH DIFFERENT COFACTORS

USC
UNIVERSIDADE DE SANTIAGO DE COMPOSTELA

5.1 INTRODUCTION

5.1.1 PRION STRAINS

The concept of "strain" is defined in microbiology as "the lineage or subtype of an organism genetically distinct from another by one or more mutations," and it is widely applied to viruses and bacteria. Nowadays, it is well-known that prions are not slow viruses and that they lack genetic material; nevertheless, the term "strain" has been applied to prions since the early 1960s [79], when it was under discussion the sort of pathogen that caused scrapie. Decades before, in 1926 Stockman had already described two syndromes in scrapie-affected sheep termed "nervous" if sheep presented lethargy, or "itching" if animals showed hyperactivity and intense scratching syndrome [441]. However, it was in 1961 when Pattison and Millson transmitted specifically two forms of the disease that emerged after serial passages of a sheep isolate in goats [79]. These strains, termed "drowsy" and "scratching" were transmitted to other individuals after inoculation with brain-derived material from animals that distinctly presented one or the other clinical syndromes, demonstrating that the nature of the inoculum determined the phenotype and, therefore, both syndromes would be caused by different scrapie strains [441]. The use of rodent models permitted an in-depth and fast study of prion isolates and allowed to distinguish a large variety of prion strains with particular phenotypes, brain tropism, and incubation period [442].

Prion strains are biologically defined by the properties mentioned above: the incubation period, the brain lesion profile, and the clinical syndrome. The incubation period of prion diseases is characterized by a long asymptomatic course followed by a short clinical stage. In mice,

USC UNIVERSIDADE DE SANTIAGO DE COMPOSTELA

the average incubation time can extend from 35 [345] to more than 500 days[443]; nonetheless, it is a reproducible parameter under controlled experimental conditions. The incubation period critically depends on three factors as well: the titer, the route of inoculation, and the genetic background of the host. The titer or titration is the concentration of infectious particles in the inoculum, and the incubation period linearly depends on the logarithmic concentration of prions [444,445]; therefore, the higher the titer, the shorter the period of incubation. The route of inoculation is also an essential factor that affects the incubation of prion diseases; consequently, direct inoculation into the CNS presents shorter incubation periods than other routes, such as intraperitoneal, intravenous, or oral[446,447]; in fact, sometimes the inoculation through peripheric routes is so slow that animals do not develop clinical signs throughout their lifespan, although the accumulation of PrP aggregates can be detected in their tissues. Regarding the host properties, the expression level of PrP significantly determines the incubation time. The long incubation time of some prion strains led to the generation of transgenic mice that overexpress the PrP protein, in this manner, the incubation time can be reduced from 131 to 60 days respecting wild-type animals [448]. Apart from the expression level, interspecies or intraspecies polymorphisms, or biochemical modification, such as the absence of N-linked glycans or GPI, dramatically affect the incubation period as well. These factors hamper the propagation and increase the incubation period, entailing a transmission barrier.

Sometimes, the incubation period of two strains coincides, and it is impossible to distinguish them by this feature. This is the case of the mouse-adapted scrapie strains ME7, 139A, and 79A; all of them have a similar period of incubation in C57BL/6 mice, ~160-170 dpi, when they are inoculated intracerebrally. Nonetheless, their tropism, or tendency to accumulate in specific brain areas, is different. While the ME7 strain presents high vacuolation in the medial thalamus and the septum, scarcely affects the white matter; on the other hand, 79A and 139A display spongiosis in the pyramidal tract, whereas they vary in the

USC UNIVERSIDADE DE SANTIAGO DE COMPOSTELA

vacuolation of the cerebellar white matter [449–451]. Therefore, the location of the spongiosis, the semiquantitative evaluation of the spongiosis severity, and the PrP^{Sc} deposition into the brain provide crucial information about the neuropathology, and they are essential for discerning or identifying prion strains [452].

The first evidence of prion disease is the clinical signs. Scrapie strains, "nervous" and "itching", fortunately showed distinct signs, so it was easy to distinguish them. However, infected animals can present a large variety of clinical signs and it is usual that different strains share symptoms; furthermore, animals commonly display more than one sign. Therefore, the clinical syndrome alone is generally not sufficient to identify a prion strain [453–455].

Prion strains can be discriminated by their biochemical properties as well. One of the most relevant biochemical features is the electrophoretic mobility of PK-resistant PrP^{Sc} fragments. Distinct migration patterns manifest biochemical or conformational differences, which are reflected as variations in the molecular weight of the PK-resistant fragments. One of the most relevant distinctions in the electrophoretic pattern is the mobility of the unglycosylated band, which can display a molecular weight of ~21 or ~19kDa. This difference provides a critical tool for diagnosing sCJD since in type 1 sCJD patients, this band migrates at ~21kDa, whereas in type 2 sCJD patients this band migrates at ~19kDa [456]. Apart from the electrophoretic pattern, the glycoform ratio is also a biochemical signature of each strain. The PrP^{C} glycosylation profile is complex and can vary regarding the tissue; nonetheless, the glycoform ratio of the PrP^{Sc} after digestion with PK is strain-specific[450,457].

Other biochemical techniques used to discern prion strains are the resistance to proteolytic degradation or to denaturalization with chaotropic agents. The relative resistance to PK has been widely used to characterize prion strains with similar electrophoretic and glycoform patterns [458,459]; in addition, this resistance to PK has also been assessed

USC UNIVERSIDADE DE SANTIAGO DE COMPOSTELA

in the presence of denaturants such as guanidine or urea, or detergents, like sarkosyl [457,458,460,461]. The effects on the different prion strains when subjected to these treatments proved their stability and, therefore, their structural differences (Fig 4.1).

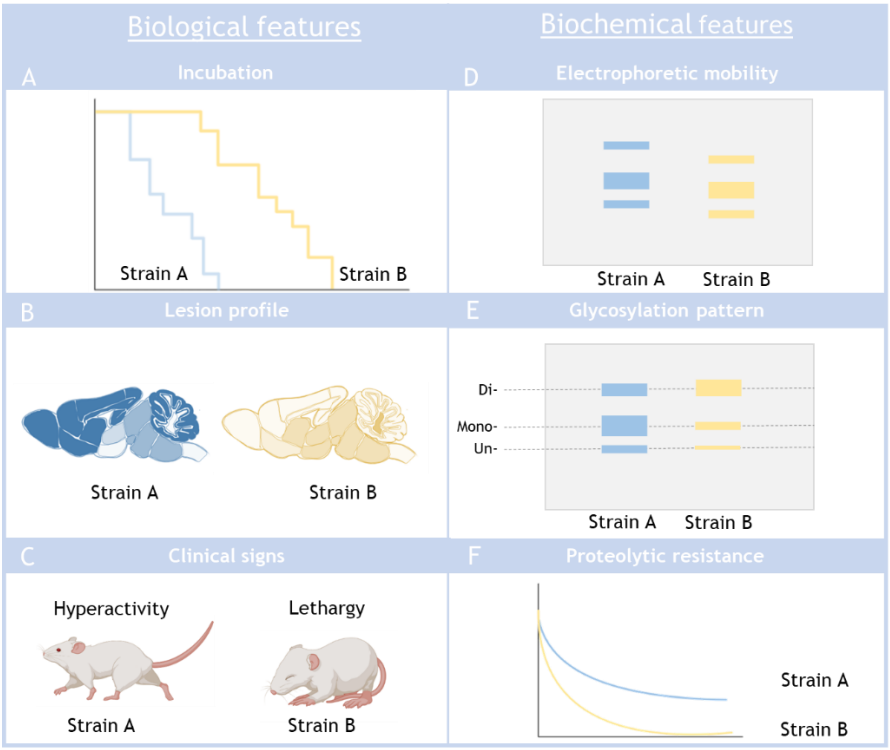


Figure 4.1. Biological and biochemical properties that define a prion strain. A) The incubation period is the time between the infection and the onset of clinical signs; this period depends on the prion strain, the route of infection, the titer of infectious particles, and the PrP^{C} expression level. B) The brain lesion profile is defined by the tropism of the prion strain for specific brain areas, and it is expressed as the brain area, the level of affectation, and the deposition of PrP^{Sc}. C) The clinical manifestations are the first evidence of prion diseases, and they vary widely depending on the prion strain, to the point of being opposite. D) The electrophoretic pattern brings information about the PK cleavage sites, manifested as changes in the

USC UNIVERSIDADE DE SANTIAGO DE COMPOSTELA

molecular weight of the bands. E) The glycoform ratio is useful to diagnose some human prion strains and consists of the proportion of the un, mono and diglycosylated forms of the PrP. F) The effect on the PrP^{Sc} of increasing concentration chaotropic agents reflects its stability and resistance. Image created with BioRender.com.

Recent cryoEM studies of some brain-derived mouse-adapted prion strains (RML, aRML, a22L, and ME7) revealed that the differences among them lied in subtle structural variations, while all of them conserved the main features of the PIRIBS core. Among the differences, the disulfide arch is the most divergent structural motif. This disulfide β-arch differs in shape and the amino acids that compose the backbone; moreover, it seems that the different glycans located in this arch could affect the flexibility of this structure [205,406]. Another structural divergence among strains is the planarity of the core. The monomer of PrP^{Sc} is non-planar; therefore, C-terminal and N-terminal lobes are staggered, and the staggered level also differs depending on the prion strain, being, for instance, 22L and ME7 flatter than RML[193,204,205].

In addition, these prion strains feature different hydrophobic and electrostatic charge distributions, allowing lateral interactions with other molecules present in the brain, such as phospholipids, glycans, or nucleic acids. Indeed, non-proteinaceous molecules were observed surrounding the fibril by cryoEM, although the nature of these cofactors was not identified [406]. These molecules, termed cofactors, were postulated to stabilize the fibril and play a key role in prion propagation. Moreover, cofactors are hypothesized to be strain-specific and to be involved in brain tropism [190,193,194,205]. Even though many advances have been made in recent years regarding the structural characterization of prion strains, further studies are necessary to shed light on the biochemical properties of prion strains, strain-specific templating activity, the role of cofactors in strain diversity, and brain tropism.

USC UNIVERSIDADE DE SANTIAGO DE COMPOSTELA

5.1.2 TRANSMISSIBILITY OF PRION STRAINS AND TRANSMISSION BARRIERS

One of the most remarkable properties of prions is their capability to be transmitted to individuals of the same species, but also to members of other species. However, when a prion strain is inoculated in a host belonging to a different species than the donor, the prion suffers from a process of adaptation, which is usually reflected in more extended incubation periods and incomplete attack rates. This inefficient cross-species transmission was first described by Pattison and colleagues who mentioned the different susceptibility to the disease between sheep and goats and termed this phenomenon as a "species barrier" [79]. A few years later, Pattison confirmed the existence of this transmission barrier by inoculating a goat isolate into sheep, goats, and mice and determining that the period of incubation was longer than inoculating sheep with a sheep-adapted strain or mice with a mouse-adapted strain[462].

The species barrier mainly resides in the divergences in the amino acid sequence of the PrP between the donor and the host[463,464]. Although PrP^C is a conserved protein in mammals, chemically distinct amino acids entail steric impediments in the template process. In fact, in some cases, direct transmission of a prion strain into a specific host is not possible, and it requires an intermediate host to adapt to the prion strain. In this regard, there is no evidence that scrapie can infect humans, so far; however, it was demonstrated that atypical Nor98 scrapie prions could be responsible for classical BSE [47], which caused vCJD in humans [29,465]; thus, it could be said that scrapie can indirectly affect human through the transmission to cattle. Furthermore, the species barrier can often be overcome by subsequent serial passages in the new host [466]; after serial transmission, the incubation time becomes shorter until getting stability and uniformity.

Apart from the interspecies barrier, an intraspecies barrier also affects prion strains that infect members of the same species. As well as for the interspecies barrier, one reason for this intraspecies transmission barrier is the intraspecies genetic variability, like polymorphisms. However,

USC UNIVERSIDADE DE SANTIAGO DE COMPOSTELA

the species barrier is also defined by an intrinsic component in the prion strain and two strains that affect the same host can present different transmission barriers [467]. This is the case of vCJD and sCJD; both affect humans with the same PrP primary sequence; however, vCJD is scarcely transmissible to humanized mice, while the species barrier between sCJD and humanized mice is almost null [468]. The intraspecies barrier is also perceived when synthetic prions are inoculated in animals bearing the same amino acid sequence. In this case, the barrier is probably due to the lack of posttranscriptional modifications, such as the glycosylphosphatidylinositol anchor and N-linked glycans, in the case of recombinant prions [469] and requires an adaptation to the host [108,470].

Sometimes, instead of a process of adaptation, strains suffer from "mutations" or mechanisms of selection. Mutations usually occur when a prion strain is inoculated in a host with a different PrP primary sequence, either because they are other species or due to polymorphisms in the case of individuals of the same species. Therefore, the term is used metaphorically and does not involve amino acid composition changes Mutations change the prion identity and are reflected in drastic changes in the prion strain properties, such as the incubation time, brain tropisms, or electrophoretic pattern[471–473]. On the contrary, a selection mechanism occurs when the prion strain was initially caused by a stable mixture of conformers that propagated together, called quasispecies. Changes in the environment, such as the inoculation into a new host, destabilize the mixture, and one of the prion strains, the one that propagates more efficiently in the new conditions, is selected and propagates over the other (Fig 4.2)[437,474,475].

USC UNIVERSIDADE DE SANTIAGO DE COMPOSTELA

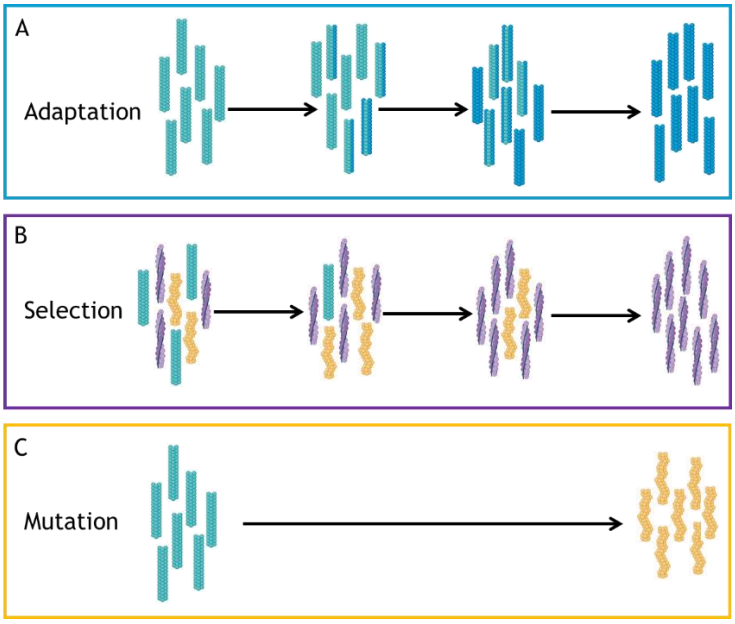


Figure 4.2. Prion strain adaptation, selection, and mutation phenomena. A) During the adaptation process, the prion strain accommodates the new host keeping the original biological and biochemical properties. B) The mechanism of prion selection involves the propagation of one strain out of a stable mixture of quasispecies; the strain that propagates is the most thermodynamically suitable to the new environment. C) A strain mutation consists of a drastic change in the strain properties and, therefore, its identity. Image created with BioRender.com

5.1.3 SYNTHETIC PRIONS AND *IN VITRO* PROPAGATION METHODS

In vitro prion propagation methods were developed for different purposes: reducing the number, costs, and time derived from studies in animals, studying the efficacy of different therapeutic molecules, getting large amounts of infectious prions for structural analysis, amplifying small amounts of prions as a tool for diagnosing or studying the minimum components necessary for obtaining infectious particles, among others.

USC UNIVERSIDADE DE SANTIAGO DE COMPOSTELA

Overall, prions generated *in vitro*, henceforth synthetic prions, can be obtained in two ways from brain-derived or bacterially expressed PrP: amplifying a minute amount of prions (seeded reaction)[178,476], where the amplified prions share the properties of the original seed; or forming prions *de novo* (unseeded reaction)[108]. The infectivity of *de novo* generated prions was discussed for a long time: while different methods obtained PK-resistant particles, their capacity for triggering prion diseases was poor or null, presenting long incubation periods, incomplete attack rates, and requiring animal models expressing truncated forms of the PrP or high expression levels that even developed spontaneous prion diseases [477–479].

In 2010, Wang and colleagues generated the first synthetic prion formed *de novo* with infectivity in wild-type CD-1 mice. This material generated from bacterially expressed full-length mouse PrP was converted into PK-resistant PrP by unseeded serial PMCA. Wild-type mice inoculated with this material succumbed to a prion disease after 166 dpi. Moreover, these mice presented the classical brain pathology that characterizes prion diseases, with vacuolation and accumulation of PrP^{res}, demonstrating that these synthetic prions were fully infectious in wild-type animals[108].

Further studies postulated that the reasons for the inefficient transmissibility of the first synthetic prions could be the necessity for a period of adaptation or the presence of low titers of infectious particles, suggesting that the *de novo* formation of prions *in vitro* could be due to a stochastic process, as well as it happens in brains of patients of sporadic prion diseases [437,480,481]. Moreover, the conditions and the composition of the conversion system, such as the cofactors, temperature, sonication, rotation, shaking, pH, salinity, presence of denaturant, etc., were demonstrated to strongly influence the final product of the conversion [424,478,482,483].

The most noteworthy methods for prion propagation *in vitro* are described below.

USC UNIVERSIDADE DE SANTIAGO DE COMPOSTELA

Cell-free conversion assays

The cell-free conversion assay was the first method of prion propagation *in vitro*. This technique consisted of mixing cell-derived hamster PrP^{C} (substrate) and brain-derived PrP^{Sc} (seed) in the presence of a chaotropic agent (Gdn), which partially denaturalized the PrP^{Sc}. The renaturalization of the PrP^{Sc} by diluting the chaotropic agent led to the conversion of the PrP^{C} into PrP^{Sc}. This fact was demonstrated using ^{35}S-PrP^{C}; thus, after incubating the labeled substrate with the seed and subsequent digestion with PK to remove the unconverted ^{35}S-PrP^{C}, Kocisko and colleagues assessed that the PK-resistant PrP^{Sc} was labeled, whereas, in the absence of the seed, there was no PK-resistant ^{35}S-PrP^{Sc}. Therefore, the ^{35}S-PrP^{C} was misfolded into ^{35}S-PrP^{Sc} using the brain-derived PrP^{Sc} as a template[98]. Unfortunately, the infectivity of the newly generated PrP^{Sc} was not demonstrated, and the yield of this method was low because the newly originated PrP^{Sc} was usually stoichiometric relative to the amount of the seed [477].

Protein Misfolding Cyclic Amplification

In 2001, Saborio and colleagues described a new method of prion propagation called Protein Misfolding Cyclic Amplification (PMCA). The perception of prion amplification by PMCA is conceptually similar to the polymerase chain reaction (PCR); thus, this method consists of adding small amounts of PrP^{Sc} (seed) to a brain homogenate (substrate) which is subjected to cyclic periods of incubation and sonication, resulting in an efficient propagation of PrP^{Sc} [99]. It is assumed that during the incubation period, PrP^{C} binds to PrP^{Sc} and is misfolded into new PrP^{Sc} forming fibrils which are fragmented during the sonication phases, generating numerous nucleation origins from which the fibrils can bind more PrP^{C}, and therefore, continue to grow. In contrast to cell-free conversion assay, this technique is extremely sensitive and, after seven serial rounds, can detect and amplify on the order of ~10^{-18}g[484].

Additionally, PrP^{Sc} amplified by PMCA maintains the strain identity, and when the product of the amplification is inoculated in wild-type

USC UNIVERSIDADE DE SANTIAGO DE COMPOSTELA

animals, they succumb to a prion disease with the same biological and biochemical features as those of the original seed[485–487]

Numerous studies support the usefulness and versatility of the PMCA. This technique has been used for testing the anti-prion activity of different therapeutic candidates [335,488], infectivity assays[487], studying the prion adaptation and transmission barriers[489], detecting prions in water[65], assessing the effectivity of decontamination procedures on surfaces or surgical material[490] and also diagnose of prion disease using different tissues, even in preclinical stages due to the high amplification rates[491].

PMCA has also been optimized for using recombinant PrP and specific cofactors instead of brain-derived PrP, allowing an exhaustive control of the substrate composition [100]. The use of recombinant PrP accelerates the conversion by increasing the amount of PrP^{C} regarding the brain homogenate; moreover, the control of the substrate composition made possible the formation of synthetic infectious prion *de novo*[108] as well as studies about the minimum requirements for prion propagation or infectivity.

Quaking-Induced Conversion

One of the drawbacks of the PMCA is the complexity of the system related to the sonication. With a view to simplifying the technology, Atarashi and colleagues developed a method that replaced the cycles of sonication by intermittent shaking, called Quaking-Induced Conversion (QuIC) reactions [476]. Initially, this reaction was developed in a microtube and required brain-derived PrP^{Sc} (seed) and recombinant PrP^{C} as substrate in a mixture of detergents and salts. QUIC was demonstrated to be faster than PMCA, amplifying on the order of ~10^{-16}g after 46h.

The adaptation of this system to a multiwell plate and the addition of ThT (an amyloidophilic dye that emits fluorescence when it binds to amyloid fibrils) allowed monitoring in real-time the formation of the

USC UNIVERSIDADE DE SANTIAGO DE COMPOSTELA

fibrils. This adaptation received the name RT-QuIC (Real-Time Quaking-Induced Conversion) and was a breakthrough for the diagnosis of prion diseases in diverse biological samples like CSF[492,493], brain [494], urine[495], saliva [496], blood [497], skin[498], and other tissues [499]. In addition, the success of RT-QUIC in the diagnosis of prion diseases extended its use to other neurodegenerative diseases, such as Parkinson's disease[500], dementia with Lewy Bodies[501] or Alzheimer's disease[502].

RT-QuIC is highly sensitive and reproducible [503]; however, it requires intensive optimization and accurate parameter selection, such as temperature, detergent concentration, shaking regimes, and incubation time in order to avoid the spontaneous generation of PrP amyloids.

Unlike the PMCA, RT-QuIC does not maintain the biochemical strain properties; in fact, immunoblotting of material subjected to serial rounds of RT-QuIC only display two C-terminal PK-resistant fragments of ~12 and ~10kDa. Such electrophoretic pattern resembles that of the recombinant amyloid generated by Bocharova and colleagues [504] and it could be hypothesized that the RT-QuIC might be propagating an amyloid instead of PrP^{Sc}. Furthermore, the product amplified by RT-QuIC is not infectious [476]. These facts make this method unsuitable for structural studies and infectivity assay.

Amyloid Seeding Assay

Similarly to RT-QuIC, the Amyloid Seeding Assay (ASA) takes advantage of the affinity of ThT for amyloid fibrils to monitor the amplification. This technique was developed by Colby and collaborators and used brain-derived PrP^{Sc} partially purified and precipitated with NaPTA as seed and recombinant PrP as substrate. Both seed and substrate are shaken together in a microplate in the presence of low concentrations of chaotropic agents and glass beads that increased the effect of the agitation [505]. Although this method was very sensitive, amplifying and detecting to the order of ~10^{-17}g Sc237 hamster prions, the high variability of the kinetics required several

USC UNIVERSIDADE DE SANTIAGO DE COMPOSTELA

replicates per sample, and the spontaneous amyloid fibril formation impeded more extensive use of this system.

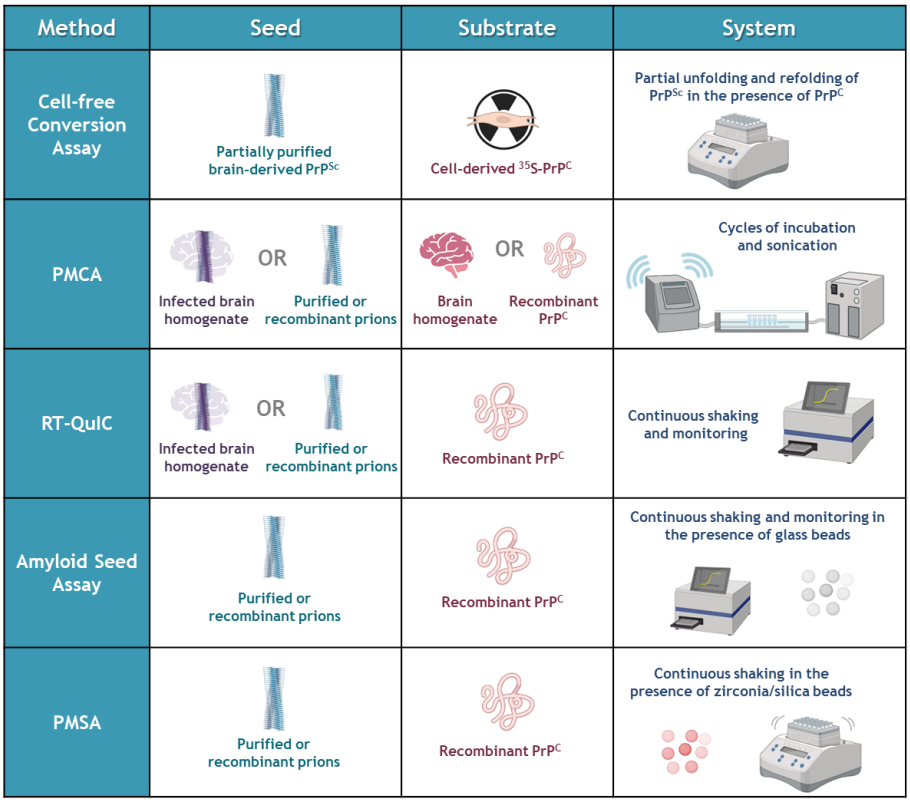


Figure 4.3. Methods of *in vitro* prion detection or propagation. General comparison of the different assays regarding the sources of PrP^{Sc} and PrP^{C}, the equipment, and the system used by each method. Image created with BioRender.com

Protein Misfolding Shaking Amplification

Recently, Eraña and colleagues designed a new method of prion propagation that, unlike the previous ones, allows obtaining large amounts of homogeneous infectious recombinant prions [101]. This technique was designated Protein Misfolding Shaking Amplification (PMSA) and consisted of submitting a PrP^{Sc} seed and recombinant PrP^{C}

USC UNIVERSIDADE DE SANTIAGO DE COMPOSTELA

mixed with salts, detergents, and cofactors, to continuous shaking in the presence of zirconia/silica beads. As well as RT-QuIC, PMSA eliminates the complexity and high cost of the sonication system, although it has not been adapted to real-time monitorization of the fibril formation. Additionally, prion strains propagated by PMSA faithfully preserved the biochemical properties of the prion strain used as seed [101,506] and recapitulated a similar prion disease to that of the original seed.

This versatile method can be easily scaled-up to obtain large amounts of recombinant PrP^{Sc} useful for structural studies since more than 2,5mg of PK-digested recombinant prions can be obtained per day. Moreover, PMSA can also be used for species barrier studies, infectivity assays, anti-prion compounds tests [507,508], and studies about the minimum components involved in prion infectivity[509].

5.1.4 ROLE OF COFACTORS IN SYNTHETIC PRIONS

Brain components involve the ideal environment for prion generation and propagation. The first methods of *in vitro* prion amplification tried to simulate as much as possible the brain scenario, using brain homogenate [99,482] or cell lysate extracts[98]. Once *bona fide* synthetic prions were obtained, studies focused on simplifying as much as possible the technical complexities and the buffer composition, as well as looking for the minimum components required for prion infectivity.

The term cofactor encompasses molecules that compose the buffer where the misfolding of PrP^{C} into PrP^{Sc} occurs and that play a vital role in the conversion process, structural stabilization of the prion fibril, preservation of the strain identity [510], and brain tropism. Cofactors are macromolecules of different natures[511] such as natural or synthetic nucleic acids, like as mouse liver RNA [108,470], plasmid DNA[482], poly(rA) (polyriboadenylic acid)[512]; phospholipids, such as POPG (1-palmitoyl-2-oleoylphosphatidylglycerol) [108,512] or PE (phosphatidylethanolamine)[513]; glycosphingolipids, such as GM1

USC UNIVERSIDADE DE SANTIAGO DE COMPOSTELA

(monosialotetrahexosylganglioside) [514]; anionic detergents, like SDS (sodium dodecyl sulfate)[420]; or polysaccharides, such as dextran sulfate [101,482]. Moreover, cofactors were hypothesized to be essential for synthetic prions infectivity since, to date, all the attempts to originate synthetic prions *de novo* without these non-protein molecules resulted in non-infectious amyloids, even though such amyloids had PK-resistant core [482,515].

The molecular mechanism of how cofactors participate in PrP conversion remains unknown; however, it has been hypothesized that cofactors could be involved in PrP^C destabilization before the unfolding; thus, polyanionic cofactors could interact with the unfolded N-terminal tail, which is positively charged, initiating the misfolding pathway [516]. In addition, Choi and colleagues spontaneously generated an infectious prion, in the absence of cofactors or detergents, from the mutated protein Y145Stop, which contains the polybasic region, and it was known to be highly amyloidogenic [421]; therefore, cofactors would be required to convert the full-length PrP^C, which α-helices provide much more stability than the Y145Stop truncated form. Moreover, recent prion structures solved by cryo-EM showed that positive charges are exposed to the lateral surface; in addition, density maps of the solved structures showed peripheral densities which would probably be interacting with the fibril [190,192–194,517]. This supports the idea that polyanionic molecules, such as those mentioned above, can be interacting with the prion fibril *in vivo*.

Definitely, the prion strain diversity is of structural and biochemical interest. Additionally, since prion strains cause specific phenotypes, the characterization of these strains is also crucial from a pharmacological perspective. Currently, there is no effective treatment for prion diseases, and one of the reasons of the therapeutical failure is the strains capability to evade the treatment by mechanisms of adaptation and selection that lead to the development of drug-resistances.

USC UNIVERSIDADE DE SANTIAGO DE COMPOSTELA

Consequently, a thorough characterization of various prion strains can provide crucial information about their differences, enabling the development of effective therapies and the mitigation adaptation and selection mechanisms that lead to therapeutic failure. *In vitro* prion amplification methods are immensely useful tools to study the properties of prion strains. They permit a tight control over all the parameters and the reagents, providing information about the role of each one on the properties of the prion strains.

Given the relevance of the properties of prion strains and their implication in the search of a therapy for prion diseases, this chapter addresses the biological, biochemical, and biophysical study of different recombinant prion strains generated de novo by PMSA with three different cofactors. This approach provides new insights into the similarities and differences between recombinant and brain derived prion strains and the role of cofactors in prion strain diversity.

USC UNIVERSIDADE DE SANTIAGO DE COMPOSTELA

5.2 SPECIFIC AIMS

The main goal of this chapter was to generate *de novo* different PrP conformers by PMSA in the presence of different polysaccharide cofactors. This global objective has been broken up into the following specific aims:

1. To determine the biological, biochemical, and biophysical properties of the recombinant conformers.

2. To compare the properties of the generated conformers to determine if they exhibit different features.

3. To assess the infectious potential of the generated conformers to determine if they exhibit characteristics of *bona fide* prions.

4. To compare the properties of the conformers *in vivo* to determine if they consist of different prion strains.

4. To compare the effect of the different cofactors on the generation of the conformers.

USC UNIVERSIDADE DE SANTIAGO DE COMPOSTELA

5.3 METHODS

Reagents, materials, buffers composition, and devices used in this doctoral thesis are described in Annexes I, II, II, IV and V.

5.3.1 De novo generation of PrPSc by PMSA with different cofactors

Recombinant BVPrP 23-231 (109I) was expressed, purified, and stored as previously detailed in section *4.3.1 Expression and purification of BVPrP 109I*. Aliquots of recombinant protein stored at -80°C with 6M Gdn were thawed on ice, diluted 1:5 in PBS, and dialyzed against PBS for 1h at rt. After dialysis, the protein was centrifuged for 15min at 19000g and 4°C in order to remove abnormally folded protein aggregates that sediment during the centrifugation. Subsequently, the protein was diluted to a final concentration of 2µM with conversion buffer (CB) supplemented with 0,1% (w/v) heparin sodium salt from porcine intestinal mucosa, 0,1%(w/v) chondroitin sulfate sodium salt from shark cartilage, or 0,1%(w/v) pentosan polysulfate sodium. The mixture containing the CB, the recombinant protein, and the corresponding cofactor was termed substrate. For PrP conversion, 500µL of substrate were aliquoted in a 2mL screwed cap, conic tubes containing ~180mg of 1mm or 0,1mm glass beads, and tubes were continuously shaken for 24h at 39°C and 700rpm.

The product of the PMSA was analyzed by SDS-PAGE and BlueSafe dye after digestion with 25µg/mL of PK at 42°C for 1h. Alternatively, the product of the PMSA was stored at -80°C for further analyses or amplification.

USC UNIVERSIDADE DE SANTIAGO DE COMPOSTELA

5.3.2 PROPAGATION OF PrP^{Sc} BY PMSA

PrP^{Sc} propagation protocol was similar to that used for the *de novo* generation of PrP^{Sc} with the following modifications. Before adding 500µL of the substrate, 1mm zirconia/silica beads were added to the 2mL conic tubes. After adding the substrate, 5µL or 50µL of the previous round of PMSA was added as seed, obtaining a final concentration of 1:100 or 1:10 (seed:substrate) [101]. The product of the amplification was digested with PK and analyzed by SDS-PAGE and BlueSafe staining.

For ssNMR experiments, the PMSA was scaled-up, and 50mL conic tubes were used with 20mL of the substrate and ~40 zirconia/silica beads. The proportions among the CB, recombinant protein, cofactors, and seed were maintained. These tubes were shaken for 24h at 39°C and 900rpm.

5.3.3 MICE INOCULATION

The ethical statement, the animal model and the housing conditions were the same that were previously described in sections *3.3.1. Ethical statement* and *3.3.2. Animal model and housing conditions.* TgVole mice expressing BVPrP (109I) were anesthetized and inoculated as previously described in section *3.3.3. Prion inoculation*. Recombinant PrP^{Sc} generated by PMSA was diluted 1:10 in PBS, and mice were inoculated intracerebrally with 20µL of the dilution.

To perform the second passage, 10% brain homogenates of mice from the first passage were diluted to a final concentration of 1% in PBS, and mice were inoculated intracerebrally with 20µL of the dilution.

5.3.4 HISTOPATHOLOGICAL AND IMMUNOHISTOCHEMICAL ANALYSES

Histopathological and immunohistochemical analyses were performed as previously described in section *3.3.8 Histopathological and immunohistochemical analyses*.

USC UNIVERSIDADE DE SANTIAGO DE COMPOSTELA

5.3.5 WESTERN BLOT OF RECOMBINANT PrP^{Sc}

The product of the PMSA was digested with 25µg/mL of PK for 1h at 42°C. The Western blot was performed as previously described in section *3.3.7. Proteinase K digestion and Western blot analysis*.

5.3.6 WESTERN BLOT OF BRAIN HOMOGENATES

For logistical reasons, Western blot analysis of the brains of mice inoculated with the conformers was performed by Hasier Eraña and Patricia Piñeiro at CIC bioGUNE, Bilbao. The brains of mice from the first and second passages were homogenized at 10% (w/v) in PBS supplemented with a Protease inhibitor cocktail, and 15µL of brain homogenates were mixed with 5µL of a buffer containing 2% (v/v) NP40 and 5%(w/v) Sarkosyl in PBS. Subsequently, samples were digested with 85µg/mL PK and were incubated for 1h at 56°C and 450rpm. The reaction was stopped by adding 1:3 of a loading buffer and heating at 99°C for 10min. Samples were run in a 4-12% acrylamide gel and transferred to a PVDF membrane using the Trans-Blot® TurboTM(BioRad) transfer system. Then, blocking, washing, and antibodies incubations were performed with the Western blot processing system iBind™ Flex Western. The monoclonal antibody used was SAF83 (1:400) (epitope 130-160), and the secondary antibody was a peroxidase-conjugated goat anti-mouse. Images were processed with the Invitrogen iBright analysis software.

5.3.6 MASS SPECTROMETRY-BASED ANALYSIS

For mass spectrometry-based analysis, 2mL of the PMSA product were digested by adding PK to a final concentration of 25ug/mL and incubation at 42°C for 1h. After digestion, samples were centrifuged for 30min at 19000g, the supernatant was discarded, and the pellet was resuspended and washed with 1mL of PBS. Subsequently, the sample

USC UNIVERSIDADE DE SANTIAGO DE COMPOSTELA

was centrifuged again for 30min at 19000g, the supernatant was discarded, and the pellet was resuspended in 50uL Gdn/HCl 6M with 3 pulses of a tip sonicator and incubated for 1h at 37°C. After incubation, TFA was added to a final concentration of 1%. From this point, the samples were processed by Susana Bravo at the Proteomic Unit of Instituto de Investigaciones Sanitarias de Santiago de Compostela (IDIS). Samples (4µl) were injected into a micro liquid chromatography system nanoLC 400, coupled to a high-speed Triple TOF 6600 mass spectrometer with a microflow source, and equipped with a silica-based reversed-phase column ChromXP C18 150×0.30 mm, 3mm particle size and 120Å pore size. A YMC-TRIART C18 trap column was connected prior to the separating column, online (3mm particle size and 120Å pore size). After sample loading and washing with 0.1% formic acid in water to remove Gdn/HCl and other non-peptide components of the sample, the flow was switched onto the analytical column, and separation proceeded at a flow rate of 5µl/min with a solvent system consisting of 0.1% formic acid in water as mobile phase A, and 0.1% formic acid in acetonitrile as mobile phase B. Peptides were separated over 40min with a gradient ranging from 2% to 90% of mobile phase B. Data acquisition was performed in a TripleTOF 6600 System using a Data dependent workflow. Source and interface conditions were the following: ionspray voltage floating (ISVF) 5500V, curtain gas (CUR) 25, collision energy (CE) 10 556and ion source gas 1 (GS1) 25. The instrument was operated with Analyst TF1.7.1 software. Switching criteria were set to ions greater than mass-to-charge ratio (m/z) 350 and smaller than m/z 1400 with a charge state of 2-5, mass tolerance 250ppm and an abundance threshold of more than 200 counts (cps). Former target ions were excluded for 15s. The instrument was automatically calibrated every 4 hours using tryptic peptides from PepCalMix as an external calibrant. For data analysis, the sample TIC was opened using the PeakView2.2 software that allows protein reconstruction. The LC-MS Peptide Reconstruct feature uses a peak finding algorithm to identify groups of peaks that form isotope series and charge series. Protein deconvolution was carried out between 800

USC UNIVERSIDADE DE SANTIAGO DE COMPOSTELA

to 20000Da. PK-resistant fragments were identified with the GPMAW software tool. PK-resistant fragments were identified based on a +/– 1 Da difference between the peak and the theoretical weight mass.

5.3.7 Expression of recombinant PrP (109I) with uniformly labeled (^{13}C, ^{15}N) phenylalanine residues

Recombinant full-length BVPrP (I109) (23-231) was expressed by *E. coli Rosetta* (DE3) Competent Cells harboring the pOPIN E expression vector containing I109 BV PRNP. Bacteria from a glycerolate stored at -80°C were grown in a 250mL Erlenmeyer flask containing 50 mL of LB broth overnight at 37°C and 225rpm. The culture was then transferred to two 2L Erlenmeyer flasks containing each 500 mL of minimal medium supplemented with a solution of uniformly labeled ^{13}C-^{15}N-L-phenylalanine and the remaining unlabeled amino acids to a final concentration of 0,1g/L, glucose, NH_4Cl, $MgSO_4$, $CaCl_2$, thiamine, biotin, and ampicillin. When the culture reached an OD_{600} of 0.8-1.2 AU, 1mM Isopropyl β-D-1-thiogalactopyranoside (IPTG) was added to induce expression of PrP for 3h under the same temperature and agitation conditions. Bacteria were pelleted, lysed, and recombinant PrP was purified as previously described in section *4.3.1 Expression and purification of BVPrP 109I.*

5.3.8 Solid-state nuclear magnetic resonance measurements (ssNMR)

Purified U^{13}C-^{15}N-Phe PrP 23-231 (109I) was converted into PrP^{Sc} by PMSA in 50mL tubes containing 20mL substrate. The product of the PMSA was pooled and treated with PK to a final concentration of 10µg/mL at 37°C for 1h. The reaction was stopped by adding PEFABLOC to a final concentration of 1mM. The samples were centrifuged at 34000g for 1h and at 25°C. The supernatant was discarded, and the pellets were resuspended in PBS and centrifuged again under the same conditions. After centrifuging, the supernatant

USC UNIVERSIDADE DE SANTIAGO DE COMPOSTELA

was discarded, and the pellets were resuspended in PBS and pooled in a final volume of 2mL; this volume was then transferred to two microtubes and centrifuged in a tabletop centrifuge for 20min at 20000g. Subsequently, the supernatant was discarded, and the pellets were resuspended and pooled in a final volume of 1mL of deionized water. The sample was centrifuged for 20min at 20000g. The supernatant was discarded, while the final pellet was dried ON at 37°C and introduced in the rotor using a Bruker rotor filling kit. The rotor was capped and placed in the solid NMR probe.

Solid-state NMR experiments were performed by Manuel Martín-Pastor at Unidade de Resonancia Magnética, CACTUS, University of Santiago de Compostela. Solid-state NMR experiments were measured at 278K in a Bruker NEO 17.6T spectrometer (proton resonance 750MHz and ^{13}C resonance 188MHz) equipped with a $^{1}H/^{13}C/^{15}N$ triple resonance solid probe for 1.3mm zirconia rotors and an available range of MAS rates from 8 to 67kHz.

The spectrometer control software was TopSpin4.0. All spectra were processed with MestreNova v14.0 (Mestrelab Research Inc.). Carbon-13 chemical shifts were referenced to the CA signal of solid glycine at 43.5 ppm. Nitrogen-15 chemical shifts were referenced to the ^{15}N peak of a solid ^{15}N labeled sample of glycine at 35.0ppm. Proton chemical shifts were referenced to the intense water peak at 4.7 ppm.

2D^{13}C-^{13}C DARR spectra were measured at 20kHz MAS (pulse sequence cpSPINDIFFof the Bruker library). The ^{13}C carrier was placed at 110 ppm, and the spectrum covered a spectral width of 220 ppm in each carbon dimension. The 1H carrier was set on the water resonance at 4.7 ppm. The initial proton/carbon cross polarization contact time was 2ms, and the proton contact pulse power used an ascending linear ramp of 50%. During the mixing time of the sequence, a DARR ^{1}H pulse was applied at 20kHz. The number of complex points acquired in t2 and t1 dimensions were 1666 and 300, respectively. The FID was acquired under heteronuclear proton decoupling at 110kHz

USC UNIVERSIDADE DE SANTIAGO DE COMPOSTELA

with SPINAL-64. The inter-scan delay was 2.5s, and the number of scans per t1 value was 88.

2.3.10 STATISTICAL ANALYSIS

Statistical analyses were performed using Graph Pad Prism 8 .

Descriptive statistics such as mean, standard deviation, or the standard error of the mean were calculated for each group of mice. Survival time was expressed as mean±SEM.

The graphical representation of survival time was plotted as the percentage of survival and was analyzed by the Kaplan-Meier test.

A Games-Howell's multiple comparison *post hoc* test, with individual variances computed for each comparison, was performed to analyze the differences in the incubation periods among the conformers and also between both passages. A ρ value$\leq$0.05 was considered statistically significant.

USC UNIVERSIDADE DE SANTIAGO DE COMPOSTELA

5.4 RESULTS

5.4.1 *DE NOVO* GENERATION OF DIVERSE CONFORMERS WITH DIFFERENT POLYSACCHARIDE COFACTORS BY PMSA

Cofactors are biomolecules not only relevant to prion diseases but also to other amyloid-related diseases, such as Alzheimer's disease [518–520], Parkinson's disease[521], type II diabetes mellitus [522] or familial amyloidosis [523], among others [524,525]. Many amyloid fibrils extracted from living organisms had associated cofactors from different natures (lipids, polysaccharides, nucleic acids,…), although these molecules were considered contaminants at first [526–529]. Hence, there is no doubt that cofactors should be biomolecules naturally existing in the cell environment. As PrP^{C} is a membrane-anchored protein and the conversion into PrP^{Sc} most likely takes place on the cell surface, it is conceivable that cofactors could be biomolecules present on the extracellular matrix, and the most abundant components present on the extracellular matrix are fibrous proteins, proteoglycans and glycosaminoglycans [530].

Glycosaminoglycans are unbranched, negatively charged polysaccharides consisting of the repetition of disaccharides. These polysaccharides share structural and biochemical functions and regulate physiological mechanisms such as cell differentiation, migration, inflammation, morphogenesis, or cell signaling [530]. Moreover, sulfated glycosaminoglycans play a crucial role in amyloid fibrillation by reducing the lag phase, as well as enhancing the conformational change from the native state to the amyloid fibril or increasing the concentration of pre-fibrillar species. Glycosaminoglycans also

USC UNIVERSIDADE DE SANTIAGO DE COMPOSTELA

accelerate the rate of fibrillation in the elongation phase and provide structural support to the amyloid assembly [524,531,532].

This work aimed to generate *de novo* recombinant *bona fide* prions with three different sulfated glycosaminoglycans: heparin, chondroitin sulfate, and pentosan polysulfate, and characterize them by different biological, biochemical, and structural methods (Fig 4.4).

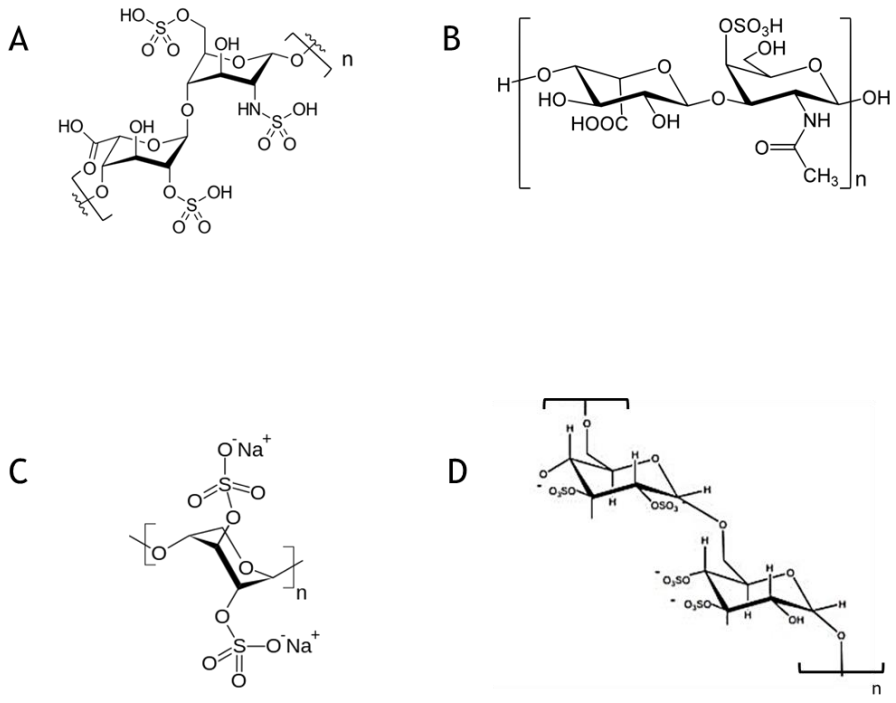


Figure 4.4 Chemical structure of four different polysaccharide cofactors. A) Chemical structure of the disaccharide unit of heparin; B) Chemical structure of the disaccharide unit of chondroitin sulfate; C) Chemical structure of the semisynthetic glycosaminoglycan unit of pentosan polysulfate; D) Chemical structure of the disaccharide unit or dextran sulfate, a glycosaminoglycan cofactor used to generate and propagate recombinant prions [101,482].

USC UNIVERSIDADE DE SANTIAGO DE COMPOSTELA

Taking advantage of the misfolding propensity of the BVPrP, recombinant BVPrP (23-231) (109I) was expressed and subjected to serial rounds of PMSA in the presence of three glycosaminoglycans as cofactors: heparin, chondroitin sulfate, or pentosan polysulfate. The initial round of PMSA was performed in the absence of any seed. To propagate the material serially, the product of the initial PMSA was diluted 1:10 into the fresh substrate and subjected to another round for 24h. Moreover, the PMSA was carried out in the presence of glass beads of different sizes, 0,1mm, and 1mm (Fig 4.5). Beads of glass were chosen over other materials since glass promotes the spontaneous generation of PK-resistant material in the absence of a seed[509].

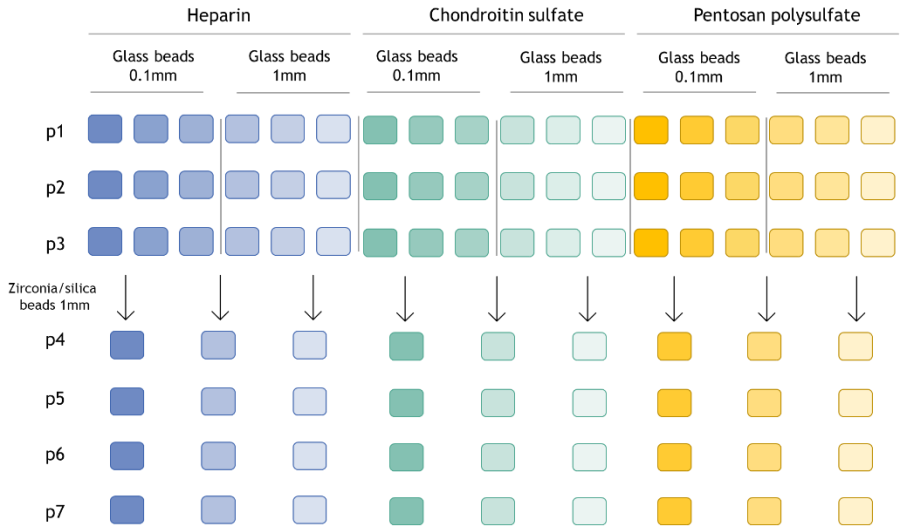
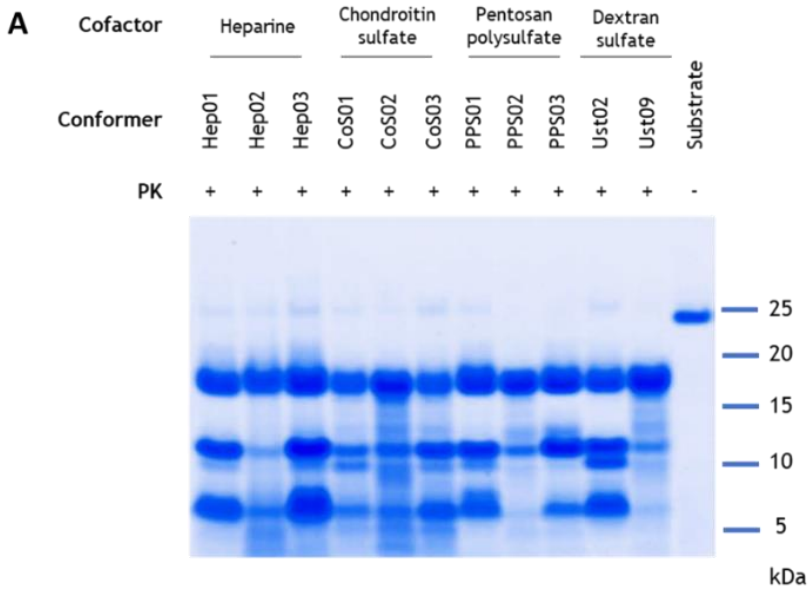


Figure 4.5. Schematic representation of the steps followed to generate the conformers. A substrate with recombinant PrP and enriched with three cofactors (heparin, chondroitin sulfate, and pentosan polysulfate) was subjected to PMSA in the presence of glass beads of 1mm or 0,1mm and by triplicate, according to the sort of beads. After three passages, three conformers generated with each cofactor were

USC UNIVERSIDADE DE SANTIAGO DE COMPOSTELA

selected and serially propagated in the presence of zirconia/silica beads of 1mm to stabilize the conformers.

Spontaneously generated PK-resistant material was detected even in the first round. Furthermore, after serial rounds of PMSA, a large variety of PK-resistant conformers were obtained. Among the different conformers, three generated with each cofactor were selected and propagated serially by PMSA with zirconia/silica beads instead of glass beads; it is known that this material promotes the amplification of the present conformers rather than generation of spontaneous ones. In addition, misfolded PrP^{Sc} remains adsorbed to the surface of these beads and could be used as seeds alternatively to the liquid product of the PMSA. The use of zirconia/silica beads also facilitates the storage and manipulation of the seeds [509,533]. After four passages, the electrophoretic pattern was compared with the original one to confirm that it did not change; therefore, the conformers were stabilized.



USC UNIVERSIDADE DE SANTIAGO DE COMPOSTELA

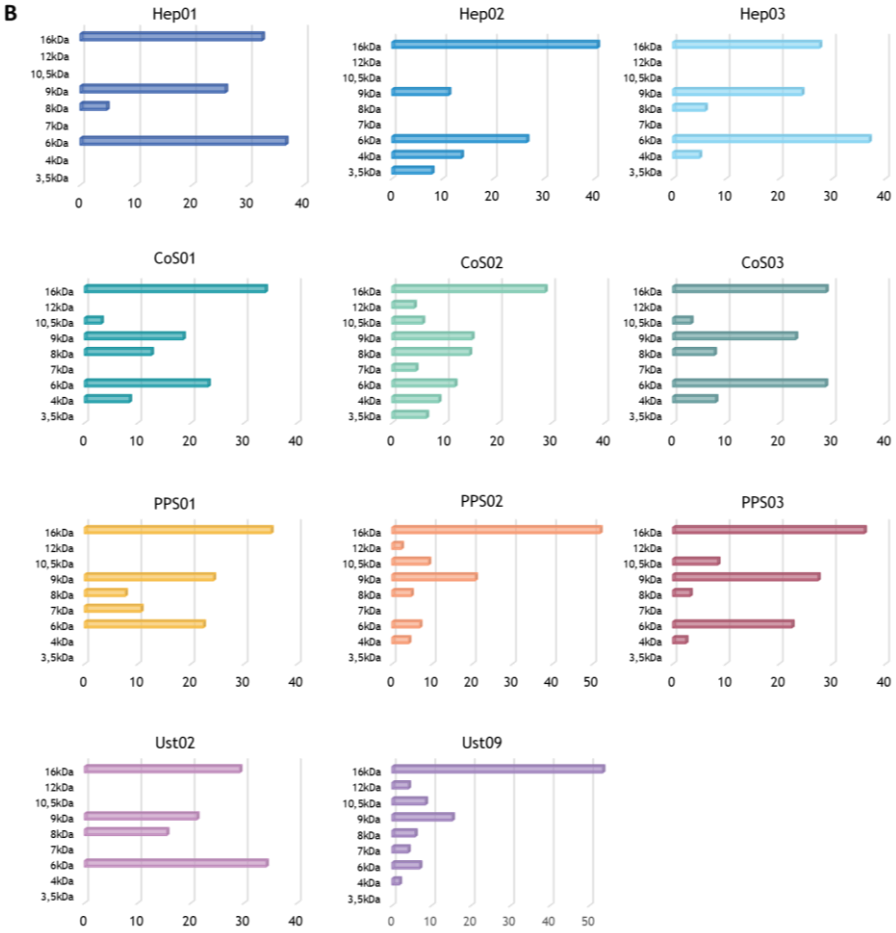


Figure 4.6. Electrophoretic pattern of different conformers after PK digestion. A) Electrophoretic pattern of the nine selected conformers; in addition, two recombinant prions strains *de novo* generated with dextran sulfate, Ust02 and Ust09, were included to compare their electrophoretic patterns. The substrate containing the recombinant protein was included as a reference. B) Bar plots represent the densitometry of each band. The X axis represent the percentage of contribution of each band to the pattern; the Y axis represents an approximate molecular weight.

USC UNIVERSIDADE DE SANTIAGO DE COMPOSTELA

Ust02 and Ust09 are two recombinant prion strains generated by PMSA using dextran sulfate as a cofactor, which demonstrated infectivity *in vivo* when they were inoculated in transgenic mice expressing ~1x BVPrP (109I) [533]; furthermore, these conformers are two distinct prion strains with different biochemical properties, such as incubation time or brain deposition. Thus, these two strains were included in the characterization of the conformers and compared together.

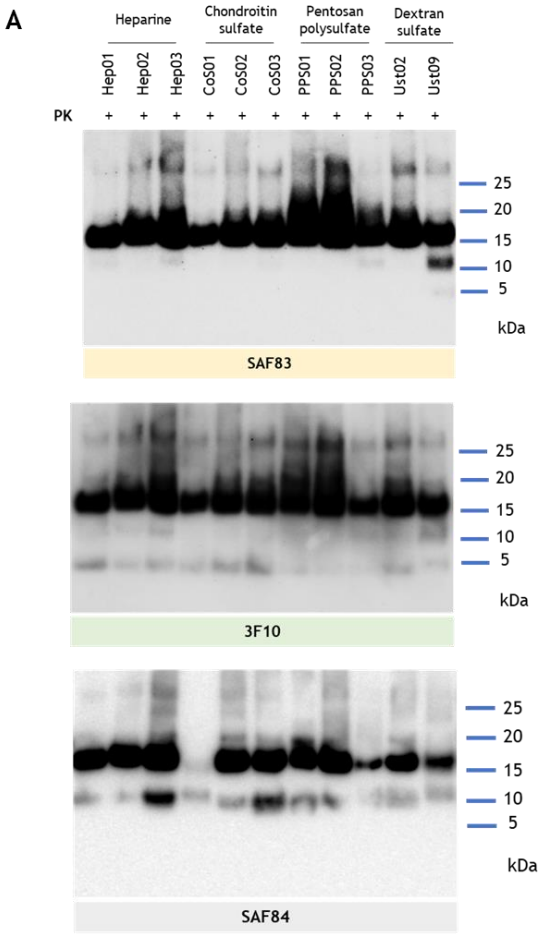
The electrophoretic separation followed by total protein staining showed that all the conformers shared three predominant bands of ~16, ~9, and ~6kDa; however, the presence of minor bands differentiated them (Fig 5.6). Moreover, although some conformers presented similar bands, such as Hep01 and Ust02, or CoS01, CoS03, and PPS03, such bands differed in their proportion, providing a unique appearance to the conformers. The differences in electrophoretic patterns suggest that the conformers were biochemically different.

The electrophoretic mobility depends on the molecular weight of the PK-resistant fragments. In order to estimate the cleavage sites of the PK and to identify the epitopes present in each PK-resistant fragment, the product of the PMSA was subjected to Western blot analysis using different antibodies that recognize the PrP. For this purpose, the conformers were digested with PK, separated electrophoretically, and transferred to a PVDF membrane. The membrane was incubated with antibodies that recognize epitopes in the C-terminal and central region of the PrP.

All the epitopes were included in the ~16kDa band of all conformers, which based on previous work [101,506], corresponds to the ~90-231 fragment. Moreover, SAF83, which recognizes a broad epitope of the central region (126-164), clearly recognized a band of lower molecular weight in Ust09; the same band seemed to be present on Hep01, Hep03, or PPS03; nonetheless, the abundance of such fragment in these conformers is lower. 3F10 recognizes an epitope also in the central region (135-150) but it is shorter than SAF83 and it is not interrupted

USC UNIVERSIDADE DE SANTIAGO DE COMPOSTELA

by the cleavage site at positions ~153/154. This antibody recognized bands of ~6kDa, which most likely corresponded to the N-terminal fragments ~90-153; moreover, in some conformers, this antibody also recognized bands of ~10kDa. On the other hand, the C-terminal antibody, SAF84 (160-170), identified bands in the region of ~8-11kDa which clearly differed in size depending on the conformer. In some cases, the bands were diffused, indicating that they could be composed of more than one fragment.



USC UNIVERSIDADE DE SANTIAGO DE COMPOSTELA

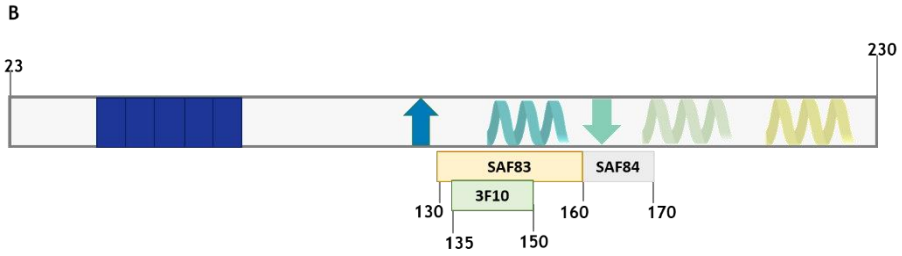


Figure 4.7 Western blot analysis of the PK-resistant fragments of the different conformers generated with polysaccharide cofactors. A) The conformers were subjected to Western blot analysis and were incubated with antibodies that recognize diverse regions of the PrP: SAF83 (1:400) recognizes the epitope 126-164; 3F10 (1:10000) recognized the epitope 135-150; SAF84 (1:400) recognizes the epitope 160-170. B) Schematic representation of the epitopes in the PrP^{C} structure.

The low resolution of the gel, added to the low abundance of some fragments, did not permit the differentiation between close bands. Moreover, the variety of epitopes tested was insufficient to cover all the possible PK-resistant fragments.

5.4.2 CHARACTERIZATION OF THE RECOMBINANT CONFORMERS BY LIMITED PROTEOLYSIS COUPLED TO MASS SPECTROMETRY

In order to obtain a detailed information about the PK-resistant fragments and the exact PK cleavage sites, a mass spectrometry-based analysis was performed after limited proteolysis with PK.

Limited proteolysis consists of the partial digestion of a protein by a protease; under non-denaturing conditions, the cleavage sites or nicksites [534,535] depend on the sequence of the protein, which dictates the hydrolysis site for which the protease has the preference, but also on the tertiary architecture of the protein, which determines the accessibility of the protease to the nicksites [534,535]. Thus, limited proteolysis also provides structural information about the protein. On

USC UNIVERSIDADE DE SANTIAGO DE COMPOSTELA

the other hand, mass spectrometry is a highly sensitive analytical technique that, applied to proteins, allows identifying peptides by their mass; therefore, with the combination of limited proteolysis with PK and mass spectrometric analysis, it would be possible to recognize each PK-resistant fragment and to identify the exact cleavage sites of the PK.

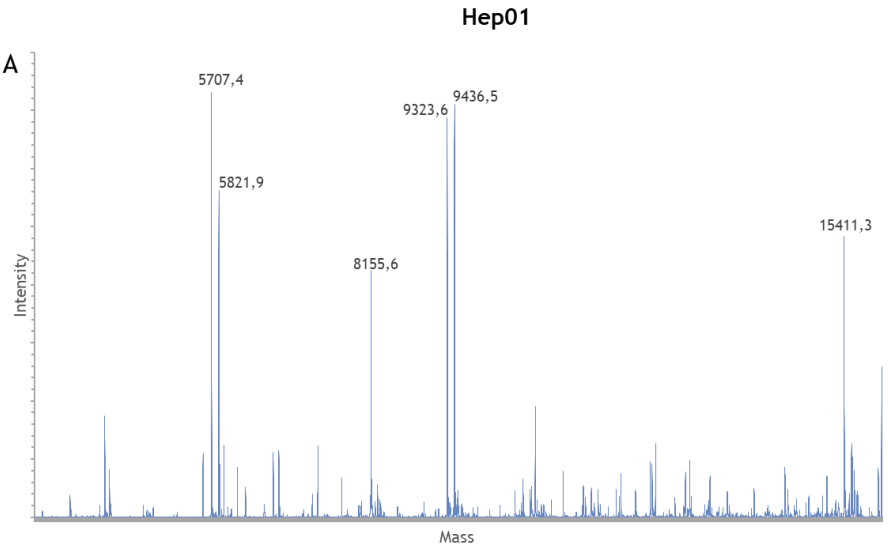
To carry out mass spectrometric analysis, the product of the PMSA was digested with PK, and the PK-resistant fragments were sedimented by centrifugation; subsequently, they were denaturalized with Gdn and separated by liquid chromatography coupled to the mass spectrometer.

Seven of the eleven conformers were analyzed: Hep01, Hep02, Hep03, CoS02, CoS03, Ust02, and Ust09. The mass spectra of Hep02, Hep03, Ust02, and Ust09 allowed a sensitive and precise identification of several PK-resistant fragments; however, Hep01, CoS02, and Cos03 mass spectra presented the high background and only the most intense peaks were identified, while other, which were visible in the total protein staining, were not distinguish, specially CoS02, that despite the fact that had a diffuse pattern that resembled Ust09, only half of the peaks were recognized.

The peaks identified by mass spectrometry were in agreement with previous works [179,180,182,183,506]. The most common cleavage sites present in all the strains were N97, Q98, Y150, N153, and M154 (Fig 4.14), which determined the peptides N97-Y150, Q98-N150, N153-S231, and M154-S231. Additionally, alternative nicksites were also recognized, although they were not present in all the conformers, such as G90, G92, H96, W99, A133, A136, F141, W145, R151, V161, Y163, or R164. Furthermore, most of these cleavage sites were previously described in *ex vivo* and recombinant prion strains, such as G90, G92, N97, A133, N153, M154, or Y163 (BV sequence). Limited proteolysis coupled to mass spectrometry, also provided the exact molecular weight of the PK-resistant peptides (Fig 4.8-4.14).

USC UNIVERSIDADE DE SANTIAGO DE COMPOSTELA

A



B

Observed mass (Da)	Theoretical mass (Da)	Sequence	Modifications
15411,3	15411,3	Q^{98}-S^{231}	-
9436,5	9436,4	N^{153}-S^{231}	-
9323,6	3922,3	M^{154}-S^{231}	-
8155,4	8155,9	Y^{163}-S^{231}	-
5821,9	5821,5	N^{97}-Y^{150}	-
5707,9	5707,4	Q^{98}-Y^{150}	-

C

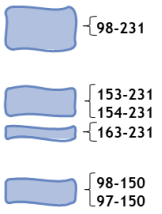
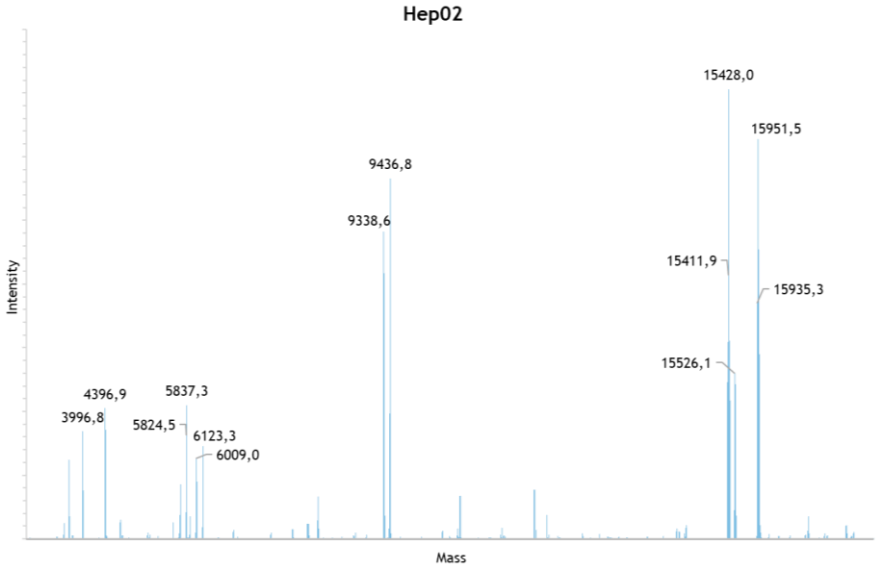


Figure 4.8 Mass spectrometry of Hep01. A) Deconvoluted spectrum of the PK-resistant fragments of Hep01; tagged peaks are those that were identified. The chromatogram and mass/charge spectrum are included in Annex VIII. B) Table of the identified peptides mass and the corresponding sequence. C) Schematic representation of bands densitometry based on the electrophoretic pattern.

USC UNIVERSIDADE DE SANTIAGO DE COMPOSTELA

A



B

Observed mass (Da)	Theoretical mass (Da)	Sequence	Modifications
15951,5	15950,5	G^{92}-S^{231}	Oxidation
15935,3	15934,5	G^{92}-S^{231}	-
15428,0	15427,3	Q^{98}-S^{231}	Oxidation
15411,9	15411,3	Q^{98}-S^{231}	-
9436,8	9436,4	N^{153}-S^{231}	-
9336,6	9338,3	M^{154}-S^{231}	Oxidation
6123,3	6122,9	Q^{98}-N^{153}	Oxidation
6009,0	6008,7	Q^{98}-E^{152}	Oxidation
5837,3	5837,6	N^{97}-Y^{150}	Oxidation
5824,5	5821,6	N^{97}-Y^{150}	-
4396,9	4396,1	W^{99}-F^{141}	Oxidation
3996,8	3996,6	N^{97}-R^{136}	-

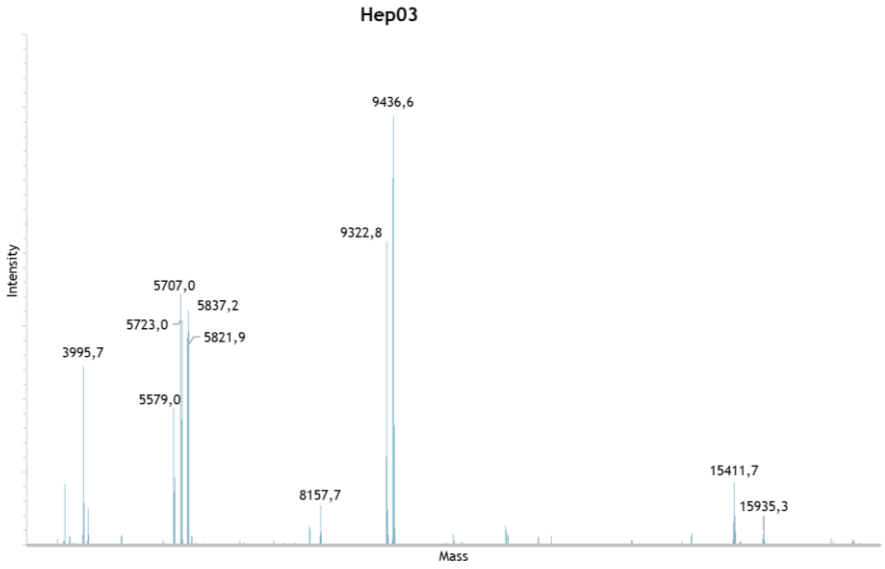
C



Figure 4.9 Mass spectrometry of Hep02. A) Deconvoluted spectrum of the PK-resistant fragments of Hep02; tagged peaks are those that were identified. The chromatogram and mass/charge spectrum are included in in Annex VIII. B) Table of the identified peptides mass and the corresponding sequence. C) Schematic representation of bands densitometry based on the electrophoretic pattern.

USC UNIVERSIDADE DE SANTIAGO DE COMPOSTELA

A



B

Observed mass (Da)	Theoretical mass (Da)	Sequence	Modifications
15935,3	15934,5	G^{92}-S^{231}	-
15411,7	15411,3	Q^{98}-S^{231}	-
9436,6	9436,4	N^{153}-S^{231}	-
9322,8	9322,2	M^{154}-S^{231}	-
8157,7	8155,9	Y^{163}-S^{231}	-
5837,2	5837,6	N^{97}-Y^{150}	Oxidation
5821,9	5821,6	N^{97}-Y^{150}	-
5723,0	5723,4	Q^{98}-Y^{150}	Oxidation
5707,0	5707,4	Q^{98}-Y^{150}	-
5579,0	5579,3	W^{99}-Y^{150}	-
3995,7	3996,6	N^{97}-R^{136}	-

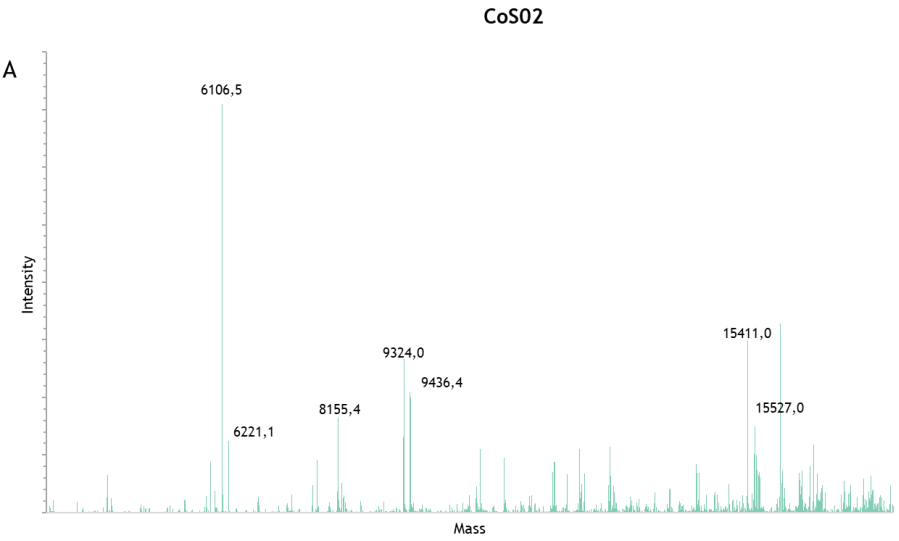
C



Figure 4.10 Mass spectrometry of Hep03. A) Deconvoluted spectrum of the PK-resistant fragments of Hep03; tagged peaks are those that were identified. The chromatogram and mass/charge spectrum are included in Annex VIII. B) Table of the identified peptides mass and the corresponding sequence. C) Schematic representation of bands densitometry based on the electrophoretic pattern.

USC UNIVERSIDADE DE SANTIAGO DE COMPOSTELA

A



B

Observed mass (Da)	Theoretical mass (Da)	Sequence	Modifications
15527,0	15525,1	N^{97}-S^{231}	-
15411,0	15411,3	Q^{98}-S^{231}	-
9436,4	9436,4	N^{153}-S^{231}	-
9324,0	3922,3	M^{154}-S^{231}	-
8155,4	8155,9	Y^{163}-S^{231}	-
6221,1	6219,8	W^{99}-Y^{150}	-
6106,2	6106,9	Q^{98}-N^{153}	-

C

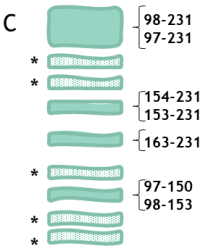
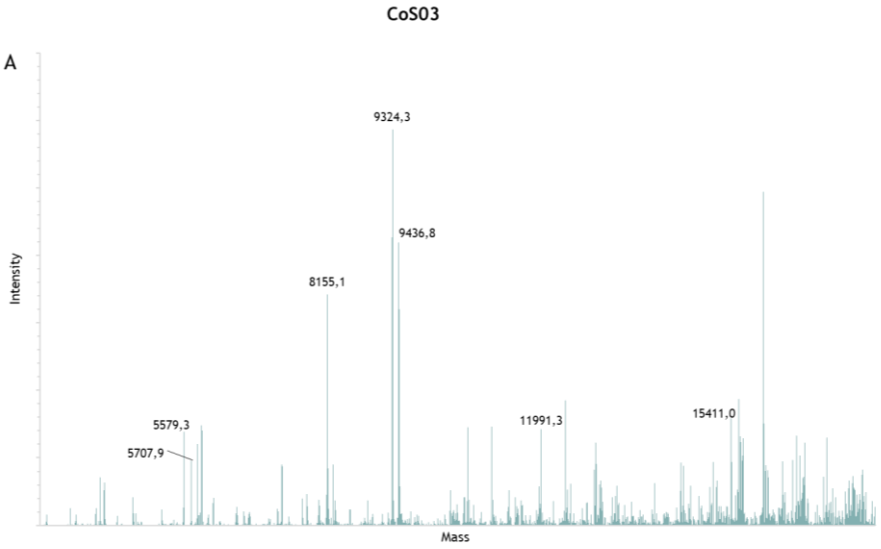


Figure 4.11 Mass spectrometry of CoS02. A) Deconvoluted spectrum of the PK-resistant fragments of CoS02; tagged peaks are those that were identified. The chromatogram and mass/charge spectrum are included in Annex VIII. B) Table of the identified peptides mass and the corresponding sequence. C) Schematic representation of bands densitometry based on the electrophoretic pattern. The asterisk(*) indicates bands visible with total protein staining but not identified by mass spectrometry.

USC UNIVERSIDADE DE SANTIAGO DE COMPOSTELA



B

Observed mass (Da)	Theoretical mass (Da)	Sequence	Modifications
15411,0	15411,3	Q^{98}-S^{231}	-
11991,3	11992,1	A^{133}-S^{231}	-
9436,8	9436,4	N^{153}-S^{231}	-
9324,3	3922,3	M^{154}-S^{231}	-
8155,4	8155,9	Y^{163}-S^{231}	-
5707,9	5707,4	Q^{98}-Y^{150}	-
5579,3	5578,6	W^{99}-Y^{150}	-

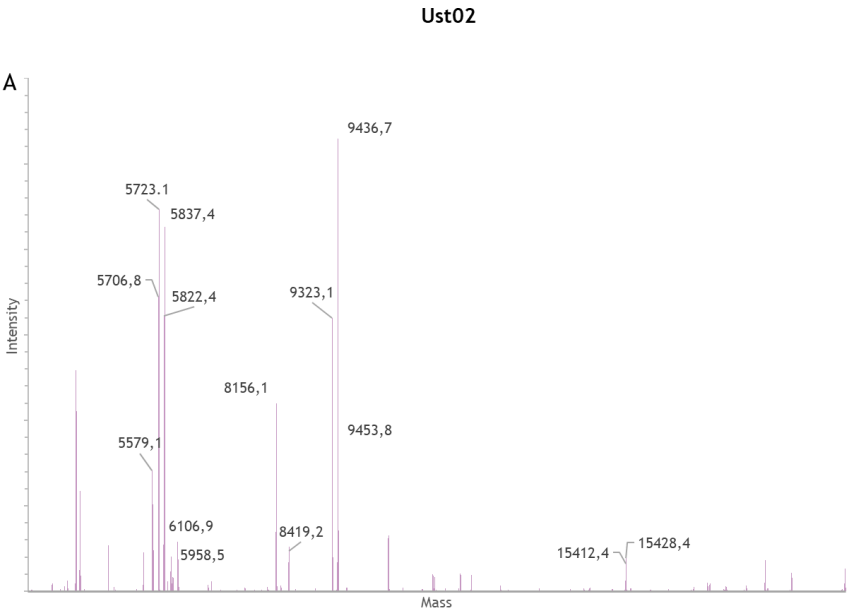
C



Figure 4.12 Mass spectrometry of CoS03. A) Deconvoluted spectrum of the PK-resistant fragments of CoS03; tagged peaks are those that were identified. The chromatogram and mass/charge spectrum are included in Annex VIII. B) Table of the identified peptides mass and the corresponding sequence. C) Schematic representation of bands densitometry based on the electrophoretic pattern. The asterisk(*) indicates bands visible with total protein staining but not identified by mass spectrometry.

USC UNIVERSIDADE DE SANTIAGO DE COMPOSTELA

A



B

Observed mass (Da)	Theoretical mass (Da)	Sequence	Modifications
15428,4	15427,3	Q^{98}-S^{231}	Oxidation
15412,4	15411,3	Q^{98}-S^{231}	-
9453,8	9452,4	N^{153}-S^{231}	Oxidation
9436,7	9436,4	N^{153}-S^{231}	-
9323,1	3922,3	M^{154}-S^{231}	-
8419,2	8418,3	V^{161}-S^{231}	-
8156,5	8156,0	Y^{163}-S^{231}	-
6106,2	6106,9	Q^{98}-N^{153}	-
5958,5	5958,7	H^{96}-Y^{150}	-
5837,4	5837,6	N^{97}-Y^{150}	Oxidation
5822,4	5821,6	N^{97}-Y^{150}	-
5723,1	5722,5	Q^{98}-Y^{150}	Oxidation
5706,8	5707,5	Q^{98}-Y^{150}	-
5579,1	5579,4	W^{99}-Y^{150}	-

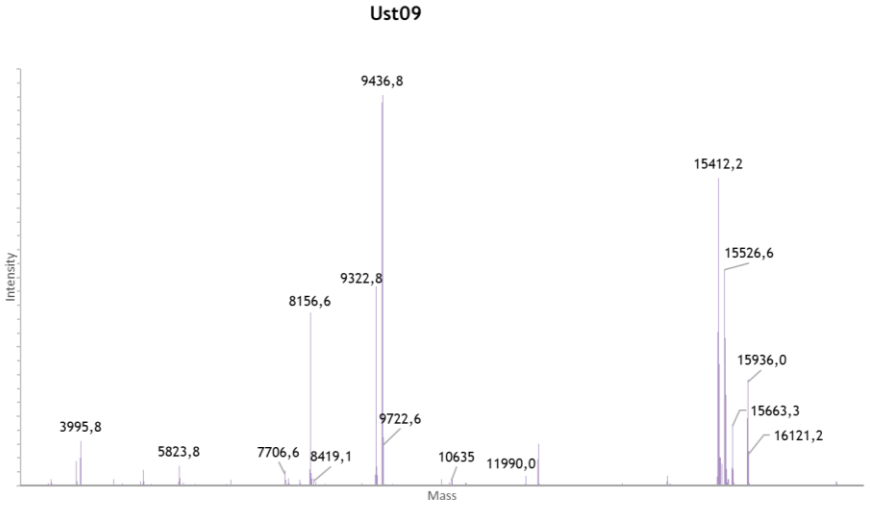
C



Figure 4.13 Mass spectrometry of Ust02. A) Deconvoluted spectrum of the PK-resistant fragments of Ust02; tagged peaks are those that were identified. The chromatogram and mass/charge spectrum are included in Annex VIII. B) Table of the identified peptides mass and the corresponding sequence. C) Schematic representation of bands densitometry based on the electrophoretic pattern.

USC UNIVERSIDADE DE SANTIAGO DE COMPOSTELA

A



B

Observed mass (Da)	Theoretical mass (Da)	Sequence	Modifications
16121,2	16119,7	G^{90}-S^{231}	-
15936,0	15934,5	G^{92}-S^{231}	-
15663,3	15662,3	H^{96}-S^{231}	-
15526,6	15525,2	N^{97}-S^{231}	-
15412,2	15411,3	Q^{98}-S^{231}	-
11990,0	11992,1	A^{133}-S^{231}	-
10635,0	10634,6	W^{145}-S^{231}	-
9722,6	9721,6	R^{151}-S^{231}	-
9436,8	9436,4	N^{153}-S^{231}	-
9322,8	9322,2	M^{154}-S^{231}	-
8419,1	8418,3	V^{161}-S^{231}	-
8156,6	8156,0	Y^{163}-S^{231}	-
7706,6	7706,6	N^{97}-R^{164}	-
5823,8	5821,6	N^{97}-Y^{150}	-
3995,8	3996,6	N^{97}-R^{136}	-

C



Figure 4.14 Mass spectrometry of Ust09. A) Deconvoluted spectrum of the PK-resistant fragments of Ust09; tagged peaks are those that were identified. The chromatogram and mass/charge spectrum are included in Annex VIII. B) Table of the identified peptides mass and the corresponding sequence. C) Schematic representation of bands densitometry based on the electrophoretic pattern.

USC UNIVERSIDADE DE SANTIAGO DE COMPOSTELA

Of the seven conformers that were analyzed, none of them presented the same distribution of PK-resistant peptides: even though Hep01 and Ust02 shared an electrophoretic pattern with similar ~16, ~9, ~8, and ~6kDa bands, mass spectrometry revealed that the cleavage sites were not precisely the same; for example, the contribution to the ~6kDa band in the case of Hep01 was restricted to the PK-resistant peptides N97-Y150 and Q98-Y150, while the same fragment in Ust02 was comprised by N97-Y150 and Q98-Y150, but H96-Y150, Q98-N153, and W99-Y150. Since the digestion conditions were the same (regarding the concentration of proteinase, pH, temperature, or duration of the digestion), these differences, could be due to different structural arrangements, which provided better accessibility of the PK to the cleavage sites or promoted the generation of ragged ends (Fig 4.15).

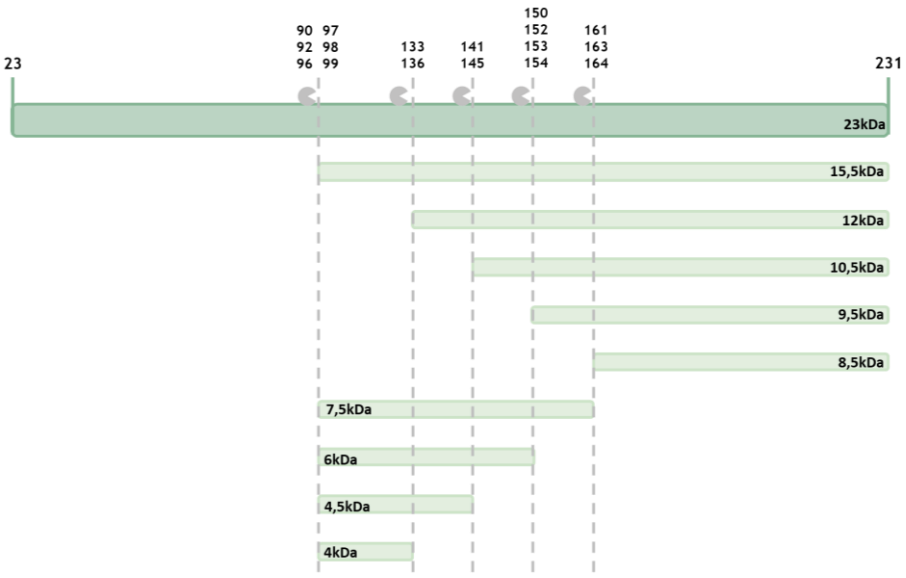


Figure 4.15 PK cleavage sites. Schematic representation of the nicksites of the PK and the resultant PK-resistant fragments.

USC UNIVERSIDADE DE SANTIAGO DE COMPOSTELA

Although the total protein staining showed a different PK-resistant fragments proportion, the mass spectrometry-based analysis is not a quantitative technique, and the intensity of the peaks is not directly related to the abundance of each peptide.

5.4.3 STUDY OF THE INFECTIVITY OF THE CONFORMERS GENERATED BY PMSA

In order to assess if the new conformers generated by PMSA with heparin, chondroitin sulfate, and pentosan polysulfate were *bona fide* prions and different strains, the product of the PMSA was inoculated intracerebrally into TgVole mice. Mice were then monitored twice a week until the onset of clinical signs; thereafter, they were observed daily until they reached the terminal stage.

All the inoculated mice developed clinical signs compatible with a transmissible spongiform encephalopathy. The prion disease was confirmed by detecting PK-resistant PrP^{Sc} in their brains by Western blot and verifying the presence of spongiosis characteristic of prion diseases.

Interestingly, the average incubation time varied widely among the conformers: Hep03 presented the shorter period of incubation, 105±2 dpi, which was similar to the average incubation time described for one of the prion strains generated with dextran, Ust02, 101±4 dpi [533]. On the other hand, the slowest conformer was Hep01, also generated using heparin as a cofactor, whose incubation period was 363±7dpi. Given that the amount of PK-resistant PrP was similar in all the conformers regarding the total protein staining, it would be reasonable to think that the difference in the incubation was not due to the titers of PrP^{Sc}; thus, the variability in the incubation would be due to intrinsic differences among the conformers, suggesting that they could be different prion strains. Moreover, one-way ANOVA and *post hoc* multiple comparisons test (Annex IX) demonstrated that conformers generated with the same cofactor presented statistically significant differences

USC UNIVERSIDADE DE SANTIAGO DE COMPOSTELA

regarding the mean incubation time. These differences, added to the variable electrophoretic mobility, supported the idea that different prion strains could be generated under the same conditions. On the contrary, the same test revealed that conformers, with different patterns, such as Hep02 and CoS01 or Hep03 and CoS03, could behave similarly from a biological point of view, and share the same average incubation time.

To further characterize these prion strains, TgVole mice were inoculated intracranially with 1% brain homogenates of mice from the first passage. Like with the first passage, mice were monitored and euthanized when in the terminal stage of the prion disease. All the inoculated animals displayed clinical signs and the attack rate was 100%; moreover, the presence of PK-resistant PrP was detected in all the brains analyzed; hence it was confirmed that the different conformers were *de novo* generated *bona fide* recombinant prions (Fig 4.16).

A

Cofactor	Strain	First passage			Second passage		
		Attack rate	PrP^{Sc}	Mean ± SEM	Attack rate	PrP^{Sc}	Mean ± SEM
Heparin	Hep01	7/7*	7/7	363 ± 7	6/6*	6/6	86 ± 5
	Hep02	6/6*	6/6	220 ± 13	6/6	5/5#	84 ± 3
	Hep03	5/5*	5/5	105 ± 2	6/6	6/6	95 ± 4
Chondroitin sulfate	CoS01	7/7	2/7	280 ± 32	6/6	6/6	101 ± 3
	CoS02	7/7	7/7	144 ± 1	6/6*	6/6	102 ± 7
	CoS03	6/6	5/6	111 ± 5	6/6	6/6	74 ± 2
Pentosan polysulfate	PPS01	6/6*	6/6	292 ± 24	6/6*	5/5#	106 ± 2
	PPS02	8/8	7/7#	141 ± 4	6/6*	6/6	79 ± 2
	PPS03	7/7	7/7	167 ± 3	6/6*	6/6	103 ± 2
Dextran sulfate	Ust02	9/9	9/9	101 ± 4	7/7	7/7	80 ± 3
	Ust09	7/7	7/7	169 ± 5	5/5	5/5	110 ± 2

USC UNIVERSIDADE DE SANTIAGO DE COMPOSTELA

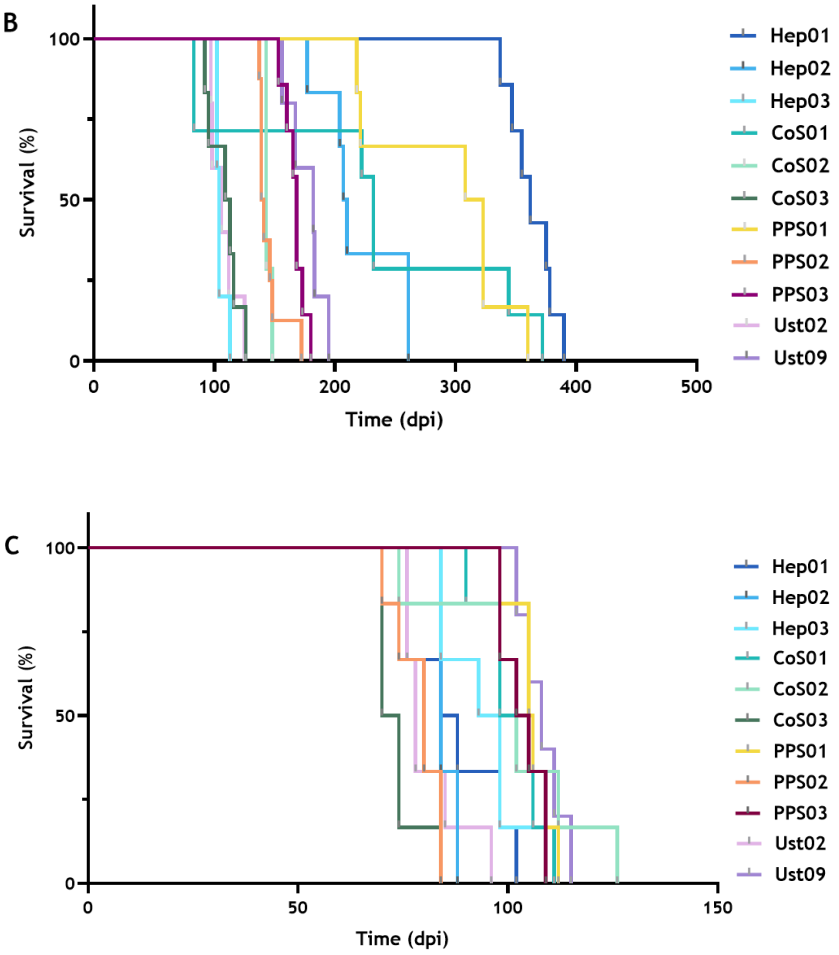


Figure 4.16 The recombinant conformers generated with different cofactors were *bona fide* prions. A) Table summarizing the average incubation time of the first and second passages. The attack rate represents the animals that presented clinical signs compatible with prion disease when euthanized. The asterisk (*) indicates that animals from those groups died of intercurrent diseases; such animals were excluded from the analysis. Hash ($^{\#}$) represents groups with animals whose brains were not possible to extract (e.g., they were found dead), although they presented clinical signs, and for this reason, the attack rate and the brains with PrP^{Sc} do not match. B) Kaplan-Meier curve of mice from the first passage. C) Kaplan-Meier curve of mice from the second passage. It should be noted that the X-axis of both curves does not have the same graduation to better distinguish the incubation time.

USC UNIVERSIDADE DE SANTIAGO DE COMPOSTELA

In general terms, the average incubation time on the second passage was shorter in comparison with the first passage, as well as the dispersion. On the first passage, the average incubation time varied between 105 and 363dpi; on the contrary, on the second passage the periods of incubation of all the stains tended to unify between 74 and 105dpi. Moreover, some conformers presented a significant decrease in the incubation period between the first and the second passages, such as Hep01, whose average incubation time moved from 363 to 86dpi. In contrast, Hep03 displayed a low variation in the incubation period, from 105 to 95 dpi. On the other hand, conformers CoS01 and PPS01 displayed similar incubation times in both passages, showing a parallel adaptation to the host; however, it is not possible to confirm that they consist of the same strain just based on this feature, since different prion strains can share the same period of incubation [449].

Overall, these data revealed that all the strains had to adapt to the brain PrP, although such adaptation was different depending on the strain: while some strains suffered from an important adaptation reflected in a great reduction of the incubation period, other strains most likely had a structure in which fully glycosylated brain PrP fitted efficiently.

5.4.4 BIOCHEMICAL FEATURES OF THE DIFFERENT RECOMBINANT PRION STRAINS

Brains of mice belonging to both passages were subjected to Western blot analysis in order to assess the presence of PrP^{Sc}. A clear accumulation of classical PrP^{Sc} was detected in all groups of animals and on both passages, supporting the idea that these recombinant conformers are *bona fide* prions. the nature. Interestingly, after PK digestion, all the conformers present a predominance of the diglycosylated band, and they greatest variety was perceived in the non-glycosylated band. This band highly varied in intensity, and molecular weight.

USC UNIVERSIDADE DE SANTIAGO DE COMPOSTELA

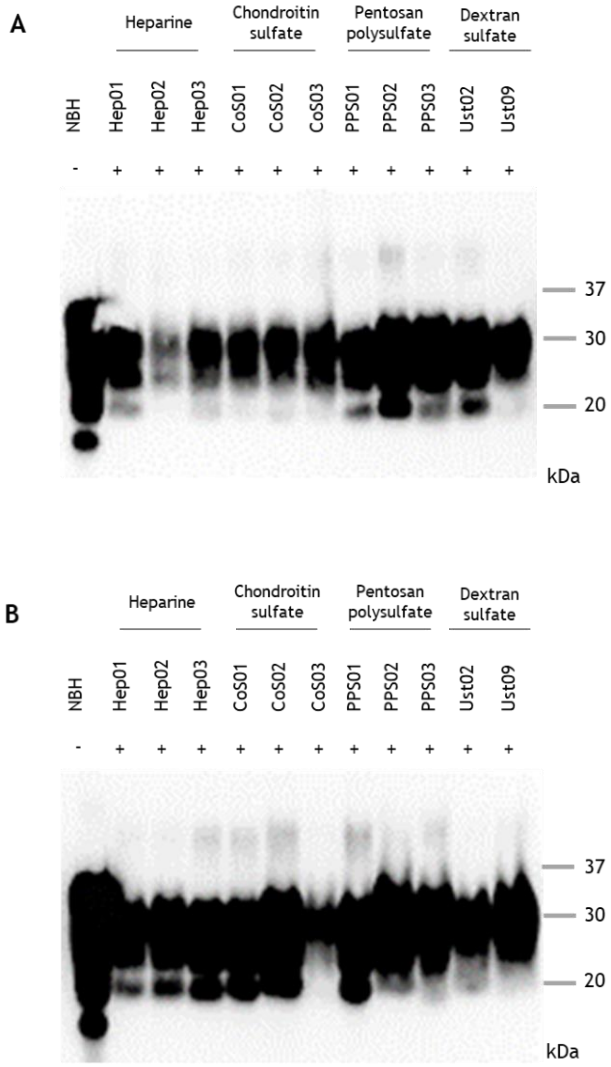


Figure 4.17 Western blot of brain homogenates of mice inoculated with conformers generated with different cofactors. A) Western blot of brain homogenates of terminally ill mice inoculated with different conformers generated by PMSA using different cofactors. B) Western blot of brain homogenates of terminally ill mice from the second passage. These animals were inoculated intracranially with brain homogenates of mice from the first passage and succumbed

USC UNIVERSIDADE DE SANTIAGO DE COMPOSTELA

to prion disease. A non-digested normal brain homogenate (NBH) was included as a reference.

Regarding the second passage, while the non-glycosylated band of PPS02, PPS03, Ust02 or Ust09 presented a weak intensity, or it was even absent, like in CoS03, such band showed a strong presence in Hep03, CoS01, CoS02 or PPS01. In terms of the electrophoretic mobility, the non-glycosylated band seemed to display a higher molecular weight in CoS02, PPS02 or Ust09. Also with respect to electrophoretic mobility in the second passage, CoS03 and PPS01 seemed to have a diglycosylated band of lower molecular weight than the other conformers (Fig 4.17). These differences would suggest structural differences among the conformers.

To better characterize the material that is propagating in the brains of the mice inoculated with the different conformers and also with the aim of assessing that the conformers give place to different prion strains, fixed brains were examined in search of spongiform changes and PrP^{res} deposits. Notwithstanding brains of animals from the first passage were inspected to confirm the presence of vacuolation and deposits of PrP^{res}, a detailed histopathological characterization was performed with the brains of mice from the second passage. The reason why an in-depth analysis was only performed with the second passage was that on the first passage the recombinant prion strains are not completely adapted to the host, as was reflected in the reduction in the incubation period, and we most likely would find certain variability in the brains of mice from the same inoculum. Since all the mice were culled in the terminal stage of the disease, it was assumed that the differences in terms of severity of the spongiform changes or in the amount of PrP^{res} depositions were characteristic properties of the strain.

USC UNIVERSIDADE DE SANTIAGO DE COMPOSTELA

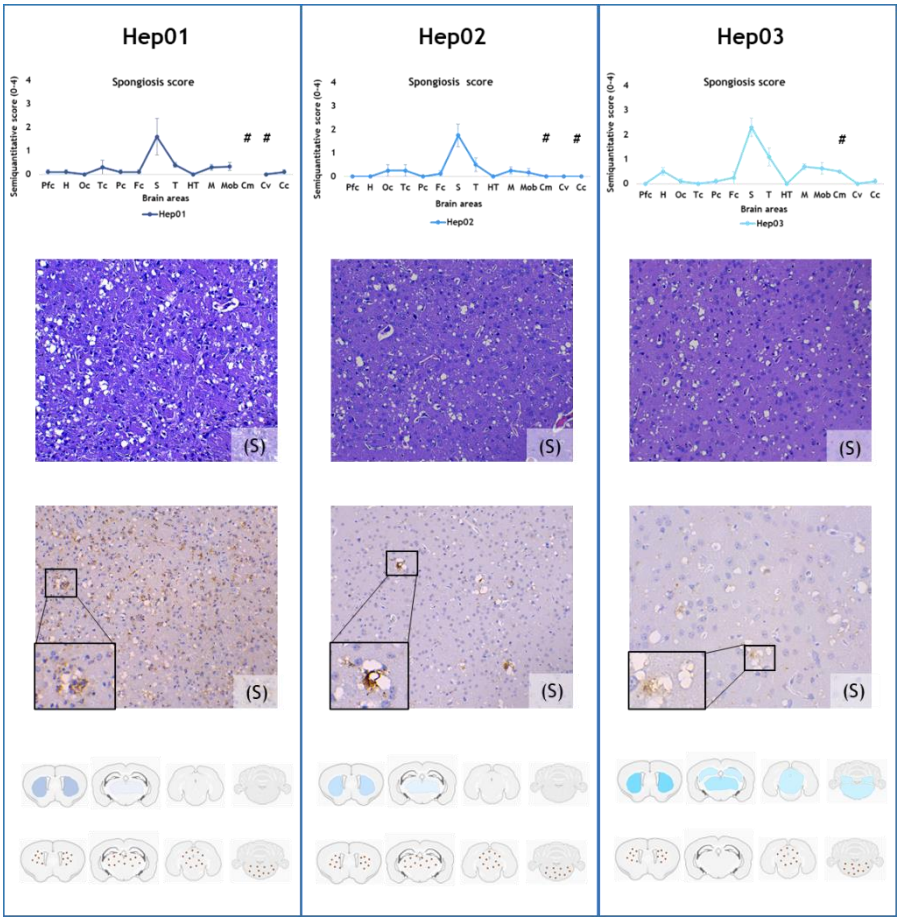


Figure 4. 18. Histopathological features of TgVole mice inoculated with conformers generated with heparin. The histopathological profile represents the mean semi-quantitative scoring (0–4, vertical axis) of the spongiform lesions against these brain regions: Pfc: piriform cortex, H: hippocampus, Oc: occipital cortex, Tc: temporal cortex, Pc: parietal cortex, Fc: frontal cortex, S: striatum, T: thalamus, HT: hypothalamus, M: mesencephalon, Mob: medulla oblongata, Cm: cerebellar nuclei, Cv: cerebellar vermis, Cc: cerebellar cortex. Hash (#) indicates that the pointed-out brain area could not be examined in all the samples. Hematoxylin-eosin staining revealed vacuolation and PrP immunolabeling showed PK-resistant PrP deposits; the brain areas from which the images were obtained are indicated in parenthesis. A schematic representation of the different brain areas summarizes the histopathological features of each conformer. The intensity of the color is in accordance with the semiquantitative score of spongiform changes and the brown dots indicate the areas where PK-resistant PrP was found.

USC UNIVERSIDADE DE SANTIAGO DE COMPOSTELA

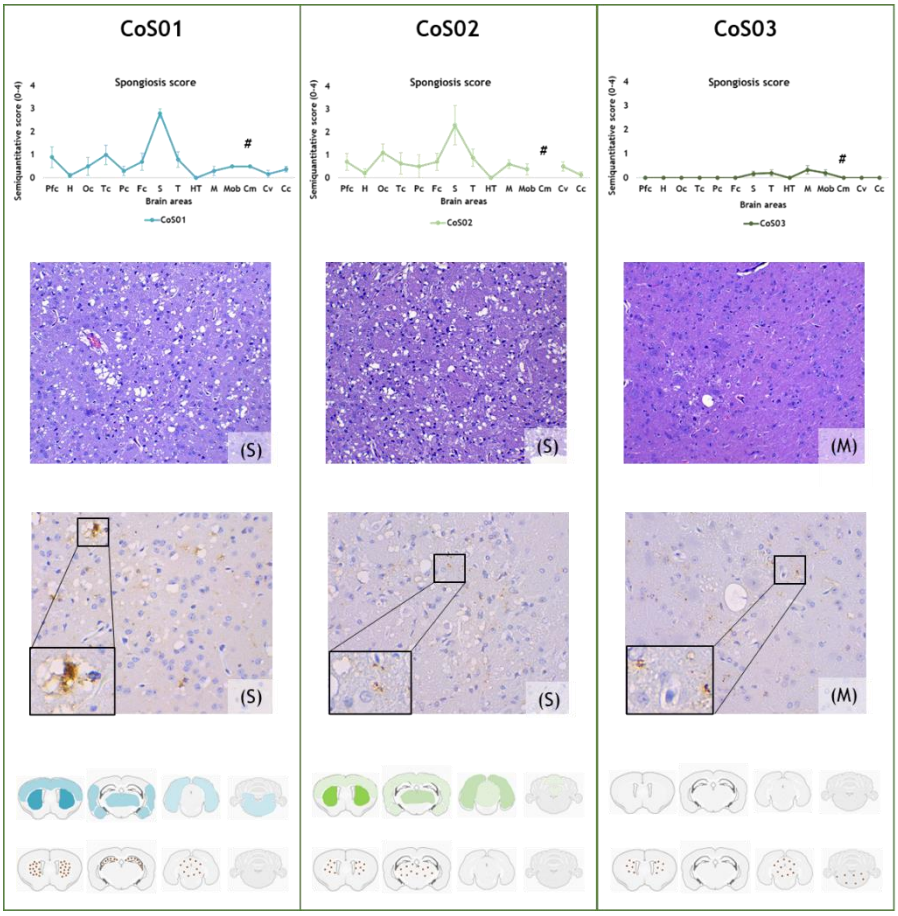


Figure 4. 19. Histopathological features of TgVole mice inoculated with conformers generated with chondroitin sulfate. The histopathological profile represents the mean semi-quantitative scoring (0–4, vertical axis) of the spongiform lesions against these brain regions: Pfc: piriform cortex, H: hippocampus, Oc: occipital cortex, Tc: temporal cortex, Pc: parietal cortex, Fc: frontal cortex, S: striatum, T: thalamus, HT: hypothalamus, M: mesencephalon, Mob: medulla oblongata, Cm: cerebellar nuclei, Cv: cerebellar vermis, Cc: cerebellar cortex. Hash (#) indicates that the pointed-out brain area could not be examined in all the samples. Hematoxylin-eosin staining revealed vacuolation and PrP immunolabeling showed PK-resistant PrP deposits; the brain areas from which the images were obtained are indicated in parenthesis. A schematic representation of the different brain areas summarizes the histopathological features of each conformer. The intensity of the color is in accordance with the semiquantitative score of spongiform changes and the brown dots indicate the areas where PK-resistant PrP were found.

USC UNIVERSIDADE DE SANTIAGO DE COMPOSTELA

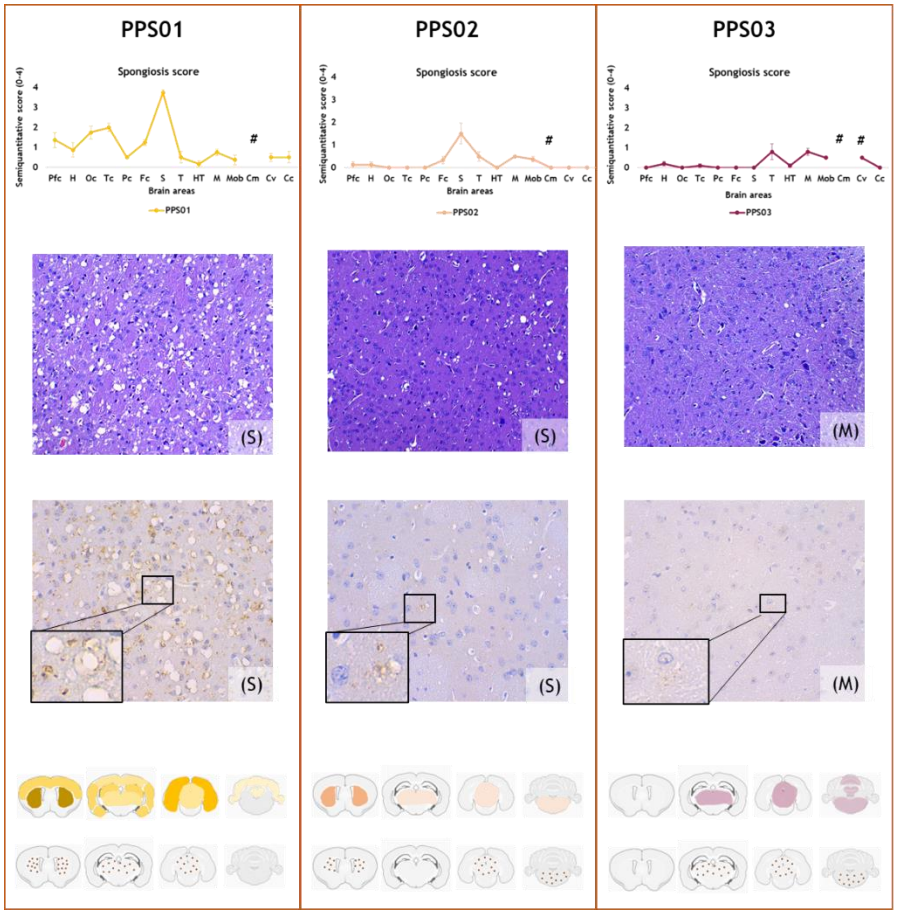


Figure 4. 20. Histopathological features of TgVole mice inoculated with conformers generated with pentosan polysulfate. The histopathological profile represents the mean semi-quantitative scoring (0–4, vertical axis) of the spongiform lesions against these brain regions: Pfc: piriform cortex, H: hippocampus, Oc: occipital cortex, Tc: temporal cortex, Pc: parietal cortex, Fc: frontal cortex, S: striatum, T: thalamus, HT: hypothalamus, M: mesencephalon, Mob: medulla oblongata, Cm: cerebellar nuclei, Cv: cerebellar vermis, Cc: cerebellar cortex. Hash (#) indicates that the pointed-out brain area could not be examined in all the samples. Hematoxylin-eosin staining revealed vacuolation and PrP immunolabeling showed PK-resistant PrP deposits; the brain areas from which the images were obtained are indicated in parenthesis. A schematic representation of the different brain areas summarizes the histopathological features of each conformer. The intensity of the color is in accordance with the semiquantitative score of spongiform changes and the brown dots indicate the areas where PK-resistant PrP were found.

USC UNIVERSIDADE DE SANTIAGO DE COMPOSTELA

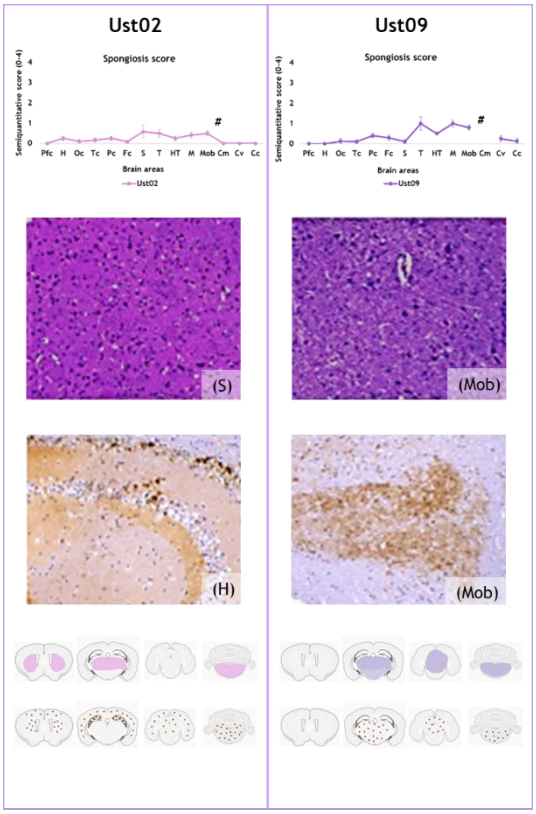


Figure 4. 21. Histopathological features of TgVole mice inoculated with conformers generated with dextran sulfate. The histopathological profile represents the mean semi-quantitative scoring (0–4, vertical axis) of the spongiform lesions against these brain regions: Pfc: piriform cortex, H: hippocampus, Oc: occipital cortex, Tc: temporal cortex, Pc: parietal cortex, Fc: frontal cortex, S: striatum, T: thalamus, HT: hypothalamus, M: mesencephalon, Mob: medulla oblongata, Cm: cerebellar nuclei, Cv: cerebellar vermis, Cc: cerebellar cortex. Hash (#) indicates that the pointed-out brain area could not be examined in all the samples. Hematoxylin-eosin staining revealed vacuolation and PrP immunolabeling showed PK-resistant PrP deposits; the brain areas from which the images were obtained are indicated in parenthesis. A schematic representation of the different brain areas summarizes the histopathological features of each conformer. The intensity of the color is in accordance with the semiquantitative score of spongiform changes and the brown dots indicate the areas where PK-resistant PrP were found. Adapted from Lopez-Moreno and Eraña et al[533]

USC UNIVERSIDADE DE SANTIAGO DE COMPOSTELA

Pathological characterization of brains of mice inoculated with conformers generated with heparin showed clear spongiform changes and PK-resistant PrP deposits. The lesion profile indicated a common affectation in the corpus striatum of the three strains, with incipient spongiosis in the thalamus. In addition, Hep03 also presented a weak vacuolation in the hippocampus and brain stem, with the exception of the hypothalamus. Regarding the PK-resistant PrP immunolabeling, these conformers displayed a faint punctuate deposition and occasional granular deposits surrounding confluent vacuoles in the striatum. Besides, the presence of PK-resistant PrP was detected in the thalamus, mesencephalon and medulla oblongata in mice inoculated with Hep01 and Hep02, although the thalamus was spared in Hep03. Since Hep01 and Hep02 share similar periods of incubation times (86 and 84dpi, respectively), they are present an indistinguishable electrophoretic pattern and brain tropism, both could be considered the same strain. On the contrary, the identity of Hep03 is not so evident given that this conformer presented a slightly longer period of incubation (95dpi), the electrophoretic pattern showed a higher intensity of the diglycosylated band, and it displayed an affinity for the hippocampus and the cerebellar cortex. Taken together, the results suggest that Hep03 could be a different entity from Hep01 and Hep02, although more data would be necessary to confirm this hypothesis (Fig 4.18).

Regarding the conformers generated with chondroitin sulfate, CoS01 and CoS02, had both similar periods of incubation and similar lesion profiles, characterized by intense striatal vacuolation and slight affectation of the neocortex and cerebellar cortex with certain variability among individuals. Although the spongiform changes looked similar, both conformers showed different PK-resistant PrP accumulation. CoS01 presented granular deposits in the striatum and hippocampus and diffuse punctuate in the mesencephalon; on the other hand, animals inoculated with CoS02 displayed diffuse punctuate deposition in the striatum and some small perinuclear plaques in the thalamus. Intriguingly, CoS03 showed distinct and unique properties.

USC UNIVERSIDADE DE SANTIAGO DE COMPOSTELA

Hardly any vacuole was observed to the point that it was considered that the animals inoculated with this conformer had a negative histopathology. Notwithstanding, these mice presented PK-resistant deposit in their brains, predominantly in the striatum, although in some animals were also found in the mesencephalon and medulla oblongata. In the mesencephalon, these deposits were granular intraneuronal and also diffuse punctuate in the neuropil. CoS03, importantly differed in the period of incubation, since it was the fastest conformer in the second passage (74dpi) and presented a different electrophoretic mobility as well, with less accumulation of PrP^{Sc} which was mainly diglycosylated. These data would hint at three different strains could had been generated with chondroitin sulfate (Fig 4.19).

Concerning the conformers generated with pentosan polysulfate, the three conformers gave rise to three clearly distinguishable anatomopathological patterns. On one hand, PPS01 was the conformer that caused the most intense spongiform changes, with vacuolation in all the brain areas unless hypothalamus, medulla oblongata, which was so weak that was considered negative, and cerebellar nuclei, which could not be examined. The spongiosis was accompanied by PK-resistant PrP deposits in the corpus striatum, thalamus and mesencephalon, as punctuate deposits in the neuropil and also perivacuolar granular deposits. On the other hand, the anatomopathological changes triggered by PPS02 resemble of those caused by Hep01 and Hep02, with moderate vacuolation in the striatum, mild affectation of the brain stem, and diffuse punctuate PK-resistant PrP depositions in the striatum, mesencephalon and medulla oblongata. Oppositely, PPS03 presented slight spongiform changes, only perceivable in the thalamus, mesencephalon, medulla oblongata and cerebellar vermis, despite this brain area could not be examined in all the mice. In contrast to the previous conformers, PPS03 neither trigger spongiosis in the striatum nor PK-resistant PrP deposits in this brain area. Such deposits were located in the brain stem, as faint punctuate accumulations in the neuropil. Likewise, mice inoculated with the three

USC UNIVERSIDADE DE SANTIAGO DE COMPOSTELA

conformers generated with PPS also presented different electrophoretic pattern; PPS01 apparently had a lower molecular weight diglycosylated band than PPS02 and PPS03. Additionally, all differed in the intensity and molecular weight of the non-glycosylated band, indicating that they might differ structurally. These results suggest that three different strains could had been generated with PPS (Fig 4.20).

In relation to the conformers generated in the presence of dextran sulfate, Ust02 and Ust09 consist of two different strains, as was previously reported [533]. Ust02 displayed mild vacuolation with predominant affectation of the striatum, thalamus and medulla oblongata; regarding the PK-resistant PrP deposits, they presented a clear hippocampal tropism, where plaques could be observed; interestingly, PK-resistant PrP deposits could be recognized in brain areas without spongiform changes, such as the neocortex or the mesencephalon. Alike PPS03, Ust09 presented the peculiarity that the striatum was spared of vacuolation, and the spongiform changes were located in the brain stem, where PK-resistant PrP deposits were also focused, as intraneuronal granular deposits distributed throughout the neuropil (Fig 4.21).

Taken together, these data suggest that different *bona fide* prion strains could be generated by PMSA in the presence of the same cofactor. Likewise, regarding the similar biochemical and biological properties of certain conformers generated with different cofactors, these results would also advocate that some conformers would give rise the same prion strain after inoculation in TgVole mice. Since it is possible that the conformers have not yet fully adapted to the PrP of the host, it would be ideal to perform a third passage to better compare the biological and biochemical properties of the conformers.

USC UNIVERSIDADE DE SANTIAGO DE COMPOSTELA

5.4.5 CHARACTERIZATION OF DIFFERENT STRAINS GENERATED WITH DEXTRAN SULFATE BY SSNMR

Nuclear magnetic resonance spectroscopy is a spectroscopic technique that can provide atomic resolution of a molecule based on the behavior of atomic nuclei when electromagnetic radiation is applied with a specific frequency. NMR spectroscopy has been used to acquire structural information about amyloid fibrils; however, since amyloids are heterogeneous insoluble assemblies that tend to aggregate, structural studies are adapted to an NMR variant termed, solid-state NMR (ssNMR) that, as its name suggests, uses solid particles rather than in solution [175,536].

Our group has recently made use of ssNMR spectroscopy to study a vole-adapted CWD prion strain propagated by PMSA[537], called Sst01 [533]. This prion strain has its origin in a CWD isolate which was inoculated in BVs bearing the 109I polymorphism[345]. Subsequently, a brain homogenate from a terminally sick BV was inoculated in transgenic mice expressing BVPrP, which are easier to breed and handle in the laboratory than voles. Brain homogenates of these mice in which the vole-adapted CWD strain was propagating, were used as seed for a PMCA and serially amplified by this technique using recombinant PrP as substrate[482]; afterward, the strain adapted to PMCA was used as seed for PMSA[483] and propagated using dextran sulfate as a cofactor.

One of the aforementioned advantages of the PMSA above other methods of prion propagation is its scalability. Scaling-up permits to obtain large amounts of material in a short period of time and can be used to carry out biochemical or biophysical techniques that require larger amounts of material. Thus, taking advantage of this benefit, our laboratory generated large amounts of Sst01 and characterized it by FTIR, ssNMR [189,537], and mass spectrometry-based analysis [538]. Regarding the structural characterization by ssNMR, one of the experiments carried out was ^{13}C-^{13}C Dipolar Assisted Rotational Resonance (DARR) spectra. This assay consisted of the transfer of the magnetization from one hydrogen to ^{13}C nuclei, and from these nuclei

USC UNIVERSIDADE DE SANTIAGO DE COMPOSTELA

to other intra or intermolecular ^{13}C nuclei that are close in space[539,540] (Fig 4.22). Since this experiment was performed with U-(^{13}C, ^{15}N)-Phe full-length BVPrP, it would provide information about the chemical shift of phenylalanines. In case of showing similar chemical shifts, the results would provide evidence that the three phenylalanine residues shared conformational environments. On the contrary, in case that they presented different chemical shifts, these results would suggest that the phenylalanine residues are in different conformational environments with different levels of rigidity. Depending on the chemical shift, the results would support that the chemical environment of phenylalanines would be compatible with a PIRIBS or 4RβS architectures. It should be noted that this experiment was performed before the structural resolution of the 263K strain by cryo-EM.

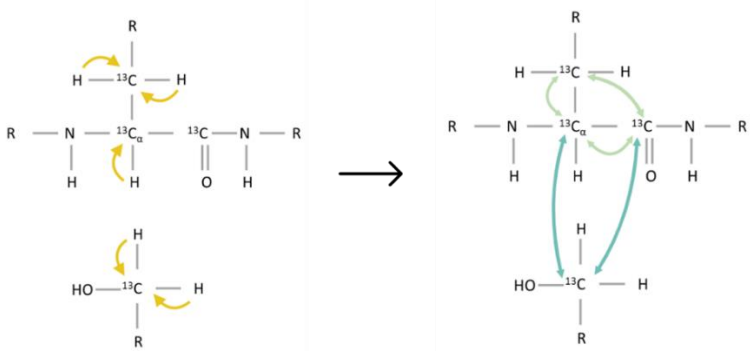


Figure 4.22 Schematic representation of the basis of ^{13}C-^{13}C Dipolar Assisted Rotational Resonance (DARR). Hydrogen magnetization is transferred to ^{13}C nuclei (yellow arrows). Subsequently, magnetized ^{13}C nuclei transfer the magnetization to other nearby intra (light green arrows) or intermolecular (cyan arrows) ^{13}C nuclei. Image created with bioRender.com adapted from https://protein-nmr.org.uk/[541]

Intriguingly, the Sst01 ^{13}C-^{13}C-DARR spectrum presented two sets with three signals for each set, while only one signal for each

USC UNIVERSIDADE DE SANTIAGO DE COMPOSTELA

phenylalanine was expected. Moreover, the chemical shift of one set of signals was more characteristic of a coil, while the other one was compatible with a β-sheet secondary structure [542]; although it was not possible to make a further interpretation of these data from the structural point of view, this experiment evidenced that phenylalanines would be in different chemical environments; therefore, more than one conformer would be present in Sst01.

In order to characterize more recombinant prion strains by ssNMR and to compare their spectra, large amounts of U-(^{13}C, ^{15}N)-Phe Ust02 and Ust09 were obtained by PMSA. Like Sst01, these strains were propagated in the presence of dextran sulfate as a cofactor, with the aim to reduce variability among strains, since the interaction between glycosaminoglycans can vary amyloids DARR chemical shift[543]. After amplification, the recombinant prion strains were digested with PK, pelleted, dried, and loaded in a 1.3mm rotor.

Interestingly, like Sst01, Ust02 and Ust09 spectra also presented two sets of three signals, indicating that phenylalanine residues are located in structures with different levels of rigidity: the chemical shift of one set would be compatible with a relatively rigid coil or a flexible β-sheet, and the other set would present a chemical shift compatible with a more rigid β-sheet (Fig 4.23)[542]. Comparing the three spectra it can be noticed that the signals were not completely overlapped, indicating that the chemical environment of the phenylalanines of the three strains was significatively different.

While some of the coil signals of Sst01 and Ust02 could be superposed, Ust09 presented a chemical shift slightly displaced. On the other hand, β-sheet chemical shift signals of Sst01 and Ust09 were completely overlapped; whereas only one of the signals of the β-sheet chemical shifts set of Ust02 merged with the corresponding signals of Sst01 and Ust09. Definitely, these results demonstrated distinct structural arrangements among the recombinant prion strains.

USC UNIVERSIDADE DE SANTIAGO DE COMPOSTELA

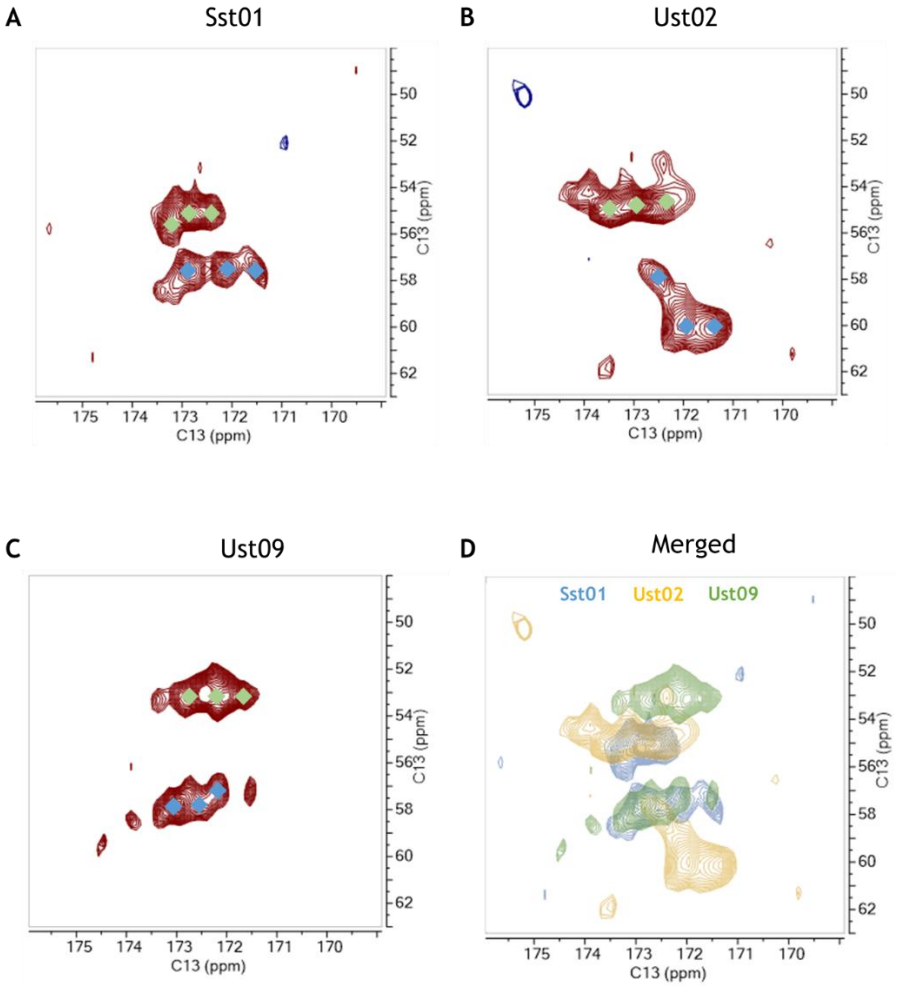


Figure 4.23 ^{13}C-^{13}C DARR spectra (τ_{mix}=100ms; MAS 20kHz). Spectra of expanded CO/CA regions of A) Sst01, B)Ust02, and C) Ust09. Diamonds indicate peaks corresponding to phenylalanine signals with chemical shifts characteristic of a coil (green) or ß-sheet (blue). D) Merged spectra of the three recombinant prion strains: Sst01 (blue), Ust02 (yellow), and Ust09 (green).

USC UNIVERSIDADE DE SANTIAGO DE COMPOSTELA

5.5 DISCUSSION

5.5.1 GENERATION AND CHARACTERIZATION OF DIFFERENT RECOMBINANT PRIONS STRAINS *DE NOVO* GENERATED BY PMSA WITH DIFFERENT COFACTORS

The wide variety of prion strains is of structural and biochemical interest. However, since prion strains cause specific pathological phenotypes, the characterization of these conformers is of vital importance from a pharmacological point of view, as well. Currently, there is no effective treatment for prion diseases, and one of the reasons is the strains capability to evade the treatment by mechanisms of adaptation and selection[474,544]. The presence of pharmacological compounds modifies the environment of prion propagation, which triggers the emergence of drug-resistant conformers[415,472]; therefore, a comprehensive characterization of diverse strains can provide crucial information about the underlying differences among them, enabling the design of effective therapies and to tackle the adaptation and selection mechanisms that lead to therapeutic failure.

It has been suggested that cofactors are biomolecules involved in maintaining the biological and biochemical features of prion strains and closely related to prion infectivity[545]; additionally, cofactors have also been associated with prion strain selection. Since PrP is a membrane protein, it would be reasonable to consider as possible cofactors molecules that are present in the extracellular matrix and with which PrP could interact; thus, such molecules include membrane phospholipids, proteoglycans, glycosaminoglycans, and other proteins. Although prions isolated from infected animals had associated different cofactors, glycosaminoglycans are frequently related to amyloid

USC UNIVERSIDADE DE SANTIAGO DE COMPOSTELA

deposits, and *in vitro* assays demonstrated that they play a crucial role in amyloid formation and fibril stabilization[546]; additionally, in some amyloidoses, glycosaminoglycans have also been associated with cytotoxicity[522]. Moreover, heparan sulfate, which is the most common glycosaminoglycan present in the cell membrane, has been associated with diverse amyloidoses, such as Alzheimer's disease, Parkinson's disease, type II diabetes or light chain amyloidosis [524]. In prion diseases, heparan sulfate affects the kinetics of propagation[547] and the brain deposition *in vivo*, therefore, it changes the strain properties[548].

The aim of this work was to generate different synthetic conformers by PMSA using natural or synthetic glycosaminoglycans cofactors and characterize them by different biological, biochemical, and biophysical methods. This characterization would enable us to assess their infectivity and their properties; therefore, it would make it possible to confirm whether they are different *bona fide* prion strains.

Nine different conformers were *de novo* generated by PSMA using recombinant full-length BVPrP (109I) and heparin, chondroitin sulfate, or pentosan polysulfate as cofactors. Concretely, three different conformers were generated with each cofactor. These conformers were stabilized by serial passages and compared with two recombinant prion strains generated by the same methodology but using dextran sulfate as a cofactor[533].

Attending to the electrophoretic pattern and independently of the cofactor, all the conformers shared three PK-resistant fragments detectable with total protein staining and Western blot of ~16, ~9, and ~6kDa; particularly, the ~16kDa PK-resistant fragment is present in recombinant infectious prions propagated by PMSA[101] or *de novo* generated by PMCA using recombinant PrP [108], and corresponds to the PrP27-30 PK-resistant core of *bona fide* prions[92].

The characterization of the conformers by limited proteolysis coupled to mass spectrometry turned out to be an exceptionally revealing technique. It must be noted that the bases of limited proteolysis

USC UNIVERSIDADE DE SANTIAGO DE COMPOSTELA

establish that the tertiary structure, rather than the sequence of the protein, determines the site of proteolysis [534]. Thus, loops, unstructured and flexible regions exposed to the solvent would be primarily cleaved since local deformations are required to reach the active site of the enzyme. Oppositely, β-strands are rigid structures, stabilized by inter and intrachain hydrogen bonds that involve energetic constraints and can hardly be deformed [535], for these reasons, limited proteolysis provided structural information. Moreover, the combination with mass spectrometry-based analysis permitted the identification of exact cleavage sites and the PK-resistant fragments that composed each conformer. In addition, although the intensity of the peaks was not directly related to the abundance of the peptide, a semiquantitative approach could be done by attending to the total protein staining, taking into consideration the intensity and the molecular weight of the bands.

As well as the electrophoretic migration, mass spectrometry-based analysis showed that all the conformers shared three bands, identifying common cleavage sites at positions 98, 150, 153, and 154 which yielded the peptides 98-231, 153-231, 154-231, and 98-150, and corresponded to the aforementioned bands observed in the total protein staining. Apart from these common nicksites, specific cleavage sites were recognized for each conformer that agreed with the electrophoretic pattern. Moreover, all these conformers present a PK-sensitive 23-89 region, which is in complete agreement with previous works and with PrP^{Sc} solved structures [110,179,180,190,193,194,506,549].

Nevertheless, we found the first particularity in the region 89-99, which corresponds with the frontier between the unstructured N-terminal domain and the C-terminal PIRIBS core. Different works have demonstrated that the PK-resistant core of some *ex vivo* wild-type prion strains from patients with the GSS P102L variant [549], sCJD [181], or from prion-infected hamsters,[179] and mice [180] started at position ~74-81 with ragged termini fragments that could be extended until position 92. However, the PK-resistant core of mouse and BV prion strains propagated by PMCA[506] or PMSA started at positions ~90-99. When

USC UNIVERSIDADE DE SANTIAGO DE COMPOSTELA

these cleavage sites were projected into the different structures available for mouse prion strains, aRML[194], RML[190], ME7[193], and a22L[205], most of them were placed in a region that corresponds to a β-sheet which extend from position ~94 to ~99. Additionally, the size of the ~90-231 region determines the PK-resistant core of brain-derived prions, known as PrP27-30. In this regard, the cleavage site at the N-terminal extreme determines the electrophoretic mobility, differentiating between type 1 or type 2 patterns. Therefore, dominant nicksites at positions 78, 82, or 90 are preponderant in 263K or PrP^{Sc} derived from type 1 CJD patients, whereas Dy or PrP^{Sc} derived from type 2 CJD patients have preponderant cleavage sites at positions 92, 97, or 101[179,550]. Based on these data, BV recombinant strains propagated PMSA present common cleavage sites at positions 92, 97, or 98; therefore, it would be reasonable to expect a Dy-like electrophoretic mobility after inoculation (Annex VII Fig S2).

Another cleavage site in the region ~150-154 was identified in all the recombinant prion strains studied in the present work, and two reciprocal fragments arise from this cleavage site ~90-150 and ~154-231. These fragments, together with ~90-231, represent the most common PK-resistant fragments in recombinant prion strains [101,506]. Additionally, cleavage sites at these positions have also been described in brain-derived classical[179,180,182] and atypical[181,183,549,551] prions. Notwithstanding, while in recombinant prion strains these cleavage sites are predominant, in brain-derived PrP^{Sc} these nicksites were detected in a very low proportion[179,180]. Although these cleavage sites were identified in both, classical and atypical PrP^{Sc}, the presence of the resultant N-terminal fragment, ~90-150, was widely associated with atypical PrP^{Sc} such as GSS P102L[549], sCJD[183], Nor98[552], or VPSPr[551] among others. On the contrary, the C-terminal fragment resultant of the cleave, ~154-231, involves the most resistant region of the PrP^{Sc} core to PK digestion or denaturalization [179,182].

Many of the strains generated by PMSA presented a major nicksite at position ~163, which originated the complementary peptides ~97-163

USC UNIVERSIDADE DE SANTIAGO DE COMPOSTELA

and ~163-231. While fragment ~97-163 was very unusual, the ~163-231 peptide, together with the fragment ~153-231, were reflected as an intense doublet of ~9kDa in the electrophoretic pattern. Although this cleavage site was also described in *ex vivo* aRML[180], the presence of this fragment in classical prion strains was minimal. However, this ~163-231 C-terminal truncated fragment, together with ~154-231 fragment, also known as CTF12/13, are much more common in brain-derived samples from patients with different subtypes of CJD[553], such as sCJD[181,183] iCJD[554], CJD E200K[555], or M232R[554], where they were found in coexistence with PrP27-30. Interestingly, recombinant PrP amyloids also present this ~163-231 PK-resistant core [413]. When this cleavage site is projected into the available PrP^{Sc} structures, it could be perceived that it is placed in a β-sheet; thus, the cleavage at this residue should be unlikely. Zou et al suggested that this fragment would be generated following a different pathway than PrP27-30[181]. This idea suggests the existence of a mixture of distinct PrP^{Sc} conformers with slight differences in the tertiary structure; nonetheless, the role of the ~163-231 C-terminal fragments in human pathogenesis remains unclear[556]. Regarding the recombinant prion strains generated by PMSA, the simultaneous origin of a mixture of species with a slightly different architecture would be a reasonable explanation for the coexistence of both truncated forms: ~163-231 and ~153-231; and it is supported by the evidence that *in vitro* amplification techniques, like PMCA, can generate heterogeneous populations[186,557,558]. Overall, the data obtained by mass spectrometry-based analysis after digestion with PK indicate that the presence of different PK-resistant fragments in the different conformers is compatible with different structural arrangements, reinforcing the idea that they consist of different strains. Moreover, this information strongly suggests the existence of different conformational arrangements between wild-type and synthetic prion strains generated by PMSA, reflected in a higher sensitivity to PK digestion and the presence of different cleavage sites. Such structural differences could be a consequence of the lack of the bulky glycans that could interfere sterically in the adopted conformation.

USC UNIVERSIDADE DE SANTIAGO DE COMPOSTELA

Cleavage sites at positions 117/119 have been broadly described in both, *ex vivo* and recombinant prion strains; in fact, Kraus and colleagues proposed that these nicksites would be responsible for local destabilizations which would trigger partial unfolding and separation of residues ~90-118. This hypothesis would be supported by the fact that the hydrophobic clusters provide lateral and longitudinal intra and interchain polar interactions which stabilize the structure; the proteolytic digestion could disrupt these interactions causing local structural destabilizations[559]. Moreover, this phenomenon would allow the access of the solvent and PK to the hydrophobic region 120-140[192] where minor cleavage sites have been also identified at positions 133, 135, or 139 (BV numbering)[179,180,506]. In contrast to this evidence, none of the recombinant conformers presented nick sites at positions 117/119, although cleavage sites at positions 133 and 136 were identified. Since in these samples nicksites at residues 133 and 136 generated the peptides 97-136 and 133-231, they are most likely independent cleavage sites rather than complementary; thus, there are some reasonable explanations for their existence that are not exclusive. One hypothesis for this event would be that cleavage sites at position 117 and 119 were present in the conformers, although they were not identified due to the low intensity of the peaks; moreover, reciprocal peptides, ~97-117 or ~97-119, would have such a low molecular weight that an accurate and precise identification would not be possible. This hypothesis would explain the origin of the peptides 133-231 recognized in CoS03 and Ust09 spectra. Another option would be that these strains generated by PMSA structurally differ from *ex vivo* or other recombinant prion strains. This idea would be supported by the fact that the cleavage site at position 136 exists in the absence of the nicksites at positions 117 and 119, since the peptide 97-136 was identified in Hep02, Hep03, and Ust09. This peptide would not exist if the cleavage site at 136 were a consequence of a primary cleavage at positions 117 or 119; on the other hand, based on Kraus's hypothesis, this cleavage site would be secondary to an initial nick at residues 153-154, which are present in all the strains studied. Another interpretation is that the

USC UNIVERSIDADE DE SANTIAGO DE COMPOSTELA

structural arrangements of PMSA-generated recombinant BV strains expose some cleavage sites to the solvent and to the PK, while in wild-type strains these nicksites are buried in hydrophobic cores.

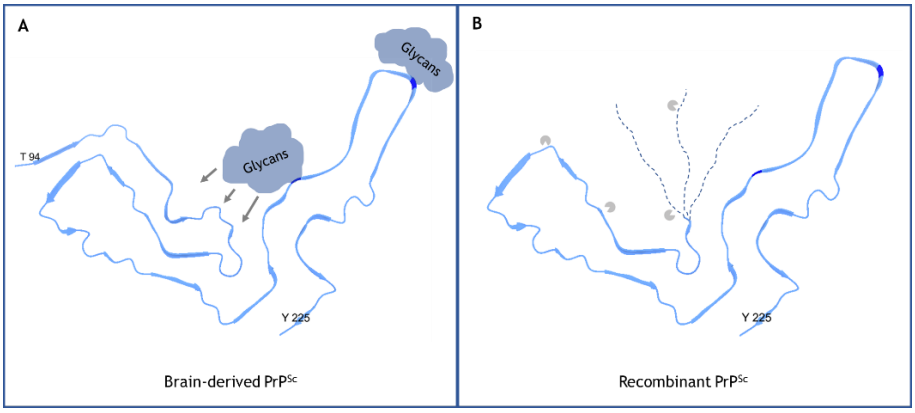


Figure 4.24 Hypothetical structural differences between brain-derived and recombinant prion strains. A) Structure of RML with the representation of glycans as dark blue clouds. Gray arrows represent glycans demanding space that force the interaction of the N-terminal lobe. B) Hypothetical representation of a recombinant prion strain generated with recombinant PrP; therefore, lacking glycans. Dashed line indicates a flexible ~90-118 region, and gray icons illustrate how PK could access to different cleavage sites identified by mass spectrometry-based analysis. Image created with ChimeraX with the RML structure (PDB 7QIG)[197]

Since most of the differences regarding the PK cleavage sites between recombinant and brain-derived strains affect the N-terminal region of the PrP^{Sc}, it could be hypothesized that there exist structural differences in this area. Such structural divergences would affect the flexibility or the degree of compaction of the N-terminal lobe, leading to a higher accessibility of the PK to certain cleavage sites, which are unavailable in brain-derived prion strains. It is possible that in brain-derived strains the presence of bulky glycans at position 180 (mouse numbering) pushes region ~90-118, forcing it to interact with the region ~120-145. In case of prion strains generated *in vitro* from recombinant PrP, the

USC UNIVERSIDADE DE SANTIAGO DE COMPOSTELA

absence of glycans allows a greater mobility of the ~90-118 region, permitting the access of the PK (Fig 4.24).

In order to characterize the biological properties of these conformers, they were inoculated in TgVole mice expressing ~1x BVPrP (109I). On the first passage, all the conformers had an attack rate of 100%, demonstrating that they are *bona fide* prions. The conformers characterized in this work presented a wide variety of incubation periods on the first passage. Interestingly, among the strains generated with each conformer it was possible to identify fast, moderate and slow conformers, demonstrating that they propagated in the brain in a different fashion.

The period of incubation is an intrinsic feature of the strain; however, it is known that certain synthetic prions generated from recombinant PrP and inoculated in animals require a period of adaptation in which the PrP^{Sc} structure is adapted to a substrate that contains post-translational modifications, like N-linked glycans and the GPI anchor. Moreover, these post-translational modifications mean that there is an intraspecies barrier, therefore, the period of adaptation increases the proper incubation time of the strain, according to how well brain PrP^{C} fits in the recombinant PrP^{Sc} structure [511]. A complete adaptation is obtained after serial transmission when there is no difference in the incubation period consecutive passages. Despite the fact that this phenomenon of adaptation was reflected in several recombinant prion strains [101,510,560], there have also been described synthetic prions which did not showed a reduction in the period of incubation after serial transmission [108,470]. Such synthetic prions presented from the first passage a period of incubation comparable to brain-derived prions, indicating that their architecture might be similar.

Regarding the second passage, conformers experienced a clear adaptation to the host reflected in the shortening of the incubation time, since the average incubation time of all the conformers trended to unify between 73 and 110dpi. Despite this unification, certain conformers still

USC UNIVERSIDADE DE SANTIAGO DE COMPOSTELA

presenting clear distinctions in the incubation period, suggesting that different strains would have arisen under the same conditions of propagation. This idea was also supported by the biochemical characterization of the PK-resistant material present in brains of mice inoculated with the conformers, since the immunoblotting of the second passage clearly showed different electrophoretic mobility patterns. Finally, anatomopathological analysis provided crucial information that confirmed the existence of different prion strains. The different lesion profiles and location of PrP^{res} deposits indicated a specific brain tropism by certain conformers which were clearly distinguishable from others. As suggested by the average incubation times and electrophoretic patterns, different strains could have been generated under the same propagation conditions and with the same cofactor. On the other hand, some conformers generated with different cofactors displayed similar biological and biochemical properties, suggesting that the same strain could have been generated in the presence of different cofactors.

Previous works suggest that cofactors govern the conformation and strain properties of PrP^{Sc}. Moreover, it was proposed that prion strains preferentially propagate in the presence of determined endogenous cofactors. Such cofactors would be enriched in different proportions in the brain areas and would determine the brain tropism of the strains, since the cofactor would promote the propagation of the PrP^{Sc} strain; this idea was termed cofactor selection model of neurotropism[515]. This model would be supported by experiments performed by PMCA, in which the presence of a concrete pure cofactor leads the propagation of one single PrP^{Sc} conformer, while different conformers would be obtained using different pure cofactors or their combination[482,510], indicating that the PrP^{Sc} diversity would be limited by the cofactor.

Nevertheless, since our results showed that more than one recombinant prion strain would be generated from the same PrP sequence, in the presence of the same cofactor and under the same condition of propagation, it could be suggested that the PrP sequence or the method

USC UNIVERSIDADE DE SANTIAGO DE COMPOSTELA

of amplification, rather that the cofactors, would govern the PrP^{Sc} diversity.

Regarding the structural information obtained by ssNMR, DARR spectra showed that the phenylalanines of the three strains have different chemical shifts, therefore, their chemical environment is slightly different. This evidence confirmed that the prion strains generated by PMSA with dextran sulfate are structurally different; unfortunately, no further conclusions about the architecture can be drawn from these spectra.

Interestingly, all the strains analyzed by ssNMR presented signal multiplicity since two different sets of signals were detected for U-(^{15}N, ^{13}C)-phenylalanines, while only one signal or less (in case their chemical shifts coincided) were expected. The presence of signal multiplicity could also be artifactual, caused by intermolecular interactions between different fibrils. This event is most likely due to the lateral associations between fibrils, which have been observed by TEM. Additionally, this phenomenon could be also caused by the collapse or structural reorganization of assemblies as a consequence of the PK digestion; nonetheless, this is an unlike possibility since undigested Sst01 also showed signal multiplicity (Fig 4.25)[189,537]. The most reasonable explanation for these results is that, instead of being pure strains, a mixture of different conformers was present in these samples. The selection of specific cofactors, such as dextran sulfate [101,482], or the use of zirconia/silica beads instead of glass beads to perform the PMSA[509], are known to reduce the heterogeneity of the samples. Nevertheless, due to the stochastic origin of prions[480], it could not be rejected the idea that more than one conformer was propagating simultaneously as a stable mixture in these samples. The likelihood of a mixture of conformers would also explain the tendency of the average incubation times to unify upon the second passage and the common histopathological features that shared some conformers. These data would suggest that a predominant prion strain, which adapted faster to brain PrP^{C} would be present and dominated over others. Mixtures of

USC UNIVERSIDADE DE SANTIAGO DE COMPOSTELA

strains are commonly found in nature, in brains of sCJD patients[427,466,561]; furthermore, the PMCA has also been demonstrated to generate heterogeneous populations of PrP^{Sc} after serial passages[186,557,558]; thus, this possibility must be also contemplated. Moreover, since glycosaminoglycans promote and accelerate the fibrillation of amyloidogenic proteins, they could also be responsible for the diversity of conformers and possible mixtures[562,563].

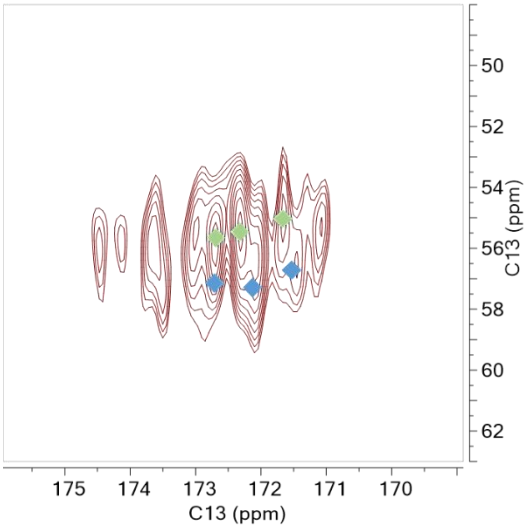


Figure 4.25. ^{13}C-^{13}C DARR spectra (τ_{mix}=100ms; MAS 20kHz) of non-digested Sst01. Spectra of expanded CO/CA regions of non-digested Sst01. Diamonds indicate peaks corresponding to phenylalanine signals with chemical shifts characteristic of a coil (green) or ß-sheet (blue).

Overall, these results demonstrate that the PMSA turned out to be a versatile technique to generate, propagate and amplify large amounts of multiple PK-resistant conformers. These conformers were generated *de novo* in the presence of different polysaccharide cofactors and their inoculation in TgVole mice demonstrate that they consist of *bona fide* prions. Moreover, conformers generated with the same cofactor displayed distinct biochemical and biological properties suggesting that they consist of different strains. This fact challenges the previous conception about the role of cofactors in prion strain diversity.

USC UNIVERSIDADE DE SANTIAGO DE COMPOSTELA

5.6 SALIENT REMARKS

1. Multiple conformers have been spontaneously generated by PMSA in the presence of three different cofactors.

2. Biochemical and biophysical analyses determined that the conformers present different structural properties.

3. Mass spectrometry-based analysis determined that the recombinant conformers presented structural differences in comparison with brain-derived prions.

3. Inoculation of the conformers in TgVole mice demonstrated that they consist of *bona fide* prions.

4. The biological and biochemical features of the conformers after serial transmission suggest that more than one strain emerged under the same conditions of propagation.

4. ssNMR analysis indicates that the analyzed conformers are structurally different.

5. ssNMR analysis suggests that a mixture of conformers would be present in the same sample.

USC UNIVERSIDADE DE SANTIAGO DE COMPOSTELA

6. CONCLUSIONS

USC
UNIVERSIDADE DE SANTIAGO DE COMPOSTELA

1. The molecular chaperone, Fe(III)-TMPyP, neither had effect on the survival nor the pathology of TgVole mice inoculated with a vole adapted-CWD strain after a chronic treatment.

2. A chronic treatment with Fe(III)-TMPyP reduced the accumulation of PrP^{Sc} in the brain of mice inoculated with a vole adapted-CWD strain.

3. A preliminary kinetic evaluation of Fe(III)-TMPyP showed that the tetrapyrrole cannot diffuse throughout the brain parenchyma.

4. Given the poor penetrance of Fe(III)-TMPyP, the reduction in the accumulation of PrP^{Sc} might be due to a local effect in the site of administration.

5. The conformational antibody, scFv-G1, neither had effect on the survival nor the pathology of TgVole mice inoculated with a vole adapted-CWD strain after a chronic treatment.

6. The prophylactic administration of the recombinant PrP amyloid, termed theraloid, had no effect on the survival of prion infected mice.

7. Animals treated with the theraloid presented distinct histopathological features, indicating that the theraloid was propagating.

8. The theraloid resulted infectious in TgVole mice, triggering a prion disease in those animals that were solely inoculated with the amyloid.

9. Mice inoculated with the theraloid accumulated and propagated two different prion strains.

USC UNIVERSIDADE DE SANTIAGO DE COMPOSTELA

10. The amyloid was serially transmitted to TgVole mice, indicating that the recombinant PrP amyloid was a *bona fide* prion.
11. The biological and biochemical properties of the amyloid were maintained after serial transmission.
12. Multiple conformers have been spontaneously generated by PMSA in the presence of three different cofactors.
13. Biochemical and biophysical analyses determined that the conformers present different structural properties.
14. Mass spectrometry-based analysis determined that the recombinant conformers presented structural differences in comparison with brain-derived prions.
15. Inoculation of the conformers in TgVole mice demonstrated that they consist of *bona fide* prions.
16. The biological and biochemical features of the conformers after serial transmission suggest that more than one strain emerged under the same conditions of propagation.
17. ssNMR analysis indicates that the analyzed conformers are structurally different.
18. ssNMR analysis suggests that a mixture of conformers would be present in the same sample.

USC UNIVERSIDADE DE SANTIAGO DE COMPOSTELA

7. REFERENCES

1. Hartl, F. U. Protein Misfolding Diseases. *Annu. Rev. Biochem* **86**, (2017).
2. Parchi, P. *et al.* Classification of Sporadic Creutzfeldt-Jakob Disease Based on Molecular and Phenotypic Analysis of 300 Subjects. *American Neurological Association* **46**, 224–233 (1999).
3. Parchi, P. & Saverioni, D. Molecular pathology, classification, and diagnosis of sporadic human prion disease variants. *Folia Neuropathol* **50**, 20–45 (2012).
4. Raymond, G. J. *et al.* Antisense oligonucleotides extend survival of prion-infected mice. *JCI Insight* **4**, (2019).
5. Watson, N. *et al.* The importance of ongoing international surveillance for Creutzfeldt–Jakob disease. *Nat Rev Neurol* **17**, 362 (2021).
6. Will, R. G. & Ironside, J. W. Sporadic and infectious human prion diseases. *Cold Spring Harb Perspect Med* **7**, 1–22 (2017).
7. Centro Nacional de Epidemiología, I. de S. C. III. Vigilancia Epidemiológica de las Encefalopatías Espongiformes Transmisibles Humanas. https://www.isciii.es/QueHacemos/Servicios/VigilanciaSaludPublicaRENAVE/EnfermedadesTransmisibles/Documents/archivos%20A-Z/EETH/informe%20RNEETH_2021.pdf (2021).
8. Zerr, I. & Parchi, P. Sporadic Creutzfeldt–Jakob disease. in *Handbook of Clinical Neurology* vol. 153 155–174 (Elsevier B.V., 2018).
9. Capellari, S., Strammiello, R., Saverioni, D., Kretzschmar, H. & Parchi, P. Genetic Creutzfeldt-Jakob disease and fatal familial insomnia: insights into phenotypic variability and disease pathogenesis. *Acta Neuropathol* **121**, 21–37 (2011).
10. Gambetti, P. *et al.* A novel human disease with abnormal prion protein sensitive to protease. *Ann Neurol* **63**, 697–708 (2008).

USC UNIVERSIDADE DE SANTIAGO DE COMPOSTELA

11. Zou, W. *et al.* Variably Protease-Sensitive Prionopathy: A New Sporadic Disease of the Prion Protein. *Ann Neurol* **68**, 162–172 (2010).

12. Notari, S., Appleby, B. S. & Gambetti, P. Variably protease-sensitive prionopathy. in *Handbook of Clinical Neurology* vol. 153 175–190 (Elsevier B.V., 2018).

13. Kim, M. O., Takada, L. T., Wong, K., Forner, S. A. & Geschwind, M. D. Genetic PrP Prion Diseases. *Cold Spring Harb Perspect Biol* **10**, (2018).

14. Takada, L. T. *et al.* Genetic prion disease: Experience of a rapidly progressive dementia center in the United States and a review of the literature. *American Journal of Medical Genetics, Part B: Neuropsychiatric Genetics* vol. 174 36–69 Preprint at https://doi.org/10.1002/ajmg.b.32505 (2017).

15. Minikel, E. V. *et al.* Quantifying prion disease penetrance using large population control cohorts. *Sci Transl Med* **8**, (2016).

16. Hsiao, K. *et al.* Mutation of the prion protein in Libyan Jews with Creutzfeldt-Jakob disease. *N Engl J Med* **324**, 1091–1097 (1991).

17. Lee, H. S. *et al.* Ancestral origins and worldwide distribution of the PRNP 200K mutation causing familial Creutzfeldt-Jakob disease. *Am J Hum Genet* **64**, 1063–1070 (1999).

18. Mitrová, E. & Belay, G. Creutzfeldt-Jakob disease with E200K mutation in Slovakia: characterization and development. *Acta Virol* **46**, 31–39 (2002).

19. Ladogana, A. *et al.* High incidence of genetic human transmissible spongiform encephalopathies in Italy. *Neurology* **64**, 1592–1597 (2005).

20. Dlouhy, S. R. *et al.* Linkage of the Indiana kindred of Gerstmann-Sträussler-Scheinker disease to the prion protein gene. *Nat Genet* **1**, 64–67 (1992).

21. Lugaresi, E. *et al.* Fatal familial insomnia and dysautonomia with selective degeneration of thalamic nuclei. *N Engl J Med* **315**, 997–1003 (1986).

22. Montagna, P., Gambetti, P., Cortelli, P. & Lugaresi, E. Familial and sporadic fatal insomnia. *Lancet Neurology* **2**, 167–176 (2003).

23. Gajdusek, D. C. & Zigas, V. Degenerative disease of the central nervous system in New Guinea; the endemic occurrence of kuru in the native population. *N Engl J Med* **257**, 974–978 (1957).

USC UNIVERSIDADE DE SANTIAGO DE COMPOSTELA

24. Liberski, P. P. Historical overview of prion diseases: a view from afar. *Folia neuropathologica* **50**, 1–12 (2012).

25. Gajdusek, D. C., Gibbs, C. J. & Alpers, M. Experimental transmission of a Kuru-like syndrome to chimpanzees. *Nature* **209**, 794–796 (1966).

26. Gajdusek, D. C., Gibbs, C. J., Asher, D. M. & David, E. Transmission of experimental kuru to the spider monkey (Ateles geoffreyi). *Science* **162**, 693–694 (1968).

27. Wadsworth, J. D. F. *et al.* Kuru prions and sporadic Creutzfeldt-Jakob disease prions have equivalent transmission properties in transgenic and wild-type mice. *Proc Natl Acad Sci U S A* **105**, 3885–3890 (2008).

28. Will, R. G. *et al.* A new variant of Creutzfeldt-Jakob disease in the UK. *The Lancet* **347**, 921–925 (1996).

29. Bruce, M. E. *et al.* Transmissions to mice indicate that 'new variant' CJD is caused by the BSE agent. *Nature* **389**, 498–501 (1997).

30. Ritchie, D. L., Peden, A. H. & Barria, M. A. Variant cjd: Reflections a quarter of a century on. *Pathogens* **10**, (2021).

31. Duffy, P., Wolf, J., Collins, G., De Vof, A. G. & Cowen, D. Possible person-to-person transmission of Creutzfeldt-Jakob disease. *New England Journal of Medicine* **290**, 692 (1974).

32. Nevin, S., Mcmenemey, W. H., Behrman, S. & Jones, D. P. Subacute spongiform encephalopathy--a subacute form of encephalopathy attributable to vascular dysfunction (spongiform cerebral atrophy). *Brain* **83**, 519–564 (1960).

33. Gibbs, C. J. *et al.* Transmission of Creutzfeldt-Jakob disease to a chimpanzee by electrodes contaminated during neurosurgery. *J Neurol Neurosurg Psychiatry* **57**, 757–758 (1994).

34. Asher, D. M. & Gregori, L. *Human transmissible spongiform encephalopathies: historic view*. *Handbook of Clinical Neurology* vol. 153 (Elsevier B.V., 2018).

35. Gill, O. N. *et al.* Prevalence in Britain of abnormal prion protein in human appendices before and after exposure to the cattle BSE epizootic. *Acta Neuropathol* **139**, 965–976 (2020).

USC UNIVERSIDADE DE SANTIAGO DE COMPOSTELA

36. Hilton, D. A. *et al.* Prevalence of lymphoreticular prion protein accumulation in UK tissue samples. *J Pathol* **203**, 733–739 (2004).

37. Gill, N. O. *et al.* Prevalent abnormal prion protein in human appendixes after bovine spongiform encephalopathy epizootic: Large scale survey. *BMJ (Online)* **347**, (2013).

38. Morand, S., McIntyre, K. M. & Baylis, M. Domesticated animals and human infectious diseases of zoonotic origins: Domestication time matters. *Infection, Genetics and Evolution* **24**, 76–81 (2014).

39. Benestad, S. L. *et al.* Cases of scrapie with unusual features in Norway and designation of a new type, Nor98. *Vet Rec* **153**, 202–208 (2003).

40. Moore, S. J., Simmons, M., Chaplin, M. & Spiropoulos, J. Neuroanatomical distribution of abnormal prion protein in naturally occurring atypical scrapie cases in Great Britain. *Acta Neuropathol* **116**, 547–559 (2008).

41. Benestad, S. L., Arsac, J. N., Goldmann, W. & Nöremark, M. Atypical/Nor98 scrapie: properties of the agent, genetics, and epidemiology. *Vet Res* **39**, (2008).

42. Aguilar-Calvo, P., García, C., Espinosa, J. C., Andreoletti, O. & Torres, J. M. Prion and prion-like diseases in animals. *Virus Res* **207**, 82–93 (2014).

43. Houston, F. & Andréoletti, O. Animal prion diseases: the risks to human health. *Brain Pathol* **29**, 248–262 (2019).

44. Wells, G. A. *et al.* A novel progressive spongiform encephalopathy in cattle. *Vet Rec* **121**, 419–420 (1987).

45. The legacy of BSE. *New Sci* **209**, 3 (2011).

46. Wilesmith, J. W., Ryan, J. B. & Atkinson, M. J. Bovine spongiform encephalopathy: epidemiological studies on the origin. *Vet Rec* **128**, 199–203 (1991).

47. Huor, A. *et al.* The emergence of classical BSE from atypical/Nor98 scrapie. *Proc.Natl.Acad.Sci.U.S.A* **116**, 26853–26862 (2019).

48. Hill, A. F. *et al.* Molecular screening of sheep for bovine spongiform encephalopathy. *Neurosci Lett* **255**, 159–162 (1998).

49. Baron, T. *et al.* Emergence of classical BSE strain properties during serial passages of H-BSE in wild-type mice. *PLoS One* **6**, (2011).

USC UNIVERSIDADE DE SANTIAGO DE COMPOSTELA

50. Torres, J. M. *et al.* Spontaneous generation of infectious prion disease in transgenic mice. *Emerg Infect Dis* **19**, 1938–1947 (2013).

51. Colchester, A. C. F. & Colchester, N. T. H. The origin of bovine spongiform encephalopathy: the human prion disease hypothesis. *Lancet* **366**, 856–861 (2005).

52. Sigurdson, C. J. & Miller, M. W. Other animal prion diseases. *Br Med Bull* **66**, 199–212 (2003).

53. Casalone, C. *et al.* Identification of a second bovine amyloidotic spongiform encephalopathy: Molecular similarities with sporadic Creutzfeldt-Jakob disease. *Proc Natl Acad Sci U S A* **101**, 3065–3070 (2004).

54. Biacabe, A. G., Laplanche, J. L., Ryder, S. & Baron, T. Distinct molecular phenotypes in bovine prion diseases. *EMBO Rep* **5**, 110–115 (2004).

55. Béringue, V. *et al.* Isolation from cattle of a prion strain distinct from that causing bovine spongiform encephalopathy. *PLoS Pathog* **2**, 0956–0963 (2006).

56. Béringue, V. *et al.* A bovine prion acquires an epidemic bovine spongiform encephalopathy strain-like phenotype on interspecies transmission. *Journal of Neuroscience* **27**, 6965–6971 (2007).

57. Béringue, V. *et al.* Transmission of atypical bovine prions to mice transgenic for human prion protein. *Emerg Infect Dis* **14**, 1898–1901 (2008).

58. Torres, J. M. *et al.* Classical bovine spongiform encephalopathy by transmission of H-type prion in homologous prion protein context. *Emerg Infect Dis* **17**, 1636–1644 (2011).

59. Tranulis, M. A. *et al.* Chronic wasting disease in Europe: new strains on the horizon. *Acta Vet Scand* **63**, 48 (2021).

60. Miller, M. W., Williams, E. S., Hobbs, N. T. & Wolfe, L. L. Environmental sources of prion transmission in mule deer. *Emerg Infect Dis* **10**, 1003–1006 (2004).

61. Tamgüney, G. *et al.* Salivary prions in sheep and deer. *Prion* **6**, 52–61 (2012).

62. Haley, N. J., Seelig, D. M., Zabel, M. D., Telling, G. C. & Hoover, E. A. Detection of CWD prions in urine and saliva of deer by transgenic mouse bioassay. *PLoS One* **4**, (2009).

USC UNIVERSIDADE DE SANTIAGO DE COMPOSTELA

63. Pulford, B. *et al.* Detection of PrPCWD in feces from naturally exposed Rocky Mountain elk (Cervus elaphus nelsoni) using protein misfolding cyclic amplification. *J Wildl Dis* **48**, 425–434 (2012).

64. Kuznetsova, A., McKenzie, D., Banser, P., Siddique, T. & Aiken, J. M. Potential role of soil properties in the spread of CWD in western Canada. *Prion* **8**, (2014).

65. Nichols, T. A. *et al.* Detection of protease-resistant cervid prion protein in water from a CWD-endemic area. *Prion* **3**, 171–183 (2009).

66. Mathiason, C. K. *et al.* Infectious prions in the saliva and blood of deer with chronic wasting disease. *Science* **314**, 133–136 (2006).

67. DeVivo, M. T. *et al.* Endemic chronic wasting disease causes mule deer population decline in Wyoming. *PLoS One* **12**, e0186512 (2017).

68. Kurt, T. D. & Sigurdson, C. J. Cross-species transmission of CWD prions. *Prion* **10**, 83 (2016).

69. Marsh, R. F., Bessen, R. A., Lehmann, S. & Hartsough, G. R. Epidemiological and experimental studies on a new incident of transmissible mink encephalopathy. *J Gen Virol* **72 (Pt 3)**, 589–594 (1991).

70. Hartsough, G. R. & Burger, D. Encephalopathy of mink. I. Epizootiologic and clinical observations. *J Infect Dis* **115**, 387–392 (1965).

71. Babelhadj, B. *et al.* Prion Disease in Dromedary Camels, Algeria. *Emerg Infect Dis* **24**, 1029–1036 (2018).

72. *Camel prion disease: a possible emerging disease in dromedary camel populations?* www.oiebulletin.com.

73. Schneider, K., Fangerau, H., Michaelsen, B. & Raab, W. H. M. The early history of the transmissible spongiform encephalopathies exemplified by scrapie. *Brain Res Bull* **77**, 343–355 (2008).

74. Gordon, W. S. Advances in veterinary research. *Vet Rec* **58**, 516–25 (1946).

75. Liberski, P. P., Gajos, A., Sikorska, B. & Lindenbaum, S. Kuru, the First Human Prion Disease. *Viruses* **11**, (2019).

76. Klatzo, I., Gajdusek, D. C. & Zigas, V. Pathology of Kuru. *Lab Invest* **8**, 799–847 (1959).

77. Hadlow, W. J. Scrapie and kuru. *The Lancet* **274**, 289–290 (1959).

USC UNIVERSIDADE DE SANTIAGO DE COMPOSTELA

78. Gibbs, C. J. *et al.* Creutzfeldt-Jakob disease (spongiform encephalopathy): transmission to the chimpanzee. *Science* **161**, 388–389 (1968).

79. Pattison, I. H., Gordon, W. S. & Millson, G. C. Experimental Production of Scrapie in Goats. *Journal of Comparative Pathology and Therapeutics* **69**, 300-IN20 (1959).

80. Chandler, R. L. Encephalopathy in mice produced by inoculation with scrapie brain material. *Lancet* **1**, 1378–1379 (1961).

81. Pattison, I. & Sansom, B. Dialysis of the scrapie agent. *Res. vet. Sci* **5**, 340–347 (1964).

82. Pattison, I. H. & Jones, K. M. The possible nature of the transmissible agent of scrapie. *Vet Rec* **80**, 2–9 (1967).

83. Alper, T., Haig, D. A. & Clarke, M. C. The exceptionally small size of the scrapie agent. *Biochem Biophys Res Commun* **22**, 278–284 (1966).

84. Griffith, J. S. Self-replication and scrapie. *Nature* **215**, 1043–1044 (1967).

85. Crick, F. Central Dogma of Molecular Biology. *Nature* **229**, 561–564 (1970).

86. Cho, H. J. Requirement of a protein component for scrapie infectivity. *Intervirology* **14**, 213–216 (1980).

87. Prusiner, S. B. *et al.* Molecular properties, partial purification, and assay by incubation period measurements of the hamster scrapie agent. *Biochemistry* **19**, 4883–4891 (1980).

88. Bolton, D. C., Mckinley, M. P. & Prusiner, S. B. Identification of a protein that purifies with the scrapie prion. *Science* **218**, 1309–1311 (1982).

89. Prusiner, S. B. Novel Proteinaceous Infectious Particles Cause Scrapie. *Science (1979)* **216**, 136–144 (1982).

90. Staniforth, G. L. & Tuite, M. F. Fungal prions. in *Progress in Molecular Biology and Translational Science* vol. 107 417–456 (Elsevier B.V., 2012).

91. Chesebro, B. *et al.* Identification of scrapie prion protein-specific mRNA in scrapie-infected and uninfected brain. *Nature* **315**, 331–333 (1985).

92. Oesch, B. *et al.* A cellular gene encodes scrapie PrP 27-30 protein. *Cell* **40**, 735–746 (1985).

USC UNIVERSIDADE DE SANTIAGO DE COMPOSTELA

93. Hsiao, K. *et al.* Linkage of a prion protein missense variant to Gerstmann-Sträussler syndrome. *Nature* **338**, 342–345 (1989).

94. WEISSMANN, C. *et al.* PrP-deficient Mice Are Resistant to Scrapie. *Ann N Y Acad Sci* **724**, 235–240 (1994).

95. Büeler, H. *et al.* High prion and PrPSc levels but delayed onset of disease in scrapie-inoculated mice heterozygous for a disrupted PrP gene. *Mol Med* **1**, 19–30 (1994).

96. Büeler, H. *et al.* Mice devoid of PrP are resistant to scrapie. *Cell* **73**, 1339–1347 (1993).

97. Sailer, A., Büeler, H., Fischer, M., Aguzzi, A. & Weissmann, C. No propagation of prions in mice devoid of PrP. *Cell* **77**, 967–968 (1994).

98. Kocisko, D. A. *et al.* Cell-free formation of protease-resistant prion protein. *Nature* **370**, 471–474 (1994).

99. Saborio, G. P., Permanne, B. & Soto, C. Sensitive detection of pathological prion protein by cyclic amplification of protein misfolding. *Nature* **411**, 810–3 (2001).

100. Atarashi, R. *et al.* Ultrasensitive detection of scrapie prion protein using seeded conversion of recombinant prion protein. *Nat Methods* **4**, 645–650 (2007).

101. Eraña, H. *et al.* Development of a new largely scalable in vitro prion propagation method for the production of infectious recombinant prions for high resolution structural studies. *PLoS Pathog* **15**, (2019).

102. Riek, R. *et al.* NMR structure of the mouse prion protein domain PrP(121-231). *Nature* **382**, 180–182 (1996).

103. Knaus, K. J. *et al.* Crystal structure of the human prion protein reveals a mechanism for oligomerization. *Nat Struct Biol* **8**, 770–774 (2001).

104. Merz, P. A., Somerville, R. A., Wisniewski, H. M. & Iqbal, K. Abnormal fibrils from scrapie-infected brain. *Acta Neuropathol* **54**, 63–74 (1981).

105. Merz, P. A., Somerville, R. A., Wisniewski, H. M., Manuelidis, L. & Manuelidis, E. E. Scrapie-associated fibrils in Creutzfeldt-Jakob disease. *Nature* **306**, 474–476 (1983).

USC UNIVERSIDADE DE SANTIAGO DE COMPOSTELA

106. Pan, K. M. *et al.* Conversion of α-helices into β-sheets features in the formation of the scrapie prion proteins. *Proc Natl Acad Sci U S A* **90**, 10962–10966 (1993).

107. Safar, J., Roller, P. P., Gajdusek, D. C. & Gibbs, C. J. Conformational transitions, dissociation, and unfolding of scrapie amyloid (prion) protein. *Journal of Biological Chemistry* **268**, 20276–20284 (1993).

108. Wang, F., Wang, X., Yuan, C. G. & Ma, J. Generating a prion with bacterially expressed recombinant prion protein. *Science (1979)* **327**, 1132–1135 (2010).

109. Spagnolli, G., Requena, J. R. & Biasini, E. Understanding prion structure and conversion. *Prog Mol Biol Transl Sci* **175**, 19–30 (2020).

110. Kraus, A. *et al.* High-resolution structure and strain comparison of infectious mammalian prions. *Mol Cell* **81**, 4540-4551.e6 (2021).

111. Stahl, N., Borchelt, D. R., Hsiao, K. & Prusiner, S. B. Scrapie prion protein contains a phosphatidylinositol glycolipid. *Cell* **51**, 229–240 (1987).

112. Liao, A. Y. J. *et al.* Human Prion Protein cDNA : Molecular Cloning , Chromosomal Mapping , and Biological Implications. *Science (1979)* **233**, 364–367 (1986).

113. Kretzschmar, H. A. *et al.* Molecular cloning of a human prion protein cDNA. *DNA* **5**, 315–324 (1986).

114. Prusiner, S. B. Molecular biology of prion deseases. *Science (1979)* **252**, 1515–1522 (1991).

115. Martin, R., Gallet, P.-F., Rocha, D. & Petit, D. *Polymorphism of the Prion Protein in Mammals: A Phylogenetic Approach*. *Recent Patents on DNA & Gene Sequences* vol. 3 http://www.ncbi.nlm.nih. (2009).

116. Wopfner, F. *et al.* Analysis of 27 mammalian and 9 avian PrPs reveals high conservation of flexible regions of the prion protein. *J Mol Biol* **289**, 1163–1178 (1999).

117. Calzolai, L., Lysek, D. A., Pérez, D. R., Güntert, P. & Wüthrich, K. Prion protein NMR structures of chickens, turtles, and frogs. *Proc Natl Acad Sci U S A* **102**, 651–655 (2005).

118. Premzl, M. & Gamulin, V. Comparative genomic analysis of prion genes. *BMC Genomics* **8**, (2007).

USC UNIVERSIDADE DE SANTIAGO DE COMPOSTELA

119. Brown, H. R. *et al.* The mRNA encoding the scrapie agent protein is present in a variety of non-neuronal cells. *Acta Neuropathol* **80**, 1–6 (1990).

120. Bosque, P. J. *et al.* Prions in skeletal muscle. *Proc.Natl.Acad.Sci.U.S.A* **99**, 3812–3817 (2002).

121. Stahl, N. *et al.* Glycosylinositol phospholipid anchors of the scrapie and cellular prion proteins contain sialic acid. *Biochemistry* **31**, 5043–5053 (1992).

122. Vey, M. *et al.* Subcellular colocalization of the cellular and scrapie prion proteins in caveolae-like membranous domains. *Proc Natl Acad Sci U S A* **93**, 14945–14949 (1996).

123. Taylor, D. R. & Hooper, N. M. The low-density lipoprotein receptor-related protein 1 (LRP1) mediates the endocytosis of the cellular prion protein. *Biochem J* **402**, 17–23 (2007).

124. Peters, P. J. *et al.* Trafficking of prion proteins through a caveolae-mediated endosomal pathway. *J Cell Biol* **162**, 703–717 (2003).

125. Sarnataro, D. *et al.* PrP(C) association with lipid rafts in the early secretory pathway stabilizes its cellular conformation. *Mol Biol Cell* **15**, 4031–4042 (2004).

126. Sunyach, C. *et al.* The mechanism of internalization of glycosylphosphatidylinositol-anchored prion protein. *EMBO J* **22**, 3591–3601 (2003).

127. Endres, K., Mitteregger, G., Kojro, E., Kretzschmar, H. & Fahrenholz, F. Influence of ADAM10 on prion protein processing and scrapie infectiosity in vivo. *Neurobiol Dis* **36**, 233–241 (2009).

128. Lewis, V. *et al.* Prion protein 'gamma-cleavage': characterizing a novel endoproteolytic processing event. *Cell Mol Life Sci* **73**, 667–683 (2016).

129. Linsenmeier, L. *et al*. Diverse functions of the prion protein - Does proteolytic processing hold the key? *Biochim Biophys Acta Mol Cell Res* **1864**, 2128–2137 (2017).

130. Büeler, H. *et al.* Normal development and behaviour of mice lacking the neuronal cell-surface PrP protein. *Nature* **356**, 577–582 (1992).

USC UNIVERSIDADE DE SANTIAGO DE COMPOSTELA

131. Manson, J. C. *et al.* 129/Ola mice carrying a null mutation in PrP that abolishes mRNA production are developmentally normal. *Mol Neurobiol* **8**, 121–127 (1994).

132. Benestad, S. L., Austbø, L., Tranulis, M. A., Espenes, A. & Olsaker, I. Healthy goats naturally devoid of prion protein. *Vet Res* **43**, (2012).

133. Salvesen, Ø. *et al.* Goats naturally devoid of PrPC are resistant to scrapie. *Vet Res* **51**, (2020).

134. Walter, E. D., Stevens, D. J., Visconte, M. P. & Millhauser, G. L. The prion protein is a combined zinc and copper binding protein: Zn 2+ alters the distribution of Cu2+ coordination modes. *J Am Chem Soc* **129**, 15440–15441 (2007).

135. Brown, D. R. *et al.* The cellular prion protein binds copper in vivo. *Nature 1997 390:6661* **390**, 684–687 (1997).

136. Castle, A. R. & Gill, A. C. Physiological Functions of the Cellular Prion Protein. *Front Mol Biosci* **4**, 1–25 (2017).

137. Watt, N. T., Routledge, M. N., Wild, C. P. & Hooper, N. M. Cellular prion protein protects against reactive-oxygen-species-induced DNA damage. *Free Radic Biol Med* **43**, 959–967 (2007).

138. Singh, A. *et al.* Prion protein regulates iron transport by functioning as a ferrireductase. *J Alzheimers Dis* **35**, 541–552 (2013).

139. Singh, A. *et al.* Prion protein (PrP) knock-out mice show altered iron metabolism: a functional role for PrP in iron uptake and transport. *PLoS One* **4**, (2009).

140. Bremer, J. *et al.* Axonal prion protein is required for peripheral myelin maintenance. *Nat Neurosci* **13**, 310–318 (2010).

141. Wulf, M., Senatore, A. & Aguzzi, A. The biological function of the cellular prion protein : an update. *BMC Biol* **15**, 1–13 (2017).

142. Collinge, J. *et al.* Prion protein is necessary for normal synaptic function. *Nature* **370**, 295–297 (1994).

143. Parkin, E. T. *et al.* Cellular prion protein regulates beta-secretase cleavage of the Alzheimer's amyloid precursor protein. *Proc Natl Acad Sci U S A* **104**, 11062–11067 (2007).

USC UNIVERSIDADE DE SANTIAGO DE COMPOSTELA

144. Whitehouse, I. J., Jackson, C., Turner, A. J. & Hooper, N. M. Prion protein is reduced in aging and in sporadic but not in familial Alzheimer's disease. *J Alzheimers Dis* **22**, 1023–1031 (2010).

145. Whitehouse, I. J. *et al.* Ablation of Prion Protein in Wild Type Human Amyloid Precursor Protein (APP) Transgenic Mice Does Not Alter The Proteolysis of APP, Levels of Amyloid-β or Pathologic Phenotype. *PLoS One* **11**, (2016).

146. Laurén, J., Gimbel, D. A., Nygaard, H. B., Gilbert, J. W. & Strittmatter, S. M. Cellular prion protein mediates impairment of synaptic plasticity by amyloid-beta oligomers. *Nature* **457**, 1128–1132 (2009).

147. Chen, S., Yadav, S. P. & Surewicz, W. K. Interaction between human prion protein and amyloid-beta (Abeta) oligomers: role OF N-terminal residues. *J Biol Chem* **285**, 26377–26383 (2010).

148. Chen, R. J., Chang, W. W., Lin, Y. C., Cheng, P. L. & Chen, Y. R. Alzheimer's amyloid-β oligomers rescue cellular prion protein induced tau reduction via the Fyn pathway. *ACS Chem Neurosci* **4**, 1287–1296 (2013).

149. Ferreira, D. G. *et al.* α-synuclein interacts with PrPC to induce cognitive impairment through mGluR5 and NMDAR2B. *Nature Neuroscience 2017 20:11* **20**, 1569–1579 (2017).

150. Aulić, S. *et al.* α-Synuclein Amyloids Hijack Prion Protein to Gain Cell Entry, Facilitate Cell-to-Cell Spreading and Block Prion Replication. *Scientific Reports 2017 7:1* **7**, 1–12 (2017).

151. Collins, S., McLean, C. A. & Masters, C. L. Gerstmann-Sträussler-Scheinker syndrome,fatal familial insomnia, and kuru: a review of these less common human transmissible spongiform encephalopathies. *J Clin Neurosci* **8**, 387–397 (2001).

152. Tobler, I., Deboer, T. & Fischer, M. Sleep and sleep regulation in normal and prion protein-deficient mice. *J Neurosci* **17**, 1869–1879 (1997).

153. Tobler, I. *et al.* Altered circadian activity rhythms and sleep in mice devoid of prion protein. *Nature* **380**, 639–642 (1996).

154. Brown, D. R., Nicholas, R. S. J. & Canevari, L. Lack of prion protein expression results in a neuronal phenotype sensitive to stress. *J Neurosci Res* **67**, 211–224 (2002).

USC UNIVERSIDADE DE SANTIAGO DE COMPOSTELA

155. Cagampang, F. R. A. *et al.* Circadian regulation of prion protein messenger RNA in the rat forebrain: a widespread and synchronous rhythm. *Neuroscience* **91**, 1201–1204 (1999).

156. Black, S. A. G., Stys, P. K., Zamponi, G. W. & Tsutsui, S. Cellular prion protein and NMDA receptor modulation: Protecting against excitotoxicity. *Front Cell Dev Biol* **2**, (2014).

157. Khosravani, H. *et al.* Prion protein attenuates excitotoxicity by inhibiting NMDA receptors. *J Cell Biol* **181**, 551–555 (2008).

158. Shyu, W. C. *et al.* Overexpression of PrPC by adenovirus-mediated gene targeting reduces ischemic injury in a stroke rat model. *J Neurosci* **25**, 8967–8977 (2005).

159. James Haddon, D. *et al.* Prion protein expression and release by mast cells after activation. *J Infect Dis* **200**, 827–831 (2009).

160. Gadotti, V. M. & Zamponi, G. W. Cellular prion protein protects from inflammatory and neuropathic pain. *Mol Pain* **7**, (2011).

161. Manni, G. *et al.* The cellular prion protein beyond prion diseases. *Swiss Medical Weekly 2020 :17* **150**, w20222 (2020).

162. Li, Q. Q. *et al.* Cellular prion protein promotes glucose uptake through the Fyn-HIF-2α-Glut1 pathway to support colorectal cancer cell survival. *Cancer Sci* **102**, 400–406 (2011).

163. Liang, J. *et al.* Inhibition of PI3K/Akt partially leads to the inhibition of PrPC-induced drug resistance in gastric cancer cells. *FEBS J* **276**, 685–694 (2009).

164. Du, J. *et al.* Overexpression and significance of prion protein in gastric cancer and multidrug-resistant gastric carcinoma cell line SGC7901/ADR. *Int J Cancer* **113**, 213–220 (2005).

165. Pan, Y. *et al.* Cellular prion protein promotes invasion and metastasis of gastric cancer. *The FASEB Journal* **20**, 1886–1888 (2006).

166. Wiegmans, A. P. *et al.* Secreted cellular prion protein binds doxorubicin and correlates with anthracycline resistance in breast cancer. *JCI Insight* **4**, (2019).

167. Prusiner, S. B. *et al.* Scrapie prions aggregate to form amyloid-like birefringent rods. *Cell* **35**, 349–358 (1983).

USC UNIVERSIDADE DE SANTIAGO DE COMPOSTELA

168. Sim, V. L. & Caughey, B. Ultrastructures and strain comparison of under-glycosylated scrapie prion fibrils. *Neurobiol Aging* **30**, 2031–2042 (2009).

169. Wille, H. *et al.* Natural and synthetic prion structure from X-ray fiber diffraction. *Proc Natl Acad Sci U S A* **106**, 16990–16995 (2009).

170. Caughey, B. W. *et al.* Secondary Structure Analysis of the Scrapie-Associated Protein PrP 27–30 in Water by Infrared Spectroscopy. *Biochemistry* **30**, 7672–7680 (1991).

171. Baron, G. S. *et al.* Effect of glycans and the glycophosphatidylinositol anchor on strain dependent conformations of scrapie prion protein: Improved purifications and infrared spectra. *Biochemistry* **50**, 4479–4490 (2011).

172. Cobb, N. J., Sönnichsen, F. D., Mchaourab, H. & Surewicz, W. K. Molecular architecture of human prion protein amyloid: A parallel, in-register β-structure. *Proc Natl Acad Sci U S A* **104**, 18946–18951 (2007).

173. Nguyen, J. T. *et al.* X-ray Diffraction of Scrapie Prion Rods and PrP Peptides. *J Mol Biol* **252**, 412–422 (1995).

174. Requena, J. R. & Wille, H. *The Structure of the Infectious Prion Protein and Its Propagation*. *Progress in Molecular Biology and Translational Science* vol. 150 (Elsevier Inc., 2017).

175. Siemer, A. B., Ritter, C., Ernst, M., Riek, R. & Meier, B. H. High-resolution solid-state NMR spectroscopy of the prion protein HET-s in its amyloid conformation. *Angewandte Chemie - International Edition* **44**, 2441–2444 (2005).

176. Van Melckebeke, H. *et al.* Atomic-resolution three-dimensional structure of HET-s(218-289) amyloid fibrils by solid-state nmr spectroscopy. *J Am Chem Soc* **132**, 13765–13775 (2010).

177. Wegmann, S., Miesbauer, M., Winklhofer, K. F., Tatzelt, J. & Muller, D. J. Observing fibrillar assemblies on scrapie-infected cells. *Pflugers Arch* **456**, 83–93 (2008).

178. Piro, J. R. *et al.* Seeding specificity and ultrastructural characteristics of infectious recombinant prions. *Biochemistry* **50**, 7111–7116 (2011).

179. Sajnani, G., Pastrana, M. A., Dynin, I., Onisko, B. & Requena, J. R. Scrapie prion protein structural constraints obtained by limited proteolysis and mass spectrometry. *J Mol Biol* **382**, 88–98 (2008).

USC UNIVERSIDADE DE SANTIAGO DE COMPOSTELA

180. Vázquez-Fernández, E. *et al.* Structural Organization of Mammalian Prions as Probed by Limited Proteolysis. *PLoS One* **7**, 1–8 (2012).

181. Zou, W. Q. *et al.* Identification of Novel Proteinase K-resistant C-terminal Fragments of PrP in Creutzfeldt-Jakob Disease. *Journal of Biological Chemistry* **278**, 40429–40436 (2003).

182. Kocisko, D. A., Lansbury, P. T. & Caughey, B. Partial Unfolding and Refolding of Scrapie-Associated Prion Protein: Evidence for a Critical 16-kDa C-Terminal Domain. *Biochemistry* **35**, 13434–13442 (1996).

183. Zanusso, G. *et al.* Identification of distinct N-terminal truncated forms of prion protein in different Creutzfeldt-Jakob disease subtypes. *Journal of Biological Chemistry* **279**, 38936–38942 (2004).

184. Silva, C. J., Vázquez-Fernández, E., Onisko, B. & Requena, J. R. Proteinase K and the structure of PrPSc: The good, the bad and the ugly. *Virus Res* (2015) doi:10.1016/j.virusres.2015.03.008.

185. Lu, X., Wintrode, P. L. & Surewicz, W. K. Beta-sheet core of human prion protein amyloid fibrils as determined by hydrogen/deuterium exchange. *Proc Natl Acad Sci U S A* **104**, 1510–5 (2007).

186. Smirnovas, V. *et al.* Distinct Structures of Scrapie Prion Protein (PrPSc)-seeded Versus Spontaneous Recombinant Prion Protein Fibrils Revealed by Hydrogen/Deuterium Exchange. *J Biol Chem* **284**, 24233 (2009).

187. Lu, J. X. *et al.* XMolecular structure of β-amyloid fibrils in alzheimer's disease brain tissue. *Cell* **154**, 1257 (2013).

188. Paravastu, A. K., Leapman, R. D., Yau, W. M. & Tycko, R. Molecular structural basis for polymorphism in Alzheimer's β-amyloid fibrils. *Proc Natl Acad Sci U S A* **105**, 18349–18354 (2008).

189. Martín-pastor, M., Codeseira, Y. B., Spagnolli, G. & Eraña, H. Solid state NMR reveals a parallel in register architecture for an infectious recombinant prion. *bioRxiv* (2021).

190. Manka, S. W. *et al.* 2.7 Å cryo-EM structure of ex vivo RML prion fibrils. *Nat Commun* **13**, (2022).

191. Vázquez-Fernández, E. *et al.* The Structural Architecture of an Infectious Mammalian Prion Using Electron Cryomicroscopy. *PLoS Pathog* **12**, 1–21 (2016).

USC UNIVERSIDADE DE SANTIAGO DE COMPOSTELA

192. Kraus, A. *et al.* Structure of an infectious mammalian prion. *bioRxiv* (2021) doi:10.1101/2021.02.14.431014.

193. Manka, S. W. *et al.* A structural basis for prion strain diversity. *Nat Chem Biol* (2023) doi:10.1038/s41589-022-01229-7.

194. Hoyt, F. *et al.* Cryo-EM structure of anchorless RML prion reveals variations in shared motifs between distinct strains. *Nat Commun* **13**, (2022).

195. Kajava, A. V. & Steven, A. C. β-Rolls, β-Helices, and Other β-Solenoid Proteins. *Advances in Protein Chemistry* vol. 73 55–96 Preprint at https://doi.org/10.1016/S0065-3233(06)73003-0 (2006).

196. Spagnolli, G. *et al.* Full atomistic model of prion structure and conversion. *PLoS Pathog* **15**, e1007864 (2019).

197. Pettersen, E. F. *et al.* UCSF ChimeraX: Structure visualization for researchers, educators, and developers. *Protein Sci* **30**, 70–82 (2021).

198. Margittai, M. & Langen, R. Fibrils with parallel in-register structure constitute a major class of amyloid fibrils: Molecular insights from electron paramagnetic resonance spectroscopy. *Q Rev Biophys* **41**, 265–297 (2008).

199. Groveman, B. R. *et al.* Parallel in-register intermolecular β-sheet architectures for prion-seeded prion protein (PrP) amyloids. *Journal of Biological Chemistry* **289**, 24129–24142 (2014).

200. Gallagher-Jones, M. *et al.* Sub-ångström cryo-EM structure of a prion protofibril reveals a polar clasp. *Nat Struct Mol Biol* **25**, 131–134 (2018).

201. Li, Q., Jaroniec, C. P. & Surewicz, W. K. Cryo-EM structure of disease-related prion fibrils provides insights into seeding barriers. *Nature Structural & Molecular Biology 2022 29:10* **29**, 962–965 (2022).

202. Wang, L. Q. *et al.* Genetic prion disease–related mutation E196K displays a novel amyloid fibril structure revealed by cryo-EM. *Sci Adv* **7**, (2021).

203. Glynn, C. *et al.* Cryo-EM structure of a human prion fibril with a hydrophobic, protease-resistant core. *Nat Struct Mol Biol* **27**, 417–423 (2020).

204. Artikis, E., Kraus, A. & Caughey, B. Structural biology of ex vivo mammalian prions. *Journal of Biological Chemistry* **298**, (2022).

205. Hoyt, F. *et al.* Cryo-EM of prion strains from the same genotype of host identifies conformational determinants. *PLoS Pathog* **18**, e1010947 (2022).

USC UNIVERSIDADE DE SANTIAGO DE COMPOSTELA

206. Brandner, S. *et al.* Normal host prion protein (PrPC) is required for scrapie spread within the central nervous system. *Proc Natl Acad Sci U S A* **93**, 13148–13151 (1996).

207. Mallucci, G. *et al.* Depleting neuronal PrP in prion infection prevents disease and reverses spongiosis. *Science* **302**, 871–874 (2003).

208. Sandberg, M. K., Al-Doujaily, H., Sharps, B., Clarke, A. R. & Collinge, J. Prion propagation and toxicity in vivo occur in two distinct mechanistic phases. *Nature* **470**, 540–542 (2011).

209. Sandberg, M. K. *et al.* Prion neuropathology follows the accumulation of alternate prion protein isoforms after infective titre has peaked. *Nat Commun* **5**, (2014).

210. Benilova, I. *et al.* Highly infectious prions are not directly neurotoxic. *Proc Natl Acad Sci U S A* **117**, 23815–23822 (2020).

211. Biasini, E., Turnbaugh, J. A., Unterberger, U. & Harris, D. A. Prion protein at the crossroads of physiology and disease. *Trends in Neurosciences* vol. 35 92–103 Preprint at https://doi.org/10.1016/j.tins.2011.10.002 (2012).

212. Otero, A. *et al.* Prion-Associated Neurodegeneration Causes Both Endoplasmic Reticulum Stress and Proteasome Impairment in a Murine Model of Spontaneous Disease. *Int J Mol Sci* **22**, 1–21 (2021).

213. McKinnon, C. *et al.* Prion-mediated neurodegeneration is associated with early impairment of the ubiquitin–proteasome system. *Acta Neuropathol* **131**, 411–425 (2016).

214. Ironside, J. W., McCardle, L., Hayward, P. A. R. & Bell, J. E. Ubiquitin immunocytochemistry in human spongiform encephalopathies. *Neuropathol Appl Neurobiol* **19**, 134–140 (1993).

215. Aguzzi, A., Lakkaraju, A. K. K. & Frontzek, K. Toward Therapy of Human Prion Diseases. *Annu Rev Pharmacol Toxicol* **58**, annurev-pharmtox-010617-052745 (2018).

216. Zattoni, M. & Legname, G. Tackling prion diseases: a review of the patent landscape. *Expert Opin Ther Pat* **31**, 1097–1115 (2021).

217. Astolfi, A., Spagnolli, G., Biasini, E. & Barreca, M. L. The Compelling Demand for an Effective PrPC-Directed Therapy against Prion Diseases. *ACS Med Chem Lett* **11**, 2063–2067 (2020).

USC UNIVERSIDADE DE SANTIAGO DE COMPOSTELA

218. Zafar, S., Noor, A. & Zerr, I. Therapies for prion diseases. *Handb Clin Neurol* **165**, 47–58 (2019).

219. Vallabh, S. M., Minikel, E. V., Schreiber, S. L. & Lander, E. S. Towards a treatment for genetic prion disease: trials and biomarkers. *Lancet Neurol* **19**, 361–368 (2020).

220. Ma, Y. & Ma, J. Immunotherapy against Prion Disease. *Pathogens* **9**, (2020).

221. Terzano, M. G., Montanari, E., Calzetti, S., Mancia, D. & Lechi, A. The effect of amantadine on arousal and EEG patterns in Creutzfeldt-Jakob disease. *Arch Neurol* **40**, 555–559 (1983).

222. Otto, M. *et al.* Efficacy of flupirtine on cognitive function in patients with CJD: A double-blind study. *Neurology* **62**, 714–718 (2004).

223. Haïk, S. *et al.* Doxycycline in Creutzfeldt-Jakob disease: a phase 2, randomised, double-blind, placebo-controlled trial. *Lancet Neurol* **13**, 150–158 (2014).

224. Collinge, J. *et al.* Safety and efficacy of quinacrine in human prion disease (PRION-1 study): a patient-preference trial. *Lancet Neurol* **8**, 334–344 (2009).

225. Geschwind, M. D. *et al.* Quinacrine treatment trial for sporadic creutzfeldt-Jakob disease. *Neurology* **81**, 2015–2023 (2013).

226. Haïk, S. *et al.* Compassionate use of quinacrine in Creutzfeldt-Jakob disease fails to show significant effects. *Neurology* **63**, 2413–2415 (2004).

227. Varges, D. *et al.* Doxycycline in early CJD: a double-blinded randomised phase II and observational study. *J Neurol Neurosurg Psychiatry* **88**, 119–125 (2017).

228. Mead, S. *et al.* Prion protein monoclonal antibody (PRN100) therapy for Creutzfeldt–Jakob disease: evaluation of a first-in-human treatment programme. *Lancet Neurol* **21**, 342–354 (2022).

229. Colini Baldeschi, A., Vanni, S., Zattoni, M. & Legname, G. Novel regulators of PrPC expression as potential therapeutic targets in prion diseases. *Expert Opin Ther Targets* **24**, 759–776 (2020).

230. Fire, A. *et al.* Potent and specific genetic interference by double-stranded RNA in Caenorhabditis elegans. *Nature* **391**, 806–811 (1998).

USC UNIVERSIDADE DE SANTIAGO DE COMPOSTELA

231. Tilly, G., Chapuis, J., Vilette, D., Laude, H. & Vilotte, J. L. Efficient and specific down-regulation of prion protein expression by RNAi. *Biochem Biophys Res Commun* **305**, 548–551 (2003).

232. Lehmann, S. *et al.* Systemic delivery of siRNA down regulates brain prion protein and ameliorates neuropathology in prion disorder. *PLoS One* **9**, (2014).

233. Kumar, P. *et al.* Transvascular delivery of small interfering RNA to the central nervous system. *Nature* **448**, 39–43 (2007).

234. Pulford, B. *et al.* Liposome-siRNA-peptide complexes cross the blood-brain barrier and significantly decrease PrP on neuronal cells and PrP in infected cell cultures. *PLoS One* **5**, (2010).

235. Bender, H. *et al.* PrPC knockdown by liposome-siRNA-peptide complexes (LSPCs) prolongs survival and normal behavior of prion-infected mice immunotolerant to treatment. *PLoS One* **14**, (2019).

236. Ahn, M. *et al.* Convection-Enhanced Delivery of AAV2-PrPshRNA in Prion-Infected Mice. *PLoS One* **9**, e98496 (2014).

237. Tabrizi, S. J. *et al.* Targeting Huntingtin Expression in Patients with Huntington's Disease. *New England Journal of Medicine* **380**, 2307–2316 (2019).

238. Stein, C. A., Subasinghe, C., Shinozuka, K. & Cohen, J. S. Physicochemical properties of phosphorothioate oligodeoxynucleotides. *Nucleic Acids Res* **16**, 3209–3221 (1988).

239. Mummery, C. J. *et al.* Results of the first-in-human, randomized, double-blind, placebo-controlled phase 1b study of lumbar intrathecal bolus administrations of antisense oligonucleotide (ISIS 814907; BIIB080) targeting tau mRNA in patients with mild Alzheimer's disease. *Alzheimer's & Dementia* **17**, e051871 (2021).

240. A Study to Assess if BIIB080 Can Change Clinical Dementia Rating-Sum of Boxes Scores, and BIIB080 Safety and Tolerability When Injected Into the Cerebrospinal Fluid of Participants With Mild Cognitive Impairment Due to Alzheimer's Disease (AD) or Mild AD Dementia Between 50 to 80 Years of Age - Full Text View - ClinicalTrials.gov. https://clinicaltrials.gov/ct2/show/NCT05399888.

USC UNIVERSIDADE DE SANTIAGO DE COMPOSTELA

241. Finkel, R. S. *et al.* Treatment of infantile-onset spinal muscular atrophy with nusinersen: a phase 2, open-label, dose-escalation study. *Lancet* **388**, 3017–3026 (2016).

242. FDA approves first drug for spinal muscular atrophy | FDA. https://www.fda.gov/news-events/press-announcements/fda-approves-first-drug-spinal-muscular-atrophy.

243. Friberg, K. N. *et al.* Intracerebral infusion of antisense oligonucleotides into prion-infected mice. *Mol Ther Nucleic Acids* **1**, 1–12 (2012).

244. Minikel, E. V. *et al.* Prion protein lowering is a disease-modifying therapy across prion disease stages, strains, and endpoints. *Nucleic Acids Res.* **48**, 10615–10631 (2020).

245. Bertsch, U. *et al.* Systematic Identification of Antiprion Drugs by High-Throughput Screening Based on Scanning for Intensely Fluorescent Targets. *J Virol* **79**, 7785–7791 (2005).

246. Giles K, Olson SH & Prusiner SB. Developing Therapeutics for PrP Prion Diseases. *Cold Spring Harb Perspect Med* **7**, 4 (2017).

247. Kocisko, D. A. & Caughey, B. Searching for anti-prion compounds: cell-based high-throughput in vitro assays and animal testing strategies. *Methods Enzymol* **412**, 223–234 (2006).

248. Breydo, L., Bocharova, O. V. & Baskakov, I. V. Semiautomated cell-free conversion of prion protein: Applications for high-throughput screening of potential antiprion drugs. *Anal Biochem* **339**, 165–173 (2005).

249. Barreca, M., Iraci, N., Biggi, S., Cecchetti, V. & Biasini, E. Pharmacological Agents Targeting the Cellular Prion Protein. *Pathogens* **7**, 27 (2018).

250. Kamatari, Y. O., Hayano, Y., Yamaguchi, K. I., Hosokawa-Muto, J. & Kuwata, K. Characterizing antiprion compounds based on their binding properties to prion proteins: Implications as medical chaperones. *Protein Science* **22**, 22–34 (2013).

251. Kocisko, D. A. *et al.* A porphyrin increases survival time of mice after intracerebral prion infection. *Antimicrob Agents Chemother* **50**, 759–761 (2006).

252. Rajora, M. A., Lou, J. W. H. & Zheng, G. Advancing porphyrin's biomedical utility: Via supramolecular chemistry. *Chemical Society Reviews* vol. 46 6433–6469 Preprint at https://doi.org/10.1039/c7cs00525c (2017).

USC UNIVERSIDADE DE SANTIAGO DE COMPOSTELA

253. Whittle, I. R., Knight, R. S. G. & Will, R. G. Unsuccessful intraventricular pentosan polysulphate treatment of variant Creutzfeldt-Jakob disease. *Acta Neurochir (Wien)* **148**, 677–678 (2006).

254. Bone, I., Belton, L., Walker, A. S. & Darbyshire, J. Intraventricular pentosan polysulphate in human prion diseases: An observational study in the UK. *Eur J Neurol* **15**, 458–464 (2008).

255. Todd, N. V *et al.* Cerebroventricular infusion of pentosan polysulphate in human variant Creutzfeldt – Jakob disease. *Journal of Infection* **50**, 394–396 (2005).

256. Tsuboi, Y., Doh-Ura, K. & Yamada, T. Continuous intraventricular infusion of pentosan polysulfate: Clinical trial against prion diseases: Symposium: Prion diseases - Updated. in *Neuropathology* vol. 29 632–636 (2009).

257. Familiar Fatal Insomnia: Preventive Treatment With Doxycycline in Subject With Disease Risk - Full Text View - ClinicalTrials.gov. https://clinicaltrials.gov/ct2/show/NCT04846335?cond=NCT04846335&draw=2&rank=1.

258. Caughey, B. & Race, R. E. Potent inhibition of scrapie-associated PrP accumulation by congo red. *J Neurochem* **59**, 768–771 (1992).

259. Margalith, I. *et al.* Polythiophenes inhibit prion propagation by stabilizing prion protein (PrP) aggregates. *J Biol Chem* **287**, 18872–18887 (2012).

260. Ingrosso, L., Ladogana, A. & Pocchiari, M. Congo Red Prolongs the Incubation Period in Scrapie-Infected Hamsters. *J Virol* **69**, 506–508 (1995).

261. Caspi, S. *et al.* The anti-prion activity of Congo red. Putative mechanism. *J Biol Chem* **273**, 3484–3489 (1998).

262. Poli, G. *et al. Evaluation of Anti-Prion Activity of Congo Red and its Derivatives in Experimentally Infected Hamsters*. *Arzneim.-Forsch./Drug Res* vol. 54 (2004).

263. Yakupova, E. I., Bobyleva, L. G., Vikhlyantsev, I. M. & Bobylev, A. G. Congo Red and amyloids: history and relationship. *Biosci Rep* **39**, (2019).

264. Sigurdson, C. J. *et al.* Prion strain discrimination using luminescent conjugated polymers. *Nat Methods* **4**, 1023–1030 (2007).

265. Herrmann, U. S. *et al.* Prion infections and anti-PrP antibodies trigger converging neurotoxic pathways. *PLoS Pathog* **11**, (2015).

USC UNIVERSIDADE DE SANTIAGO DE COMPOSTELA

266. Soto, C. *et al.* Beta-sheet breaker peptides inhibit fibrillogenesis in a rat brain model of amyloidosis: implications for Alzheimer's therapy. *Nat Med* **4**, 822–826 (1998).

267. Soto, C. *et al.* Reversion of prion protein conformational changes by synthetic β-sheet breaker peptides. *Lancet* **355**, 192–197 (2000).

268. Filesi, I., Cardinale, A., Mattei, S. & Biocca, S. Selective re-routing of prion protein to proteasomes and alteration of its vesicular secretion prevent PrP(Sc) formation. *J Neurochem* **101**, 1516–1526 (2007).

269. McNally, K. L., Ward, A. E. & Priola, S. A. Cells expressing anchorless prion protein are resistant to scrapie infection. *J Virol* **83**, 4469–4475 (2009).

270. Biggi, S. *et al.* Identification of compounds inhibiting prion replication and toxicity by removing PrPC from the cell surface. *J Neurochem* **152**, 136–150 (2020).

271. Daniel, J. A. *et al.* Phenothiazine-derived antipsychotic drugs inhibit dynamin and clathrin-mediated endocytosis. *Traffic* **16**, 635–654 (2015).

272. Stincardini, C. *et al.* An antipsychotic drug exerts anti-prion effects by altering the localization of the cellular prion protein. *PLoS One* **12**, (2017).

273. Benito-León, J. Combined quinacrine and chlorpromazine therapy in fatal familial insomnia. *Clin Neuropharmacol* **27**, 201–203 (2004).

274. Drisaldi, B. *et al.* Mutant PrP is delayed in its exit from the endoplasmic reticulum, but neither wild-type nor mutant PrP undergoes retrotranslocation prior to proteasomal degradation. *J Biol Chem* **278**, 21732–21743 (2003).

275. Fregno, I. & Molinari, M. Proteasomal and lysosomal clearance of faulty secretory proteins: ER-associated degradation (ERAD) and ER-to-lysosome-associated degradation (ERLAD) pathways. *Crit Rev Biochem Mol Biol* **54**, 153–163 (2019).

276. Spagnolli, G. *et al.* Pharmacological protein inactivation by targeting folding intermediates. *Commun Biol* **4**, (2021).

277. Shim, S. Y., Karri, S., Law, S., Schatzl, H. M. & Gilch, S. Prion infection impairs lysosomal degradation capacity by interfering with rab7 membrane attachment in neuronal cells. *Sci Rep* **6**, (2016).

USC UNIVERSIDADE DE SANTIAGO DE COMPOSTELA

278. Yao, H., Zhao, D., Khan, S. H. & Yang, L. Role of autophagy in prion protein-induced neurodegenerative diseases. *Acta Biochim Biophys Sin (Shanghai)* **45**, 494–502 (2013).

279. Doh-ura, K., Iwaki, T. & Caughey, B. Lysosomotropic agents and cysteine protease inhibitors inhibit scrapie-associated prion protein accumulation. *J Virol* **74**, 4894–4897 (2000).

280. Supattapone, S., Nguyen, H. O. B., Cohen, F. E., Prusiner, S. B. & Scott, M. R. Elimination of prions by branched polyamines and implications for therapeutics. *Proc Natl Acad Sci U S A* **96**, 14529–14534 (1999).

281. Karapetyan, Y. E. *et al.* Unique drug screening approach for prion diseases identifies tacrolimus and astemizole as antiprion agents. *Proc Natl Acad Sci U S A* **110**, 7044–7049 (2013).

282. Nakagaki, T. *et al.* FK506 reduces abnormal prion protein through the activation of autolysosomal degradation and prolongs survival in prion-infected mice. *Autophagy* **9**, 1386–1394 (2013).

283. Supattapone, S. *et al.* Branched polyamines cure prion-infected neuroblastoma cells. *J Virol* **75**, 3453–3461 (2001).

284. Collinge, J. *et al.* Transmission of fatal familial insomnia to laboratory animals. *Lancet* **346**, 569–570 (1995).

285. Lasmézas, C. I. *et al.* Transmission of the BSE agent to mice in the absence of detectable abnormal prion protein. *Science* **275**, 402–405 (1997).

286. Benilova, I. *et al.* Highly infectious prions are not directly neurotoxic. *Proc Natl Acad Sci U S A* **117**, 23815–23822 (2020).

287. Ron, D. & Walter, P. Signal integration in the endoplasmic reticulum unfolded protein response. *Nat Rev Mol Cell Biol* **8**, 519–529 (2007).

288. Bravo, R. *et al.* Endoplasmic reticulum and the unfolded protein response: dynamics and metabolic integration. *Int Rev Cell Mol Biol* **301**, 215–290 (2013).

289. Moreno, J. A. *et al.* Sustained translational repression by eIF2α-P mediates prion neurodegeneration. *Nature* **485**, 507–511 (2012).

290. Thapa, S., Abdelaziz, D. H., Abdulrahman, B. A. & Schatzl, H. M. Sephin1 Reduces Prion Infection in Prion-Infected Cells and Animal Model. *Mol Neurobiol* **57**, 2206–2219 (2020).

USC UNIVERSIDADE DE SANTIAGO DE COMPOSTELA

291. Sevigny, J. *et al.* The antibody aducanumab reduces Aβ plaques in Alzheimer's disease. *Nature* **537**, 50–56 (2016).

292. Jankovic, J. *et al.* Safety and Tolerability of Multiple Ascending Doses of PRX002/RG7935, an Anti-α-Synuclein Monoclonal Antibody, in Patients With Parkinson Disease: A Randomized Clinical Trial. *JAMA Neurol* **75**, 1206–1214 (2018).

293. Feigin, A. *et al.* Pepinemab antibody blockade of SEMA4D in early Huntington's disease: a randomized, placebo-controlled, phase 2 trial. *Nat Med* **28**, (2022).

294. Sassa, Y., Kataoka, N., Inoshima, Y. & Ishiguro, N. Anti-PrP antibodies detected at terminal stage of prion-affected mouse. *Cell Immunol* **263**, 212–218 (2010).

295. Senatore, A. *et al.* Protective anti-prion antibodies in human immunoglobulin repertoires. *EMBO Mol Med* **12**, (2020).

296. Polymenidou, M. *et al.* Humoral immune response to native eukaryotic prion protein correlates with anti-prion protection. *Proc Natl Acad Sci U S A* **101 Suppl 2**, 14670–14676 (2004).

297. Grégoire, S. *et al.* The murine B cell repertoire is severely selected against endogenous cellular prion protein. *J Immunol* **175**, 6443–6449 (2005).

298. Souan, L. *et al.* Modulation of proteinase-K resistant prion protein by prion peptide immunization. *Eur. J. Immunol.* **31**, 2338–2346 (2001).

299. Abdelaziz, D. H. *et al.* Immunization of cervidized transgenic mice with multimeric deer prion protein induces self-antibodies that antagonize chronic wasting disease infectivity in vitro. *Sci Rep* **7**, (2017).

300. Abdelaziz, D. H. *et al.* Recombinant prion protein vaccination of transgenic elk PrP mice and reindeer overcomes self-tolerance and protects mice against chronic wasting disease. *J Biol Chem* **293**, 19812–19822 (2018).

301. Bachy, V. *et al.* Mouse vaccination with dendritic cells loaded with prion protein peptides overcomes tolerance and delays scrapie. *J Gen Virol* **91**, 809–820 (2010).

302. Ishibashi, D. *et al.* Immunization with recombinant bovine but not mouse prion protein delays the onset of disease in mice inoculated with a mouse-adapted prion. *Vaccine* **25**, 985–992 (2007).

USC UNIVERSIDADE DE SANTIAGO DE COMPOSTELA

303. Magri, G. *et al.* Decrease in pathology and progression of scrapie after immunisation with synthetic prion protein peptides in hamsters. *Vaccine* **23**, 2862–2868 (2005).

304. Tal, Y. *et al.* Complete Freund's adjuvant immunization prolongs survival in experimental prion disease in mice. *J Neurosci Res* **71**, 286–290 (2003).

305. Goñi, F. *et al.* Mucosal vaccination delays or prevents prion infection via an oral route. *Neuroscience* **133**, 413–421 (2005).

306. Goñi, F. *et al.* High titers of mucosal and systemic anti-PrP antibodies abrogate oral prion infection in mucosal-vaccinated mice. *Neuroscience* **153**, 679–686 (2008).

307. Rosset, M. B. *et al.* Breaking Immune Tolerance to the Prion Protein Using Prion Protein Peptides Plus Oligodeoxynucleotide-CpG in Mice. *The Journal of Immunology* **172**, 5168–5174 (2004).

308. Sethi, S., Lipford, G., Wagner, H. & Kretzschmar, H. Postexposure prophylaxis against prion disease with a stimulator of innate immunity. *Lancet* **360**, 229–230 (2002).

309. Carlson, G. A. Postexposure prophylaxis against transmissible spongiform encephalopathies: CpG oligodeoxynucleotides in mice. *Lancet* **360**, 184 (2002).

310. Marciniuk, K. *et al.* Development of a multivalent, PrP(Sc)-specific prion vaccine through rational optimization of three disease-specific epitopes. *Vaccine* **32**, 1988–1997 (2014).

311. Taschuk, R. *et al.* Safety, specificity and immunogenicity of a PrP(Sc)-specific prion vaccine based on the YYR disease specific epitope. *Prion* **8**, (2014).

312. Taschuk, R. *et al.* Induction of PrPSc-specific systemic and mucosal immune responses in white-tailed deer with an oral vaccine for chronic wasting disease. *Prion* **11**, 368–380 (2017).

313. Wood, M. E. *et al.* Accelerated onset of chronic wasting disease in elk (Cervus canadensis) vaccinated with a PrPSc-specific vaccine and housed in a prion contaminated environment. *Vaccine* **36**, 7737–7743 (2018).

314. Kascsak, R. J. *et al.* Mouse polyclonal and monoclonal antibody to scrapie-associated fibril proteins. *J Virol* **61**, 3688–3693 (1987).

USC UNIVERSIDADE DE SANTIAGO DE COMPOSTELA

315. Polymenidou, M. *et al.* The POM Monoclonals: A Comprehensive Set of Antibodies to Non-Overlapping Prion Protein Epitopes. *PLoS One* **3**, 3872 (2008).

316. Sonati, T. *et al.* The toxicity of antiprion antibodies is mediated by the flexible tail of the prion protein. *Nature* **501**, 102–106 (2013).

317. White, A. R. *et al.* Monoclonal antibodies inhibit prion replication and delay the development of prion disease. *Nature* **422**, 80–83 (2003).

318. Klöhn, P. C. *et al.* PrP antibodies do not trigger mouse hippocampal neuron apoptosis. *Science* **335**, 52 (2012).

319. Reimann, R. R. *et al.* Differential Toxicity of Antibodies to the Prion Protein. *PLoS Pathog* **12**, (2016).

320. Song, C. H. *et al.* Effect of intraventricular infusion of anti-prion protein monoclonal antibodies on disease progression in prion-infected mice. *Journal of General Virology* **89**, 1533–1544 (2008).

321. Ericson, T., Singla, P. & Kohan, L. Intrathecal Pumps. *Phys Med Rehabil Clin N Am* **33**, 409–424 (2022).

322. Zubair, A. & De Jesus, O. Ommaya Reservoir. *Statpearls* https://pubmed.ncbi.nlm.nih.gov/32644437/ (2022) doi:10.32388/n772ha.

323. Kawasaki, Y. *et al.* Orally Administered Amyloidophilic Compound Is Effective in Prolonging the Incubation Periods of Animals Cerebrally Infected with Prion Diseases in a Prion Strain-Dependent Manner. *J Virol* **81**, 12889–12898 (2007).

324. Hannaoui, S. *et al.* Cycline efficacy on the propagation of human prions in primary cultured neurons is strain-specific. *J Infect Dis* **209**, 1144–1148 (2014).

325. Miller-Vedam, L. & Ghaemmaghami, S. Strain specificity and drug resistance in anti-prion therapy. *Curr Top Med Chem* **13**, 2397–2406 (2013).

326. Berry, D. B. *et al.* Drug resistance confounding prion therapeutics. *Proc Natl Acad Sci U S A* **110**, (2013).

327. Ghaemmaghami, S. *et al.* Continuous quinacrine treatment results in the formation of drug-resistant prions. *PLoS Pathog* **5**, (2009).

USC UNIVERSIDADE DE SANTIAGO DE COMPOSTELA

328. Burke, C. M., Mark, K. M. K., Kun, J., Beauchemin, K. S. & Supattapone, S. Emergence of prions selectively resistant to combination drug therapy. *PLoS Pathog* **16**, (2020).

329. Appleby, B. S., Connor, A. & Wang, H. Therapeutic strategies for prion disease: a practical perspective. *Curr Opin Pharmacol* **44**, 15–19 (2019).

330. Harrison, K. L. *et al.* Developing neuropalliative care for sporadic Creutzfeldt-Jakob Disease. *Prion* **16**, 23–39 (2022).

331. Bailey, B., Aranda, S., Quinn, K. & Kean, H. Creutzfeldt-Jakob disease: extending palliative care nursing knowledge. *Int J Palliat Nurs* **6**, 131–139 (2000).

332. Caughey, W. S. *et al.* Cyclic tetrapyrrole sulfonation, metals, and oligomerization in antiprion activity. *Antimicrob Agents Chemother* **51**, 3887–3894 (2007).

333. Gupta, A. N. *et al.* Pharmacological chaperone reshapes the energy landscape for folding and aggregation of the prion protein. *Nature Communications* vol. 7 (2016).

334. Caughey, W. S., Raymond, L. D., Horiuchi, M. & Caughey, B. Inhibition of protease-resistant prion protein formation by porphyrins and phthalocyanines. *Proc Natl Acad Sci U S A* **95**, 12117–12122 (1998).

335. Massignan, T. *et al.* A cationic tetrapyrrole inhibits toxic activities of the cellular prion protein. *Sci Rep* **6**, 1–14 (2016).

336. López Lorenzo, N. Evaluación De Las Propiedades Antipriónicas De Diferentes Tetrapirroles En Un Modelo Celular De Propagación De Priones. (Universidad Francisco de Vitoria, 2019).

337. Chandler, R. L. & Turfrey, B. A. Inoculation of Voles, Chinese Hamsters, Gerbils and Guinea-pigs with Scrapie Brain Material. *Res Vet Sci* **13**, 219–226 (1972).

338. Nonno, R. *et al.* Efficient transmission and characterization of Creutzfeldt-Jakob disease strains in bank voles. *PLoS Pathog* **2**, 0112–0120 (2006).

339. Agrimi, U. *et al.* Prion protein amino acid determinants of differential susceptibility and molecular feature of prion strains in mice and voles. *PLoS Pathog* **4**, (2008).

USC UNIVERSIDADE DE SANTIAGO DE COMPOSTELA

340. Pirisinu, L. *et al.* Biochemical characterization of prion strains in bank voles. *Pathogens* **2**, 446–456 (2013).

341. di Bari, M. A. *et al.* Chronic wasting disease in bank voles: characterisation of the shortest incubation time model for prion diseases. *PLoS Pathog* **9**, (2013).

342. Watts, J. C. *et al.* Evidence that bank vole PrP is a universal acceptor for prions. *PLoS Pathog* **10**, e1003990 (2014).

343. Cartoni, C. *et al.* Identification of the pathological prion protein allotypes in scrapie-infected heterozygous bank voles (Clethrionomys glareolus) by high-performance liquid chromatography-mass spectrometry. *J Chromatogr A* **1081**, 122–126 (2005).

344. Arshad, H., Bourkas, M. E. C. & Watts, J. C. The utility of bank voles for studying prion disease. *Prog Mol Biol Transl Sci* **175**, 179–211 (2020).

345. Di Bari, M. A. *et al.* Chronic Wasting Disease in Bank Voles: Characterisation of the Shortest Incubation Time Model for Prion Diseases. *PLoS Pathog* **9**, (2013).

346. Priola, S. A., Raines, A. & Caughey, W. S. Porphyrin and phthalocyanine antiscrapie compounds. *Science (1979)* **287**, 1503–1506 (2000).

347. Kimberlin, R. H. & Walker, C. A. The antiviral compound HPA-23 can prevent scrapie when administered at the time of infection. *Arch Virol* **78**, 9–18 (1983).

348. Mathiasen, J. R. & Moser, V. C. The Irwin Test and Functional Observational Battery (FOB) for Assessing the Effects of Compounds on Behavior, Physiology, and Safety Pharmacology in Rodents. *Curr Protoc Pharmacol* **83**, (2018).

349. Lefebvre-Roque, M. *et al.* Toxic effects of intracerebral PrP antibody administration during the course of BSE infection in mice. *Prion* **1**, 198–206 (2007).

350. Sisó, S., Ordóñez, M., Cordón, I., Vidal, E. & Pumarola, M. Distribution of PrP(res) in the brains of BSE-affected cows detected by active surveillance in Catalonia, Spain. *Vet Rec* **155**, 524–525 (2004).

351. Tolar, M., Abushakra, S., Hey, J. A., Porsteinsson, A. & Sabbagh, M. Aducanumab, gantenerumab, BAN2401, and ALZ-801-the first wave of

USC UNIVERSIDADE DE SANTIAGO DE COMPOSTELA

amyloid-targeting drugs for Alzheimer's disease with potential for near term approval. *Alzheimers Res Ther* **12**, (2020).

352. Henderson, R. D. *et al.* Phase 1b dose-escalation, safety, and pharmacokinetic study of IC14, a monoclonal antibody against CD14, for the treatment of amyotrophic lateral sclerosis. *Medicine* **100**, e27421 (2021).

353. Vázquez-Fernández, E. *et al.* The Structural Architecture of an Infectious Mammalian Prion Using Electron Cryomicroscopy. *PLoS Pathog* **12**, (2016).

354. Wasmer, C. *et al.* Amyloid fibrils of the HET-s(218-289) prion form a β solenoid with a triangular hydrophobic core. *Science (1979)* **319**, 1523–1526 (2008).

355. Zerr, I. Prion 2022 Conference abstracts: pushing the boundaries. *Prion* **16**, 95–253 (2022).

356. Keough, K., Greenlee, J. & Caughey, B. PRION 2019 emerging concepts. *Prion* **13**, 1–141 (2019).

357. Holger Wille, PhD | Creutzfeldt-Jakob Disease Foundation. https://cjdfoundation.org/holger-wille-phd-0.

358. Varadi, M. *et al.* AlphaFold Protein Structure Database: massively expanding the structural coverage of protein-sequence space with high-accuracy models. *Nucleic Acids Res* **50**, D439–D444 (2022).

359. Zahn, R. *et al.* NMR solution structure of the human prion protein. *Proc Natl Acad Sci U S A* **97**, 145–150 (2000).

360. Sigurdsson, E. M. *et al.* Anti-prion antibodies for prophylaxis following prion exposure in mice. *Neurosci Lett* **336**, 185–187 (2003).

361. Sadowski, M. J. *et al.* Anti-PrP Mab 6D11 suppresses PrP(Sc) replication in prion infected myeloid precursor line FDC-P1/22L and in the lymphoreticular system in vivo. *Neurobiol Dis* **34**, 267–278 (2009).

362. Petsch, B. *et al.* Biological effects and use of PrPSc- and PrP-specific antibodies generated by immunization with purified full-length native mouse prions. *J Virol* **85**, 4538–4546 (2011).

363. Uttamlal, M. & Sheila Holmes-Smith, A. The excitation wavelength dependent fluorescence of porphyrins. *Chem Phys Lett* **454**, 223–228 (2008).

USC UNIVERSIDADE DE SANTIAGO DE COMPOSTELA

364. Park, J. M., Hong, K. I., Lee, H. & Jang, W. D. Bioinspired Applications of Porphyrin Derivatives. *Acc Chem Res* **54**, 2249–2260 (2021).

365. Nicoll, A. J. *et al.* Pharmacological chaperone for the structured domain of human prion protein. *Proc Natl Acad Sci U S A* **107**, 17610–17615 (2010).

366. Masone, A. *et al.* A tetracationic porphyrin with dual anti-prion activity. *iScience* **26**, 107480 (2023).

367. Bajracharya, R., Caruso, A. C., Vella, L. J. & Nisbet, R. M. Current and Emerging Strategies for Enhancing Antibody Delivery to the Brain. *Pharmaceutics* **13**, (2021).

368. Terstappen, G. C., Meyer, A. H., Bell, R. D. & Zhang, W. Strategies for delivering therapeutics across the blood–brain barrier. *Nature Reviews Drug Discovery 2021 20:5* **20**, 362–383 (2021).

369. Carter, P. J. & Rajpal, A. Designing antibodies as therapeutics. *Cell* **185**, 2789–2805 (2022).

370. Gao, Y., Zhu, J. & Lu, H. Single domain antibody-based vectors in the delivery of biologics across the blood-brain barrier: a review. *Drug Deliv Transl Res* **11**, 1818–1828 (2021).

371. Bélanger, K. *et al.* Single-Domain Antibodies as Therapeutic and Imaging Agents for the Treatment of CNS Diseases. *Antibodies (Basel)* **8**, (2019).

372. Ruiz-López, E. & Schuhmacher, A. J. Transportation of Single-Domain Antibodies through the Blood–Brain Barrier. *Biomolecules 2021, Vol. 11, Page 1131* **11**, 1131 (2021).

373. Lindroth, K., Mastache, E. F., Roos, I., Fernández, Á. G. & Fernández, C. Understanding thymus-independent antigen-induced reduction of thymus-dependent immune responses. *Immunology* **112**, 413–419 (2004).

374. Korth, C. *et al.* Prion (PrPSc)-specific epitope defined by a monoclonal antibody. *Nature 1997 390:6655* **390**, 74–77 (1997).

375. Paramithiotis, E. *et al.* A prion protein epitope selective for the pathologically misfolded conformation. *Nat Med* **9**, 893–899 (2003).

376. Jones, M. *et al.* An antibody to the aggregated synthetic prion protein peptide (PrP106-126) selectively recognizes disease-associated prion protein (PrP) from human brain specimens. *Brain Pathol* **19**, 293–302 (2009).

USC UNIVERSIDADE DE SANTIAGO DE COMPOSTELA

377. Abbas, A. K., Lichtman, A. H. & Pillai, S. B Cell Activation and Antibody Production. in *Cellular and Molecular Immunology* 251–273 (2018).

378. Padilla, D. *et al.* Sheep and Goat BSE Propagate More Efficiently than Cattle BSE in Human PrP Transgenic Mice. *PLoS Pathog* **7**, e1001319 (2011).

379. Patel, M. M. & Patel, B. M. Crossing the Blood–Brain Barrier: Recent Advances in Drug Delivery to the Brain. *CNS Drugs 2017 31:2* **31**, 109–133 (2017).

380. Bonakdar, M., Graybill, P. M. & Davalos, R. V. A microfluidic model of the blood-brain barrier to study permeabilization by pulsed electric fields. *RSC Adv* **7**, 42811–42818 (2017).

381. Li, Q. *et al.* Application of low-intensity ultrasound by opening blood-brain barrier for enhanced brain-targeted drug delivery. *Int J Pharm* **642**, 123191 (2023).

382. Liu, J. *et al.* Label-Free Assessment of Mannitol Accumulation Following Osmotic Blood–Brain Barrier Opening Using Chemical Exchange Saturation Transfer Magnetic Resonance Imaging. *Pharmaceutics* **14**, (2022).

383. Dobson, C. M. Protein folding and misfolding. *Nature* **426**, 884–890 (2003).

384. Brunori, M., Gianni, S., Giri, R., Morrone, A. & Travaglini-Allocatelli, C. Morphogenesis of a protein: folding pathways and the energy landscape. *Biochem Soc Trans* **40**, 429–432 (2012).

385. Strodel, B. Energy Landscapes of Protein Aggregation and Conformation Switching in Intrinsically Disordered Proteins: Energy landscapes of IDPs and protein aggregation. *Journal of Molecular Biology* vol. 433 Preprint at https://doi.org/10.1016/j.jmb.2021.167182 (2021).

386. Chiti, F. & Dobson, C. M. Protein Misfolding, Amyloid Formation, and Human Disease: A Summary of Progress Over the Last Decade. *Annu. Rev. Biochem* **86**, 35.1-35.42 (2017).

387. Subedi, S., Sasidharan, S., Nag, N., Saudagar, P. & Tripathi, T. Amyloid Cross-Seeding: Mechanism, Implication, and Inhibition. *Molecules* vol. 27 Preprint at https://doi.org/10.3390/molecules27061776 (2022).

388. Wagner, J. *et al.* Medin co-aggregates with vascular amyloid-β in Alzheimer's disease. *Nature* **612**, 123–131 (2022).

USC UNIVERSIDADE DE SANTIAGO DE COMPOSTELA

389. Taylor, A. I. P. & Staniforth, R. A. General Principles Underpinning Amyloid Structure. *Front Neurosci* **16**, 817 (2022).

390. Margittai, M. & Langen, R. Template-assisted filament growth by parallel stacking of tau. *Proc Natl Acad Sci U S A* **101**, 10278–10283 (2004).

391. Benzinger, T. L. S. *et al.* Propagating structure of Alzheimer's beta-amyloid(10-35) is parallel beta-sheet with residues in exact register. *Proc Natl Acad Sci U S A* **95**, 13407–13412 (1998).

392. Der-Sarkissiant, A., Jao, C. C., Chen, J. & Langen, R. Structural Organization of α-Synuclein Fibrils Studied by Site-directed Spin Labeling. *Journal of Biological Chemistry* **278**, 37530–37535 (2003).

393. Hallinan, G. I. *et al.* Cryo-EM structures of prion protein filaments from Gerstmann–Sträussler–Scheinker disease. *Acta Neuropathol* **144**, 509–520 (2022).

394. Otzen, D. & Riek, R. Functional Amyloids. *Cold Spring Harb Perspect Biol* **11**, (2019).

395. Wang, L. Q. *et al.* Cryo-EM structure of an amyloid fibril formed by full-length human prion protein. *Nat Struct Mol Biol* **27**, 598–602 (2020).

396. Terry, C. *et al.* Structural features distinguishing infectious ex vivo mammalian prions from non-infectious fibrillar assemblies generated in vitro. *Sci Rep* **9**, (2019).

397. Jackson, W. S. *et al.* Spontaneous generation of prion infectivity in fatal familial insomnia knockin mice. *Neuron* **63**, 438–450 (2009).

398. Yang, W. *et al.* A new transgenic mouse model of Gerstmann-Sträussler-Scheinker syndrome caused by the A117V mutation of PRNP. *Journal of Neuroscience* **29**, 10072–10080 (2009).

399. Friedman-Levi, Y. *et al.* Fatal prion disease in a mouse model of genetic E200K Creutzfeldt-Jakob disease. *PLoS Pathog* **7**, (2011).

400. Makarava, N. *et al.* Genesis of mammalian prions: From non-infectious amyloid fibrils to a transmissible prion disease. *PLoS Pathog* **7**, (2011).

401. Diack, A. B. *et al.* Variably Protease-Sensitive Prionopathy, a Unique Prion Variant with Inefficient Transmission Properties - Volume 20, Number 12—December 2014 - Emerging Infectious Diseases journal - CDC. *Emerg Infect Dis* **20**, 1969–1979 (2014).

USC UNIVERSIDADE DE SANTIAGO DE COMPOSTELA

402. Notari, S. *et al.* Transmission Characteristics of Variably Protease-Sensitive Prionopathy - Volume 20, Number 12—December 2014 - Emerging Infectious Diseases journal - CDC. *Emerg Infect Dis* **20**, 2006–2014 (2014).

403. Bouybayoune, I. *et al.* Transgenic fatal familial insomnia mice indicate prion infectivity-independent mechanisms of pathogenesis and phenotypic expression of disease. *PLoS Pathog* **11**, (2015).

404. Asante, E. A. *et al.* Transmission Properties of Human PrP 102L Prions Challenge the Relevance of Mouse Models of GSS. *PLoS Pathog* **11**, (2015).

405. Asante, E. A. *et al.* Spontaneous generation of prions and transmissible PrP amyloid in a humanised transgenic mouse model of A117V GSS. *PLoS Biol* **18**, (2020).

406. Manka, S. W. *et al.* A structural basis for prion strain diversity. *bioRxiv* (2022) doi:10.1101/2022.05.17.492259.

407. Tagliavini, F. *et al.* Amyloid protein of Gerstmann-Straussler-Scheinker disease (Indiana kindred) is an 11 kd fragment of prion protein with an N-terminal glycine at codon 58. *EMBO Journal* **10**, 513–519 (1991).

408. Kitamoto, T., Iizuka, R. & Tateishi, J. An amber mutation of prion protein in Gerstmann-Sträussler syndrome with mutant PrP plaques. *Biochem Biophys Res Commun* **192**, 525–531 (1993).

409. Theint, T., Nadaud, P. S., Surewicz, K., Surewicz, W. K. & Jaroniec, C. P. 13C and 15N chemical shift assignments of mammalian Y145Stop prion protein amyloid fibrils. *Biomol NMR Assign* **11**, 75–80 (2017).

410. Theint, T. *et al.* Structural Studies of Amyloid Fibrils by Paramagnetic Solid-State Nuclear Magnetic Resonance Spectroscopy. *J Am Chem Soc* **140**, 13161–13166 (2018).

411. Peoc'h, K. *et al.* Identification of three novel mutations (E196K, V203I, E211Q) in the prion protein gene (PRNP) in inherited prion diseases with Creutzfeldt-Jakob disease phenotype. *Hum Mutat* **15**, 482 (2000).

412. Baskakov, I. V. & Bocharova, O. V. In vitro conversion of mammalian prion protein into amyloid fibrils displays unusual features. *Biochemistry* **44**, 2339–2348 (2005).

413. Bocharova, O. V, Breydo, L., Salnikov, V. V, Gill, A. C. & Baskakov, I. V. Synthetic prions generated in vitro are similar to a newly identified

USC UNIVERSIDADE DE SANTIAGO DE COMPOSTELA

subpopulation of PrPSc from sporadic Creutzfeldt-Jakob Disease. *Protein Sci* **14**, 1222–32 (2005).

414. Makarava, N. & Baskakov, I. V. Genesis of tramsmissible protein states via deformed templating. *Prion* **6**, 252–255 (2012).

415. Makarava, N. & Baskakov, I. V. The evolution of transmissible prions: the role of deformed templating. *PLoS Pathog* **9**, 1–3 (2013).

416. Makarava, N. *et al.* Recombinant prion protein induces a new transmissible prion disease in wild-type animals. *Acta Neuropathol* **119**, 177–187 (2010).

417. Diaz-Espinoza, R. *et al.* Treatment with a Non-toxic, Self-replicating Anti-prion Delays or Prevents Prion Disease In vivo. *Mol Psychiatry* **23**, 777 (2018).

418. Torrent, J. *et al.* Pressure Reveals Unique Conformational Features in Prion Protein Fibril Diversity. *Sci Rep* **9**, (2019).

419. Wenborn, A. *et al.* A novel and rapid method for obtaining high titre intact prion strains from mammalian brain. *Sci Rep* **5**, (2015).

420. Kim, J. Il *et al.* Mammalian prions generated from bacterially expressed prion protein in the absence of any mammalian cofactors. *Journal of Biological Chemistry* **285**, 14083–14087 (2010).

421. Choi, J. K. *et al.* Amyloid fibrils from the N-terminal prion protein fragment are infectious. *Proc Natl Acad Sci U S A* **113**, 13851–13856 (2016).

422. Baskakov, I. V. Switching in amyloid structure within individual fibrils: implication for strain adaptation, species barrier and strain classification. *FEBS Lett* **583**, 2618–2622 (2009).

423. Timmes, A. G., Moore, R. A., Fischer, E. R. & Priola, S. A. Recombinant Prion Protein Refolded with Lipid and RNA Has the Biochemical Hallmarks of a Prion but Lacks In Vivo Infectivity. *PLoS One* **8**, (2013).

424. Wang, F. *et al.* Self-propagating, protease-resistant, recombinant prion protein conformers with or without in vivo pathogenicity. *PLoS Pathog* **13**, (2017).

425. Makarava, N. *et al.* Stabilization of a prion strain of synthetic origin requires multiple serial passages. *J Biol Chem* **287**, 30205–30214 (2012).

USC UNIVERSIDADE DE SANTIAGO DE COMPOSTELA

426. Fischer, M. *et al.* Prion protein (PrP) with amino-proximal deletions restoring susceptibility of PrP knockout mice to scrapie. *EMBO J* **15**, 1255–1264 (1996).

427. Cassard, H. *et al.* Prions from Sporadic Creutzfeldt-Jakob Disease Patients Propagate as Strain Mixtures. *mBio* **11**, 1–19 (2020).

428. Tranulis, M. A., Benestad, S. L., Baron, T. & Kretzschmar, H. Atypical prion diseases in humans and animals. *Top Curr Chem* **305**, 23–50 (2011).

429. Kimberlin, R. H. & Walker, C. A. Competition between strains of scrapie depends on the blocking agent being infectious. *Intervirology* **23**, 74–81 (1985).

430. Bessen, R. A. & Marsh, R. F. Identification of two biologically distinct strains of transmissible mink encephalopathy in hamsters. *Journal of General Virology* **73**, 329–334 (1992).

431. Watts, J. C. *et al.* Spontaneous generation of rapidly transmissible prions in transgenic mice expressing wild-type bank vole prion protein. *Proceedings of the National Academy of Sciences* **109**, 3498–3503 (2012).

432. Watts, J. C. *et al.* Towards authentic transgenic mouse models of heritable PrP prion diseases. *Acta Neuropathol* **132**, 593–610 (2016).

433. Otero, A. *et al.* A Single Amino Acid Substitution, Found in Mammals with Low Susceptibility to Prion Diseases, Delays Propagation of Two Prion Strains in Highly Susceptible Transgenic Mouse Models. *Mol Neurobiol* **56**, 6501–6511 (2019).

434. Marín-Moreno, A., Espinosa, J. C. & Torres, J. M. Transgenic mouse models for the study of prion diseases. in *Progress in Molecular Biology and Translational Science* vol. 175 147–177 (Elsevier B.V., 2020).

435. Nazor, K. E. *et al.* Immunodetection of disease-associated mutant PrP, which accelerates disease in GSS transgenic mice. *EMBO J* **24**, 2472–2480 (2005).

436. Dickinson, A. G., Fraser, H., Meikle, V. M. H. & Outram, G. H. Competition between different scrapie agents in mice. *Nat New Biol* **237**, 244–245 (1972).

437. Collinge, J. & Clarke, A. R. A general model of prion strains and their pathogenicity. *Science (1979)* **318**, 930–936 (2007).

USC UNIVERSIDADE DE SANTIAGO DE COMPOSTELA

438. Langenfeld, K. A., Shikiya, R. A., Kincaid, A. E. & Bartz, J. C. Incongruity between Prion Conversion and Incubation Period following Coinfection. *J Virol* **90**, 5715–5723 (2016).

439. Bartz, J. C., Aiken, J. M. & Bessen, R. A. Delay in onset of prion disease for the HY strain of transmissible mink encephalopathy as a result of prior peripheral inoculation with the replication-deficient DY strain. *J Gen Virol* **85**, 265–273 (2004).

440. Bartz, J. C. *et al.* Prion interference is due to a reduction in strain-specific PrPSc levels. *J Virol* **81**, 689–697 (2007).

441. Pattison I. H. & Millson, G. C. Scrapie Produced Experimentally in Goats With Special Reference To the Clinical Syndrome. *Journal of Comparative Pathology and Therapeutics* **71**, 101-IN10 (1961).

442. Bruce, M. E. TSE strain variation. *Br Med Bull* **66**, 99–108 (2003).

443. Outram, G. W. The pathogenesis of scrapie in mice. *Front Biol* **44**, 325–357 (1976).

444. Prusiner, S. B., Cochran, S. P., Downey, D. E. & Groth, D. F. Determination of scrapie agent titer from incubation period mesurements in hamsters. *Adv Exp Med Biol* **134**, 385–399 (1981).

445. Prusiner, S. B. *et al.* Measurement of the scrapie agent using an incubation time interval assay. *Ann Neurol* **11**, 353–358 (1982).

446. Kimberlin, R. H. & Walker, C. A. Pathogenesis of mouse scrapie: dynamics of agent replication in spleen, spinal cord and brain after infection by different routes. *J Comp Pathol.* **89**, 551–562 (1979).

447. Vickery, C. M., Beck, K. E., Simmons, M. M., Hawkins, S. A. C. & Spiropoulos, J. Disease characteristics of bovine spongiform encephalopathy following inoculation into mice via three different routes. *Int J Exp Pathol* **94**, 320–328 (2013).

448. Bruce, M. E. & Dickinson, A. G. Genetic control of amyloid plaque production and incubation period in scrapie-infected mice. *J Neuropathol Exp Neurol* **44**, 285–294 (1985).

449. Bruce, M. E., McConnell, I., Fraser, H. & Dickinson, A. G. The disease characteristics of different strains of scrapie in Sinc congenic mouse lines: Implications for the nature of the agent and host control of pathogenesis. *Journal of General Virology* **72**, 595–603 (1991).

USC UNIVERSIDADE DE SANTIAGO DE COMPOSTELA

450. Carroll, J. A. *et al.* Prion Strain Differences in Accumulation of PrPSc on Neurons and Glia Are Associated with Similar Expression Profiles of Neuroinflammatory Genes: Comparison of Three Prion Strains. *PLoS Pathog* **12**, e1005551 (2016).

451. Hilton, K. J., Cunningham, C., Reynolds, R. A. & Perry, V. H. Early Hippocampal Synaptic Loss Precedes Neuronal Loss and Associates with Early Behavioural Deficits in Three Distinct Strains of Prion Disease. *PLoS One* **8**, (2013).

452. Fraser, H. & Dickinson, A. G. The sequential development of the brain lesion of scrapie in three strains of mice. *J Comp Pathol* **78**, (1968).

453. Outram, G. W. Changes in drinking and feeding habits of mice with experimental scrapie. *J Comp Pathol* **82**, 415–427 (1972).

454. Marsh, R. F. & Kimberlin, R. H. Comparison of scrapie and transmissible mink encephalopathy in hamsters. II. Clinical signs, pathology, and pathogenesis. *J Infect Dis* **131**, 104–110 (1975).

455. Cunningham, C. *et al.* Neuropathologically distinct prion strains give rise to similar temporal profiles of behavioral deficits. *Neurobiol Dis* **18**, 258–269 (2005).

456. Parchi, P. *et al.* Molecular Basis of Phenotypic Variability in Sporadc Creudeldt-Jakob Disease. *Ann. Neurol.* **39**, 767–778 (1996).

457. Thackray, A. M., Hopkins, L., Klein, M. A. & Bujdoso, R. Mouse-Adapted Ovine Scrapie Prion Strains Are Characterized by Different Conformers of PrPSc. *J Virol* **81**, 12119 (2007).

458. Bessen, R. A. & Marsh, R. F. Biochemical and physical properties of the prion protein from two strains of the transmissible mink encephalopathy agent. *J Virol* **66**, 2096–2101 (1992).

459. Kuczius, T. & Groschup, M. H. Differences in proteinase K resistance and neuronal deposition of abnormal prion proteins characterize bovine spongiform encephalopathy (BSE) and scrapie strains. *Molecular Medicine* **5**, 406–418 (1999).

460. Bett, C. *et al.* Biochemical Properties of Highly Neuroinvasive Prion Strains. *PLoS Pathog* **8**, e1002522 (2012).

461. Safar, J. *et al.* Eight prion strains have PrP(Sc) molecules with different conformations. *Nat Med* **4**, 1157–1165 (1998).

USC UNIVERSIDADE DE SANTIAGO DE COMPOSTELA

462. Pattison, I. H. The relative susceptibility of sheep, goats, and mice to two types of the goat scrapie agent. *Res. Vet. Sci* **7**, 207–212 (1966).

463. Bartz, J. C., McKenzie, D. I., Bessen, R. A., Marsh, R. F. & Aiken, J. M. Transmissible mink encephalopathy species barrier effect between ferret and mink: PrP gene and protein analysis. *J Gen Virol* **75 (Pt 11)**, 2947–53 (1994).

464. Kocisko, D. A. *et al.* Species specificity in the cell-free conversion of prion protein to protease-resistant forms: a model for the scrapie species barrier. *Proc Natl Acad Sci U S A* **92**, 3923–3927 (1995).

465. Ironside, J. W. *et al.* A new variant of Creutzfeldt-Jakob disease: Neuropathological and clinical features. *Cold Spring Harb Symp Quant Biol* **61**, 523–530 (1996).

466. Kimberlin, R. H. & Walker, C. A. Evidence that the Transmission of One Source of Scrapie Agent to Hamsters Involves Separation of Agent Strains from a Mixture. *J. gen. Virol.* **39**, 487–496 (1978).

467. Collinge, J. Human prion diseases and bovine spongiform encephalopathy (BSE). *Hum Mol Genet* **6**, 1699–1705 (1997).

468. Hill, A. F. *et al.* The same prion strain causes vCJD and BSE. *Nature* **389**, 448–450 (1997).

469. Katorcha, E., Makarava, N., Savtchenko, R., d′Azzo, A. & Baskakov, I. V. Sialylation of Prion Protein Controls the Rate of Prion Amplification, the Cross-Species Barrier, the Ratio of PrPSc Glycoform and Prion Infectivity. *PLoS Pathog* **10**, (2014).

470. Zhang, Z. *et al.* De novo generation of infectious prions with bacterially expressed recombinant prion protein. *FASEB J* **27**, 4768–4775 (2013).

471. Bruce, M. E. & Dickinson, A. G. Biological evidence that scrapie agent has an independent genome. *J Gen Virol* **68 (Pt 1)**, 79–89 (1987).

472. Collinge, J. Prion strain mutation and selection. *Science* **328**, 1111–2 (2010).

473. Gonzalez-Montalban, N., Lee, Y. J., Makarava, N., Savtchenko, R. & Baskakov, I. V. Changes in prion replication environment cause prion strain mutation. *FASEB J* **27**, 3702–3710 (2013).

474. Bartz, J. C., Bessen, R. A., McKenzie, D., Marsh, R. F. & Aiken, J. M. Adaptation and Selection of Prion Protein Strain Conformations following

USC UNIVERSIDADE DE SANTIAGO DE COMPOSTELA

Interspecies Transmission of Transmissible Mink Encephalopathy. *J Virol* **74**, 5542 (2000).

475. Ghaemmaghami, S. *et al.* Conformational transformation and selection of synthetic prion strains. *J Mol Biol* **413**, 527–542 (2011).

476. Atarashi, R. *et al.* Simplified ultrasensitive prion detection by recombinant PrP conversion with shaking. *Nat Methods* **5**, 211–212 (2008).

477. Hill, A. F., Antoniou, M. & Collinge, J. Protease-resistant prion protein produced in vitro lacks detectable infectivity. *J Gen Virol* **80 (Pt 1)**, 11–14 (1999).

478. Baskakov, I. V., Legname, G., Baldwin, M. A., Prusiner, S. B. & Cohen, F. E. Pathway complexity of prion protein assembly into amyloid. *J Biol Chem* **277**, 21140–21148 (2002).

479. Legname, G. *et al.* Synthetic mammalian prions. *Science (1979)* **305**, 673–676 (2004).

480. Cohen, F. E. *et al.* Structural clues to prion replication. *Science (1979)* **264**, 530–531 (1994).

481. Schmidt, C. *et al.* A systematic investigation of production of synthetic prions from recombinant prion protein. *Open Biol* **5**, (2015).

482. Fernández-Borges, N. *et al.* Cofactors influence the biological properties of infectious recombinant prions. *Acta Neuropathol* **135**, 179–199 (2018).

483. Eraña, H. *et al.* Development of a new largely scalable in vitro prion propagation method for the production of infectious recombinant prions for high resolution structural studies. *PLoS Pathog* **15**, (2019).

484. Saá, P., Castilla, J. & Soto, C. Ultra-efficient replication of infectious prions by automated protein misfolding cyclic amplification. *Journal of Biological Chemistry* **281**, 35245–35252 (2006).

485. Castilla, J. *et al.* Cell-free propagation of prion strains. *EMBO Journal* **27**, 2557–2566 (2008).

486. Shikiya, R. A., Ayers, J. I., Schutt, C. R., Kincaid, A. E. & Bartz, J. C. Coinfecting Prion Strains Compete for a Limiting Cellular Resource. *J Virol* **84**, 5706–5714 (2010).

USC UNIVERSIDADE DE SANTIAGO DE COMPOSTELA

487. Cali, I. *et al.* PMCA-replicated PrPD in urine of vCJD patients maintains infectivity and strain characteristics of brain PrPD: Transmission study. *Sci Rep* **9**, (2019).

488. Wagner, J. *et al.* Anle138b: a novel oligomer modulator for disease-modifying therapy of neurodegenerative diseases such as prion and Parkinson's disease. *Acta Neuropathol* **125**, 795–813 (2013).

489. Fernández-Borges, N., De Castro, J. & Castilla, J. In vitro studies of the transmission barrier. *Prion* **3**, (2009).

490. Bélondrade, M. *et al.* Correlation between Bioassay and Protein Misfolding Cyclic Amplification for Variant Creutzfeldt-Jakob Disease Decontamination Studies. *mSphere* **5**, (2020).

491. Saá, P., Castilla, J. & Soto, C. Presymptomatic detection of prions in blood. *Science* **313**, 92–94 (2006).

492. Hermann, P. *et al.* Biomarkers and diagnostic guidelines for sporadic Creutzfeldt-Jakob disease. *Lancet Neurol* **20**, 235–246 (2021).

493. Orrù, C. D. *et al.* RT-QuIC Assays for Prion Disease Detection and Diagnostics. *Methods Mol Biol* **1658**, 185–203 (2017).

494. Peden, A. H. *et al.* Sensitive and specific detection of sporadic Creutzfeldt-Jakob disease brain prion protein using real-time quaking-induced conversion. *J Gen Virol* **93**, (2012).

495. John, T. R., Schätzl, H. M. & Gilch, S. Early detection of chronic wasting disease prions in urine of pre-symptomatic deer by real-time quaking-induced conversion assay. *Prion* **7**, 253–258 (2013).

496. Henderson, D. M. *et al.* Rapid antemortem detection of CWD prions in deer saliva. *PLoS One* **8**, (2013).

497. Orrú, C. D. *et al.* Prion disease blood test using immunoprecipitation and improved quaking-induced conversion. *mBio* **2**, (2011).

498. Orrú, C. D. *et al.* Prion seeding activity and infectivity in skin samples from patients with sporadic Creutzfeldt-Jakob disease. *Sci Transl Med* **9**, (2017).

499. Bongianni, M. *et al.* Diagnosis of Human Prion Disease Using Real-Time Quaking-Induced Conversion Testing of Olfactory Mucosa and Cerebrospinal Fluid Samples. *JAMA Neurol* **74**, 155–162 (2017).

USC UNIVERSIDADE DE SANTIAGO DE COMPOSTELA

500. Groveman, B. R. *et al.* Rapid and ultra-sensitive quantitation of disease-associated α-synuclein seeds in brain and cerebrospinal fluid by αSyn RT-QuIC. *Acta Neuropathol Commun* **6**, (2018).

501. Koga, S., Sekiya, H., Kondru, N., Ross, O. A. & Dickson, D. W. Neuropathology and molecular diagnosis of Synucleinopathies. *Mol Neurodegener* **16**, (2021).

502. Saijo, E. *et al.* Ultrasensitive RT-QuIC Seed Amplification Assays for Disease-Associated Tau, α-Synuclein, and Prion Aggregates. *Methods Mol Biol* **1873**, 19–37 (2019).

503. Mok, T. H. *et al.* Bank vole prion protein extends the use of RT-QuIC assays to detect prions in a range of inherited prion diseases. *Sci Rep* **11**, (2021).

504. Bocharova, O. V. *et al.* Annealing prion protein amyloid fibrils at high temperature results in extension of a proteinase K-resistant core. *Journal of Biological Chemistry* **281**, 2373–2379 (2006).

505. Colby, D. W. *et al.* Prion detection by an amyloid seeding assay. *Proc Natl Acad Sci U S A* **104**, 20914–20919 (2007).

506. Sevillano, A. M. *et al.* Recombinant PrPScshares structural features with brain-derived PrPSc: Insights from limited proteolysis. *PLoS Pathog* **14**, 1–21 (2018).

507. Charco, J. M. Desarrollo de un nuevo sistema de cribado masivo basado en la propagación in vitro de priones recombinantes infecciosos para la detección de compuestos con actividad anti-priónica. (2018).

508. Miranda, E. G. Adaptación de un sistema de propagación de priones in vitro para el cribado masivo de compuestos específicos frente a las Encefalopatías Espongiformes Transmisibles humanas. (2020).

509. Pérez-Castro, M. Á. Generación de distintas cepas de priones recombinantes como herramienta parael estudio del malplegamiento espontáneo en las enfermedades priónicas. (Universidad del País Vasco, 2021).

510. Deleault, N. R. *et al.* Cofactor molecules maintain infectious conformation and restrict strain properties in purified prions. *Proc Natl Acad Sci U S A* **109**, E1938-46 (2012).

511. Ma, J., Zhang, J. & Yan, R. Recombinant Mammalian Prions: The "Correctly" Misfolded Prion Protein Conformers. *Viruses* **14**, 1940 (2022).

USC UNIVERSIDADE DE SANTIAGO DE COMPOSTELA

512. Wang, F. *et al.* Genetic informational RNA is not required for recombinant prion infectivity. *J Virol* **86**, 1874–1876 (2012).

513. Deleault, N. R. *et al.* Isolation of phosphatidylethanolamine as a solitary cofactor for prion formation in the absence of nucleic acids. *Proceedings of the National Academy of Sciences* **109**, 8546–8551 (2012).

514. Kim, C. *et al.* Artificial strain of human prions created in vitro. *Nat Commun* **9**, 1–11 (2018).

515. Supattapone, S. Cofactor molecules: Essential partners for infectious prions. *Prog Mol Biol Transl Sci* **175**, 53–75 (2020).

516. Kazlauskaite, J., Sanghera, N., Sylvester, I., Vénien-Bryan, C. & Pinheiro, T. J. T. Structural changes of the prion protein in lipid membranes leading to aggregation and fibrillization. *Biochemistry* **42**, 3295–3304 (2003).

517. Jack, K., Jackson, G. S. & Bieschke, J. Essential Components of Synthetic Infectious Prion Formation De Novo. *Biomolecules* **12**, (2022).

518. Hasegawa, M., Crowther, R. A., Jakes, R. & Goedert, M. Alzheimer-like changes in microtubule-associated protein tau induced by sulfated glycosaminoglycans. Inhibition of microtubule binding stimulation of phosphorylation filament assembly depend on the degree of sulfation. *Journal of Biological Chemistry* **272**, 33118–33124 (1997).

519. Brunden, K. R., Richter-Cook, N. J., Chaturvedi, N. & Frederickson, R. C. A. pH-dependent binding of synthetic beta-amyloid peptides to glycosaminoglycans. *J Neurochem* **61**, 2147–2154 (1993).

520. Luo, Y. *et al.* Molecular insights into the reversible formation of tau protein fibrils. *Chem Commun (Camb)* **49**, 3582–3584 (2013).

521. Holmes, B. B. *et al.* Heparan sulfate proteoglycans mediate internalization and propagation of specific proteopathic seeds. *Proc Natl Acad Sci U S A* **110**, (2013).

522. De Carufel, C. A., Nguyen, P. T., Sahnouni, S. & Bourgault, S. New insights into the roles of sulfated glycosaminoglycans in islet amyloid polypeptide amyloidogenesis and cytotoxicity. *Biopolymers* **100**, 645–655 (2013).

523. Bourgault, S., Solomon, J. P., Reixach, N. & Kelly, J. W. Sulfated glycosaminoglycans accelerate transthyretin amyloidogenesis by quaternary structural conversion. *Biochemistry* **50**, 1001–1015 (2011).

USC UNIVERSIDADE DE SANTIAGO DE COMPOSTELA

524. Quittot, N., Sebastiao, M. & Bourgault, S. Modulation of amyloid assembly by glycosaminoglycans: from mechanism to biological significance. *Biochem Cell Biol* **95**, 329–337 (2017).

525. Madine, J. Cofactor-mediated amyloidogenesis. *Biosci Rep* **39**, (2019).

526. Kisilevsky, R. The relation of proteoglycans, serum amyloid P and apo E to amyloidosis current status, 2000. *Amyloid* **7**, 23–25 (2000).

527. Alexandrescu, A. T. Amyloid accomplices and enforcers. *Protein Sci* **14**, 1–12 (2005).

528. Gellermann, G. P. *et al.* Raft lipids as common components of human extracellular amyloid fibrils. *Proc Natl Acad Sci U S A* **102**, 6297–6302 (2005).

529. Ancsin, J. B. Amyloidogenesis: historical and modern observations point to heparan sulfate proteoglycans as a major culprit. *Amyloid* **10**, 67–79 (2003).

530. Theocharis, A. D., Skandalis, S. S., Gialeli, C. & Karamanos, N. K. Extracellular matrix structure. *Adv Drug Deliv Rev* **97**, 4–27 (2016).

531. Aguilera, J. J., Zhang, F., Beaudet, J. M., Linhardt, R. J. & Colón, W. Divergent effect of glycosaminoglycans on the in vitro aggregation of serum amyloid A. *Biochimie* **104**, 70–80 (2014).

532. McLaurin, J. A., Franklin, T., Zhang, X., Deng, J. & Fraser, P. E. Interactions of Alzheimer amyloid-β peptides with glycosaminoglycans. *Eur J Biochem* **266**, 1101–1110 (1999).

533. López-Moreno, R. Estudio de la diversidad y estabilidad de diferentes priones recombinantes infecciosos para dilucidar los mecanismos moleculares que rigen el fenómeno de cepa. (2021).

534. Hubbard, S. J. The structural aspects of limited proteolysis of native proteins. *Biochim Biophys Acta* **1382**, 191–206 (1998).

535. Fontana, A. *et al.* Probing protein structure by limited proteolysis. *Acta Biochim Pol* **51**, 299–321 (2004).

536. Naito, A. & Kawamura, I. Solid-state NMR as a method to reveal structure and membrane-interaction of amyloidogenic proteins and peptides. *Biochimica et Biophysica Acta - Biomembranes* vol. 1768 1900–1912 Preprint at https://doi.org/10.1016/j.bbamem.2007.03.025 (2007).

USC UNIVERSIDADE DE SANTIAGO DE COMPOSTELA

537. Codeseira, Y. B. Structural characterization of recombinant PrPSc prions using biochemical and biophysical techniques. (2022).

538. Fernández, L. C. Probing the structure of a recombinant prion using limited proteolysis coupled to mass spectrometry. (University of Santiago de Compostela, 2020).

539. Takegoshi, K., Nakamura, S. & Terao, T. 13C–1H dipolar-driven 13C–13C recoupling without 13C rf irradiation in nuclear magnetic resonance of rotating solids. *J Chem Phys* **118**, 2325 (2003).

540. Takegoshi, K., Nakamura, S. & Terao, T. 13C–1H dipolar-assisted rotational resonance in magic-angle spinning NMR. *Chem Phys Lett* **344**, 631–637 (2001).

541. DARR | Protein NMR. https://protein-nmr.org.uk/solid-state-mas-nmr/spectrum-descriptions/darr/.

542. Zhang, H., Neal, S. & Wishart, D. S. RefDB: a database of uniformly referenced protein chemical shifts. *J Biomol NMR* **25**, 173–195 (2003).

543. Madine, J. *et al.* Site-Specific Identification of an Aβ Fibril–Heparin Interaction Site by Using Solid-State NMR Spectroscopy. *Angewandte Chemie International Edition* **51**, 13140–13143 (2012).

544. Bistaffa, E. *et al.* Synthetic Prion Selection and Adaptation. *Mol Neurobiol* **56**, 2978–2989 (2019).

545. Supattapone, S. Elucidating the role of cofactors in mammalian prion propagation. *Prion* **8**, (2014).

546. Iannuzzi, C., Irace, G. & Sirangelo, I. The effect of glycosaminoglycans (GAGs) on amyloid aggregation and toxicity. *Molecules* **20**, 2510–2528 (2015).

547. Wong, C. *et al.* Sulfated glycans and elevated temperature stimulate PrP(Sc)-dependent cell-free formation of protease-resistant prion protein. *EMBO J* **20**, 377–386 (2001).

548. Aguilar-Calvo, P. *et al.* Post-translational modifications in PrP expand the conformational diversity of prions in vivo. *Sci Rep* **7**, (2017).

549. Parchi, P. *et al. Different patterns of truncated prion protein fragments correlate with distinct phenotypes in P102L Gerstmann-Sträussler-Scheinker disease*. *Neurobiology* vol. 95 www.pnas.org. (1998).

USC UNIVERSIDADE DE SANTIAGO DE COMPOSTELA

550. Parchi, P. *et al.* Genetic influence on the structural variations of the abnormal prion protein. *Proc Natl Acad Sci U S A* **97**, 10168–10172 (2000).

551. Pirisinu, L. *et al.* Small Ruminant Nor98 Prions Share Biochemical Features with Human Gerstmann-Strä ussler-Scheinker Disease and Variably Protease-Sensitive Prionopathy. *PLoS One* **8**, 1–13 (2013).

552. Klingeborn, M. *et al.* Characterization of proteinase K-resistant N- and C-terminally truncated PrP in Nor98 atypical scrapie. *J Gen Virol* **87**, 1751–1760 (2006).

553. Notari, S. *et al.* Characterization of truncated forms of abnormal prion protein in Creutzfeldt-Jakob disease. *Journal of Biological Chemistry* **283**, 30557–30565 (2008).

554. Satoh, K. *et al.* Association of an 11 - 12 kDa protease-resistant prion protein fragment with subtypes of dura graft-associated Creutzfeldt-Jakob disease and other prion diseases. *Journal of General Virology* **84**, 2885–2893 (2003).

555. Capellari, S. *et al.* Effect of the E200K Mutation on Prion Protein Metabolism : Comparative Study of a Cell Model and Human Brain. *Am J Pathol* **157**, 613 (2000).

556. Xiao, X. *et al.* Comparative Study of Prions in Iatrogenic and Sporadic Creutzfeldt-Jakob Disease. *J Clin Cell Immunol* **5**, (2014).

557. Vanni, I. *et al.* In vitro replication highlights the mutability of prions. *Prion* **8**, 154 (2014).

558. Walsh, D. J., Schwind, A. M., Noble, G. P. & Supattapone, S. Conformational diversity in purified prions produced in vitro. *PLoS Pathog* **19**, e1011083 (2023).

559. Manka, S. W., Wenborn, A., Collinge, J. & Wadsworth, J. D. F. Prion strains viewed through the lens of cryo-EM. *Cell Tissue Res* (2022) doi:10.1007/S00441-022-03676-Z.

560. Burke, C. *et al.* Full restoration of specific infectivity and strain properties from pure mammalian prion protein. *PLoS Pathog* **15**, (2019).

561. Barrio, T. *et al.* Mixtures of prion substrains in natural scrapie cases revealed by ovinised murine models. *Sci Rep* **10**, (2020).

USC UNIVERSIDADE DE SANTIAGO DE COMPOSTELA

562. Pérez, M., Wandosell, F., Colaço, C. & Avila, J. Sulphated glycosaminoglycans prevent the neurotoxicity of a human prion protein fragment. *Biochem J* **335 (Pt 2)**, 369–374 (1998).

563. Bazar, E. & Jelinek, R. Divergent heparin-induced fibrillation pathways of a prion amyloidogenic determinant. *Chembiochem* **11**, 1997–2002 (2010).

USC UNIVERSIDADE DE SANTIAGO DE COMPOSTELA

USC
UNIVERSIDADE
DE SANTIAGO
DE COMPOSTELA

8. SUPPLEMENTARY INFORMATION

ANNEX I: LISTING OF MATERIALS USED IN THIS THESIS

Material	Reference	Brand
0.22µm filter	JCAS 045025K	Cytiva
0.45µm filter	SLGP033RS	Filter lab
JA-10 rotor tubes	31410500	Thermo Scientific
JA-20 rotor tubes	55.517	Sarstedt
PMSA tubes	3468	Thermo Scientific
Immobilon P PVDF membrane	IPVH00010	Millipore
Blotting paper	RPN6101M	Cytiva
3mL Slide-A-Lyzer dialysis cassettes G2	87718	Thermo
Scalpel blade 21	0207	Swann-Morton
Black-bottom 96-wells plate	353945	Falcon
96-wells plate	M600	Deltalab
29-gauge needle (built-in syringe)	320926	BD Medical
25-gauge needle (built-in syringe)	4657853	Braun
His Trap HP column	17524802	Cytiva
1mm Zirconia/Silica beads	11079110z	Biospec products
1mm Glass beads	11079110	Biospec products
0.1mm Glass beads	11079101	Biospec products
2.3mm Zirconia/Silica beads	11079125z	Biospec products

USC UNIVERSIDADE DE SANTIAGO DE COMPOSTELA

ChromXP C18 150×0.30 mm column	5022436	SCIEX
Centrifugal filters ultracel 3K Amicon Ultra 15	UFC900324	Merck
mPAGE 4-12% Bis-Tris gels	MP41G10	Sigma
70Ti rotor tubes	355618	Beckman Coulter
YMC-TRIART C18 trap column	TA12S03-1503PTH	Tecnokroma

USC UNIVERSIDADE DE SANTIAGO DE COMPOSTELA

ANNEX II: LISTING OF REAGENTS USED IN THE PRESENT THESIS

Reagent	Reference	Brand
2,2,2-tribromoethanol	T48402	Sigma
2-mercaptoethanol	M3148	Sigma
2-methyl-2-butanol	152483	Sigma
Ampicillin sodium salt	A9518	Sigma
Anti-ß-tubulin antibody	MA5-16308	Invitrogen
APS (Ammonium persulfate)	A6761	Sigma
APS (ammonium persulfate)	A3678	Sigma
Benzonase Nuclease	70746	Millipore
Biotin	B4501	Sigma
BlueSafe	MB15201	NZYtech
Bromophenol blue	114391	Sigma
C0mplete (protease inhibition cocktail)	11697498001	Merck
Ca2Cl (Calcium chloride)	2083	Merck
Chondroitin sulfate from shark cartilage	C4384	Sigma
ClNH4 (Ammonium chloride)	A9434	Sigma
D+Glucose	G7021	Sigma
Dextran sodium sulfate 6500-10000	D4911	Sigma
DNAse	04536282001	Merck
E. coli Rossetta (DE3) Competent Cells	69450	Novagen
EDTA (Ethylenediaminetetraacetic acid)	E9884	Sigma
Fe(III)-TMPyP [Fe(III) meso-Tetra (N-Methyl-4-Pyridyl) porphine pentachloride]	1-800-364-9897	Cayman Chemical Company

USC UNIVERSIDADE DE SANTIAGO DE COMPOSTELA

Glycerol	G9012	Sigma
Goat anti-mouse IgG (HRP)	Ab6789	Abcam
Guanidine - HCl	A13543.01	Alfa Aesar
H2SO4 (Sulfuric acid)		
HCl (Chlorhydric acid)	30721	Sigma
Heparin sodium from porcine mucosa	SRE0027	Sigma
Imidazole	I2399	Sigma
Immobilon Forte Western Substrate	WBLUF0100	Millipore
IPTG (Isopropil ß-D-1-thiogalactopyranoside)	IS758	Sigma
KCl (Potassium chloride)	9541	Sigma
KH2PO4 [Potassium dihydrogen phosphate]	1.04873.1000	Merck
L-alanine	AL00300100	Scharlau
L-arginine	AR12500100	Scharlau
L-asparagine	AS00150100	Scharlau
L-aspartic acid	AC05290100	Scharlau
LB growth media	L3022	Sigma
L-cysteine	CI03050025	Scharlau
L-glutamic acid	AC12250250	Scharlau
L-glutamine	GL01650100	Scharlau
L-glycine	G7126	Sigma
L-histidine	HI03950100	Scharlau
L-isoleucine	IS01400025	Scharlau
L-leucine	LE00550025	Scharlau
L-lysine	LI00351000	Scharlau

USC UNIVERSIDADE DE SANTIAGO DE COMPOSTELA

L-methionine	152882.1606	Panreac
L-phenylalanine	FE01800100	Scharlau
L-proline	PR00550100	Scharlau
L-serine	SE01050100	Scharlau
L-threonine	BP394-100	Fisher Bioreagents
L-tryptophan	TR04000025	Scharlau
L-tyrosine	TI03250100	Scharlau
L-valine	VA00550025	Scharlau
Lysozyme from chicken egg white	62980	Sigma
MES (morfolino etanesulfonic acid monohydrate)	1.06126.0250	Merck
Methanol	20847.360	Normapur Reagents
$MgCl_2$ Magnesium chloride	MA00360500	Scharlau
$MgSO_4$ Magnesium sulfate	M7506	Sigma
Molecular weight marker	161-0377	BioRad
Na_2HPO_4 (Sodium hydrogen phosphate)	1.06586.1000	Merck
NaAcO (Sodium acetate trihydrate)	S7670	Sigma
NaCl (Sodium chloride)	39781	Serva
NaH_2PO_4 (Sodium hydrogen phosphate monohydrate)	1.06346.0500	Merck
NaOH (Sodium hydroxide)	30620	Sigma
NaPTA (sodium phosphotungstate dibasic hydrate)	P6395	Sigma
$NiSO_4$ [Nickel (III) sulfate-6-hydrate]	131445.1209	Panreac
NuPAGE LDS Sample Buffer 4x	NP0008	Thermo Fisher Scientific
NuPAGE MES SDS Running buffer 20x	NP0002	Thermo Fisher Scientific
Optiprep (Iodixanol density gradient medium)	DI556	Sigma

USC UNIVERSIDADE DE SANTIAGO DE COMPOSTELA

Paraformaldehyde, 4% in PBS	J61899	AlfaAesar
Pefabloc	76307	Sigma
Pierce BCA Protein Assay Kit	23227	Thermo Fisher Scientific
Pierce ECL Western Blotting Substrate	32106	Thermo Fisher Scientific
PMSF (phenylmethylsulfonyl fluoride)	78830	Sigma
PNGase F	P0704L	New England Labs
PPS (Pentosan polysulfate sodium)		
Pronase E from Stretomyces griseus	1.07433.0001	Merck
Proteinase K recombinant PCR grade	03115801001	Roche
SAF83	A03207	Bertin Bioreagents
SAF84	A03208	Bertin Bioreagents
Sarkosyl (N-laurosyl salkosine sodium salt)	8.14715.0500	Sigma
SDS (sodium dodecyl sulfate)	L4509	Sigma
Skim milk powder	70166	Sigma
SOC medium	S1797	Sigma
TEMED	1.10732.0100	Millipore
TFA (trifluoroacetic acid)	363317	Panreac
Thioflavin T (ThT)	8.40072.0005	Merck
Tiamine hydrocloride	T4625	Sigma
Tris Base	A1379.1000	Panreac
Triton Tx-100	T8787	Sigma
Tween-20	P9416	Sigma
Uniformly labeled L-phenylalanine	CC2000P1	Cortecnet

USC UNIVERSIDADE DE SANTIAGO DE COMPOSTELA

ANNEX III: LISTING OF BUFFERS USED IN THE PRESENT THESIS AND THEIR COMPOSITION

Binding buffer (Ni-NTA column)

Tris	20mM
NaCl	500mM
Imidazole	5mM
Gdn/HCl	2M
Water	q.s.
pH	8

Elution buffer (Ni-NTA column)

Tris	20mM
NaCl	500mM
Imidazole	500mM
Gdn/HCl	2M
Water	q.s.
pH	8

Stripping buffer (Ni-NTA column)

Na2HPO4	20mM
NaCl	500mM
EDTA	50mM
Water	q.s.
pH	7.4

Anesthesia

Tribromoethanol	1,2%(w/v)
Tert-amyl alcohol	1,2% (v/v)
PBS	q.s.

Minimum Medium

Na2HPO4	42mM
KHPO4	22mM
NaCl	8,5mM
NH4Cl	0,1%
Glucose	0,3%
MgSO4	1mM
CaCl2	0,1mM
Thiamine	10µg/mL
Biotin	10µg/mL
Ampicillin	20µg/mL
Water	q.s.
pH	7.0

Lysis buffer

Tris-HCl	50mM
EDTA	5mM
MgCl2	20mM
Triton X-100	1% (v/v)
PMSF	1mM
Lysozyme	10µg/mL
DNase	30U/mL
Water	q.s.
pH	8.0

Inclusion bodies solubilization buffer

Tris/HCl	20mM
NaCl	0,5M
Gdn/HCl	6M
Water	q.s.
pH	8

Transfer buffer

Tris base	25mM
Glycine	200mM
Methanol	20% (v/v)
Water	q.s.
pH	8.3

USC UNIVERSIDADE DE SANTIAGO DE COMPOSTELA

Blocking buffer

Skim milk powder	5%
TBS-T	q.s.

LB growth media

LB	2% (w/v)
Ampicillin	50µg/mL
Water	q.s.

Laemmli 5x

Glycerol	50%
ß-mercaptoethanol	25%
SDS	10% (w/v)
Tris pH 6,8	125mM
Bromophenol blue	Traces
Water	q.s.

TBS-T

Tris base	20mM
NaCl	150mM
Tween 20	0.1% (v/v)
Water	q.s.
pH	7.6

Conversion buffer

Triton X-100	1% (w/v)
NaCl	150mM
PBS	q.s.

Fibrillation buffer

MES	50mM
Gdn/HCl	2M
Water	q.s.
pH	6

Stripping buffer (Western blot)

SDS	2%
Tris/HCl pH6,8	62,5mM
ß-mercaptoethanol	0,8% (v/v)
Water	q.s.

PBS-T

Tween 20	0,1% (v/v)
PBS	q.s.

Wash buffer (Prion concentration protocol)

Iodixanol	17,5%
Sarkosyl	0,1%
PBS	q.s.

ThT binding assay buffer

AcONa pH5	10mM
ThT	10µM
Protein	13µg/mL

USC UNIVERSIDADE DE SANTIAGO DE COMPOSTELA

ANNEX IV: LISTING OF APPARATUS USED IN THIS THESIS

Equipment	Model	Brand
Analytical balance	TB-124A	Denver Instrument
Balance	S-402	Denver Instrument
Centrifuge	Microfuge 22R centrifuge	Beckman Coulter
Electron microscope	JEOL JEM-F200CF-HR	JEOL Ltd.
Electrophorese cell	Mini-cell	Novex
High-speed centrifuge	Avanti J-26 XPI Centrifuge	Beckman Coulter
High-speed centrifuge rotors	JA-20	Beckman Coulter
	JA-10	
Homogenizer	Dounze Homogenizer	
IR lamp	IR 100	Medisana
Magnetic stirrer	-	Super
Mass spectrometer	Triple TOF 6600	SCIEX
Microscope	Leica DM4 B	Leica
NMR spectrometer	Bruker NEO 17.6T	Bruker
micro liquid chromatography system	nanoLC 400	SCIEX
Orbital incubator	MaxQ 8000	Thermo Scientific
Peristaltic pump	Econopump EP1	BioRad
pHmeter	MicropH 2002	Crison
Plate reader	Mithras LB 940	Berthold Technologies
Power supply	Power Pac Universal	BioRad
Semi-dry transfer cell	Transblot SD	BioRad
Shakers	Thermomixer C	Eppendorf

USC UNIVERSIDADE DE SANTIAGO DE COMPOSTELA

	Digital Shaking Drybath	Thermo Scientific
Sonicator	4710 Series Ultrasonic Homogenizer	Cole Parmer
Spectrophotometer	UV-II	Lon Optics
	Nanodrop One	Thermo Scientific
Spectrophotometer cuvettes	Cuvettes PMMA 4,5mL 4 cleaner sides (PN 1961)	Dispolab Kartell
ssNMR rotor		
Tabletop ultracentrifuge	Optima TLX	Beckman Coulter
Tabletop ultracentrifuge rotor	TLA 120.1	Beckman Coulter
Transfer system	TransBlot TurboTM	BioRad
Ultracentrifuge	Optima L-100XP Ultracentrifuge	Beckman Coulter
Ultracentrifuge rotor	70Ti	Beckman Coulter
Western blot processing system	iBind™ Flex Western	ThermoFisher Scientific
Western blot visualizer (I)	ChemiDoc MD	BioRad
Western blot visualizer (II)	Invitrogen iBright	ThermoFisher Scientific

USC UNIVERSIDADE DE SANTIAGO DE COMPOSTELA

ANNEX V: LISTING OF SOFTWARE USED IN THIS THESIS

Utility	Software	Brand
Histological slides visualizer system	EnVision	EnVision
Mass spectrometer operator software	Analyst TF1.7.1	SCIEX
Microscope image processing	Leica Application Suite X	Leica
Molecular visualization	ChimeraX	University of California
NMR spectrometer control software	TopSpin4.0	Bruker
NMR spectrometer spectra processing software	MestreNova v14.0	Mestrelab Research Inc
Online tool for creating science figures	biorender.com	BioRender
Peptides identification	GPMAW	Lighthouse data
Protein reconstruction software	PeakView2.2	PeakView
Statistical analyses	Graph Pad Prism 8	GraphPad
Western blot image processing software (I)	ImageLab	BioRad
Western blot image processing software (II)	Invitrogen iBright	ThermoFisher Scientific

USC UNIVERSIDADE DE SANTIAGO DE COMPOSTELA

ANNEX VI: BANK VOLE PRP 23-231 109I SEQUENCE

23KKRPKPGGWNTGGSRYPGQGSPGGNRYPPQGGGTWGQPHG
GGWGQPHGGGWGQPHGGGWGQPHGGGWGQGGGTHNQWN
KPSKPKTNIKHVAGAAAAGAVVGGLGGYMLGSAMSRPMIHF
GNDWEDRYYRENMNRYPNQVYYRPVDQYNNQNNFVHDCVN
ITIKQHTVTTTTKGENFTETDVKMMERVVEQMCVTQYQKESQ
AYYEGRSS231

Bank vole PrP 23-231 109I sequence. The 109I polymorphism is highlighted in blue, the phenylalanine positions are highlighted in green, and cysteines involved in the disulfide bridge are listed in yellow.

USC UNIVERSIDADE DE SANTIAGO DE COMPOSTELA

ANNEX VII: SUPPLEMENTARY IMAGES

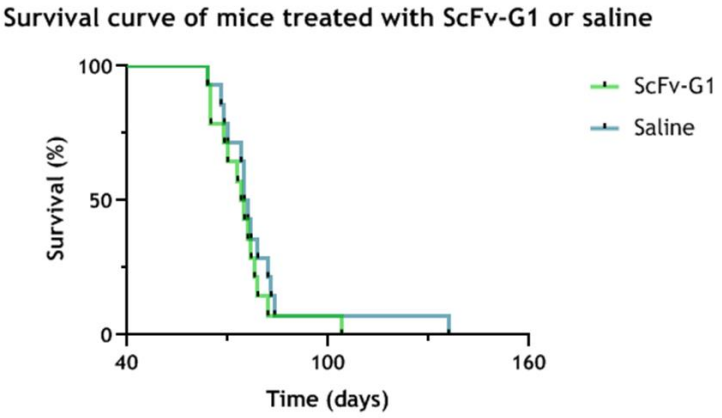


Figure S1. Survival curve of mice inoculated with 0,1% vole-adapted CWD inoculum and treated chronically with scFv-G1 including the outliers.

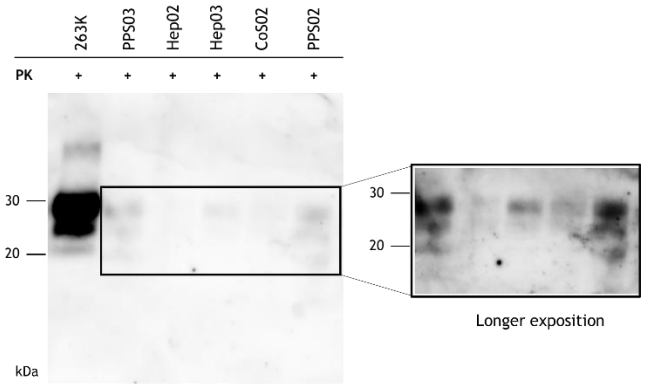


Figure S2. Comparison of the electrophoretic mobility of five recombinant prion strains inoculated in TgVole mice and 263K.

USC UNIVERSIDADE DE SANTIAGO DE COMPOSTELA

ANNEX VIII: CHROMATOGRAM AND MASS/CHARGE SPECTRA

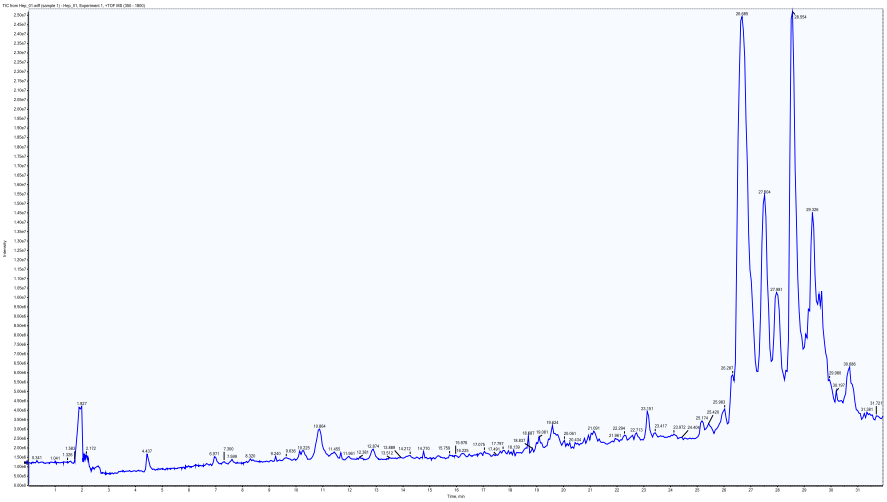


Figure 1. Chromatogram of Hep01

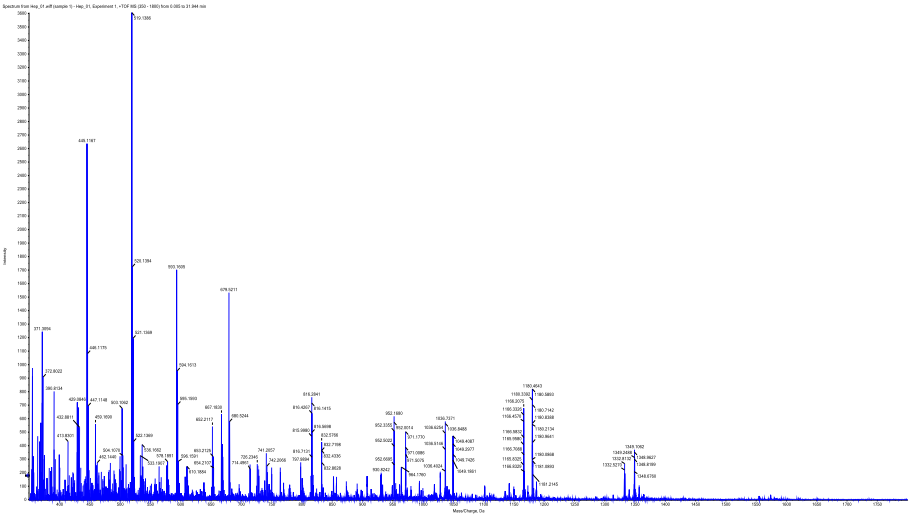


Figure 2. Mass/charge spectrum of Hep01

USC UNIVERSIDADE DE SANTIAGO DE COMPOSTELA

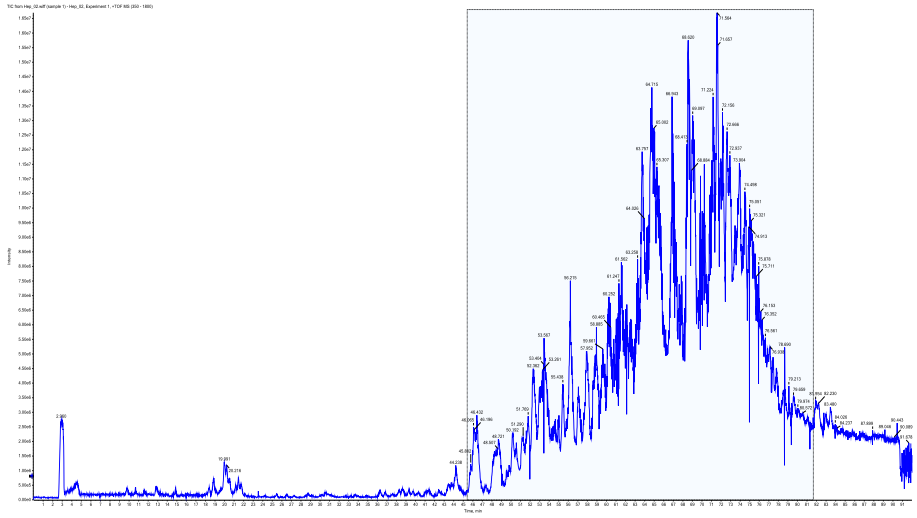


Figure 3. Chromatogram of Hep02

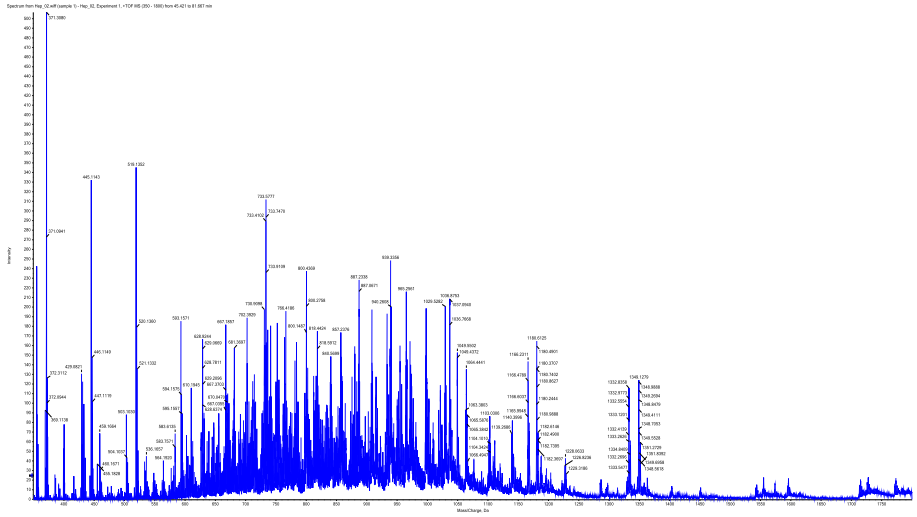


Figure 4. Mass/charge spectrum of Hep02

USC UNIVERSIDADE DE SANTIAGO DE COMPOSTELA

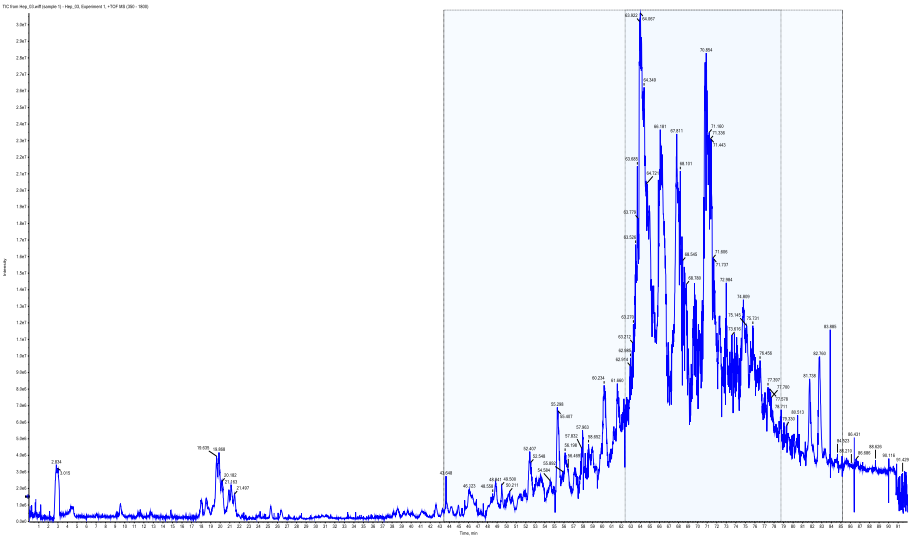


Figure 5. Chromatogram of Hep03

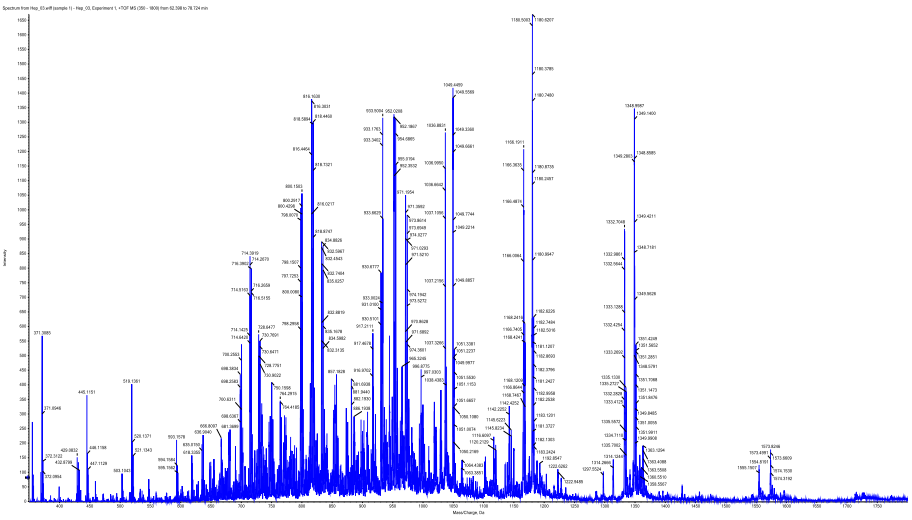


Figure 6. Mass/charge spectrum of Hep03

USC UNIVERSIDADE DE SANTIAGO DE COMPOSTELA

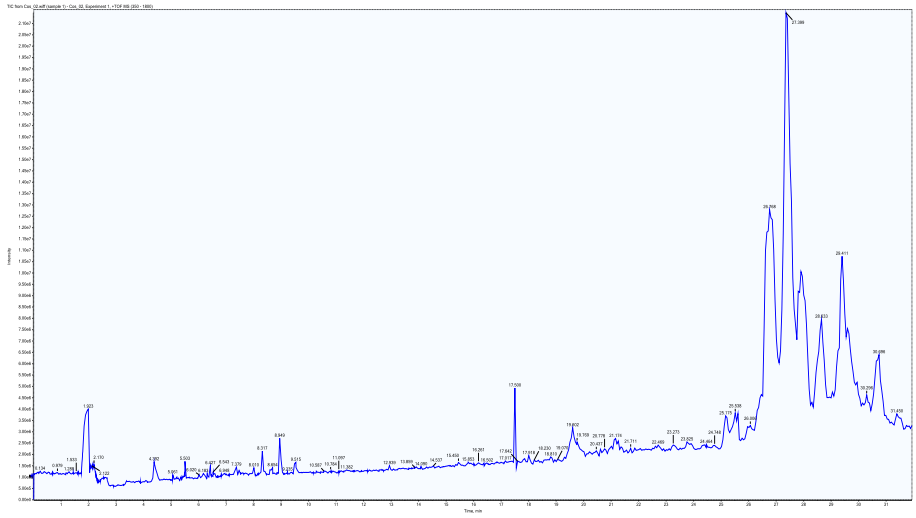


Figure 7. Chromatogram of CoS02

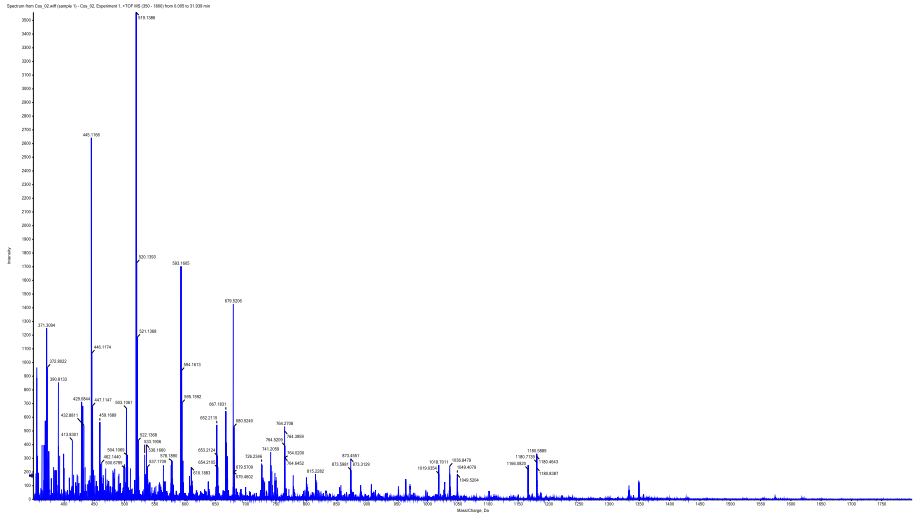


Figure 8. Mass/charge spectrum of CoS02

USC UNIVERSIDADE DE SANTIAGO DE COMPOSTELA

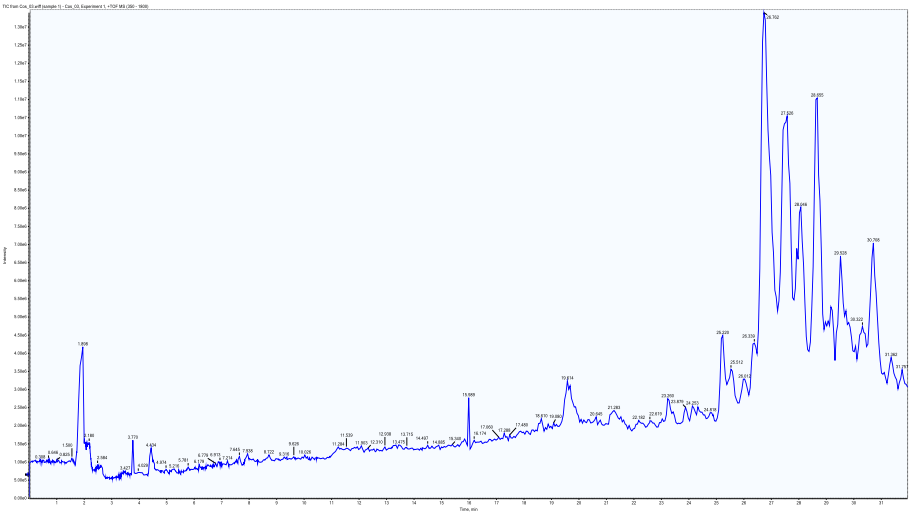


Figure 9. Chromatogram of CoS03

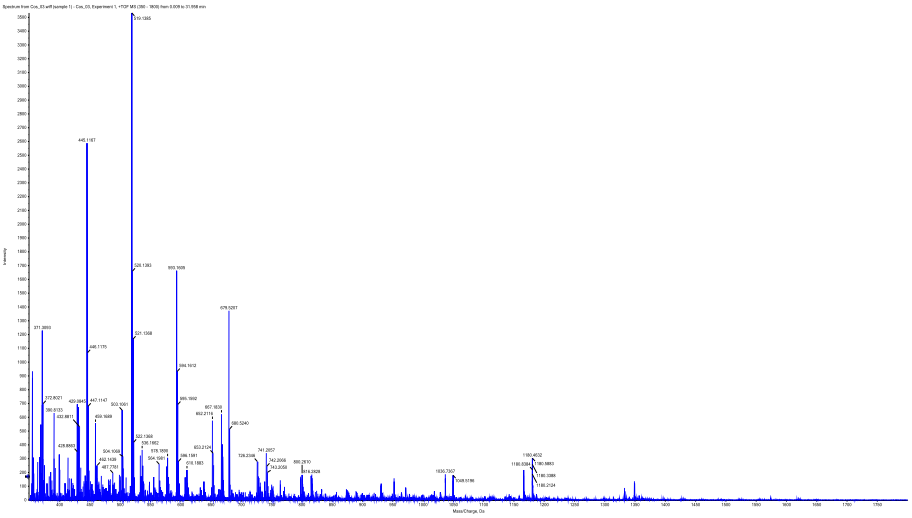


Figure 10. Mass/charge spectrum of CoS03

USC UNIVERSIDADE DE SANTIAGO DE COMPOSTELA

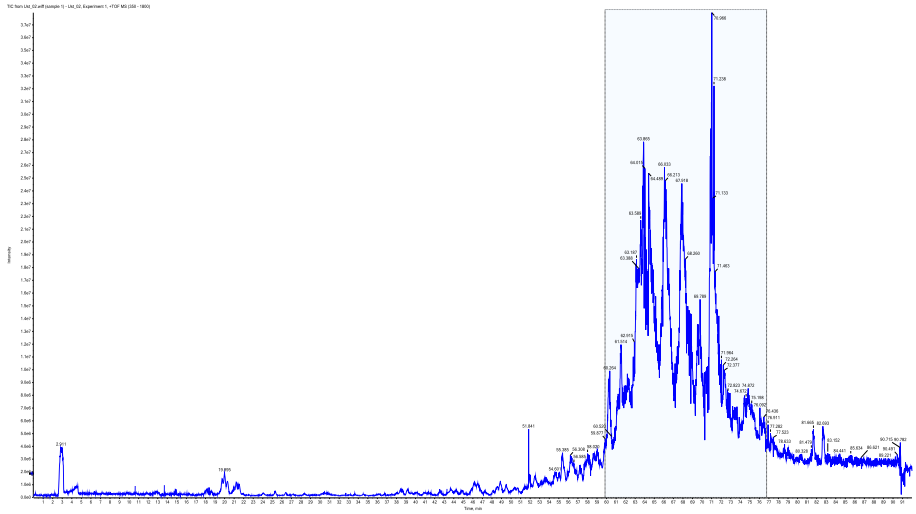


Figure 11. Chromatogram of Ust02

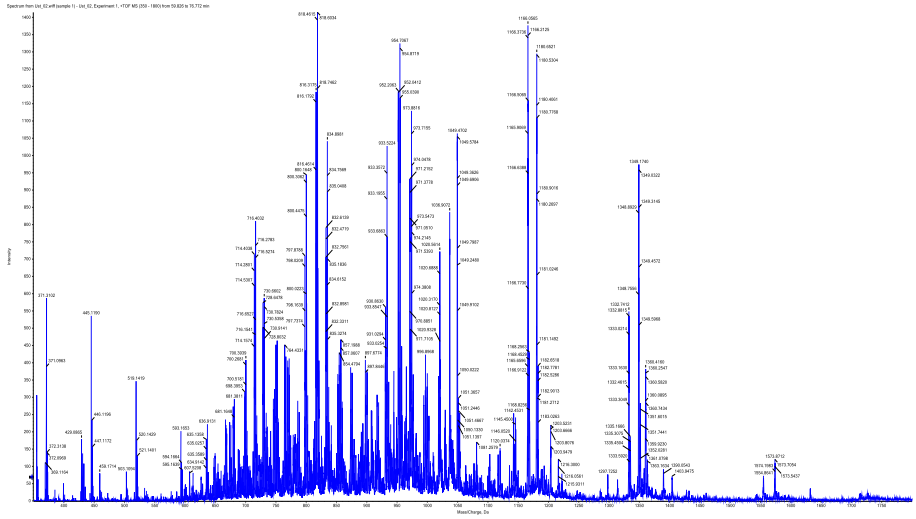


Figure 12. Mass/charge spectrum of Ust02

USC UNIVERSIDADE DE SANTIAGO DE COMPOSTELA

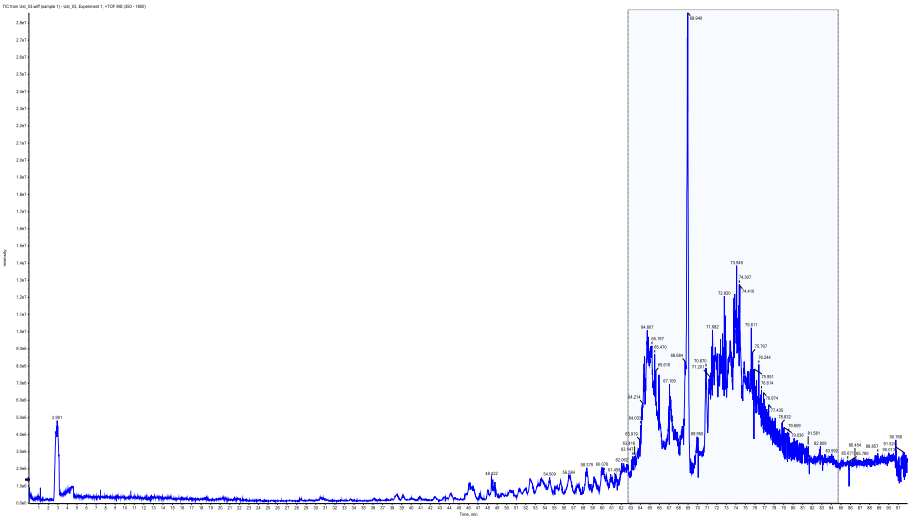


Figure 13. Chromatogram of Ust09

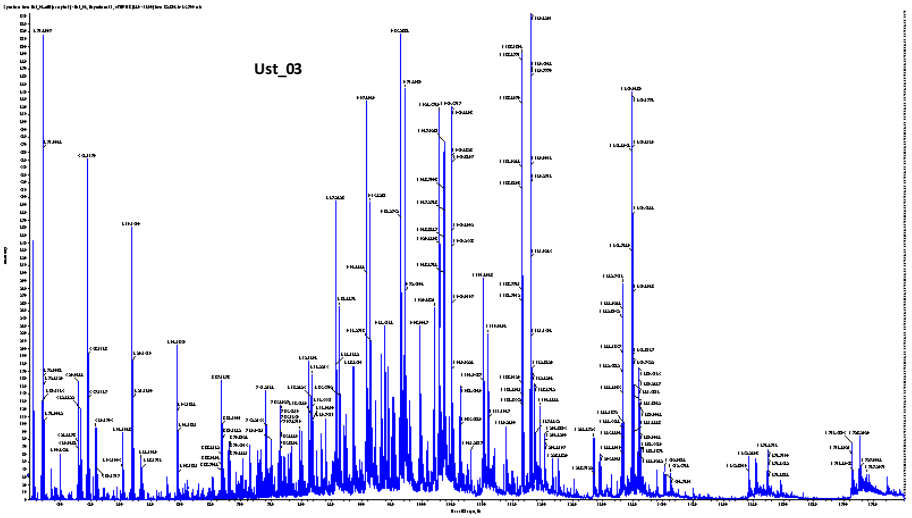


Figure 14. Mass/charge spectrum of Ust09

USC UNIVERSIDADE DE SANTIAGO DE COMPOSTELA

USC UNIVERSIDADE DE SANTIAGO DE COMPOSTELA

ANNEX IX: GAMES-HOWELL'S MULTIPLE COMPARISON *POST HOC* TEST OF THE CONFORMERS.

Table S1. Multiple comparison tests of the conformers from the first passage.

Games-Howell's multiple comparisons test	Hep01 vs. Hep02	Hep01 vs. Hep03	Hep01 vs. CoS01	Hep01 vs. CosS02	Hep01 vs. CoS03	Hep01 vs. PPS01	Hep01 vs. PPS02	Hep01 vs. PPS03	Hep02 vs. Hep03
Mean 1	363,4	363,4	363,4	363,4	363,4	363,4	363,4	363,4	220
Mean 2	220	105	280,4	144,4	111,2	292,2	141,3	166,7	105
Mean Diff,	143,4	258,4	83,03	219	252,2	71,26	222,1	196,7	115
95,00% CI of diff,	79,00 to 207,9	227,2 to 289,6	-84,78 to 250,8	187,6 to 250,4	217,5 to 286,9	-41,59 to 184,1	190,9 to 253,4	165,4 to 228,0	49,01 to 181,0
Significant?	Yes	Yes	No	Yes	Yes	No	Yes	Yes	Yes
Summary	***	****	ns	****	****	ns	****	****	**
Adjusted P Value	0,0004	<0,0001	0,3946	<0,0001	<0,0001	0,2667	<0,0001	<0,0001	0,0042

USC UNIVERSIDADE DE SANTIAGO DE COMPOSTELA

Hep02 vs. CoS01	Hep02 vs. CosS02	Hep02 vs. CoS03	Hep02 vs. PPS01	Hep02 vs. PPS02	Hep02 vs. PPS03	Hep03 vs. CoS01	Hep03 vs. CosS02	Hep03 vs. CoS03	Hep03 vs. PPS01	Hep03 vs. PPS02	Hep03 vs. PPS03	CoS01 vs. CosS02
220	220	220	220	220	220	105	105	105	105	105	105	280,4
280,4	144,4	111,2	292,2	141,3	166,7	280,4	144,4	111,2	292,2	141,3	166,7	144,4
-60,4	75,57	108,8	-72,17	78,71	53,29	-175,4	-39,43	-6,2	-187,2	-36,29	-61,71	136
-221,9 to 101,1	9,182 to 142,0	44,17 to 173,4	-185,3 to 40,94	12,52 to 144,9	-12,06 to 118,6	-347,2 to -3,612	-49,72 to -29,14	-34,54 to 22,14	-302,4 to -71,93	-46,73 to -25,84	-76,89 to -46,54	-36,16 to 308,1
No	Yes	Yes	No	Yes	No	Yes	Yes	No	Yes	Yes	Yes	No
ns	*	**	ns	*	ns	*	****	ns	**	****	****	ns
0,7189	0,0296	0,0033	0,31	0,0245	0,1115	0,0466	<0,0001	0,9616	0,0062	<0,0001	<0,0001	0,1071

CoS01 vs. CoS03	CoS01 vs. PPS01	CoS01 vs. PPS02	CoS01 vs. PPS03	CosS02 vs. CoS03	CosS02 vs. PPS01	CosS02 vs. PPS02	CosS02 vs. PPS03	CoS03 vs. PPS01	CoS03 vs. PPS02	CoS03 vs. PPS03	PPS01 vs. PPS02	PPS01 vs. PPS03
280,4	280,4	280,4	280,4	144,4	144,4	144,4	144,4	111,2	111,2	111,2	292,2	292,2
111,2	292,2	141,3	166,7	111,2	292,2	141,3	166,7	292,2	141,3	166,7	141,3	166,7
169,2	-11,77	139,1	113,7	33,23	-147,7	3,143	-22,29	-181	-30,09	-55,51	150,9	125,5
-0,1375 to 338,5	-176,3 to 152,7	-32,85 to 311,1	-57,45 to 284,8	3,795 to 62,66	-263,2 to -32,25	-3,872 to 10,16	-36,83 to -7,742	-294,7 to -67,28	-58,86 to -1,309	-83,26 to -27,77	35,51 to 266,3	10,67 to 240,2
No	No	No	No	Yes	Yes	No	Yes	Yes	Yes	Yes	Yes	Yes
ns	ns	ns	ns	*	*	ns	**	**	*	**	*	*
0,0501	>0,9999	0,0997	0,1801	0,0324	0,0181	0,7153	0,0051	0,0059	0,0423	0,0011	0,0164	0,0348

PPS02 vs. PPS03	141,3	166,7	-25,43	-40,02 to -10,84	Yes	**	0,0015

USC UNIVERSIDADE DE SANTIAGO DE COMPOSTELA

Table S2. Multiple comparison tests of the conformers from the second passage.

Games-Howell's multiple comparisons test	Hep01 vs. Hep02	Hep01 vs. Hep03	Hep01 vs. CoS01	Hep01 vs. CosS02	Hep01 vs. CoS03	Hep01 vs. PPS01	Hep01 vs. PPS02	Hep01 vs. PPS03	Hep02 vs. Hep03	Hep02 vs. CoS01	Hep02 vs. CosS02
Mean 1	86	86	86	86	86	86	86	86	83,6	83,6	83,6
Mean 2	83,6	94,83	101,5	102,3	73,67	105,8	78,67	103,5	94,83	101,5	102,3
Mean Diff,	2,4	-8,833	-15,5	-16,33	12,33	-19,83	7,333	-17,5	-11,23	-17,9	-18,73
95,00% CI of diff,	-21,93 to 26,73	-35,04 to 17,37	-40,01 to 9,013	-50,65 to 17,99	-11,86 to 36,53	-44,07 to 4,406	-16,86 to 31,53	-41,71 to 6,712	-31,66 to 9,197	-33,82 to -1,982	-51,55 to 14,08
Significant?	No	No	No	No	No	No	No	No	No	Yes	No
Summary	ns	ns	ns	ns	ns	ns	ns	ns	ns	*	ns
Adjusted P Value	>0,9999	0,906	0,322	0,6442	0,4951	0,1161	0,9054	0,1853	0,4574	0,0258	0,3661

USC UNIVERSIDADE DE SANTIAGO DE COMPOSTELA

Hep02 vs. CoS03	Hep02 vs. PPS01	Hep02 vs. PPS02	Hep02 vs. PPS03	Hep03 vs. CoS01	Hep03 vs. CosS02	Hep03 vs. CoS03	Hep03 vs. PPS01	Hep03 vs. PPS02	Hep03 vs. PPS03	CoS01 vs. CosS02	CoS01 vs. CoS03	CoS01 vs. PPS01
83,6	83,6	83,6	83,6	94,83	94,83	94,83	94,83	94,83	94,83	101,5	101,5	101,5
73,67	105,8	78,67	103,5	101,5	102,3	73,67	105,8	78,67	103,5	102,3	73,67	105,8
9,933	-22,23	4,933	-19,9	-6,667	-7,5	21,17	-11	16,17	-8,667	-0,8333	27,83	-4,333
-3,681 to 23,55	-35,39 to -9,080	-8,825 to 18,69	-33,22 to -6,576	-27,55 to 14,22	-40,72 to 25,72	1,094 to 41,24	-31,01 to 9,012	-3,938 to 36,27	-28,69 to 11,36	-33,52 to 31,86	12,80 to 42,87	-19,02 to 10,35
No	Yes	No	Yes	No	No	Yes	No	No	No	No	Yes	No
ns	**	ns	**	ns	ns	*	ns	ns	ns	ns	***	ns
0,204	0,0023	0,8579	0,0048	0,9211	0,9855	0,0383	0,4255	0,1339	0,6727	>0,9999	0,0008	0,939

CoS01 vs. PPS02	CoS01 vs. PPS03	CosS02 vs. CoS03	CosS02 vs. PPS01	CosS02 vs. PPS02	CosS02 vs. PPS03	CoS03 vs. PPS01	CoS03 vs. PPS02	CoS03 vs. PPS03	PPS01 vs. PPS02	PPS01 vs. PPS03	PPS02 vs. PPS03
101,5	101,5	102,3	102,3	102,3	102,3	73,67	73,67	73,67	105,8	105,8	78,67
78,67	103,5	73,67	105,8	78,67	103,5	105,8	78,67	103,5	78,67	103,5	103,5
22,83	-2	28,67	-3,5	23,67	-1,167	-32,17	-5	-29,83	27,17	2,333	-24,83
7,684 to 37,98	-16,82 to 12,82	-4,219 to 61,55	-36,52 to 29,52	-9,189 to 56,52	-34,13 to 31,79	-43,54 to -20,79	-17,31 to 7,308	-41,49 to -18,17	15,55 to 38,79	-8,513 to 13,18	-36,72 to -12,94
Yes	No	No	No	No	No	Yes	No	Yes	Yes	No	Yes
**	ns	ns	ns	ns	ns	****	ns	****	****	ns	***
0,0037	0,9996	0,0887	0,9997	0,18	>0,9999	<0,0001	0,8017	<0,0001	<0,0001	0,9925	0,0002

USC

Table 3. Multiple comparison tests of the first and second passages of the same conformer.

Tamhane's T2 multiple comparisons test	Hep01 vs. Hep01	Hep02 vs. Hep02	Hep03 vs. Hep03	CoS01 vs. CoS01	CosS02 vs. CosS02	CoS03 vs. CoS03	PPS01 vs. PPS01	PPS02 vs. PPS02	PPS03 vs. PPS03
Mean 1	363,4	220	105	280,4	144,4	111,2	292,2	141,3	166,7
Mean 2	86	83,6	94,83	101,5	102,3	73,67	105,8	78,67	103,5
Mean Diff,	277,4	136,4	10,17	178,9	42,1	37,53	186,3	62,62	63,21
95,00% CI of diff,	247,1 to 307,7	73,71 to 199,1	-8,441 to 28,77	7,511 to 350,3	9,992 to 74,20	10,62 to 64,44	75,57 to 297,1	52,66 to 72,58	49,55 to 76,88
Significant?	Yes	Yes	No	Yes	Yes	Yes	Yes	Yes	Yes
Summary	****	**	ns	*	*	*	**	****	****
Adjusted P Value	<0,0001	0,0012	0,477	0,0429	0,0152	0,0112	0,0049	<0,0001	<0,0001

USC UNIVERSIDADE DE SANTIAGO DE COMPOSTELA

ANNEX X: ETHICS COMMITTEE REPORT / INFOME DEL COMITÉ DE ÉTICA

USC UNIVERSIDADE DE SANTIAGO DE COMPOSTELA

XUNTA DE GALICIA
DELEGACIÓN TERRITORIAL
DA CORUÑA
Xefatura Territorial
da Consellería do Medio Rural

Edificio Administrativo Monelos
Vicente Ferrer, 2
15071 A Coruña

galicia

REXISTRO XERAL DA XUNTA DE GALICIA
REXISTRO DO EDIFICIO ADMINISTRATIVO DA CORUÑA
A CORUÑA

SAÍDA 130925 / RX 1805782 Data: 09/11/2016 17:20:41

José Manuel Cifuentes Martínez
Departamento de Anatomía
Facultade de Veterinaria
Campus Universitario
27002 Lugo

NOTIFICACIÓN DE RESOLUCIÓN DE AUTORIZACIÓN DE PROXECTOS DE EXPERIMENTACIÓN ANIMAL

Expediente núm.: 15005/16/006
Interesado: Jesús Rodriguez Requena
Procedemento: resolución de autorización

Data de inicio: 26-10-2016
Forma de inicio: solicitude do interesado

Notificolle que con data 8 de novembro de 2016, o xefe territorial da Consellería do Medio Rural emitiu unha resolución de autorización do proxecto de experimentación animal, cuxo texto íntegro é o seguinte:

ANTECEDENTES

A persoa interesada, como representante do centro CIMUS (Universidade de Santiago de Compostela), presentou con data 26-10-2016 e rexistro de entrada 126861 RX 2805241, unha solicitude para a realización do proxecto de experimentación animal cuxos datos se detallan a continuación:

Denominación do proxecto: Bioensaios co axente do scrapie utilizando ratos
Nome do centro usuario: CIMUS (USC)
Persoa responsable do proxecto: Jesús Rodriguez Requena
Establecemento onde se realizarán os procedementos do proxecto (ou lugar xeográfico no caso de traballos de campo): Facultade de Medicina
Clasificación do proxecto : Tipo I ☐ Tipo II ☐ Tipo III ☒

CONSIDERACIÓNS LEGAIS E TÉCNICAS

1. O Real decreto 53/2013, de 1 de febreiro (BOE 34, do 8 de febreiro), polo que se establecen as normas básicas aplicables para a protección dos animais utilizados en experimentación e outros fins científicos, incluíndo a docencia, establece no seu artigo 33 as condicións de autorizacións dos proxectos con animais de experimentación.

USC UNIVERSIDADE DE SANTIAGO DE COMPOSTELA

2. O artigo 88 da Lei 39/2015, de 1 de outubro, do procedemento administrativo común das administracións públicas (BOE 236, do 2 de outubro de 2015), establece que a resolución que poña fin o procedemento decidirá todas as cuestións expostas polos interesados e aquelas outras derivadas deste.

3. O Servizo de Gandaría da Coruña revisou a documentación achegada na solicitude e o resultado favorable da avaliación do proxecto, realizada polo órgano habilitado da Sección de Experimentación Animal do Comité de Bioética da Universidade de Santiago de Compostela.

Esta xefatura territorial é competente para ditar unha resolución, de conformidade co artigo 11 do Decreto 245/2009 de 3 de abril, polo que se regulan as delegacións territoriais da Xunta de Galicia e o Decreto 166/2015, de 13 de novembro, polo que se aproba a estrutura orgánica da Consellería do Medio Rural.

De acordo con todo o indicado, RESOLVO:

1. Autorizar o proxecto solicitado.
2. Notificarlle esta resolución á persoa interesada.

O mencionado proxecto precisa someterse a unha avaliación retrospectiva aos tres anos da concesión desta autorización.

A autorización deste proxecto terá unha duración de 5 anos, transcorridos os cales, deberá ser renovada esta autorización.

A citada autorización é unicamente válida nas condicións que figuran no expediente. Ante calquera cambio significativo no proxecto que poida ter efectos negativos sobre o benestar dos animais, deberá solicitar a confirmación da autorización ao Servizo Provincial de Gandaría.

Esta autorización poderá ser suspendida, no caso de que o proxecto non se leve a cabo de acordo coas condicións de autorización e retirala, previo expediente tramitado ao que se lle dará audiencia.

Contra a presente resolución, que non pon fin á vía administrativa, poderá interpor recurso de alzada ante a conselleira de Medio Rural no prazo dun mes contado a partir da recepción da notificación da presente resolución, conforme coa Lei 39/2015, de 1 de outubro, (BOE 236, do 2 de outubro de 2015), do procedemento administrativo común das administracións públicas.

A Coruña, 9 de novembro de 2016
O xefe do Servizo de Gandaría

Eugenio Romero Senande

USC UNIVERSIDADE DE SANTIAGO DE COMPOSTELA

ANNEX XI: COPYRIGHT PERMISSIONS

USC UNIVERSIDADE DE SANTIAGO DE COMPOSTELA

Marketplace

This is a License Agreement between Nuria López Lorenzo ("User") and Copyright Clearance Center, Inc. ("CCC") on behalf of the Rightsholder identified in the order details below. The license consists of the order details, the Marketplace Permissions General Terms and Conditions below, and any Rightsholder Terms and Conditions which are included below.

All payments must be made in full to CCC in accordance with the Marketplace Permissions General Terms and Conditions below.

Order Date	08-Aug-2023	Type of Use	Republish in a thesis/dissertation
Order License ID	1383935-1		
ISSN	2379-3708	Publisher	American Society for Clinical Investigation
		Portion	Image/photo/illustration

LICENSED CONTENT

Publication Title	JCI insight	Rightsholder	American Society for Clinical Investigation
Article Title	Antisense oligonucleotides extend survival of prion-infected mice.	Publication Type	e-Journal
		Issue	16
Author/Editor	American Society for Clinical Investigation,	Volume	5
		URL	https://insight.jci.org/
Date	01/01/2016		
Language	English		
Country	United States of America		

REQUEST DETAILS

Portion Type	Image/photo/illustration	Distribution	Worldwide
Number of Images / Photos / Illustrations	1	Translation	Original language of publication
Format (select all that apply)	Print	Copies for the Disabled?	No
		Minor Editing Privileges?	Yes
Who Will Republish the Content?	Academic institution	Incidental Promotional Use?	No
Duration of Use	Life of current edition	Currency	EUR
Lifetime Unit Quantity	Up to 499		
Rights Requested	Main product		

NEW WORK DETAILS

Title	Therapeutical approaches for prion diseases and characterization of recombinant prion strains from different perspectives	Institution Name	University of Santiago de Compostela
		Expected Presentation Date	2023-10-26
Instructor Name	Nuria López Lorenzo		

ADDITIONAL DETAILS

Order Reference Number	N/A	The Requesting Person/Organization to Appear on the License	Nuria López Lorenzo

REQUESTED CONTENT DETAILS

Title, Description or Numeric Reference of the Portion(s)	Figure 4	**Title of the Article/Chapter the Portion Is From**	Antisense oligonucleotides extend survival of prion-infected mice.
Editor of Portion(s)	Raymond et al.	**Author of Portion(s)**	Raymond et al.
Volume / Edition	5	**Issue, if Republishing an Article From a Serial**	16
Page or Page Range of Portion	7	**Publication Date of Portion**	2019-08-22

Marketplace Permissions General Terms and Conditions

The following terms and conditions ("General Terms"), together with any applicable Publisher Terms and Conditions, govern User's use of Works pursuant to the Licenses granted by Copyright Clearance Center, Inc. ("CCC") on behalf of the applicable Rightsholders of such Works through CCC's applicable Marketplace transactional licensing services (each, a "Service").

1) **Definitions.** For purposes of these General Terms, the following definitions apply:

"License" is the licensed use the User obtains via the Marketplace platform in a particular licensing transaction, as set forth in the Order Confirmation.

"Order Confirmation" is the confirmation CCC provides to the User at the conclusion of each Marketplace transaction. "Order Confirmation Terms" are additional terms set forth on specific Order Confirmations not set forth in the General Terms that can include terms applicable to a particular CCC transactional licensing service and/or any Rightsholder-specific terms.

"Rightsholder(s)" are the holders of copyright rights in the Works for which a User obtains licenses via the Marketplace platform, which are displayed on specific Order Confirmations.

"Terms" means the terms and conditions set forth in these General Terms and any additional Order Confirmation Terms collectively.

"User" or "you" is the person or entity making the use granted under the relevant License. Where the person accepting the Terms on behalf of a User is a freelancer or other third party who the User authorized to accept the General Terms on the User's behalf, such person shall be deemed jointly a User for purposes of such Terms.

"Work(s)" are the copyright protected works described in relevant Order Confirmations.

2) **Description of Service.** CCC's Marketplace enables Users to obtain Licenses to use one or more Works in accordance with all relevant Terms. CCC grants Licenses as an agent on behalf of the copyright rightsholder identified in the relevant Order Confirmation.

3) **Applicability of Terms.** The Terms govern User's use of Works in connection with the relevant License. In the event of any conflict between General Terms and Order Confirmation Terms, the latter shall govern. User acknowledges that Rightsholders have complete discretion whether to grant any permission, and whether to place any limitations on any grant, and that CCC has no right to supersede or to modify any such discretionary act by a Rightsholder.

4) **Representations; Acceptance.** By using the Service, User represents and warrants that User has been duly authorized by the User to accept, and hereby does accept, all Terms.

5) **Scope of License; Limitations and Obligations.** All Works and all rights therein, including copyright rights, remain the sole and exclusive property of the Rightsholder. The License provides only those rights expressly set forth in the terms and conveys no other rights in any Works

6) **General Payment Terms.** User may pay at time of checkout by credit card or choose to be invoiced. If the User chooses to be invoiced, the User shall: (i) remit payments in the manner identified on specific invoices, (ii) unless otherwise specifically stated in an Order Confirmation or separate written agreement, Users shall remit payments upon receipt of the relevant invoice from CCC, either by delivery or notification of availability of the invoice via the Marketplace platform, and (iii) if the User does not pay the invoice within 30 days of receipt, the User may incur a service charge of 1.5% per month or the maximum rate allowed by applicable law, whichever is less. While User may exercise the rights in the License immediately upon receiving the Order Confirmation, the License is automatically revoked and is null and void, as if it had never been issued, if CCC does not receive complete payment on a timely basis.

7) **General Limits on Use.** Unless otherwise provided in the Order Confirmation, any grant of rights to User (i) involves only the rights set forth in the Terms and does not include subsequent or additional uses, (ii) is non-exclusive and non-transferable, and (iii) is subject to any and all limitations and restrictions (such as, but not limited to, limitations on duration of use or circulation) included in the Terms. Upon completion of the licensed use as set forth in the Order Confirmation, User shall either secure a new permission for further use of the Work(s) or immediately cease any new use of the Work(s) and shall render inaccessible (such as by deleting or by removing or severing links or other locators) any further copies of the Work. User may only make alterations to the Work if and as expressly set forth in the Order Confirmation. No Work may be used in any way that is unlawful, including without limitation if such use would violate applicable sanctions laws or regulations, would be defamatory, violate the rights of third parties (including such third parties' rights of copyright, privacy, publicity, or other tangible or intangible property), or is otherwise illegal, sexually explicit, or obscene. In addition, User may not conjoin a Work with any other material that may result in damage to the reputation of the Rightsholder. Any unlawful use will render any licenses hereunder null and void. User agrees to inform CCC if it becomes aware of any infringement of any rights in a Work and to cooperate with any reasonable request of CCC or the Rightsholder in connection therewith.

8) **Third Party Materials.** In the event that the material for which a License is sought includes third party materials (such as photographs, illustrations, graphs, inserts and similar materials) that are identified in such material as having been used by permission (or a similar indicator), User is responsible for identifying, and seeking separate licenses (under this Service, if available, or otherwise) for any of such third party materials; without a separate license, User may not use such third party materials via the License.

9) **Copyright Notice.** Use of proper copyright notice for a Work is required as a condition of any License granted under the Service. Unless otherwise provided in the Order Confirmation, a proper copyright notice will read substantially as follows: "Used with permission of [Rightsholder's name], from [Work's title, author, volume, edition number and year of copyright]; permission conveyed through Copyright Clearance Center, Inc." Such notice must be provided in a reasonably legible font size and must be placed either on a cover page or in another location that any person, upon gaining access to the material which is the subject of a permission, shall see, or in the case of republication Licenses, immediately adjacent to the Work as used (for example, as part of a by-line or footnote) or in the place where substantially all other credits or notices for the new work containing the republished Work are located. Failure to include the required notice results in loss to the Rightsholder and CCC, and the User shall be liable to pay liquidated damages for each such failure equal to twice the use fee specified in the Order Confirmation, in addition to the use fee itself and any other fees and charges specified.

10) **Indemnity.** User hereby indemnifies and agrees to defend the Rightsholder and CCC, and their respective employees and directors, against all claims, liability, damages, costs, and expenses, including legal fees and expenses, arising out of any use of a Work beyond the scope of the rights granted herein and in the Order Confirmation, or any use of a Work which has been altered in any unauthorized way by User, including claims of defamation or infringement of rights of copyright, publicity, privacy, or other tangible or intangible property.

11) **Limitation of Liability.** UNDER NO CIRCUMSTANCES WILL CCC OR THE RIGHTSHOLDER BE LIABLE FOR ANY DIRECT, INDIRECT, CONSEQUENTIAL, OR INCIDENTAL DAMAGES (INCLUDING WITHOUT LIMITATION DAMAGES FOR LOSS OF BUSINESS PROFITS OR INFORMATION, OR FOR BUSINESS INTERRUPTION) ARISING OUT OF THE USE OR INABILITY TO USE A WORK, EVEN IF ONE OR BOTH OF THEM HAS BEEN ADVISED OF THE POSSIBILITY OF SUCH DAMAGES. In any event, the total liability of the Rightsholder and CCC (including their respective employees and directors) shall not exceed the total amount actually paid by User for the relevant License. User assumes full liability for the actions and omissions of its principals, employees, agents, affiliates, successors, and assigns.

12) **Limited Warranties.** THE WORK(S) AND RIGHT(S) ARE PROVIDED "AS IS." CCC HAS THE RIGHT TO GRANT TO USER THE RIGHTS GRANTED IN THE ORDER CONFIRMATION DOCUMENT. CCC AND THE RIGHTSHOLDER DISCLAIM ALL OTHER WARRANTIES RELATING TO THE WORK(S) AND RIGHT(S), EITHER EXPRESS OR IMPLIED, INCLUDING WITHOUT LIMITATION IMPLIED WARRANTIES OF MERCHANTABILITY OR FITNESS FOR A PARTICULAR PURPOSE. ADDITIONAL RIGHTS MAY BE REQUIRED TO USE ILLUSTRATIONS, GRAPHS, PHOTOGRAPHS, ABSTRACTS, INSERTS, OR OTHER PORTIONS OF THE WORK (AS OPPOSED TO THE ENTIRE WORK) IN A MANNER CONTEMPLATED BY USER; USER UNDERSTANDS AND AGREES THAT NEITHER CCC NOR THE RIGHTSHOLDER MAY HAVE SUCH ADDITIONAL RIGHTS TO GRANT.

13) **Effect of Breach.** Any failure by User to pay any amount when due, or any use by User of a Work beyond the scope of the License set forth in the Order Confirmation and/or the Terms, shall be a material breach of such License. Any breach not cured within 10 days of written notice thereof shall result in immediate termination of such License without further notice. Any unauthorized (but licensable) use of a Work that is terminated immediately upon notice thereof may be liquidated by payment of the Rightsholder's ordinary license price therefor; any unauthorized (and unlicensable) use that is not terminated immediately for any reason (including, for example, because materials containing the Work cannot reasonably be recalled) will be subject to all remedies available at law or in equity, but in no event to a payment of less than three times the Rightsholder's ordinary license price for the most closely analogous licensable use plus Rightsholder's and/or CCC's costs and expenses incurred in collecting such payment.

14) **Additional Terms for Specific Products and Services.** If a User is making one of the uses described in this Section 14, the additional terms and conditions apply:

a) ***Print Uses of Academic Course Content and Materials (photocopies for academic coursepacks or classroom handouts).*** For photocopies for academic coursepacks or classroom handouts the following additional terms apply:

i) The copies and anthologies created under this License may be made and assembled by faculty members individually or at their request by on-campus bookstores or copy centers, or by off-campus copy shops and other similar entities.

ii) No License granted shall in any way: (i) include any right by User to create a substantively non-identical copy of the Work or to edit or in any other way modify the Work (except by means of deleting material immediately preceding or following the entire portion of the Work copied) (ii) permit "publishing ventures" where any particular anthology would be systematically marketed at multiple institutions.

iii) Subject to any Publisher Terms (and notwithstanding any apparent contradiction in the Order Confirmation arising from data provided by User), any use authorized under the academic pay-per-use service is limited as follows:

A) any License granted shall apply to only one class (bearing a unique identifier as assigned by the institution, and thereby including all sections or other subparts of the class) at one institution;

B) use is limited to not more than 25% of the text of a book or of the items in a published collection of essays, poems or articles;

C) use is limited to no more than the greater of (a) 25% of the text of an issue of a journal or other periodical or (b) two articles from such an issue;

D) no User may sell or distribute any particular anthology, whether photocopied or electronic, at more than one institution of learning;

E) in the case of a photocopy permission, no materials may be entered into electronic memory by User except in order to produce an identical copy of a Work before or during the academic term (or analogous period) as to which any particular permission is granted. In the event that User shall choose to retain materials that are the subject of a photocopy permission in electronic memory for purposes of producing identical copies more than one day after such retention (but still within the scope of any permission granted), User must notify CCC of such fact in the applicable permission request and such retention shall constitute one copy actually sold for purposes of calculating permission fees due; and

F) any permission granted shall expire at the end of the class. No permission granted shall in any way include any right by User to create a substantively non-identical copy of the Work or to edit or in any other way modify the Work (except by means of deleting material immediately preceding or following the entire portion of the Work copied).

iv) Books and Records; Right to Audit. As to each permission granted under the academic pay-per-use Service, User shall maintain for at least four full calendar years books and records sufficient for CCC to determine the numbers of copies made by User under such permission. CCC and any representatives it may designate shall have the right to audit such books and records at any time during User's ordinary business hours, upon two days' prior notice. If any such audit shall determine that User shall have underpaid for, or underreported, any photocopies sold or by three percent (3%) or more, then User shall bear all the costs of any such audit; otherwise, CCC shall bear the costs of any such audit. Any amount determined by such audit to have been underpaid by User shall immediately be paid to CCC by User, together with interest thereon at the rate of 10% per annum from the date such amount was originally due. The provisions of this paragraph shall survive the termination of this License for any reason.

b) ***Digital Pay-Per-Uses of Academic Course Content and Materials (e-coursepacks, electronic reserves, learning management systems, academic institution intranets).*** For uses in e-coursepacks, posts in electronic reserves, posts in learning management systems, or posts on academic institution intranets, the following additional terms apply:

i) The pay-per-uses subject to this Section 14(b) include:

A) **Posting e-reserves, course management systems, e-coursepacks for text-based content,** which grants authorizations to import requested material in electronic format, and allows electronic access to this material to members of a designated college or university class, under the direction of an instructor designated by the college or university, accessible only under appropriate electronic controls (e.g., password);

B) **Posting e-reserves, course management systems, e-coursepacks for material consisting of photographs or other still images not embedded in text,** which grants not only the authorizations described in Section 14(b)(i)(A) above, but also the following authorization: to include the requested material in course materials

for use consistent with Section 14(b)(i)(A) above, including any necessary resizing, reformatting or modification of the resolution of such requested material (provided that such modification does not alter the underlying editorial content or meaning of the requested material, and provided that the resulting modified content is used solely within the scope of, and in a manner consistent with, the particular authorization described in the Order Confirmation and the Terms), but not including any other form of manipulation, alteration or editing of the requested material;

C) **Posting e-reserves, course management systems, e-coursepacks or other academic distribution for audiovisual content,** which grants not only the authorizations described in Section 14(b)(i)(A) above, but also the following authorizations: (i) to include the requested material in course materials for use consistent with Section 14(b)(i)(A) above; (ii) to display and perform the requested material to such members of such class in the physical classroom or remotely by means of streaming media or other video formats; and (iii) to "clip" or reformat the requested material for purposes of time or content management or ease of delivery, provided that such "clipping" or reformatting does not alter the underlying editorial content or meaning of the requested material and that the resulting material is used solely within the scope of, and in a manner consistent with, the particular authorization described in the Order Confirmation and the Terms. Unless expressly set forth in the relevant Order Conformation, the License does not authorize any other form of manipulation, alteration or editing of the requested material.

ii) Unless expressly set forth in the relevant Order Confirmation, no License granted shall in any way: (i) include any right by User to create a substantively non-identical copy of the Work or to edit or in any other way modify the Work (except by means of deleting material immediately preceding or following the entire portion of the Work copied or, in the case of Works subject to Sections 14(b)(1)(B) or (C) above, as described in such Sections) (ii) permit "publishing ventures" where any particular course materials would be systematically marketed at multiple institutions.

iii) Subject to any further limitations determined in the Rightsholder Terms (and notwithstanding any apparent contradiction in the Order Confirmation arising from data provided by User), any use authorized under the electronic course content pay-per-use service is limited as follows:

A) any License granted shall apply to only one class (bearing a unique identifier as assigned by the institution, and thereby including all sections or other subparts of the class) at one institution;

B) use is limited to not more than 25% of the text of a book or of the items in a published collection of essays, poems or articles;

C) use is limited to not more than the greater of (a) 25% of the text of an issue of a journal or other periodical or (b) two articles from such an issue;

D) no User may sell or distribute any particular materials, whether photocopied or electronic, at more than one institution of learning;

E) electronic access to material which is the subject of an electronic-use permission must be limited by means of electronic password, student identification or other control permitting access solely to students and instructors in the class;

F) User must ensure (through use of an electronic cover page or other appropriate means) that any person, upon gaining electronic access to the material, which is the subject of a permission, shall see:

- a proper copyright notice, identifying the Rightsholder in whose name CCC has granted permission,
- a statement to the effect that such copy was made pursuant to permission,
- a statement identifying the class to which the material applies and notifying the reader that the material has been made available electronically solely for use in the class, and
- a statement to the effect that the material may not be further distributed to any person outside the class, whether by copying or by transmission and whether electronically or in paper form, and User must also ensure that such cover page or other means will print out in the event that the person accessing the material chooses to print out the material or any part thereof.

G) any permission granted shall expire at the end of the class and, absent some other form of authorization, User is thereupon required to delete the applicable material from any electronic storage or to block electronic access to the applicable material.

iv) Uses of separate portions of a Work, even if they are to be included in the same course material or the same university or college class, require separate permissions under the electronic course content pay-per-use Service.

Unless otherwise provided in the Order Confirmation, any grant of rights to User is limited to use completed no later than the end of the academic term (or analogous period) as to which any particular permission is granted.

v) Books and Records; Right to Audit. As to each permission granted under the electronic course content Service, User shall maintain for at least four full calendar years books and records sufficient for CCC to determine the numbers of copies made by User under such permission. CCC and any representatives it may designate shall have the right to audit such books and records at any time during User's ordinary business hours, upon two days' prior notice. If any such audit shall determine that User shall have underpaid for, or underreported, any electronic copies used by three percent (3%) or more, then User shall bear all the costs of any such audit; otherwise, CCC shall bear the costs of any such audit. Any amount determined by such audit to have been underpaid by User shall immediately be paid to CCC by User, together with interest thereon at the rate of 10% per annum from the date such amount was originally due. The provisions of this paragraph shall survive the termination of this license for any reason.

c) ***Pay-Per-Use Permissions for Certain Reproductions (Academic photocopies for library reserves and interlibrary loan reporting) (Non-academic internal/external business uses and commercial document delivery).*** The License expressly excludes the uses listed in Section (c)(i)-(v) below (which must be subject to separate license from the applicable Rightsholder) for: academic photocopies for library reserves and interlibrary loan reporting; and non-academic internal/external business uses and commercial document delivery.

i) electronic storage of any reproduction (whether in plain-text, PDF, or any other format) other than on a transitory basis;

ii) the input of Works or reproductions thereof into any computerized database;

iii) reproduction of an entire Work (cover-to-cover copying) except where the Work is a single article;

iv) reproduction for resale to anyone other than a specific customer of User;

v) republication in any different form. Please obtain authorizations for these uses through other CCC services or directly from the rightsholder.

Any license granted is further limited as set forth in any restrictions included in the Order Confirmation and/or in these Terms.

d) ***Electronic Reproductions in Online Environments (Non-Academic-email, intranet, internet and extranet).*** For "electronic reproductions", which generally includes e-mail use (including instant messaging or other electronic transmission to a defined group of recipients) or posting on an intranet, extranet or Intranet site (including any display or performance incidental thereto), the following additional terms apply:

i) Unless otherwise set forth in the Order Confirmation, the License is limited to use completed within 30 days for any use on the Internet, 60 days for any use on an intranet or extranet and one year for any other use, all as measured from the "republication date" as identified in the Order Confirmation, if any, and otherwise from the date of the Order Confirmation.

ii) User may not make or permit any alterations to the Work, unless expressly set forth in the Order Confirmation (after request by User and approval by Rightsholder); provided, however, that a Work consisting of photographs or other still images not embedded in text may, if necessary, be resized, reformatted or have its resolution modified without additional express permission, and a Work consisting of audiovisual content may, if necessary, be "clipped" or reformatted for purposes of time or content management or ease of delivery (provided that any such resizing, reformatting, resolution modification or “clipping” does not alter the underlying editorial content or meaning of the Work used, and that the resulting material is used solely within the scope of, and in a manner consistent with, the particular License described in the Order Confirmation and the Terms.

15) **Miscellaneous.**

a) User acknowledges that CCC may, from time to time, make changes or additions to the Service or to the Terms, and that Rightsholder may make changes or additions to the Rightsholder Terms. Such updated Terms will replace the prior terms and conditions in the order workflow and shall be effective as to any subsequent Licenses but shall not apply to Licenses already granted and paid for under a prior set of terms.

b) Use of User-related information collected through the Service is governed by CCC's privacy policy, available online at www.copyright.com/about/privacy-policy/.

c) The License is personal to User. Therefore, User may not assign or transfer to any other person (whether a natural person or an organization of any kind) the License or any rights granted thereunder; provided, however, that, where applicable, User may assign such License in its entirety on written notice to CCC in the event of a transfer of all or substantially all of User's rights in any new material which includes the Work(s) licensed under this Service.

d) No amendment or waiver of any Terms is binding unless set forth in writing and signed by the appropriate parties, including, where applicable, the Rightsholder. The Rightsholder and CCC hereby object to any terms contained in any writing prepared by or on behalf of the User or its principals, employees, agents or affiliates and purporting to govern or otherwise relate to the License described in the Order Confirmation, which terms are in any way inconsistent with any Terms set forth in the Order Confirmation, and/or in CCC's standard operating procedures, whether such writing is prepared prior to, simultaneously with or subsequent to the Order Confirmation, and whether such writing appears on a copy of the Order Confirmation or in a separate instrument.

e) The License described in the Order Confirmation shall be governed by and construed under the law of the State of New York, USA, without regard to the principles thereof of conflicts of law. Any case, controversy, suit, action, or proceeding arising out of, in connection with, or related to such License shall be brought, at CCC's sole discretion, in any federal or state court located in the County of New York, State of New York, USA, or in any federal or state court whose geographical jurisdiction covers the location of the Rightsholder set forth in the Order Confirmation. The parties expressly submit to the personal jurisdiction and venue of each such federal or state court.

Last updated October 2022

USC
UNIVERSIDADE DE SANTIAGO DE COMPOSTELA

SPRINGER NATURE LICENSE TERMS AND CONDITIONS

Aug 14, 2023

This Agreement between Ms. Nuria Lopez Lorenzo ("You") and Springer Nature ("Springer Nature") consists of your license details and the terms and conditions provided by Springer Nature and Copyright Clearance Center.

License Number	5604120540741
License date	Aug 08, 2023
Licensed Content Publisher	Springer Nature
Licensed Content Publication	Nature Reviews Neurology
Licensed Content Title	The importance of ongoing international surveillance for Creutzfeldt–Jakob disease
Licensed Content Author	Neil Watson et al
Licensed Content Date	May 10, 2021
Type of Use	Thesis/Dissertation
Requestor type	academic/university or research institute
Format	print and electronic
Portion	figures/tables/illustrations
Number of figures/tables/illustrations	1
Would you like a high resolution image with your order?	no
Will you be translating?	no
Circulation/distribution	1 - 29
Author of this Springer Nature content	no
Title	Therapeutical approaches for prion diseases and characterization of recombinant prion strains from different perspectives
Institution name	University of Santiago de Compostela
Expected presentation date	Oct 2023
Portions	Figure 7
Requestor Location	Ms. Nuria Lopez Lorenzo Av Barcelona CIMUS SSL6 Santiago de Compostela, A Coruña 15782 Spain Attn: Ms. Nuria Lopez Lorenzo
Billing Type	Invoice
Billing Address	Ms. Nuria Lopez Lorenzo Castelao 42, 1A Bueu, Spain 36930 Attn: Ms. Nuria Lopez Lorenzo
Total	**0.00 EUR**

Terms and Conditions

Springer Nature Customer Service Centre GmbH Terms and Conditions

The following terms and conditions ("Terms and Conditions") together with the terms specified in your [RightsLink] constitute the License ("License") between you as Licensee and Springer Nature Customer Service Centre GmbH as

Licensor. By clicking 'accept' and completing the transaction for your use of the material ("Licensed Material"), you confirm your acceptance of and obligation to be bound by these Terms and Conditions.

1. Grant and Scope of License

1. 1. The Licensor grants you a personal, non-exclusive, non-transferable, non-sublicensable, revocable, world-wide License to reproduce, distribute, communicate to the public, make available, broadcast, electronically transmit or create derivative works using the Licensed Material for the purpose(s) specified in your RightsLink Licence Details only. Licenses are granted for the specific use requested in the order and for no other use, subject to these Terms and Conditions. You acknowledge and agree that the rights granted to you under this License do not include the right to modify, edit, translate, include in collective works, or create derivative works of the Licensed Material in whole or in part unless expressly stated in your RightsLink Licence Details. You may use the Licensed Material only as permitted under this Agreement and will not reproduce, distribute, display, perform, or otherwise use or exploit any Licensed Material in any way, in whole or in part, except as expressly permitted by this License.

1. 2. You may only use the Licensed Content in the manner and to the extent permitted by these Terms and Conditions, by your RightsLink Licence Details and by any applicable laws.

1. 3. A separate license may be required for any additional use of the Licensed Material, e.g. where a license has been purchased for print use only, separate permission must be obtained for electronic re-use. Similarly, a License is only valid in the language selected and does not apply for editions in other languages unless additional translation rights have been granted separately in the License.

1. 4. Any content within the Licensed Material that is owned by third parties is expressly excluded from the License.

1. 5. Rights for additional reuses such as custom editions, computer/mobile applications, film or TV reuses and/or any other derivative rights requests require additional permission and may be subject to an additional fee. Please apply to journalpermissions@springernature.com or bookpermissions@springernature.com for these rights.

2. Reservation of Rights

Licensor reserves all rights not expressly granted to you under this License. You acknowledge and agree that nothing in this License limits or restricts Licensor's rights in or use of the Licensed Material in any way. Neither this License, nor any act, omission, or statement by Licensor or you, conveys any ownership right to you in any Licensed Material, or to any element or portion thereof. As between Licensor and you, Licensor owns and retains all right, title, and interest in and to the Licensed Material subject to the license granted in Section 1.1. Your permission to use the Licensed Material is expressly conditioned on you not impairing Licensor's or the applicable copyright owner's rights in the Licensed Material in any way.

3. Restrictions on use

3. 1. Minor editing privileges are allowed for adaptations for stylistic purposes or formatting purposes provided such alterations do not alter the original meaning or intention of the Licensed Material and the new figure(s) are still accurate and representative of the Licensed Material. Any other changes including but not limited to, cropping, adapting, and/or omitting material that affect the meaning, intention or moral rights of the author(s) are strictly prohibited.

3. 2. You must not use any Licensed Material as part of any design or trademark.

3. 3. Licensed Material may be used in Open Access Publications (OAP), but any such reuse must include a clear acknowledgment of this permission visible at the same time as the figures/tables/illustration or abstract and which must indicate that the Licensed Material is not part of the governing OA license but has been reproduced with permission. This may be indicated according to any standard referencing system but must include at a minimum 'Book/Journal title, Author, Journal Name (if applicable), Volume (if applicable), Publisher, Year, reproduced with permission from SNCSC'.

4. STM Permission Guidelines

4. 1. An alternative scope of license may apply to signatories of the STM Permissions Guidelines ("STM PG") as amended from time to time and made available at https://www.stm-assoc.org/intellectual-property/permissions/permissions-guidelines/.

4. 2. For content reuse requests that qualify for permission under the STM PG, and which may be updated from time to time, the STM PG supersede the terms and conditions contained in this License.

4. 3. If a License has been granted under the STM PG, but the STM PG no longer apply at the time of publication, further permission must be sought from the Rightsholder. Contact journalpermissions@springernature.com or bookpermissions@springernature.com for these rights.

5. Duration of License

5. 1. Unless otherwise indicated on your License, a License is valid from the date of purchase ("License Date") until the end of the relevant period in the below table:

Reuse in a medical communications project	Reuse up to distribution or time period indicated in License
Reuse in a dissertation/thesis	Lifetime of thesis
Reuse in a journal/magazine	Lifetime of journal/magazine
Reuse in a book/textbook	Lifetime of edition
Reuse on a website	1 year unless otherwise specified in the License
Reuse in a presentation/slide kit/poster	Lifetime of presentation/slide kit/poster. Note: publication whether electronic or in print of presentation/slide kit/poster may require further permission.
Reuse in conference proceedings	Lifetime of conference proceedings
Reuse in an annual report	Lifetime of annual report
Reuse in training/CME materials	Reuse up to distribution or time period indicated in License
Reuse in newsmedia	Lifetime of newsmedia
Reuse in coursepack/classroom materials	Reuse up to distribution and/or time period indicated in license

6. Acknowledgement

6. 1. The Licensor's permission must be acknowledged next to the Licensed Material in print. In electronic form, this acknowledgement must be visible at the same time as the figures/tables/illustrations or abstract and must be hyperlinked to the journal/book's homepage.

6. 2. Acknowledgement may be provided according to any standard referencing system and at a minimum should include "Author, Article/Book Title, Journal name/Book imprint, volume, page number, year, Springer Nature".

7. Reuse in a dissertation or thesis

7. 1. Where 'reuse in a dissertation/thesis' has been selected, the following terms apply: Print rights of the Version of Record are provided for; electronic rights for use only on institutional repository as defined by the Sherpa guideline (www.sherpa.ac.uk/romeo/) and only up to what is required by the awarding institution.

7. 2. For theses published under an ISBN or ISSN, separate permission is required. Please contact journalpermissions@springernature.com or bookpermissions@springernature.com for these rights.

7. 3. Authors must properly cite the published manuscript in their thesis according to current citation standards and include the following acknowledgement: '*Reproduced with permission from Springer Nature*'.

8. License Fee

You must pay the fee set forth in the License Agreement (the "License Fees"). All amounts payable by you under this License are exclusive of any sales, use, withholding, value added or similar taxes, government fees or levies or other assessments. Collection and/or remittance of such taxes to the relevant tax authority shall be the responsibility of the party who has the legal obligation to do so.

USC DE SANTIAGO DE COMPOSTELA

9. Warranty

9. 1. The Licensor warrants that it has, to the best of its knowledge, the rights to license reuse of the Licensed Material. **You are solely responsible for ensuring that the material you wish to license is original to the Licensor and does not carry the copyright of another entity or third party (as credited in the published version).** If the credit line on any part of the Licensed Material indicates that it was reprinted or adapted with permission from another source, then you should seek additional permission from that source to reuse the material.

9. 2. EXCEPT FOR THE EXPRESS WARRANTY STATED HEREIN AND TO THE EXTENT PERMITTED BY APPLICABLE LAW, LICENSOR PROVIDES THE LICENSED MATERIAL "AS IS" AND MAKES NO OTHER REPRESENTATION OR WARRANTY. LICENSOR EXPRESSLY DISCLAIMS ANY LIABILITY FOR ANY CLAIM ARISING FROM OR OUT OF THE CONTENT, INCLUDING BUT NOT LIMITED TO ANY ERRORS, INACCURACIES, OMISSIONS, OR DEFECTS CONTAINED THEREIN, AND ANY IMPLIED OR EXPRESS WARRANTY AS TO MERCHANTABILITY OR FITNESS FOR A PARTICULAR PURPOSE. IN NO EVENT SHALL LICENSOR BE LIABLE TO YOU OR ANY OTHER PARTY OR ANY OTHER PERSON OR FOR ANY SPECIAL, CONSEQUENTIAL, INCIDENTAL, INDIRECT, PUNITIVE, OR EXEMPLARY DAMAGES, HOWEVER CAUSED, ARISING OUT OF OR IN CONNECTION WITH THE DOWNLOADING, VIEWING OR USE OF THE LICENSED MATERIAL REGARDLESS OF THE FORM OF ACTION, WHETHER FOR BREACH OF CONTRACT, BREACH OF WARRANTY, TORT, NEGLIGENCE, INFRINGEMENT OR OTHERWISE (INCLUDING, WITHOUT LIMITATION, DAMAGES BASED ON LOSS OF PROFITS, DATA, FILES, USE, BUSINESS OPPORTUNITY OR CLAIMS OF THIRD PARTIES), AND WHETHER OR NOT THE PARTY HAS BEEN ADVISED OF THE POSSIBILITY OF SUCH DAMAGES. THIS LIMITATION APPLIES NOTWITHSTANDING ANY FAILURE OF ESSENTIAL PURPOSE OF ANY LIMITED REMEDY PROVIDED HEREIN.

10. Termination and Cancellation

10. 1. The License and all rights granted hereunder will continue until the end of the applicable period shown in Clause 5.1 above. Thereafter, this license will be terminated and all rights granted hereunder will cease.

10. 2. Licensor reserves the right to terminate the License in the event that payment is not received in full or if you breach the terms of this License.

11. General

11. 1. The License and the rights and obligations of the parties hereto shall be construed, interpreted and determined in accordance with the laws of the Federal Republic of Germany without reference to the stipulations of the CISG (United Nations Convention on Contracts for the International Sale of Goods) or to Germany´s choice-of-law principle.

11. 2. The parties acknowledge and agree that any controversies and disputes arising out of this License shall be decided exclusively by the courts of or having jurisdiction for Heidelberg, Germany, as far as legally permissible.

11. 3. This License is solely for Licensor's and Licensee's benefit. It is not for the benefit of any other person or entity.

Questions? For questions on Copyright Clearance Center accounts or website issues please contact springernaturesupport@copyright.com or +1-855-239-3415 (toll free in the US) or +1-978-646-2777. For questions on Springer Nature licensing please visit https://www.springernature.com/gp/partners/rights-permissions-third-party-distribution

Other Conditions:

Version 1.4 - Dec 2022

Questions? E-mail us at customercare@copyright.com.

USC UNIVERSIDADE DE SANTIAGO DE COMPOSTELA

ELSEVIER LICENSE TERMS AND CONDITIONS

Aug 14, 2023

This Agreement between Ms. Nuria Lopez Lorenzo ("You") and Elsevier ("Elsevier") consists of your license details and the terms and conditions provided by Elsevier and Copyright Clearance Center.

License Number	5604141097492
License date	Aug 08, 2023
Licensed Content Publisher	Elsevier
Licensed Content Publication	Molecular Cell
Licensed Content Title	High-resolution structure and strain comparison of infectious mammalian prions
Licensed Content Author	Allison Kraus,Forrest Hoyt,Cindi L. Schwartz,Bryan Hansen,Efrosini Artikis,Andrew G. Hughson,Gregory J. Raymond,Brent Race,Gerald S. Baron,Byron Caughey
Licensed Content Date	Nov 4, 2021
Licensed Content Volume	81
Licensed Content Issue	21
Licensed Content Pages	18
Start Page	4540
End Page	4551.e6
Type of Use	reuse in a thesis/dissertation
Portion	figures/tables/illustrations
Number of figures/tables/illustrations	1
Format	both print and electronic
Are you the author of this Elsevier article?	No
Will you be translating?	No
Title	Therapeutical approaches for prion diseases and characterization of recombinant prion strains from different perspectives
Institution name	University of Santiago de Compostela
Expected presentation date	Oct 2023
Portions	Figure 3
Requestor Location	Ms. Nuria Lopez Lorenzo Castelao 42, 1A Bueu, Pontevedra 36930 Spain Attn: Ms. Nuria Lopez Lorenzo
Publisher Tax ID	GB 494 6272 12
Total	**0.00 EUR**
Terms and Conditions	

INTRODUCTION

1. The publisher for this copyrighted material is Elsevier. By clicking "accept" in connection with completing this licensing transaction, you agree that the following terms and conditions apply to this transaction (along with the Billing and Payment terms and conditions established by Copyright Clearance Center, Inc. ("CCC"), at the time that you opened your RightsLink account and that are available at any time at https://myaccount.copyright.com).

GENERAL TERMS

2. Elsevier hereby grants you permission to reproduce the aforementioned material subject to the terms and conditions indicated.

3. Acknowledgement: If any part of the material to be used (for example, figures) has appeared in our publication with credit or acknowledgement to another source, permission must also be sought from that source. If such permission is not obtained then that material may not be included in your publication/copies. Suitable acknowledgement to the source must be made, either as a footnote or in a reference list at the end of your publication, as follows:
"Reprinted from Publication title, Vol /edition number, Author(s), Title of article / title of chapter, Pages No., Copyright (Year), with permission from Elsevier [OR APPLICABLE SOCIETY COPYRIGHT OWNER]." Also Lancet special credit - "Reprinted from The Lancet, Vol. number, Author(s), Title of article, Pages No., Copyright (Year), with permission from Elsevier."
4. Reproduction of this material is confined to the purpose and/or media for which permission is hereby given. The material may not be reproduced or used in any other way, including use in combination with an artificial intelligence tool (including to train an algorithm, test, process, analyse, generate output and/or develop any form of artificial intelligence tool), or to create any derivative work and/or service (including resulting from the use of artificial intelligence tools).
5. Altering/Modifying Material: Not Permitted. However figures and illustrations may be altered/adapted minimally to serve your work. Any other abbreviations, additions, deletions and/or any other alterations shall be made only with prior written authorization of Elsevier Ltd. (Please contact Elsevier's permissions helpdesk here). No modifications can be made to any Lancet figures/tables and they must be reproduced in full.
6. If the permission fee for the requested use of our material is waived in this instance, please be advised that your future requests for Elsevier materials may attract a fee.
7. Reservation of Rights: Publisher reserves all rights not specifically granted in the combination of (i) the license details provided by you and accepted in the course of this licensing transaction, (ii) these terms and conditions and (iii) CCC's Billing and Payment terms and conditions.
8. License Contingent Upon Payment: While you may exercise the rights licensed immediately upon issuance of the license at the end of the licensing process for the transaction, provided that you have disclosed complete and accurate details of your proposed use, no license is finally effective unless and until full payment is received from you (either by publisher or by CCC) as provided in CCC's Billing and Payment terms and conditions. If full payment is not received on a timely basis, then any license preliminarily granted shall be deemed automatically revoked and shall be void as if never granted. Further, in the event that you breach any of these terms and conditions or any of CCC's Billing and Payment terms and conditions, the license is automatically revoked and shall be void as if never granted. Use of materials as described in a revoked license, as well as any use of the materials beyond the scope of an unrevoked license, may constitute copyright infringement and publisher reserves the right to take any and all action to protect its copyright in the materials.
9. Warranties: Publisher makes no representations or warranties with respect to the licensed material.
10. Indemnity: You hereby indemnify and agree to hold harmless publisher and CCC, and their respective officers, directors, employees and agents, from and against any and all claims arising out of your use of the licensed material other than as specifically authorized pursuant to this license.
11. No Transfer of License: This license is personal to you and may not be sublicensed, assigned, or transferred by you to any other person without publisher's written permission.
12. No Amendment Except in Writing: This license may not be amended except in a writing signed by both parties (or, in the case of publisher, by CCC on publisher's behalf).
13. Objection to Contrary Terms: Publisher hereby objects to any terms contained in any purchase order, acknowledgment, check endorsement or other writing prepared by you, which terms are inconsistent with these terms and conditions or CCC's Billing and Payment terms and conditions. These terms and conditions, together with CCC's Billing and Payment terms and conditions (which are incorporated herein), comprise the entire agreement between you and publisher (and CCC) concerning this licensing transaction. In the event of any conflict between your obligations established by these terms and conditions and those established by CCC's Billing and Payment terms and conditions, these terms and conditions shall control.
14. Revocation: Elsevier or Copyright Clearance Center may deny the permissions described in this License at their sole discretion, for any reason or no reason, with a full refund payable to you. Notice of such denial will be made using the contact information provided by you. Failure to receive such notice will not alter or invalidate the denial. In no event will Elsevier or Copyright Clearance Center be responsible or liable for any costs, expenses or damage incurred by you as a result of a denial of your permission request, other than a refund of the amount(s) paid by you to Elsevier and/or Copyright Clearance Center for denied permissions.

LIMITED LICENSE

The following terms and conditions apply only to specific license types:
15. **Translation**: This permission is granted for non-exclusive world **English** rights only unless your license was granted for translation rights. If you licensed translation rights you may only translate this content into the languages you requested. A professional translator must perform all translations and reproduce the content word for word preserving the integrity of the article.
16. **Posting licensed content on any Website**: The following terms and conditions apply as follows: Licensing material from an Elsevier journal: All content posted to the web site must maintain the copyright information line on the bottom of each image; A hyper-text must be included to the Homepage of the journal from which you are licensing at http://www.sciencedirect.com/science/journal/xxxxx or the Elsevier homepage for books at http://www.elsevier.com; Central Storage: This license does not include permission for a scanned version of the material to be stored in a central repository such as that provided by Heron/XanEdu.
Licensing material from an Elsevier book: A hyper-text link must be included to the Elsevier homepage at http://www.elsevier.com . All content posted to the web site must maintain the copyright information line on the bottom of each image.

Posting licensed content on Electronic reserve: In addition to the above the following clauses are applicable: The web site

must be password-protected and made available only to bona fide students registered on a relevant course. This permission is granted for 1 year only. You may obtain a new license for future website posting.

17. **For journal authors:** the following clauses are applicable in addition to the above:

Preprints:

A preprint is an author's own write-up of research results and analysis, it has not been peer-reviewed, nor has it had any other value added to it by a publisher (such as formatting, copyright, technical enhancement etc.).

Authors can share their preprints anywhere at any time. Preprints should not be added to or enhanced in any way in order to appear more like, or to substitute for, the final versions of articles however authors can update their preprints on arXiv or RePEc with their Accepted Author Manuscript (see below).

If accepted for publication, we encourage authors to link from the preprint to their formal publication via its DOI. Millions of researchers have access to the formal publications on ScienceDirect, and so links will help users to find, access, cite and use the best available version. Please note that Cell Press, The Lancet and some society-owned have different preprint policies. Information on these policies is available on the journal homepage.

Accepted Author Manuscripts: An accepted author manuscript is the manuscript of an article that has been accepted for publication and which typically includes author-incorporated changes suggested during submission, peer review and editor-author communications.

Authors can share their accepted author manuscript:

- immediately
    - via their non-commercial person homepage or blog
    - by updating a preprint in arXiv or RePEc with the accepted manuscript
    - via their research institute or institutional repository for internal institutional uses or as part of an invitation-only research collaboration work-group
    - directly by providing copies to their students or to research collaborators for their personal use
    - for private scholarly sharing as part of an invitation-only work group on commercial sites with which Elsevier has an agreement
- After the embargo period
    - via non-commercial hosting platforms such as their institutional repository
    - via commercial sites with which Elsevier has an agreement

In all cases accepted manuscripts should:

- link to the formal publication via its DOI
- bear a CC-BY-NC-ND license - this is easy to do
- if aggregated with other manuscripts, for example in a repository or other site, be shared in alignment with our hosting policy not be added to or enhanced in any way to appear more like, or to substitute for, the published journal article.

Published journal article (JPA): A published journal article (PJA) is the definitive final record of published research that appears or will appear in the journal and embodies all value-adding publishing activities including peer review co-ordination, copy-editing, formatting, (if relevant) pagination and online enrichment.

Policies for sharing publishing journal articles differ for subscription and gold open access articles:

Subscription Articles: If you are an author, please share a link to your article rather than the full-text. Millions of researchers have access to the formal publications on ScienceDirect, and so links will help your users to find, access, cite, and use the best available version.

Theses and dissertations which contain embedded PJAs as part of the formal submission can be posted publicly by the awarding institution with DOI links back to the formal publications on ScienceDirect.

If you are affiliated with a library that subscribes to ScienceDirect you have additional private sharing rights for others' research accessed under that agreement. This includes use for classroom teaching and internal training at the institution (including use in course packs and courseware programs), and inclusion of the article for grant funding purposes.

Gold Open Access Articles: May be shared according to the author-selected end-user license and should contain a CrossMark logo, the end user license, and a DOI link to the formal publication on ScienceDirect.

Please refer to Elsevier's posting policy for further information.

18. **For book authors** the following clauses are applicable in addition to the above: Authors are permitted to place a brief summary of their work online only. You are not allowed to download and post the published electronic version of your chapter, nor may you scan the printed edition to create an electronic version. **Posting to a repository:** Authors are permitted to post a summary of their chapter only in their institution's repository.

19. **Thesis/Dissertation**: If your license is for use in a thesis/dissertation your thesis may be submitted to your institution in either print or electronic form. Should your thesis be published commercially, please reapply for permission. These requirements include permission for the Library and Archives of Canada to supply single copies, on demand, of the complete thesis and include permission for Proquest/UMI to supply single copies, on demand, of the complete thesis. Should your thesis be published commercially, please reapply for permission. Theses and dissertations which contain embedded PJAs as part of the formal submission can be posted publicly by the awarding institution with DOI links back to the formal publications on ScienceDirect.

Elsevier Open Access Terms and Conditions

You can publish open access with Elsevier in hundreds of open access journals or in nearly 2000 established subscription journals that support open access publishing. Permitted third party re-use of these open access articles is defined by the author's choice of Creative Commons user license. See our open access license policy for more information.

Terms & Conditions applicable to all Open Access articles published with Elsevier:

Any reuse of the article must not represent the author as endorsing the adaptation of the article nor should the article be modified in such a way as to damage the author's honour or reputation. If any changes have been made, such changes must be clearly indicated.

The author(s) must be appropriately credited and we ask that you include the end user license and a DOI link to the formal publication on ScienceDirect.

If any part of the material to be used (for example, figures) has appeared in our publication with credit or acknowledgement to another source it is the responsibility of the user to ensure their reuse complies with the terms and conditions determined by the rights holder.

Additional Terms & Conditions applicable to each Creative Commons user license:

CC BY: The CC-BY license allows users to copy, to create extracts, abstracts and new works from the Article, to alter and revise the Article and to make commercial use of the Article (including reuse and/or resale of the Article by commercial entities), provided the user gives appropriate credit (with a link to the formal publication through the relevant DOI), provides a link to the license, indicates if changes were made and the licensor is not represented as endorsing the use made of the work. The full details of the license are available at http://creativecommons.org/licenses/by/4.0.

CC BY NC SA: The CC BY-NC-SA license allows users to copy, to create extracts, abstracts and new works from the Article, to alter and revise the Article, provided this is not done for commercial purposes, and that the user gives appropriate credit (with a link to the formal publication through the relevant DOI), provides a link to the license, indicates if changes were made and the licensor is not represented as endorsing the use made of the work. Further, any new works must be made available on the same conditions. The full details of the license are available at http://creativecommons.org/licenses/by-nc-sa/4.0.

CC BY NC ND: The CC BY-NC-ND license allows users to copy and distribute the Article, provided this is not done for commercial purposes and further does not permit distribution of the Article if it is changed or edited in any way, and provided the user gives appropriate credit (with a link to the formal publication through the relevant DOI), provides a link to the license, and that the licensor is not represented as endorsing the use made of the work. The full details of the license are available at http://creativecommons.org/licenses/by-nc-nd/4.0. Any commercial reuse of Open Access articles published with a CC BY NC SA or CC BY NC ND license requires permission from Elsevier and will be subject to a fee.

Commercial reuse includes:

- Associating advertising with the full text of the Article
- Charging fees for document delivery or access
- Article aggregation
- Systematic distribution via e-mail lists or share buttons

Posting or linking by commercial companies for use by customers of those companies.

20. **Other Conditions**:

v1.10

Questions? E-mail us at customercare@copyright.com.

USC UNIVERSIDADE DE SANTIAGO DE COMPOSTELA

USC
UNIVERSIDADE
DE SANTIAGO
DE COMPOSTELA

Prion diseases are rare and fatal neurodegenerative disorders for which there is no cure or treatment. They are caused by infectious proteins that result from the misfolding of the cellular prion protein, PrPC, into its pathogenic form, PrPSc. Furthermore, PrPSc can appear as conformational variants called strains that exhibit distinct phenotypes and could present resistance to anti-prion compounds.
This thesis aims to assess three different therapeutic candidates in a fast murine model of prion disease to tackle these disorders from different aspects of their biology. Additionally, due to the role of prion strains in drug resistance and their biochemical and structural interest, diverse recombinant prion strains were characterized in this thesis using biological, biochemical, and biophysical methods.